

**Supersaturation and solubilization to enhance the
oral bioavailability of poorly soluble drug molecules**

**A mechanistic investigation of their potential and
limitations**

Dissertation
zur
Erlangung des Doktorgrades (Dr. rer. nat.)
der
Mathematisch-Naturwissenschaftlichen Fakultät
der
Rheinischen Friedrich-Wilhelms-Universität Bonn

vorgelegt von
Álvaro López Mármol
aus
Madrid, Spanien

Bonn, Februar 2021

Angefertigt mit Genehmigung der Mathematisch-Naturwissenschaftlichen Fakultät der
Rheinischen Friedrich-Wilhelms-Universität Bonn

Promotionskommission:

Erstgutachter: Prof. Dr. Karl-Gerhard Wagner

Zweitgutachter: Prof. Dr. Alf Lamprecht

Fachnaher Gutachter: Prof. Dr. Gerd Bendas

Fachfremder Gutachter: Prof. Dr. Barbara Kirchner

Tag der Promotion: 29. April 2021

Erscheinungsjahr: 2021

ACKNOWLEDGEMENT

First of all, I would like to express my deepest gratitude to my doctor father, Prof. Dr. Karl G. Wagner, for giving me the opportunity to perform my doctoral thesis on this fascinating research topic within his work group. I would like to thank him not just for his continuous and excellent guidance and support throughout these years, but also personally for his understanding and empathy at the difficult moments. Without your acceptance and motivation throughout the years, my life would be probably very different nowadays. I will always be thankful for the chance and the trust you gave me on the first day we met some years ago.

I would like to thank also Prof. Dr. Alf Lamprecht, Prof. Dr. Gerd Bendas and Prof. Dr. Barbara Kirchner for accepting to be part of my examination committee.

A big thanks goes to Mrs. Martina Gerlitz for her extremely helpful support and kindness since the very first day. I highly appreciate your help especially with all the paper and administrative work at the beginning of this adventure, when I was literally *lost in translation*. Similarly, I would like to express my gratitude to Alexander Ramich, Jessica Gromand, Jürgen Hohmann, Thomas Vidua, Franz-Josef Willems, Iris Jusen and Dieter Baumert for their constant support and willingness in all technical matters.

I would also like to express my deepest gratitude to all the staff from Sirius Analytical Instruments Ltd. (UK), for their continuous help throughout the years. Here, a special thanks goes to Karl Box, Robert Taylor, John Comer, Craig Roberts, Paul Stripp, Paul Whittles, Rebecca Heys, Hayley Watson and Rebeca Ruiz for the interesting and helpful scientific discussions, for the technical support and for their kindness and interest during the time that I spent with them in Forest Row.

A very special thanks goes to the old colleagues in the Pharmaceutical Technology department: Thomas Schmal, Viktoria Riedel, Bernadette Kettel, Florian Schorr and Montserrat Armengol for their help during the first months and for quickly integrating me within the group. Also to my older and newer colleagues Ehab Ali, Tawfek Yazeyi, Markus Ries, Stefan Lorscheidt, Henusha Jhundoo, Merari Duarte, Ozan Hirlak, Veronika Hagelstein, Fabian Simons, Maryam Shetab, Kristina Steffens, Simone Putzke, Pia Steinlein, Katrin Grüneberg, Chi-Wah Yeung, Dnyaneshwar Kapote, Marius Monschke, Marius Neuwirth, Anna Krome, Alexander Denninger, Kathrin Locher, Anne Cossé and Rafael Bachmaier for the good moments shared in their company, for being valuable members of the Mensa Team and for making the lab life much easier and motivating every single day.

A big thank you goes also to my Besançon colleagues and friends Yann Pellequer, Antoine Touzet, Ryma Attia and Claire Chretien for the nice and instructive months that I was able to share with them in France and that I will always keep in good memory.

My deepest gratitude to my office colleagues and dear friends Mert Serim, Jan Kozak, Kai Berkenfeld, Bashar Ibraheem, Daris Grizic and Diana Agha, for being my biggest support in Bonn during these years, for never letting me down, for the good laughs and best moments shared together, which encouraged and motivated all of us during this common journey.

A special thanks goes also to my new AbbVie family: the Pharmaceuticals team, Dr. Mirko Koziolk and Dr. Kerstin Sauer for their understanding, support and limitless motivation in the last few months.

To my dear old (and new) colleague and friend Dr. Esther Bochmann, for the correction and review of this PhD thesis and for her always valuable comments and suggestions, but most importantly for being the best office colleague I could wish for and for demonstrating through the years her kindness, also in this new life phase.

A mis amigos y compis de Farmacia: Jorge Orquín, Marta Rúa, Diego Matas, Marta Molina, Nuria García e Irene Muñoz, por ser un apoyo muy importante durante estos años y por haber reforzado, a pesar de la distancia, la amistad que comenzamos hace ya un buen tiempo.

Alberto Pérez Morales, Cristina San Miguel y Maite Martínez, por su continua motivación, por las frecuentes videollamadas, por ser uno de mis mayores apoyos y en definitiva, por demostrarme semana a semana (y casi día a día) que ni el tiempo ni la distancia suponen ningún límite y que la amistad que hemos forjado (aún incluso más durante estos años), perdurará por siempre.

A mi familia: mi hermana Marta, por perseguir y cumplir sus sueños y porque sin su ayuda en casa en los últimos años, yo no habría podido perseguir los míos. En definitiva, por ser una valiente y luchadora. A mi padre, por representar el mejor ejemplo a seguir, por su entereza, por sacar fuerzas de donde era difícil sacarlas, por ofrecerme una sonrisa y tenderme una mano o dedicarme unas palabras motivadoras siempre, pero muy especialmente en estos últimos años. No puedo expresarte con palabras mi agradecimiento por estar al pie del cañón y en primera línea de batalla para que yo pudiera cumplir mis sueños.

Finalmente, a mi madre, mi gran pilar, porque sin ti nada de esto habría sido posible, por representar todo lo que aspiro a ser, por guiarme siempre por el buen camino y porque sé que todo esto es en gran parte mérito tuyo. Entre tú y yo, como siempre, las palabras sobran.

A mis padres

Confía en el tiempo,
que suele dar dulces salidas
a muchas amargas dificultades.

Miguel de Cervantes

Previously published parts of this work:

Poster presentations:

- I. **Álvaro López Mármol**, Karl Box, Karl G. Wagner. *Mechanistic evaluation of supersaturation and solubility enhancement for “Chasing” and “Non chasing” APIs using colloids*. 2015 AAPS Annual World Meeting, Orlando, Florida, USA
- II. **Álvaro López Mármol**, Karl G. Wagner. *A deeper insight of the physicochemical properties of Telmisartan under supersaturating conditions*. 11th World Meeting on Pharmaceutics, Biopharmaceutics and Pharmaceutical Technology 2018, Granada, Spain

Oral presentation:

- I. **Álvaro López Mármol**, Karl Box, Karl G. Wagner. *Evaluation of the supersaturated state and precipitation kinetics of two poorly soluble weak bases using colloids*. 10th World Meeting on Pharmaceutics, Biopharmaceutics and Pharmaceutical Technology 2016, Glasgow, UK

Research article:

- I. **López Mármol, Á.**, Denninger, A., Touzet, A., Dauer, K., Becker, T., Pöstges, F., Pellequer, Y., Lamprecht, A., and Wagner, K.G. (2021). *The relevance of supersaturation and solubilization in the gastrointestinal tract for oral bioavailability: An in vitro vs. in vivo approach*. International Journal of Pharmaceutics 603, 120648. DOI: [10.1016/j.ijpharm.2021.120648](https://doi.org/10.1016/j.ijpharm.2021.120648)

ABBREVIATIONS

Abbreviation	Definition
<i>A</i>	Absorption
<i>a</i>	Molar extinction coefficient
ABZ	Albendazole
ACN	Acetonitrile
AMI	Artificial membrane insert
API	Active pharmaceutical ingredient
ASD	Amorphous solid dispersion
AU	Absorbance units
<i>AUC</i>	Area under the curve
<i>AUC_{aq}</i>	Area under the curve in aqueous phase
<i>AUC_{oc}</i>	Area under the curve in organic phase
<i>b</i>	Path length
BA	Bioavailability
BCS	Biopharmaceutical classification system
BDT	Biphasic dissolution test
BioGIT	Biorelevant Gastrointestinal Transfer
<i>C</i>	Concentration
<i>C₀</i>	Starting concentration
<i>C_A</i>	Amorphous solubility
CDS	Candesartan
<i>C_{eq}</i>	Equilibrium (thermodynamic) solubility
CheqSol	Chasing equilibrium solubility
CLX	Celecoxib
<i>C_{max}</i>	Maximum concentration
CMC	Critical micelle concentration
<i>C_s</i>	Saturation solubility
<i>D</i>	Coefficient of distribution
<i>D₁₂</i>	Diffusion coefficient

DAD	Diode Array Detector
dC/dt	Precipitation rate
DCM	Dichloromethane
DCS	Developability classification system
DLS	Dynamic light scattering
DMSO	Dimethylsulfoxide
dpH/dt	Change in pH over time
DPD	Dipyridamole
DS	Degree of supersaturation
DSC	Differential scanning calorimetry
ϵ	Dielectric constant
E_a	Activation energy
Ph. Eur	European Pharmacopoeia
e.g.	Exempli gratia = for example
f_a	Absorbed fraction
FaHIF	Fasted state human intestinal fluid
FaSSGF	Fasted state simulated gastric fluid
FaSSIF	Fasted state simulated intestinal fluid
FDA	Food and Drug Administration
FeHIF	Fed state human intestinal fluid
FeSSIF	Fed state simulated intestinal fluid
G	Gibbs free energy
GI	Gastrointestinal
GIS	Gastrointestinal simulator
GIT	Gastrointestinal tract
GLPS	Glass – liquid phase separation
h	Thickness of the boundary layer
HCl	Hydrochloric acid
HIF	Human intestinal fluid
HME	Hot Melt Extrusion
HPLC	High performance liquid chromatography
HTS	High throughput screening
IS	Internal standard

ITZ	Itraconazole
IUPAC	International Union of Pure and Applied Chemistry
i.v.	Intravenous
IVVC	<i>In vitro in vivo</i> correlation
<i>J</i>	Flux
<i>k_a</i>	Absorption constant
<i>k_e</i>	Elimination constant
KTZ	Ketoconazole
KVA64	Vinylpyrrolidone-vinyl acetate copolymer
λ	wavelength
λ_{max}	Maximum absorbance wavelength
LDS	Laser diffraction spectrometry
LLPS	Liquid-liquid phase separation
LOD	Limit of detection
LOQ	Limit of quantification
LTD	Loratadine
<i>M</i>	Molar
<i>m</i>	Refractive index
μ	Chemical potential
μ_{eq}	Chemical potential in equilibrium
MA4C	Methylcellulose, Methocel™ A4C
max.	Maximum
MDT	Monophasic dissolution test
MEC	Molar extinction coefficient
MMC	Mean molecular charge
<i>M_n</i>	Average molecular weight
<i>M_W</i>	Molecular weight
NaCl	Sodium chloride
NaOH	Sodium hydroxide
NaTC	Sodium taurocholate
NCE	New chemical entity
NME	New molecular entity
OH-ITZ	Hydroxyitraconazole

OrBiTo project	Oral biopharmaceutical tools project
P	Partition coefficient
P_{app}	Apparent permeability
P_{ow}	Partition coefficient between octanol and water
PAMPA	Parallel artificial membrane permeability assay
PCA	Principal Component Analysis
PCS	Photon Correlation Spectroscopy
PDA	Photodiode array detector
PDI	Polydispersity index
PEG	Polyethylene glycol
P-gp	P-glycoprotein
Ph. Eur.	European Pharmacopoeia
PK	Pharmacokinetics
pK_a	Negative logarithm of the acidic dissociation constant
pK_a^{app}	apparent pK_a
p_sK_a	apparent pK_a in the presence of a cosolvent
PLM	Polarized light microscopy
PR	Partition rate
PS	Particle size
PSA	Polar surface area
PSD	Particle size distribution
PTFE	Polytetrafluorethylen
PVP	Polyvinyl pyrrolidone
R^2	Coefficient of determination
rpm	Revolutions per minute
RT	Retention time
SD	Standard deviation
SDDS	Supersaturating drug delivery system
SIF	Simulated intestinal fluid
SOL	Poyvinyl caprolactam – polyvinyl acetate – polyethylene glycol graft copolymer
SSPM	Standardized supersaturation and precipitation method
SSR	Supersaturation ratio

t	Time
$t_{1/2}$	Half life
T	Temperature
TBME	tert-butyl-methyl ether
TFA	Target Factor Analysis
T_g	Glass transition temperature
TIM	TNO intestinal model
TLM	Telmisartan
T_m	Melting point
t_{max}	Time to reach C_{max}
t_p	Precipitation time
USP	United States Pharmacopoeia
UV-Vis	Ultraviolet/visible
V	Volume
v/v	Volume/Volume
W/O	Aqueous/Octanol
w/V	weight/Volume
w/w	weight/weight
YS	Yasuda-Shedlovsky

TABLE OF CONTENT

1	General introduction	1
1.1	Parameters of interest	2
1.1.1	Ionization constants and pK_a	2
1.1.2	Solubility and supersaturation	3
1.1.3	Dissolution	5
1.1.4	Lipophilicity and permeability	6
1.1.5	The biopharmaceutical classification system (BCS)	9
1.2	Supersaturated solutions and precipitation, general context and thermodynamic aspects	10
1.3	Physiology of the human gastrointestinal tract and supersaturation <i>in vivo</i> .	17
1.4	<i>In vitro</i> supersaturation and dissolution models	19
1.4.1	Supersaturation evaluation of non-formulated drugs	20
1.4.2	Supersaturation evaluation of formulated drugs	22
2	Objective	26
3	Model	27
3.1	Drug substance selection	27
3.2	Pharmaceutical excipients selection	31
3.2.1	Vinylpyrrolidone-vinyl acetate copolymer (Kollidon VA64, KVA64)	31
3.2.2	Methylcellulose derivative Methocel A4C (MA4C)	32
3.2.3	Polyvinyl caprolactam-polyvinyl acetate-polyethylene glycol graft copolymer (Soluplus, SOL)	33
3.3	Part I: Physicochemical properties of poorly soluble drugs in polymeric solutions and their relationship with supersaturation and solubilization	35
3.3.1	Study on the ionization of poorly soluble drug molecules under supersaturation and solubilization conditions	35
3.3.1.1	UV-metric pK_a titration	36
3.3.1.1.1	UV-metric pK_a determination under the influence of a cosolvent	38
3.3.1.1.2	Differentiation between solubilizing and non-solubilizing drug-polymer combinations by means of the apparent shifts in the ionization properties	40

3.3.2	Solubility and solubility enhancement	44
3.3.2.1	CheqSol method	44
3.3.2.1.1	Solubility determination by means of potentiometric titration: chasers vs non-chasers ...	47
3.3.2.2	Shaking flask method	51
3.3.3	Lipophilicity: Log <i>P</i> and Log <i>D</i>	52
3.3.3.1	Chromatographic method	52
3.3.3.2	pH-metric titration	53
3.4	Part II: <i>In vitro</i> evaluation of the supersaturation and solubilization potential to enhance oral bioavailability.....	57
3.4.1	Monophasic and Biphasic Dissolution Tests (MDTs and BDTs).....	57
3.4.1.1	Apparatus design	57
3.4.1.1.1	Experimental design	60
3.4.2	Particle size distribution analysis	61
3.4.2.1	Particle size analysis via Laser diffraction	61
3.4.2.2	Dynamic Light Scattering (DLS) / Photon Correlation Spectroscopy (PCS)	62
3.4.3	Polarized Light Microscopy	63
3.5	Part III: Supersaturation and solubilization in the gastrointestinal tract and its relevance for oral bioavailability: an <i>in vitro</i> vs. <i>in vivo</i> approach	64
3.5.1	Blood extraction and quantification.....	64
3.5.2	Pharmacokinetic parameter calculation	65
3.5.3	Deconvolution and IVIVC calculation	66
4	Experimental	67
4.1	Materials	67
4.1.1	Equipment	67
4.1.2	Excipients and chemicals.....	69
4.1.3	Drug substance and formulation.....	70
4.2	Experimental conditions	71
4.2.1	Part I: Physicochemical properties of poorly soluble API in colloidal solutions and their relationship with supersaturation and oral bioavailability.....	71
4.2.1.1	UV-metric <i>pKa</i> titration.....	71
4.2.1.2	Solubility determination by means of potentiometric titration	71
4.2.1.3	Solubility determination by means of shaking flask method.....	72
4.2.1.4	Lipophilicity determination: chromatographic method	73
4.2.1.5	Rheological characterization.....	73
4.2.2	Part II: <i>In vitro</i> evaluation of the supersaturation and solubilization potential to enhance oral bioavailability	74
4.2.2.1	Monophasic and biphasic dissolution tests	74
4.2.2.1.1	Polymer and API stock solutions preparation	74

TABLE OF CONTENT

4.2.2.1.2	Pretests	74
4.2.2.1.3	Test and parameters investigated	76
4.2.2.2	Particle size analysis via laser diffraction	77
4.2.2.3	Dynamic light scattering (DLS)/ Photon correlation spectroscopy (PCS)	78
4.2.2.4	Polarized light microscopy (PLM).....	78
4.2.3	Part III: Supersaturation and solubilization in the gastrointestinal tract and its relevance for oral bioavailability: an <i>in vitro</i> vs. <i>in vivo</i> approach	79
4.2.3.1	<i>In vitro</i> biphasic dissolution tests (BDT).....	79
4.2.3.2	<i>In vivo</i> pharmacokinetics	80
4.2.3.3	Extraction and quantification of CLX	81
4.2.3.4	Extraction and quantification of TLM	81
4.2.3.5	Extraction and quantification of ITZ.....	82
5	Results and discussion	83
5.1	Part I: Physicochemical properties of poorly soluble API in colloidal solutions and the relation to supersaturation and oral bioavailability.....	83
5.1.1	Ionization constant and pK_a	83
5.1.1.1	Dipyridamole.....	84
5.1.1.2	Albendazole	85
5.1.1.3	Itraconazole	86
5.1.1.4	Loratadine.....	87
5.1.1.5	Telmisartan	88
5.1.1.6	Celecoxib.....	90
5.1.1.7	pK_a and apparent pK_a fitting.....	91
5.1.1.7.1	Kollidon VA64.....	91
5.1.1.7.2	Methocel A4C	92
5.1.1.7.3	Soluplus.....	94
5.1.2	Lipophilicity: $\text{Log}P$ and $\text{Log}D$	95
5.1.2.1	Chromatographic method	95
5.1.2.2	pH-metric titration method	96
5.1.3	Solubility and solubility enhancement	97
5.1.3.1	Chaser molecules	97
5.1.3.1.1	Dipyridamole	97
5.1.3.1.2	Celecoxib.....	98
5.1.3.2	Non-chaser molecules	100
5.1.3.2.1	Loratadine.....	100
5.1.3.2.2	Telmisartan	101
5.1.3.3	Extremely poorly soluble molecules	104
5.1.3.3.1	Albendazole	104
5.1.3.3.2	Itraconazole	105

5.1.3.4	Solubility enhancement as a function of the innate supersaturation behavior	106
5.1.3.5	Solubility enhancement mechanisms	108
5.1.3.5.1	Kollidon VA64.....	108
5.1.3.5.2	Methocel A4C	109
5.1.3.5.3	Soluplus.....	110
5.1.4	General physicochemical evaluation and underlying stabilization mechanisms	111
5.1.4.1	Relationship between pK_a shifts and solubility enhancement	111
5.1.4.1.1	Kollidon VA64.....	111
5.1.4.1.2	Methocel A4C	112
5.1.4.1.3	Soluplus.....	113
5.1.4.2	Relationship between the SOL pK_a -shifts and other physicochemical properties	114
5.1.5	Conclusion	117
5.2	Part II: <i>In vitro</i> evaluation of the interplay between supersaturation and partition by means of a biorelevant gastrointestinal dissolution tests.....	118
5.2.1	Monophasic dissolution test (MDT)	118
5.2.1.1	Chaser molecules	118
5.2.1.1.1	Dipyridamole	118
5.2.1.1.2	Celecoxib.....	125
5.2.1.2	Non chaser molecules.....	130
5.2.1.2.1	Loratadine.....	130
5.2.1.2.2	Telmisartan	133
5.2.1.3	Extremely poorly soluble molecules	139
5.2.1.3.1	Albendazole	139
5.2.1.3.2	Itraconazole	144
5.2.1.4	Monophasic dissolution tests and particle size distributions overview	150
5.2.2	Biphasic dissolution test (BDT).....	151
5.2.2.1	Chaser molecules	151
5.2.2.1.1	Dipyridamole	151
5.2.2.1.2	Celecoxib.....	154
5.2.2.1.3	Partition rate for chaser molecules	157
5.2.2.2	Non-chaser molecules	159
5.2.2.2.1	Loratadine.....	159
5.2.2.2.2	Telmisartan	161
5.2.2.2.3	Partition rate for non-chaser molecules	163
5.2.2.3	Extremely poorly soluble molecules	165
5.2.2.3.1	Albendazole	165
5.2.2.3.2	Itraconazole	167
5.2.2.3.3	Partition rate of extremely poorly soluble drug molecules.	169
5.2.2.4	Relationship between solubility enhancement and lipophilicity	170

TABLE OF CONTENT

5.2.2.4.1	Kollidon VA64.....	170
5.2.2.4.2	Methocel A4C	172
5.2.2.4.3	Soluplus.....	173
5.2.3	Conclusion	175
5.3	Part III: Supersaturation and solubilization in the gastrointestinal tract and its relevance for oral bioavailability: an <i>in vitro</i> vs. <i>in vivo</i> approach	177
5.3.1	<i>In vitro</i> biphasic dissolution tests in FaSSIF	177
5.3.1.1	Chaser molecule: Celecoxib	177
5.3.1.2	Non chaser molecule: Telmisartan	178
5.3.1.3	Extremely poorly soluble molecule: Itraconazole.....	179
5.3.2	<i>In vivo</i> pharmacokinetics.....	180
5.3.2.1	Chaser molecule: Celecoxib	180
5.3.2.2	Non chaser molecule: Telmisartan	183
5.3.2.3	Extremely poorly soluble molecule: Itraconazole.....	185
5.3.3	Deconvolution and IVIVC establishment.....	187
5.3.3.1	Chaser molecule: Celecoxib	188
5.3.3.2	Non chaser molecule: Telmisartan	189
5.3.4	Conclusion	191
6	Summary and outlook	192
7	References	197

SPECIFIC INFORMATION

It was renounced to use legally protected trademark for Kollidon, Methocel and Soluplus

1 General introduction

Since the discovery that supersaturation potentially improves the transport of active pharmaceutical ingredients (API) through biological membranes by increasing the API fraction ready for partition (Higuchi, 1960), the stabilization of the supersaturated state in solution was determined as a suitable approach to enhance the bioavailability of poorly soluble APIs (Fong et al., 2017a).

APIs suffering from poor solubility in aqueous biorelevant media, could benefit from this stabilization of the supersaturated state in the gastrointestinal (GI) tract as a pathway to circumvent their poor oral bioavailability (BA) (Brouwers et al., 2009). Additionally, since the oral administration route is the easiest intake pathway for patients (Hens et al., 2017; U.S. Food and Drug Administration, 2020), one of the main priorities in the development of oral dosage forms is the optimal dissolution and absorption properties of the drug product.

In the last few years, the increasing interest in supersaturating drug delivery systems (SDDS) led to a deeper understanding of the kinetics and thermodynamics of supersaturation, as well as it gave insight into the underlying mechanisms and critical parameters affecting this metastable state (Bauer-Brandl and Brandl, 2020; Bevernage et al., 2013; Brouwers et al., 2009; Xu and Dai, 2013a). Several supersaturation and solubilization strategies were already investigated (Rodríguez-Hornedo and Murphy, 1999 ; Aungst, 2017; Göke et al., 2018). Amongst others, water-soluble polymers enabled the stabilization of the supersaturated state and therefore limited the precipitation of poorly soluble APIs in simulated GI fluids (Bevernage et al., 2012a; Liu et al., 2015). This is a crucial point, since *in vivo* drug precipitation kinetics plays an important role in the oral absorption of supersaturated solutions (Brouwers et al., 2009; Lindfors et al., 2008; Xu and Dai, 2013a). In this context, the ability of supersaturated solutions to enhance the oral BA of drug molecules was extensively discussed and investigated in previous studies (Bevernage et al., 2012b; Mellaerts et al., 2008a; Miller et al., 2012a). However, these were mostly based on *in vitro* methodologies or focusing on the *in vivo* administration of SDDS. As a result, an isolated consideration of the real effect of pure supersaturation on bioavailability without being biased by a drug product formulation was impossible.

Despite several efforts made in the last few years (Alhalaweh et al., 2019; Bergström et al., 2003; Edueng et al., 2017; Fagerberg et al., 2015), a full understanding of the complex supersaturation/solubilization process and a further reliable prediction of solubility enhancement and IVIVC was not achieved (Bergström and Avdeef, 2019). As a result, this work focused on the establishment of a predictive model to determine suitable API/polymer combinations to improve the oral BA of poorly soluble drugs by supersaturation-related effects. Furthermore, a mechanistic understanding of the underlying process which led to a supersaturation or solubilization of the API was targeted. Finally, a rational selection of pharmaceutical excipients for supersaturation in early-stage drug formulation development will be enabled. This major goal is addressed by linking the efficacy of different supersaturation and solubilization mechanisms with the inherent supersaturation ability of the drug molecules from three different perspectives: physicochemical (thermodynamic), *in vitro* biorelevant (kinetic) and *in vivo* (physiological).

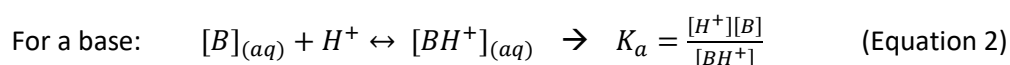
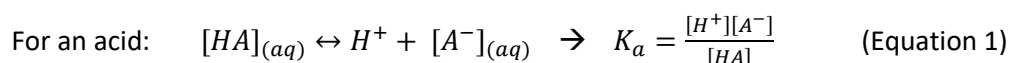
1. GENERAL INTRODUCTION

1.1 Parameters of interest

1.1.1 Ionization constants and pK_a

A large fraction of drug molecules have ionizable groups within their chemical structure. The strength of a molecule to donate or bind protons (H^+) from an aqueous medium, defines its ionization state, as well as its acidic or basic character. In general, strong acids and bases (e.g. chlorohydric acid (HCl) and sodium hydroxide (NaOH)) are fully dissociated in aqueous solution. On the contrary, the majority of drug molecules possesses weak acidic or weak basic groups within their chemical structure. The dissociation behavior of these molecules is therefore characterized by a dissociation constant (K_a or K_b , for weak acids and weak bases, respectively). It determines the ionization propensity as a function of the pH and defines the equilibrium between the ionized and unionized fractions at a certain pH.

The dissociation of a weak base or acid in water is characterized by the ability to donate or bind protons from the medium, until the ionized and neutral species fraction are in an equilibrium at a certain pH value. In this way, for a monoprotic acid or base, the equilibrium between the ionized and unionized forms can be defined as:



The strength of weak acids and bases is commonly described as pK_a and pK_b values, which are identical to the negative common logarithm of the dissociation constant. The relationship between the pH and ionization was first described by Henderson and Hasselbalch for more than 100 years ago (Hasselbalch, 1916; Henderson, 1908). In the case of a weak base, the pK_a value is calculated from the acid dissociation constant of the conjugated acid (BH^+):

$$\text{For an acid: } pK_a = pH + \log_{10} \left(\frac{[HA]}{[A^-]} \right) \quad (\text{Equation 3})$$

$$\text{For a base: } pK_a = pH + \log_{10} \left(\frac{[BH^+]}{[B]} \right) \quad (\text{Equation 4})$$

The equilibrium between the ionized and unionized forms at each pH value defines the ionization profile and determines the pH-dependent solubility and lipophilicity. From the Henderson-Hasselbalch equations, it can be deduced that the pK_a describes the pH value at which 50% of the molecular species are ionized, while the other 50% is unionized. As shown in Figure 1.1 for the weak base itraconazole, the pK_a is the pH at the crossing point of both ionization profiles.

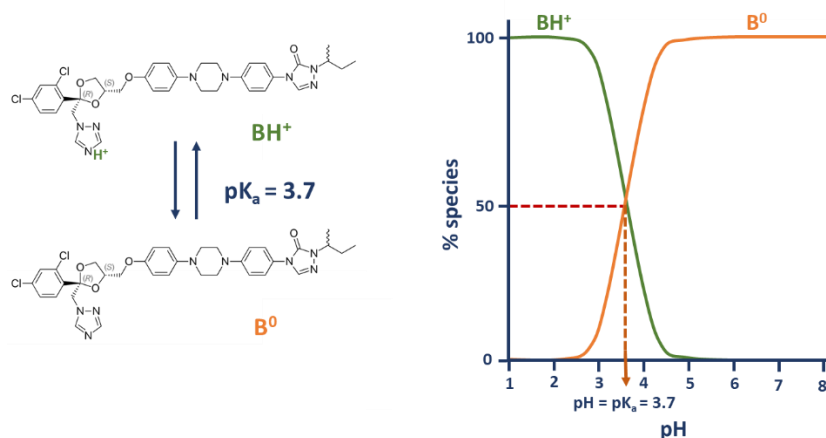


Figure 1.1: Itraconazole species formed in solution (ionized, BH^+ and non-ionized, B) as a function of the pK_a and pH -value

1.1.2 Solubility and supersaturation

The European Pharmacopoeia (Ph. Eur.) defines the solubility as the ratio of the dissolved drug substance to the volume of solvent when both, the solid and solution phase are in equilibrium (saturated solution) at room temperature (European Pharmacopoeia 9th Edition, 2017). Furthermore, the Ph. Eur. established a classification of drug molecules as a function of the volume of solvent needed to dissolve one gram of substance under equilibrated conditions (Table 1.1).

Table 1.1: Drug solubility classification according to the Ph. Eur. Edition 9.6

DESCRIPTIVE TERM	APPROXIMATE VOLUME OF SOLVENT [mL] PER GRAM OF SOLUTE	SOLUBILITY [mg/mL]
Very soluble	< 1	> 1000
Freely soluble	1-10	100-1000
Soluble	10-30	33-100
Sparingly soluble	30-100	10-33
Slightly soluble	100-1000	1-10
Very slightly soluble	1000-10000	0.1-1
Practically insoluble	> 10000	< 0.1

The Ph. Eur. solubility definition is based on the equilibrium (thermodynamic) solubility (C_{eq}) of a compound in a certain medium with a specific composition, ionic strength and pH value. In literature, this concept is often referred as saturation solubility, at which the undissolved and dissolved drug are in equilibrium (Hörter and Dressman, 1997) and therefore, the solution is saturated. Nevertheless, the complex interplay between the ionization state of a drug molecule and its solubility, imposes the need to define several other solubility-related terms:

1. GENERAL INTRODUCTION

- **Subsaturated solution.** Contains an excess of undissolved neutral species that will continue to dissolve until the equilibrium is reached.
- **Supersaturated solution.** Contains a high concentration of neutral species that cannot be dissolved by the solvent and will continue to precipitate until an equilibrium is reached.
- **Kinetic solubility.** Concentration of a compound in solution at the time when an induced precipitate first appears (Box et al., 2006). It may differ from the equilibrium solubility if a supersaturation event occurred.
- **Intrinsic solubility.** Equilibrium solubility of the neutral (unionized) acid or base form of an ionizable compound at a pH at which it is fully unionized (Box et al., 2006). In other words, this solubility represents a worst-case scenario in terms of solubility.
- **Crystalline solubility.** Equilibrium solubility of a thermodynamically stable crystalline form under defined and constant experimental conditions.
- **Amorphous solubility.** Concentration of drug in solution when it precipitates as an amorphous and kinetically stabilized form. Similar to the crystalline solubility, the amorphous solubility is pH-dependent for ionizable molecules (Indulkar et al., 2015).
- **Chaser.** Compound that possesses the ability to supersaturate in solution by itself without the influence of additional pharmaceutical excipients. These molecules are slow precipitators and tend to precipitate into a low energetic crystalline form. The kinetic solubility of chaser molecules exceeds the intrinsic solubility (Stuart and Box, 2005a).
- **Non-chaser.** Compound that does not possess the ability to supersaturate in solution by itself. In general, these molecules are fast precipitators and tend to precipitate into an amorphous form, which subsequently slowly crystallizes into a thermodynamically stable form. When a precipitation event is first detected, the solution is already in equilibrium. Therefore, the kinetic and intrinsic solubilities are identical or very similar (Stuart and Box, 2005a).

Worth to mention, the intrinsic solubility is also an equilibrium solubility value at the pH at which all drug molecules are neutral. However, the equilibrium solubility is much broader applicable and feasible for all pH-values. Given the common ionizable behavior of drug molecules, the state of ionization varies with the pH as a response to the protonation and deprotonation equilibria. Therefore, the differences in the concentration of neutral species at each pH value determine the shape of the pH-dependent solubility curve, which depends on the nature of the ionizable groups (Figure 1.2).

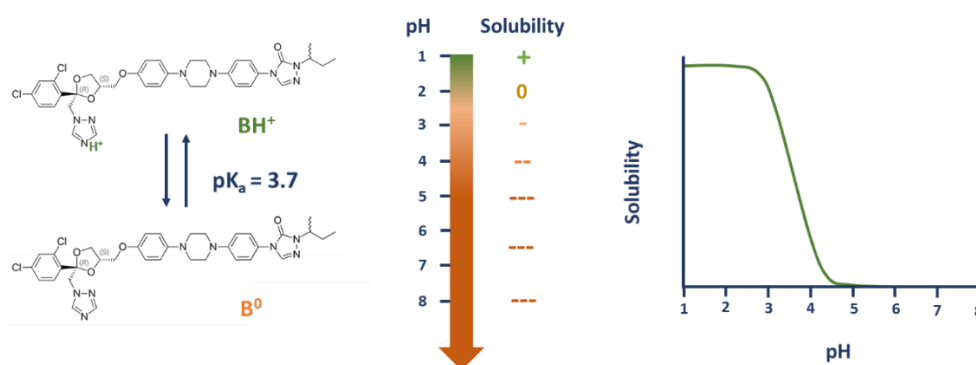


Figure 1.2: pH-dependent solubility for a weak base molecule as function of the neutral species in solution

1.1.3 Dissolution

Dissolution is described as the amount of drug substance which dissolves in a solvent over time (Mudie et al., 2010). Longer than a century ago, Noyes and Whitney described the dissolution kinetics of solids by their well-known equation (Noyes and Whitney, 1897). Especially, poorly soluble drugs suffer of low dissolution rates, as the concentration gradient between C_{eq} and the solubility of the drug is low. The Noyes-Whitney equation was refined several years later by Nernst and Brunner to account the surface of the particles (Nernst, 1904) (Equation 5).

$$\frac{dm}{dt} = \frac{D_{12} \cdot A_s \cdot (C_{eq} - C)}{h} \quad (\text{Equation 5})$$

dm/dt = dissolution rate [kg/s]

m = mass of dissolved material [kg]

t = time [s]

D_{12} = diffusion coefficient [m^2/s]

A_s = specific surface area of the solute [m^2]

h = thickness of the boundary layer of the solvent at the surface of the drug substance [m]

$C_{eq} - C$ = concentration gradient [kg/m^3]

As it can be deduced from Equation 5, the dissolution rate is directly proportional to the specific surface area of the solute, the diffusion coefficient and the concentration gradient. At the same time, it is inversely proportional to the thickness of the diffusion layer. With an increasing concentration gradient and a lower thickness of the diffusion layer, the dissolution rate would increase.

In general, poorly soluble compounds are classified as “brick dust” or “grease balls” depending on the solubility- and dissolution-limiting attribute (Bergström et al., 2016). “Brick dust” compounds have a strong crystal lattice which hinders the dissociation from the compound’s solid form into the solution. The strong intermolecular bonds in the crystal lattice counteract the pull of solvation by water. These compounds have typically a high melting point ($T_m > 200$ °C). On the other side, the solubility of “grease ball” compounds is mainly limited by their poor hydration (Figure 1.3). They are typically hydrophobic and possess a low melting point. Due to the compound’s lipophilicity, they are unable to form strong bonds with water molecules and therefore, their solubility is extremely low. In general, grease ball compounds are preferred over brick dust compounds (Bergström et al., 2007; Di et al., 2012; Hill and Young, 2010), as the traditional formulation strategies (excipients, solubilizing agents, cyclodextrins or ASDs) are more likely to improve their oral absorption (Bergström and Avdeef, 2019; Bergström et al., 2007).

1. GENERAL INTRODUCTION

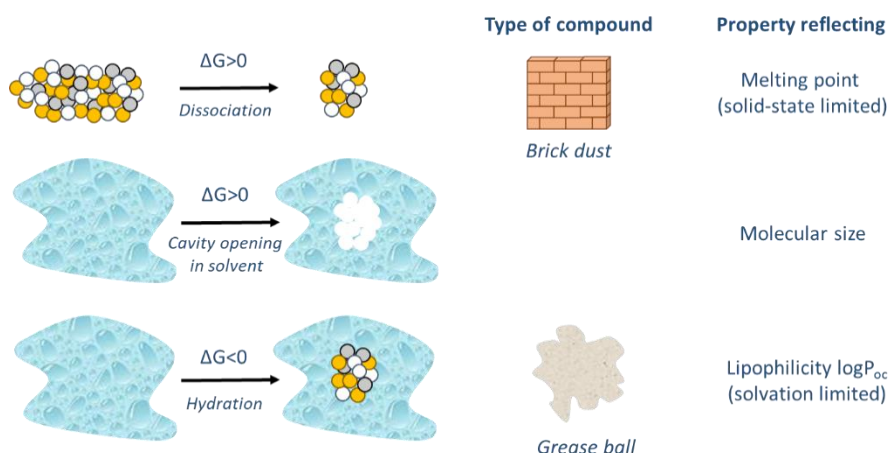
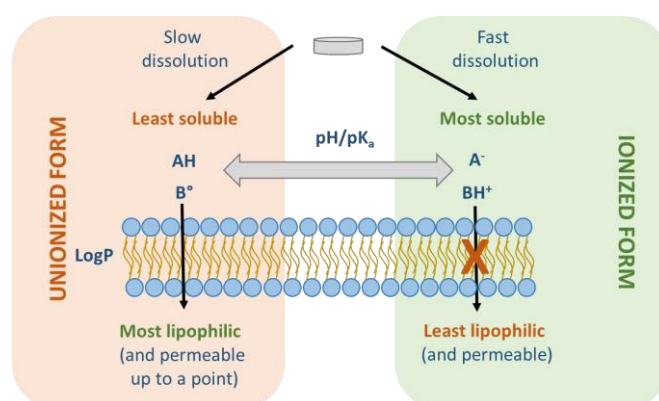


Figure 1.3: The thermodynamic principles of dissolution, limiting factors and solubility of “brick dust” and “grease ball” compounds. Adapted from Bergström et al., 2016.

1.1.4 Lipophilicity and permeability

The lipophilicity characterizes the affinity of a molecule or moiety for a lipophilic environment (van de Waterbeemd et al., 1997). In general, poorly soluble drug molecules tend to show a high lipophilicity to enable a pharmacological response within a human cell. Since biological cell membranes are composed of a lipidic bilayer made of phospholipids and cholesterol, low lipophilic molecular structures are unlikely to cross biological membranes by passive diffusion.

For ionizable drugs, the state of ionization determines the pH-dependent solubility and lipophilicity. This is an important factor for the drug uptake in the GI Tract. In here, the pH gradient throughout the GI tract drives a complex interplay between dissolution, precipitation and permeation caused by the constant change in ionization, solubility and lipophilicity of the drug molecule (1.4). The important interplay among these three physicochemical properties was highlighted by Box and Comer for 84 molecules (Box and Comer, 2008).



1.4: Interplay between the ionization, solubility and permeability of ionizable drug molecules. Adapted from “Introduction to pH-metric LogP measurement” (Sirius Analytical Instruments, 2009).

In general, the lipophilicity of a compound is defined by its partition coefficient (P). This concept was first introduced in 1872 by Berthelot and Jungfleisch (Berthelot and Jungfleisch, 1872). It is based on the ability of a dissolved drug in an aqueous medium to partition into an organic lipophilic phase, when sink conditions are applied. The extent of partition depends on the lipophilicity of the molecule or moiety. P is only valid for non-ionizable molecules or for ionizable molecules at a pH, at which the drug is fully neutral. The partition coefficient defines the unionized drug concentration ratio between two immiscible phases at equilibrium, as defined by the Equation 6.

$$P = \frac{[\text{unionized species}]_{\text{organic}}}{[\text{unionized species}]_{\text{aqueous}}} \quad (\text{Equation 6})$$

For ionizable molecules, the ratio of all species dissolved in two immiscible solvents which are in equilibrium is defined as coefficient of distribution (D) (Equation 7). In contrast to P , D is pH-dependent and is impacted by the extent of ionization in the aqueous solution. As a result, the lipophilicity curve as a function of the pH is defined by D (**¡Error! No se encuentra el origen de la referencia.**), while P is constant for each drug molecule. The shape of the lipophilicity profile directly correlates to the nature of the ionizable groups within a molecule (acid vs. base vs. ampholyte vs. zwitterion).

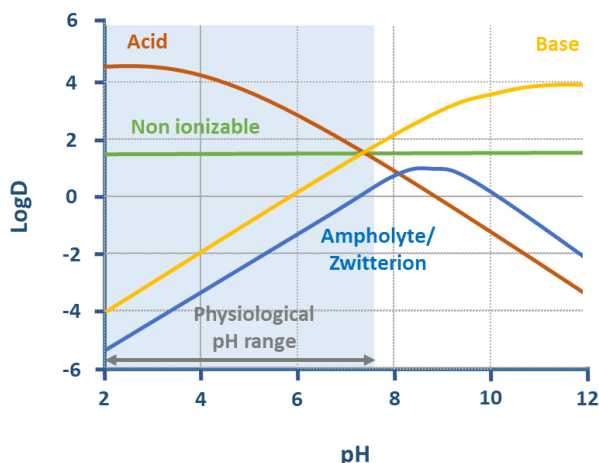
$$D = \frac{[\text{unionized+ionized species}]_{\text{organic}}}{[\text{unionized+ionized species}]_{\text{aqueous}}} \quad (\text{Equation 7})$$

Traditionally, the partition coefficient between octanol and water (P_{ow}) was used as a reference to compare the lipophilicity of molecules. For practical reasons, the lipophilicity of drug molecules is expressed in a logarithmic scale. In this way, a molecule in equilibrium with a $\text{Log}P$ of 3 exhibit 1000 times more neutral species in the organic phase as in the aqueous phase.

The lipophilicity of a drug molecule impacts their permeability through biological membranes (Camenisch et al., 1998). The permeability describes the transport through the membrane by diffusion (Mutschler et al., 2007). Therefore, it is a key parameter for intestinal drug absorption, which in turn determines the oral bioavailability and systemic drug exposure (Augustijns et al., 2014).

The $\text{Log}P$ and $\text{Log}D$ are commonly used for the prediction of absorption. Molecules exhibiting a $\text{Log}D$ in the range of 0 and 3 are considered as highly permeable while drug molecules with a $\text{Log}D$ below -1.5 or higher than 4.5 are typically low permeable compounds (Krämer, 1999). Therefore, the permeability does not increase linearly with the lipophilicity but more a bell-shaped relationship between $\text{Log}P$ and absorption was recognized by Hansch and Fujita (Hansch and Fujita, 1964). Due to the importance of the lipophilicity as a physicochemical property, several methods were developed to study the lipophilicity of molecules, as it was reviewed at the end of the 20th century (Caron et al., 1999).

1. GENERAL INTRODUCTION



1.5: Exemplary lipophilicity curves of drug molecules as a function of pH and the nature of the ionizable group. Adapted from "Introduction to pH-metric LogP measurement" (Sirius Analytical Instruments, 2009)

The permeation rate across a membrane per unit of time and surface area is defined as flux (J). The apparent permeability (P_{app}) is compound specific and is defined by the flux divided by the starting concentration (C_0) in the donor compartment.

The permeability is investigated *in vitro* by means of artificial membranes, such as applied in the parallel artificial membrane permeability assay (PAMPA), the phospholipid vesicle-based permeation assay (PVPA) or the widely used cell culture monolayers from human colon adenocarcinoma (Caco-2) (Artursson and Karlsson, 1991; Flaten et al., 2006; Kansy et al., 1998). Concretely, good relationships were established between the absorbed fraction (f_a) in humans and the P_{app} coefficient across a Caco-2 cell monolayer (Artursson and Karlsson, 1991; Grès et al., 1998; Krämer, 1999).

To predict poor drug absorption of new molecular entities (NME), the "rule of five" described by Lipinski is broadly used in drug discovery (Lipinski, 2000; Lipinski et al., 1997) and it defines the "drugability" of a NME. Due to designing synthetic molecules by computational chemistry and high-throughput screening (HTS), substances with a high molecular weight, high lipophilicity, poor water solubility and in many cases poor permeability are generated. Most of these NMEs fall in the BCS classes II or IV (see section 1.1.5), consequently having a limited oral bioavailability. In Lipinski's studies, he identified certain characteristics of an NME, including physicochemical properties and molecular descriptors, that will lead to a proper oral absorption (Lipinski, 2000). In general, good absorption is expected when the following criteria are fulfilled:

- The NME has less than 5 H-bond donors within its structure.
- The NME has less than 10 H-bond acceptors within its structure.
- The molecular weight is lower than 500 g/mol.
- The calculated LogP (cLogP) is lower than 5.

In general, the rule of five applies only to molecules that are not substrates of active transporters and that are mainly absorbed by passive diffusion. Almost two decades ago, when the rule of 5 was established, the knowledge of transporters was limited. Nowadays, thanks to the improvements of *in silico* and *in vitro* techniques, it is well known that most of the molecules are

substrates for uptake transporters. Despite this fact, the rule of 5 is still considered as valid and is used to predict poor permeability through passive diffusion.

1.1.5 The biopharmaceutical classification system (BCS)

Longer than two decades ago, Amidon first described the importance of using fundamental drug properties to improve and optimize drug product development and product quality. This thought led to the proposal of a biopharmaceutical classification system (BCS) that categorizes drug molecules regarding their solubility, dissolution rate and permeability (Amidon et al., 1995). The importance of these properties lies in its influence on oral drug absorption and exposure (Tsume et al., 2014) and it was incorporated into the FDA guidance “Dissolution Testing of Immediate Release Solid Oral Dosage Forms” (FDA Guidance for Industry, 1997).

For the first time, a further guidance “Waiver of *in vivo* Bioavailability and Bioequivalence Studies for Immediate Release Solid Oral Dosage Form Based on a Biopharmaceutics Classification System” oriented the BCS concept towards bioequivalence (BE) assessments (CDER/FDA, 2000). The concept of this guidance is based on the categorization of drug molecules into high/low solubility and high/low permeability to treat each group different in terms of the applicability of biowaiver studies. Furthermore, the BCS facilitated the decision upon drug candidate nomination and selection in drug discovery and early-stage drug product development (Kawabata et al., 2011; Ku, 2008).

In the BCS, a drug molecule is classified as *highly soluble* when the highest dose strength of an immediate release product is soluble in 250 mL or less in the pH range between 1 and 6.8 at $37 \pm 1^\circ\text{C}$ (FDA/CDER, 2017). A drug molecule is classified as *highly permeable* when the absorption in humans or through a human intestinal membrane is 85% or more of the administered dose (mass balance) or compared to an intravenous (i.v.) reference dose (FDA/CDER, 2017). Alternatively, other systems, which predict the extent of drug absorption in humans, like *in situ* animal or *in vitro* epithelial cell culture models can be applied. Furthermore, an immediate release product is considered *rapidly dissolving* when at least 85% or more of the highest dose dissolves within 30 minutes in USP apparatuses in a volume of 500 mL or less in the pH range 1 – 6.8 or in simulated gastric or intestinal fluids (FDA/CDER, 2017).

As a result of the correlation between solubility, dissolution rate and intestinal permeability with the oral BA of a molecule, the BCS and the FDA guidance categorized drugs in four groups depending on the limiting factor for oral absorption (Table 1.2).

Table 1.2. Biopharmaceutical classification system (Amidon et al., 1995; Martinez and Amidon, 2002)

CLASS	SOLUBILITY	PERMEABILITY	ABSORPTION
I	High	High	Generally very well-absorbed compounds
II	Low	High	Dissolution rate/solubility limited
III	High	Low	Permeability rate limited
IV	Low	Low	Very poor oral bioavailability

1. GENERAL INTRODUCTION

More than 50% of the known NMEs were reported to belong to class II (Miller et al., 2012b), showing a poor solubility and good permeability in the gastrointestinal tract. In this thesis, all selected compounds belong to BCS class II. It enables a study of the potential of solubility enhancement or stabilization of the supersaturation state to enhance oral absorption without affecting the oral bioavailability by a poor permeability.

Butler and Dressman developed a modified BCS classification system, called developability classification system (DCS) (Butler and Dressman, 2010), that additionally divides the compounds of class II into two subcategories in dependence of the limiting factor for oral absorption:

- IIa. Dissolution rate-limited absorption. The dissolution rate is too slow and the absorption window is shorter as the time needed for its dissolution.
- IIb. Solubility-limited absorption. The GI fluids volume is not sufficient to dissolve the entire administered drug dose.

In this way, the DCS is capable to guide the formulation design and development (Bergström et al., 2014a). In general, class IIa compounds can still be formulated as a standard dosage form by reducing their particle size without the need to change the physical state of the drug. For class IIb compounds, an enabling formulation is needed to achieve a complete absorption of the drug. Furthermore, the DCS includes the drug solubility in biorelevant media and in more realistic volumes to better simulate the *in vivo* conditions.

1.2 Supersaturated solutions and precipitation, general context and thermodynamic aspects

The complex interplay between drug absorption, distribution, metabolism and excretion (ADME) determines the *in vivo* pharmacokinetic profile of orally administered formulations. Within this context, the absorption component is determined by the Fick's first law (Equation 8), where the amount of substance diffusing through a certain unit area of the gastrointestinal barrier per unit time (flux) is proportional to the diffusion coefficient (D_{12}) and concentration gradient (dC/dx) (Comyn, 1985).

$$F = -D_{12} * (dC/dx) \quad (\text{Equation 8})$$

The absorption term is additionally influenced by the solubility of the drug molecules in the gastrointestinal (GI) lumen, since the drug dissolution is mandatory before absorption can take place by means of passive diffusion or active transport through the GI barrier. Therefore, the maximum achievable intraluminal drug concentration might limit oral absorption (Brouwers et al., 2009). Furthermore, today's state-of-the-art high-throughput screening techniques and combinatorial chemistry significantly increased the fraction of new chemical entities (NCE) suffering from poor solubility in aqueous media (Gribbon and Andreas, 2005; Lipinski, 2000; Wenlock et al., 2003). It is not surprising that a large variety of formulation approaches and technologies emerged with the aim of enhancing the poor dissolution and solubility of these drug molecules within the GIT (Stegemann et al., 2007). Amongst others, commonly applied

strategies include salt formation for ionizable compounds, micellar solubilization by surfactants, cocrystal formation, use of complexation agents like cyclodextrins and manufacturing of amorphous solid dispersions (Berge et al., 1977; Elworthy and Patel, 1982; Leuner and Dressman, 2000; Loftsson and Brewster, 2011; Vishweshwar et al., 2006). Nevertheless, it must be considered that the intraluminal concentration of a drug is not necessarily limited by its solubility in GI fluids. Within this context, drugs may exist in a state of supersaturation at a concentration above the saturation solubility (C_{eq}). In this case, the degree of supersaturation is commonly expressed as the supersaturation ratio (SSR) (Equation 9), where C is the drug concentration at a certain time point and C_{eq} represents the equilibrium (saturation) solubility.

$$SSR = \frac{C}{C_{eq}} \quad (\text{Equation 9})$$

Based on the SSR concept, a solution can be defined as unsaturated ($SSR < 1$), saturated ($SSR = 1$) and supersaturated ($SSR > 1$). In a supersaturated solution, the higher dissolved drug fraction, compared to equilibrated conditions, is responsible for an increased chemical potential (μ). Thus, supersaturation is a metastable state which contributes simultaneously to the driving force to precipitation until the solution reaches its equilibrium with a lower chemical potential (μ_{eq}) (Brouwers et al., 2009). From a thermodynamic point of view, the crystallization (precipitation) tendency is related to the difference in the chemical potential ($\Delta\mu$) between supersaturated solution and equilibrated conditions (Equation 10): the larger the SSR, the lower the stability of supersaturation and the faster precipitation will occur.

$$\Delta\mu = \mu - \mu_{eq} = RT \ln \left(\frac{a}{a_{eq}} \right) \quad (\text{Equation 10})$$

In Equation 10, R is the gas constant, T is the temperature and a and a_{eq} are the activity of the solute in a supersaturated and saturated state, respectively (Kashchiev and van Rosmalen, 2003). When the activity coefficients of the solute for supersaturated and saturated states are assumed to be identical, the Equation 10 becomes a function of the ratio between C and C_{eq} , therefore $\Delta\mu$ is related to SSR (Equation 11).

$$\Delta\mu = RT \ln \left(\frac{C}{C_{eq}} \right) = RT \ln(SSR) \quad (\text{Equation 11})$$

Addressing the higher chemical potential and energetic state of a supersaturated solution (Figure 1.6), the precipitation is the result of a thermodynamically favored exothermic process characterized by a decrease in the Gibbs free energy ($\Delta G < 0$) (Brouwers et al., 2009). From a mechanistical perspective, drug precipitation consists of two clearly differentiated processes: nucleation and crystal growth.

Nucleation involves the formation of small molecular clusters or aggregates. A phenomenon that requires an activation energy (E_a) which is attributed to the high interfacial tension between the high-curvature clusters and the solvent (γ_{ns}) (Brouwers et al., 2009). If the activation energy is

1. GENERAL INTRODUCTION

not reached, the solution remains in a supersaturated state (metastable zone) and no precipitation event takes place. However, once the activation energy is reached and the formation of clusters with maximum interfacial energy (critical clusters) is favored, nucleation occurs. The nucleation rate (J_n), defined as the net production of critical clusters per unit time and unit bulk volume, depends on the number of molecules in a unit volume (N_0), the frequency of molecular transport at the nucleus-liquid interface (ν), the Gibbs free energy change for the formation of critical clusters (ΔG^*), the Boltzmann's constant (k_b) and the temperature (T) (Equation 12).

$$J_n = N_0 \nu \exp\left(\frac{-\Delta G^*}{k_b T}\right) \quad (\text{Equation 12})$$

At the same time, the ΔG^* strongly depends on the SSR and on the γ_{ns} between the critical cluster and the solvent, and therefore the nucleation rate is also changing with SSR (Kashchiev and van Rosmalen, 2003; Lindfors et al., 2008; MILLER et al., 2007; Rodríguez-hornedo and Murphy, 1999). Furthermore, it must be considered that J_n and ΔG^* are referring to homogenous nucleation processes in solution. However, due to the presence of several surfaces and interfaces which may reduce the activation energy and therefore act as a catalyst for nucleation, heterogenous nucleation (nucleation on surfaces) is additionally expected to occur in the gastrointestinal (GI) lumen.

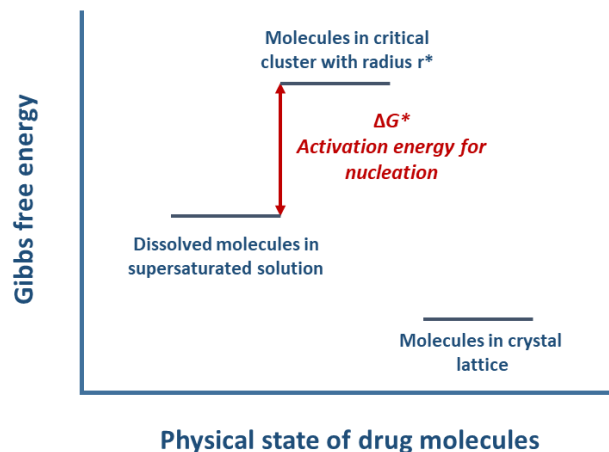


Figure 1.6: Schematic representation of the Gibbs free energy (G) of molecules in a supersaturated state in solution. Adapted from Brouwers et al., 2009.

After the energetic barrier for nucleation is exceeded (Figure 1.6), the critical clusters are susceptible to grow to macroscopic crystals. The crystal growth is in turn divided into two steps: 1) the diffusion of molecules from the supersaturated solution to the crystal interface and 2) the integration of these molecules into a crystal lattice. The increase in radius (r) of a crystal per unit time, defined as the net growth of a particle, is governed by the diffusion coefficient of a molecule (D_c), the surface integration factor (k_+), the Avogadro constant (N_A) and the difference between the bulk solute concentration and the concentration directly next to the cluster surface ($C - C_{eq}$) (Equation 13) (Lindfors et al., 2008).

$$\frac{dr}{dt} = \frac{D_c \nu N_A}{r + D/k_+} (C - C_{eq}) \quad (\text{Equation 13})$$

The crystallization time varies drastically in dependence of the drug's physicochemical properties as well as the degree of supersaturation and the experimental conditions, such as the medium composition (Indulkar et al., 2015). For slow crystallizers, a rapid generation of highly supersaturated solutions, which can be kinetically stable for a certain time frame, is known. It was attributed to the separation of the solution into two phases: a drug-rich and a drug-lean phase (Bonnett et al., 2003; Indulkar et al., 2015; Veessler et al., 2003; Zhao et al., 2012). This phenomenon is described as liquid-liquid phase separation (LLPS).

LLPS phenomena play an important role in several biological processes and assays. In the field of cell biology, LLPS is also known as promiscuous aggregation, as it is responsible for the formation of non-specific interactions between the drug-rich phase of the system and several enzymes. In many cases, this led to false positive results in biological assays (McGovern et al., 2002, 2003; Sassano et al., 2013). Furthermore, due to the formation of aberrant condensates by means of phase separation, LLPS events were recently related to pathological processes in several human diseases such as cancer, neurodegeneration and infections (Alberti et al., 2019).

From a pharmaceutical point of view, LLPS might be an advantage for poorly soluble drugs. The weak basic behavior of many drug molecules induces precipitation in the small intestine, therefore impeding their oral absorption. In this sense, the supersaturated state for slow crystallizers, with an initial precipitation by means of LLPS, offers several advantages in terms of oral absorption and exposure (Gao et al., 2003). First of all, the higher solubility of the precipitated form and its slow crystallization tendency facilitate the accessibility of dissolved drug molecules to cross the intestinal barrier. Secondly, the higher energetic state of this form decreases the energetic dissolution barrier and a quick absorption-redissolution interplay can be established (Huang and Tong, 2004), in which the drug-rich phase acts as a reservoir.

When compared to the thermodynamically stable crystalline form and despite the equilibrium between the drug-rich and the drug-lean phase, this high energetic system is metastable and therefore, crystallization is likely (Bonnett et al., 2003; Lafferrère et al., 2004; Veessler et al., 2006; Zhao et al., 2012). Furthermore, additional studies linked the phenomena of LLPS and glass-liquid phase separation (GLPS) to the amorphous solubility (Almeida e Sousa et al., 2014; Ilevbare and Taylor, 2013). It was therefore assumed that the detection of the drug concentration, at which the phase separation occurred, was a reasonable approach to determine the amorphous solubility of slow crystallizer.

From a thermodynamic perspective, the amorphous solubility (C_A) of a drug molecule is related to the free energy difference (ΔG) between the crystalline and the amorphous form (Hancock and Parks, 2000)(Figure 1.7). The relationship is defined by Equation 14, where R is the universal gas constant, T is the temperature ($37^\circ\text{C} = 310\text{ K}$), $\exp[-I(a)]$ is the factor accounting for the change in the activity of the amorphous form due to water absorption (Murdande et al., 2010) and C_{eq} is the equilibrium (thermodynamic) solubility of the crystalline form.

$$C_A = \exp\left[-\frac{\Delta G}{RT}\right] \exp[-I(a)] C_{eq} \quad (\text{Equation 14})$$

ΔG is estimated by the Hoffman equation (Equation 15) (Hoffman, 1958), which defines the relationship between the Gibbs free energy (G), the enthalpy of fusion (ΔH_f) and the melting point (T_m) of the crystalline form, by means of differential scanning calorimetry (DSC).

1. GENERAL INTRODUCTION

$$\Delta G = \frac{\Delta H_f(T_m - T)T}{T_m^2} \quad (\text{Equation 15})$$

For ionizable drug molecules, the amorphous solubility is a function of the pH (Indulkar et al., 2015), similarly to the pH-dependent solubility of the crystalline form. In this sense, the amorphous solubility at a certain pH-value depends on the neutral (unionized) fraction of the drug. If the amorphous solubility is exceeded, LLPS or GLPS occur and it results in the formation of a second drug-rich phase in the form of droplets.

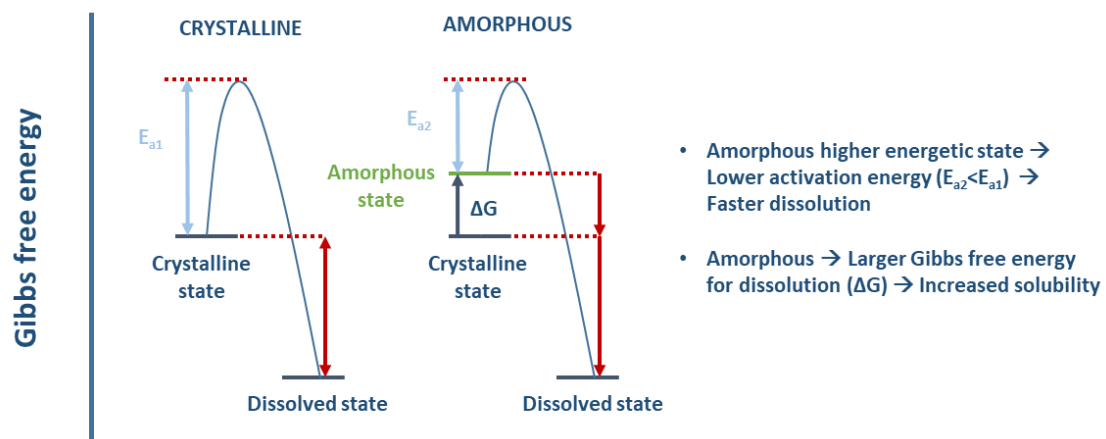


Figure 1.7: Gibbs free energy of crystalline (A) and amorphous (B) solid state forms and activation energy (E_a) needed for their dissolution. Adapted from Bauer-Brandl and Brandl, 2020.

The higher energetic state due to LLPS induces a spontaneous and thermodynamically favored crystallization, which is an exothermic process ($\Delta G < 0$). This involves the rearrangement of the precipitated drug molecules into a crystal lattice with lower entropy ($\Delta S < 0$). The low energy and low entropy of a crystal lattice (Williams, 1975) are responsible for its thermodynamic stability, but also for its lower solubility. When compared to the amorphous form, a higher energetic barrier for dissolution of the crystalline form must be overcome. The potential transitions from a supersaturated solution into a saturated and equilibrated solution are represented in Figure 1.8 (Jackson et al., 2016)

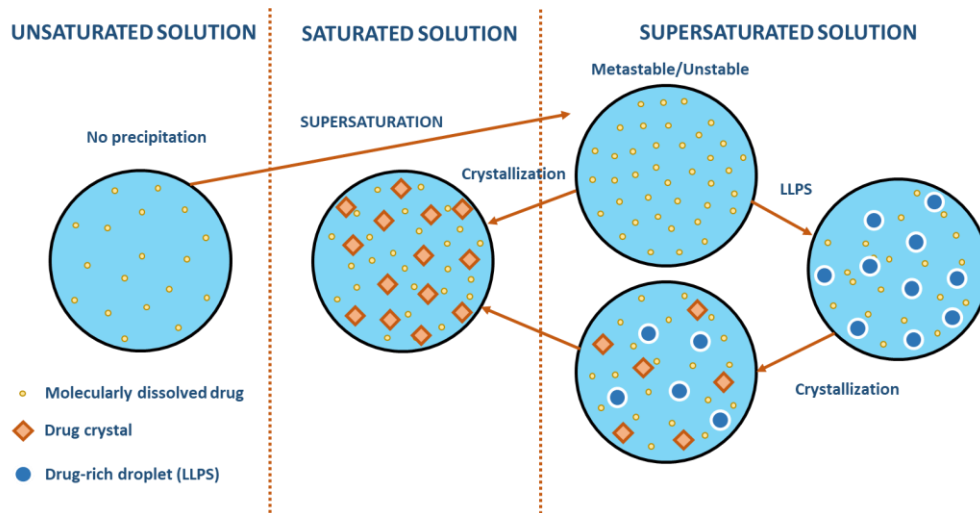


Figure 1.8: Potential phase transitions within supersaturated aqueous drug systems. Adapted from Jackson et al., 2016

The impact of pharmaceutical excipients as precipitation inhibitors is attributed to various mechanisms which interfere with the nucleation and crystal growth processes:

- Reduction of the SSR and the chemical potential of a supersaturated solution by enhancing the solubility of the drug.
- Viscosity increase which reduces molecular mobility, therefore limiting the nucleation and crystal growth.
- Increase in the cluster-liquid interfacial energy (activation energy) to further impeded nucleation.
- Adsorption onto the crystal surface, accompanied by crystal habit modification and crystal growth inhibition. The adsorption changes the level of solvation at the crystal-liquid interface and therefore hinders the integration of further drug molecules into the crystal lattice.
- Formation of intermolecular interactions between the drug molecules and pharmaceutical excipients to maintain the drug in its higher energetic state (increased chemical potential), hindering crystallization at least from a kinetic perspective.

In general, for solubility enhancement and supersaturation, a clear differentiation between solubilizing and supersaturating strategies is made. Solubility enhancement is the improvement in crystalline solubility induced by complexation or internalization of the drug with or in pharmaceutical excipients such as cyclodextrins or surfactants. In literature, the solubilization approaches were linked to a decreased permeability, even though a higher apparent solubility was obtained (Miller et al., 2012a). The goal of the supersaturation strategy is to induce a real supersaturation for a certain time, which causes subsequently drug precipitation up to a concentration of C_{eq} . This is generally the case for amorphous solid dispersions (ASDs). A true supersaturation is not generally associated with an impeded permeation, as it was reported by Frank and co-workers (Frank et al., 2012) (Figure 1.9)

1. GENERAL INTRODUCTION

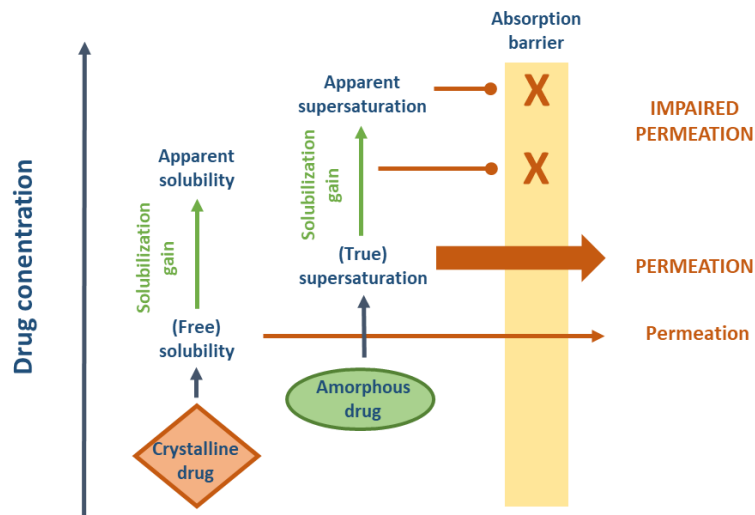


Figure 1.9: Contribution of freely dissolved drug, true supersaturation and solubilization to the permeation and absorption of drug molecules. Adapted from Bauer-Brandl and Brandl, 2020.

The contribution of all stabilizing mechanisms can be summarized in the spring and parachute approach (Figure 1.10), proposed by Guzmán and co-workers (Guzmán et al., 2004, 2007a). The model proposes that various formulation approaches applied to poorly soluble drugs, such as the amorphization of the drug, potentially induce a short-time and metastable supersaturation. Compared to the poor dissolution rate and solubility of the crystalline drug, this short-time supersaturation is defined by a “spring”, mainly attributed to the rapid dissolution and subsequent precipitation of the drug in solution. When a long-term supersaturation is targeted, the pharmaceutical excipient used acts as precipitation or crystal growth inhibitor and extends supersaturation over a longer period. Therefore, it facilitates the absorption of drug molecules from a kinetic perspective. In this way, since these excipients drive a controlled precipitation in the GI tract, their precipitation inhibition action is described as “parachute”.

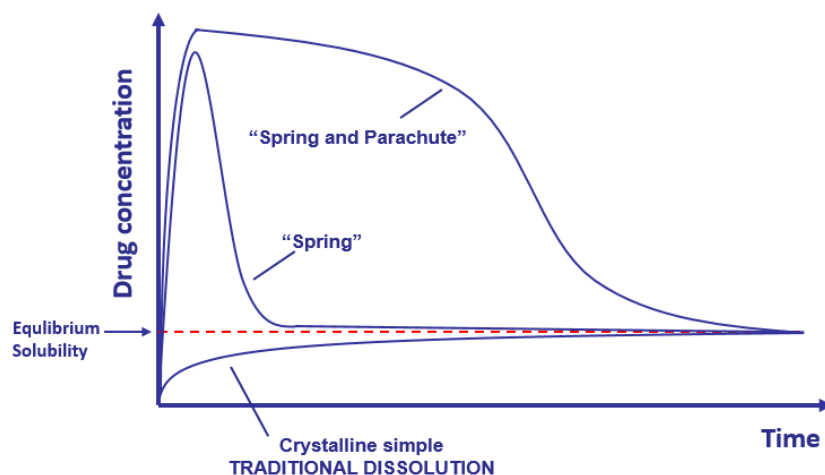


Figure 1.10: Spring and parachute approach as described by Guzmán et al., 2007. Diagram adapted from Brouwers et al., 2009.

1.3 Physiology of the human gastrointestinal tract and supersaturation *in vivo*

The anatomy and physiology of the human GIT play a crucial role in the interplay between dissolution, supersaturation and precipitation of oral dosage forms. In this sense, the regional differences along the GIT of healthy adults were reported to influence the extent on oral drug absorption (Vertzoni et al., 2019).

Following the intake of an oral dosage form, it quickly passes the esophagus and reaches the stomach within a few seconds (DeSesso and Jacobson, 2001). Under fasted conditions, the dosage form or its remains are emptied through the pylorus into the small intestine after disintegration or dissolution. Koziolok and co-workers reported a high interindividual variability in the gastric residence time (7 – 202 min, median: 30 min) and gastric pH (1.7 to 4.7) under fasted conditions, by means of the telemetric drug delivery device Intellicap® (Koziolok et al., 2015a). In the stomach, fasted state volumes between 13 and 72 mL (mean: 45 mL) were determined by magnetic resonance imaging (Schiller et al., 2005). The gastric residence times heavily varied from a few minutes to several hours depending on the dosage form, the co-administered volume (Granger et al., 1985; Locatelli et al., 2009) and the feeding state (Koziolok et al., 2014; Siegel et al., 1988). Steingoetter *et al.* determined the gastric half-emptying time of 300 mL water to be only 15 minutes (Steingoetter et al., 2006), something that can be mainly attributed to the proposed “stomach road” or “Magenstrasse” phenomenon (Pal et al., 2007). However, the gastric emptying of solid particles was a random and a highly variable process (Hunter et al., 1982; Jonsson et al., 1983).

Upon transfer into the proximal parts of the small intestine (duodenum), the Intellicap® capsule reported an increase in the pH-values (pH: 5.9 – 6.3) and it reached 7.4 – 7.8 in distal parts (ileum). Similar to gastric transit times, the small intestinal transit showed a high variability (67-532 min, median: 247 min) (Koziolok et al., 2015a). The increase in the intestinal pH was related to the lack of proton secretion (as occurring in the stomach) and the presence of bicarbonate-rich secretions which neutralize the pH (Sjögren et al., 2014).

Upon transfer into the large intestine, the colonic pH fluctuated between pH 5 and pH 8 (Koziolok et al., 2015a). The acidification of the colonic intraluminal pH is connected to the fermentation processes of the colonic microbiota (Fallingborg et al., 1989, 1990). The colon transit time is longer than the gastric and small intestinal residence times and can last up to 72 h (Rao et al., 2009).

The pH-gradient throughout the different segments of the GIT (Figure 1.11) is one of the main triggering forces influencing the dissolution, solubility and precipitation in the GI lumen for ionizable molecules, possessing pK_a values within the physiological pH-range. For instance, Brouwers and co-workers reported a strong impact of the pH-gradient on the intraluminal solubility and supersaturation of the extremely poorly soluble drug molecule itraconazole (Brouwers et al., 2017).

The large average surface area of 32 m² (Helander and Fändriks, 2014) of the small intestine is the main absorption site for drug molecules and nutritional components. It is caused by the anatomy of the small intestine with its circular folds, villi and microvilli, especially in the duodenum and the proximal half of the jejunum (DeSesso and Jacobson, 2001). As a result, the small intestinal transit time is a key parameter for bioavailability, since it defines the time in which the drug is accessible for absorption (Davis et al., 1986; Mudie et al., 2010).

1. GENERAL INTRODUCTION

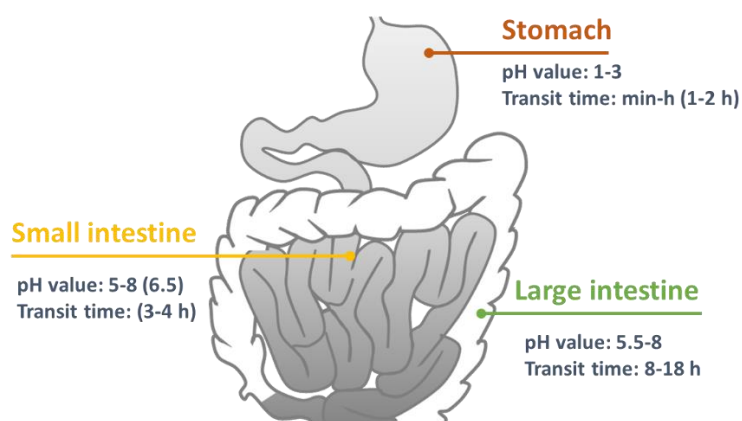


Figure 1.11: Schematic representation of the human GIT including pH-values and transit times of the relevant absorption sections. Revised from Hazzard's Geriatric Medicine and Gerontology (Halter et al., 2009).

Additionally, the medium composition plays a key role, since the present bile salts promote the solubilization of drug molecules in the intestinal milieu, as well as their absorption through the gastrointestinal barrier (Mackie and Rigby, 2015). Similarly, several other secretions, including the pancreatic juice and digestive enzymes (DeSesso and Jacobson, 2001), may impact the degree of drug molecule solubilization within lipidic species in the postprandial states. Therefore, it affects the fraction of drug accessible for absorption and leads to the so called "food effects" (Pentafragka et al., 2019).

The differentiation between the concepts of bioaccessibility and bioavailability is a key to understand the supersaturation potential in enhancing not only the dissolution and solubility of drug molecules, but also their oral absorption. The ability of a compound to go in solution (molecularly or apparently dissolved) and being accessible for absorption in the intestinal lumen is summarized into the bioaccessibility of a drug (Bean et al., 2016). In comparison, the U.S. Food and Drug Administration (FDA) defines the bioavailability as "the rate and extent to which the active drug ingredient or therapeutic moiety is absorbed from a drug product and becomes available at the site of action (or systemic circulation)" (Allam et al., 2011; Niazi, 2019). Both bioaccessibility and bioavailability might superimpose when the oral absorption is not the limiting step for the bioavailability of a drug. Nevertheless, the formation of drug/excipient species in solution which are regarded as bioaccessible but do not promote permeation, may lead to a lack of correlation between both concepts. A true supersaturation increases the molecularly dissolved fraction and thus, it increases oral absorption, while an increase in the apparent solubility by solubilization approaches may hinder the absorption of APIs (Beig et al., 2012; Dahan et al., 2010; Frank et al., 2012; Miller et al., 2012a).

In previous studies, following the aspiration of intraluminal gastric and intestinal samples from human subjects (Brouwers et al., 2017; Hens et al., 2016a, 2016b), the positive effect of supersaturation on oral absorption in humans was observed. Nevertheless, using catheters for intraluminal sampling was difficult in these studies and normally the oral absorption is investigated from blood or plasma samples as a response for the supersaturation taking place in the GIT.

1.3 Physiology of the human gastrointestinal tract and supersaturation *in vivo*

Despite the anatomical and physiological differences in the gastrointestinal tract between rats and humans (DeSesso and Jacobson, 2001), this animal model is commonly used to investigate the effect of supersaturation on oral absorption and bioavailability from enabling formulations or from supersaturated solutions (Childs et al., 2013; Gan et al., 2020; Higashino et al., 2014; Li et al., 2019; Miao et al., 2019; Miller et al., 2008a; Ruff et al., 2017; Strindberg et al., 2020). The main gap in the gastrointestinal tract physiology and anatomy of rats compared to humans is related to the lower surface area and length of the small intestine. Nevertheless, the small intestinal transit time in both species is 3 – 4 h. A major difference, which compromises the predictability of the rat model when extrapolated to humans, is the higher gastric pH in rats (3 – 5) (Kararli, 1995; McConnell et al., 2008) than in humans (1 – 2) (DeSesso and Jacobson, 2001). This fact is important for weak bases which benefit from the acidic gastric pH in terms of dissolution. Furthermore, the beagle dog model is similarly used in literature to investigate the effect of solubility enhancement on the oral bioavailability (Frank et al., 2014; Zhong et al., 2016).

1.4 *In vitro* supersaturation and dissolution models

The investigation of intraluminal supersaturation *in vivo* is often associated with practical challenges and therefore, several efforts were made to develop *in vitro* supersaturation and precipitation methods (Gao and Shi, 2012; Li et al., 1998; Wu and Khan, 2011). These *in vitro* methods target the evaluation of the supersaturation potential of drug molecules, the effectiveness of pharmaceutical excipients as precipitation inhibitors and the performance of supersaturating drug delivery systems (SDDS) (Bevernage et al., 2013).

Independently of the method applied, the *in vitro* assessment of supersaturation involves the induction of the supersaturated state and the quantification of the drug concentration in solution as a function of time. The discrepancy between the recorded drug concentration evolution over time and the equilibrium solubility (C_{eq}) of the drug in the test medium is known as the supersaturation ratio (SSR) (Equation 9, section 1.2) or degree of supersaturation (DS). Furthermore, the determination of the C_{eq} under identical experimental conditions enables the differentiation between real supersaturation and thermodynamic solubilization or solubility enhancement.

Together with the quantitative approach, which determines the concentration of supersaturated solutions over time, the detection of precipitation events is one of the main characteristics of *in vitro* supersaturation assays. In the past, this was achieved by various approaches, including visual inspection and light microscopy (Raghavan et al., 2001), spectrophotometric UV/VIS absorbance time-measurements (Chandran et al., 2011; Ozaki et al., 2012) or nephelometric turbidity determinations (Warren et al., 2010). Analysis of the physical state of the precipitating form and its ability to redissolve under favorable experimental conditions can be investigated by X-ray diffraction or polarized light microscopy (PLM) after precipitation. It enables the differentiation between amorphous and crystalline precipitates, as well as the identification of polymorphic transitions during precipitation (Linàs and Goodman, 2008; Singhal and Curatolo, 2004; Usui et al., 1997).

1. GENERAL INTRODUCTION

A broad classification of the supersaturation evaluation into non-formulated and formulated drugs can be made and is discussed in the next sections.

1.4.1 Supersaturation evaluation of non-formulated drugs

For non-formulated drugs, the supersaturation must be induced. This can be achieved by a variety of strategies including solvent evaporation or freezing, addition of ions, dissolution of unstable high energy forms or temperature changes (Rodríguez-hornedo and Murphy, 1999). Even though these techniques are well known in crystallization chemistry, for practical reasons the pH-shift and solvent shift methods are commonly used in pharmaceutical supersaturation tests (Plum et al., 2020)(Figure 1.12):

- Solvent shift method. This approach is broadly applicable for poorly water-soluble drugs with a higher solubility in any water miscible co-solvent. Due to its simplicity, convenience and low drug consumption, it is frequently used (Bevernage et al., 2013; Morrison et al., 2014; Palmelund et al., 2016; Skolnik et al., 2018). The transfer of an aliquot from a highly concentrated stock solution to the test medium generates a supersaturated solution, which will subsequently precipitate until C_{eq} is reached. Palmelund and co-workers presented a standardized supersaturation and precipitation method (SSPM) based on the solvent shift approach and confirmed the existence of a strong relationship between the initial drug concentration and the onset of precipitation (Palmelund et al., 2016). A variety of solvents were applied to induce supersaturation by the solvent shift method. Amongst others, DMSO, DMA polyethylene glycol (PEG) and propylene glycol were used (Bevernage et al., 2011; Carlert et al., 2010; Vandecruys et al., 2007; Warren et al., 2010; Yamashita et al., 2011). These studies investigated the supersaturation propensity and precipitation kinetics of drug molecules in the presence and absence of precipitation inhibitors.
- pH-shift method. This approach is based on the pH-dependent solubility of ionizable molecules. Based on the ionization equilibrium described by the Henderson-Hasselbach equation (Equations 3,4), a pre-dissolution of the drug in an aqueous solvent with a pH, in which the molecules are ionized, may induce supersaturation after a pH shift occurs (Psachoulias et al., 2011). The generated decrease in the aqueous drug solubility creates a metastable state in dependence of the compound's pK_a , its inherent supersaturation behavior, as well as the ability of the pharmaceutical excipients used to hinder or delay precipitation events. From a physiological point of view and compared to the solvent shift method, the pH-shift is more biorelevant, since the transfer of weakly basic compounds from the fasted state stomach into the small intestine induces a decrease in the ionization and supersaturation. One-compartment approaches, in which an acidic solution of a basic compound is buffered to a pH above the drug's pK_a are commonly used in literature (Carlert et al., 2010; Mellaerts et al., 2008a; Overhoff et al., 2007; Yamashita et al., 2010; Zecevic et al., 2014). Transfer models, based on the continuous infusion of a drug from an acidic compartment into a second basic compartment, mimic the gastric emptying of drug molecules in a more precise manner (Kostewicz et al., 2004; Kourentas et al., 2016a; Vatieer et al., 1994).

More recently, Plum and co-workers reported that the supersaturation and precipitation profiles induced either via solvent shift or pH shift are generally comparable for weak bases (Plum et al., 2020). However, in some cases, e.g. for extremely poor soluble drug molecules, the drug supersaturation strongly depends on the induction method. As an initial screening tool for

supersaturation and precipitation, the solvent shift method is more convenient, since it is not exclusively limited to weakly basic compounds.

- Potentiometric method. An alternative approach to investigate supersaturation of ionizable drugs is the chasing equilibrium solubility or CheqSol method introduced by Sirius Analytical Instruments (Box et al., 2009, 2006; Stuart and Box, 2005a). The method was originally developed to determine the intrinsic solubility of drug molecules, but it additionally enables the investigation of their supersaturation ability in the absence or presence of precipitation inhibitors. Briefly, the CheqSol method takes advantage of the pH-dependent solubility of ionizable drug molecules. Initially, the pH is adjusted to completely dissolve the drug in its ionized form. The generated solution is subsequently titrated back to force precipitation of the drug, while the pH and UV-absorbance are carefully monitored over test time. After precipitation, a fluctuation of the solution between the supersaturated and subsaturated state enables the identification of compounds, which possess an inherent supersaturation ability (chasers) and compounds which lack of it (non-chasers). This is based on potential differences between the kinetic and intrinsic solubility. In the case of chasers, the generated concentration-time profile of the neutral species characterizes the length and degree of supersaturation. Furthermore, the solid state properties of the precipitates can be correlated to the supersaturation behavior type. In general, short-term supersaturation was connected to crystalline precipitation and chaser behavior. Amorphous precipitation was instead associated with prolonged supersaturation and non-chaser drug molecules (Hsieh et al., 2012). Due to its importance for this work, the potentiometric test is described in more detail in the model (section 2.3.2.1) and experimental (section 3.2.1.2) section.
- High throughput supersaturation assay. To support early-stage drug product development, the use of high throughput screening (HTS) methods is mandatory. Most of these methods are based on the solvent shift method by using pharmaceutical excipients in a miniaturized scale as described by Vandecruys *et al.* (Vandecruys et al., 2007) or in a micro scale 96-well plate (Yamashita et al., 2011). The online detection of precipitation events by means of turbidity measurements was applied in HTS supersaturation assays (Warren et al., 2010) and enables a rational formulation development in early development stages.

In general, the supersaturation evaluation for non-formulated drugs is performed in standard buffers with specified pH values. It simulates the effect of pH, gastrointestinal transit and the resulting interplay between ionization, supersaturation and solubility. Nevertheless, the use of biorelevant dissolution media offers a closer counterfeit of the human GI physiology (Dressman et al., 1998). These media were developed and optimized for simulating the gastric and small intestinal conditions and capture the *in vivo* pH, osmolality, surface tension, buffer capacity, surfactants and enzyme activity (Klein, 2010). Furthermore, various media were developed to mimic fasted and fed conditions. However, the rapid and dynamic media change in the GI tract is difficult to capture and may not always be properly accounted (Lennernäs et al., 2014). The most frequently used media are fasted state simulated gastric fluid (FaSSGF), fasted state simulated intestinal fluid (FaSSIF) and fed state simulated intestinal fluid (FeSSIF). The use of biorelevant media was reported to be predictive for the *in vivo* behavior of poorly soluble drugs (Dressman and Reppas, 2000; Jantratid et al., 2008; Klein, 2010; Vertzoni et al., 2005).

1. GENERAL INTRODUCTION

Similarly, the use of human gastric fluids and human intestinal fluids (HIF) in fasted or fed state conditions (FaHIF and FeHIF, respectively) was applied (Augustijns et al., 2014; Bergström et al., 2014b; Bevernage et al., 2012a; Fuchs and Dressman, 2014). Even though the composition of these fluids is more physiologically relevant as the SIF, the inconvenience associated with their sampling through catheters from human subjects, considerably limit their applicability and therefore their use is not standardized.

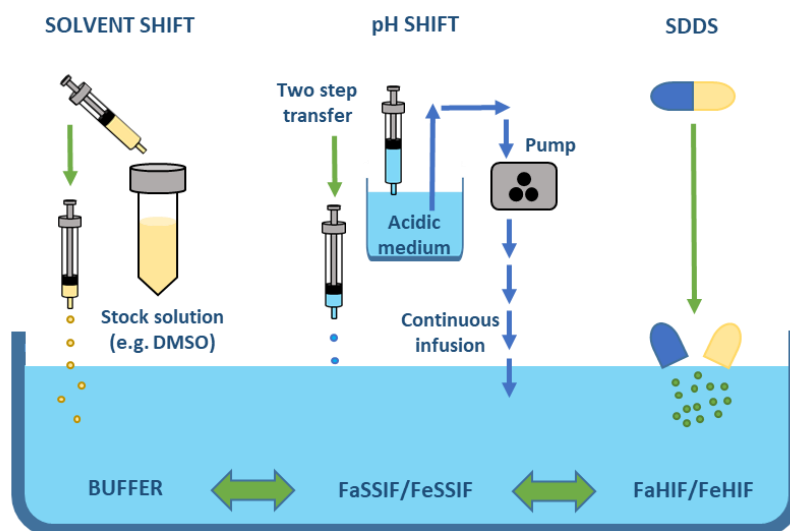


Figure 1.12: Commonly used media and approaches to generate supersaturation in in vitro assays. Adapted from Bevernage et al., 2013.

1.4.2 Supersaturation evaluation of formulated drugs

In literature, several dissolution methods for the evaluation of supersaturating drug delivery systems (SDDS) were described. In general, traditional one-compartment or monophasic setups, based on the United States Pharmacopeia (USP) I or II apparatus according to USP General Chapters <711> and <724>, can be used (USP, 2011). In quality control of dosage forms, this compendial dissolution testing is well known and the first choice (Kostewicz et al., 2014). Nevertheless, the applicability of compendial dissolution methods to test SDDS is very often limited. These tests are usually performed under sink conditions by using large dissolution volumes or high surfactant concentrations. Thus, they are only suitable to investigate the release kinetics. However, biopharmaceutical tools to evaluate formulations containing poorly soluble drugs should be performed under non-sink conditions. This is related to their poor solubility which limits their oral absorption (Bevernage et al., 2013). In this sense, the non-sink conditions enable a proper investigation of the supersaturation and precipitation. In several studies, an improved predictability of the formulation's performance was reported under non-sink conditions, compared to the compendial sink conditions (Augustijns and Brewster, 2012; Dong et al., 2007; Sun et al., 2016; Van Speybroeck et al., 2010a). Various dissolution models to simulate the conditions of the gastrointestinal lumen and to evaluate the performance of SDDS are known (Kostewicz et al., 2014). These models heavily differ in their complexity, and in their ability to capture not only the interplay between dissolution, supersaturation and precipitation, but also the permeation through membranes.

When evaluating ionizable drug molecules, a common characteristic of all these biopharmaceutical models is the simulation of gastrointestinal pH. In general, many SDDS formulations (especially those including weak bases) rely on the gastrointestinal pH-gradient to generate supersaturation and therefore, it is advisable to include an acidic phase to simulate the release under gastric conditions. Subsequently, buffering the system to intestinal conditions induces a precipitation of the drug and enables the evaluation of the interplay between supersaturation and precipitation (Bevernage et al., 2012a):

- Monophasic dissolution model (Figure 1.13A). In general, miniaturized versions of the compendial USP I and USP II apparatus are used (Kostewicz et al., 2014). One-compartment (Carlert et al., 2010; DiNunzio et al., 2008, 2010; Mellaerts et al., 2008a; Miller et al., 2007, 2008a, 2008b; Zecevic et al., 2014) and two-compartment approaches (Carlert et al., 2010; Mellaerts et al., 2008a; Van Speybroeck et al., 2010b) to investigate the supersaturation and precipitation interplay under pH-shift models are known. A general drawback of monophasic dissolution models is the absence of an absorptive sink compartment, which removes the dissolved drug from the aqueous phase and simulate the absorption into the systemic circulation. As a result, the precipitation in the aqueous phase might be overestimated, while simultaneously the supersaturation is underestimated.
- Biphasic dissolution model (Figure 1.13B). The inclusion of an upper organic phase as a sink compartment mimics the oral absorption by enabling the partition of the neutral drug molecules into the lipophilic phase (Vangani et al., 2009). This is especially important for weak bases which precipitate in the small intestine and for which the oral absorption is an alternative pathway to avoid precipitation (Bevernage et al., 2013). In this sense, the biphasic dissolution approach was postulated to be predictive for the drug fraction absorbed by passive diffusion, especially for BCS II compounds (Pestieau and Evrard, 2017; Shrivastava et al., 2019) Furthermore, it showed potential to establish IVIVC (Al Durdujji et al., 2016; Frank et al., 2014; Pestieau et al., 2017; Shi et al., 2010, 2016) to assess the supersaturation/precipitation tendency of poorly soluble drugs (Denninger et al., 2020; Heigoldt et al., 2010; Locher et al., 2016, 2018; Pestieau et al., 2015; Shi et al., 2016) and it possesses a discriminatory power (Al Durdujji et al., 2016; Amaral Silva et al., 2020; Phillips et al., 2012; Vangani et al., 2009). Consequently, the determination of the partition rate into the organic phase of a biphasic system is crucial to investigate the influence of supersaturating excipients on oral absorption by passive diffusion.
- Dissolution/permeation model (Figure 1.13C). Since the oral absorption is determined by the API dissolution and permeation in the gastrointestinal tract (Fong et al., 2017b), several *in vitro* approaches characterize these two processes in a single model. In general, these models are composed of two compartments separated by a semipermeable membrane. The models differ in their complexity, but also in the membrane type used: biological membranes (e.g. Caco-2) or artificial membranes (e.g. PAMPA or PVPA) (Buckley et al., 2012). Furthermore, artificial bio-mimetic membranes were developed, like the Permeapad® membrane (di Cagno et al., 2015; Fong et al., 2017b) which seems to be a powerful tool to investigate passive diffusion and is implementable in high-throughput permeation assays. The simplest models are composed of a donor and an acceptor compartment separated by a membrane, e.g. the model developed by Ginski and co-workers (Ginski et al., 1999). Even these simple models achieved a good correlation between the absorbed drug fraction *in human* and

1. GENERAL INTRODUCTION

the permeated amount of poorly soluble drugs in the model setup (Kataoka et al., 2003). Other complex models consider the pH change in the GIT by including a drug-dissolving vessel and a pH adjustment vessel (Kobayashi et al., 2001; Li et al., 2011; Sugawara et al., 2005). Recently, the artificial membrane insert (AMI) system (Berben et al., 2017, 2018) based on a simple regenerated cellulose membrane mounted between two plastic rings, was developed (Abrahamsson et al., 2020).

- Transfer and multi-compartment model (Figure 1.13D). The predictive power of dynamic dissolution models consisting of several compartments to simulate the various GIT segments, was already discussed a decade ago (McAllister, 2010). The general interest in these models considerably increased in the last years (Butler et al., 2019). The multi-compartmental models are mainly composed of a gastric and a duodenum compartment separated by a pump which regulates the transfer of dissolution medium from the first to the second compartment. Kostewicz *et al.* developed a simplified version, known as the transfer model (Kostewicz et al., 2004) which simulates the gastric emptying kinetics and therefore minimizes the precipitation under intestinal conditions. This mimics precisely the *in vivo* conditions where the gastric physiology decreases the precipitation of weak bases in the small intestine (Takeuchi et al., 2014). The artificial stomach duodenum model is another commonly used model composed of a gastric and an intestinal compartment (Kostewicz et al., 2014). Carino and co-workers applied the model to simulate the drug absorption of several carbamazepine crystalline forms in dogs under fasted and fed state conditions. The results correlated well with the *in vivo* rank order and bioavailability (Carino et al., 2006). The gastrointestinal simulator (GIS) was developed based on the artificial stomach duodenum model and includes a third compartment for the jejunum (Takeuchi et al., 2014). The GIS demonstrated to be a valuable tool to investigate the interplay between supersaturation and precipitation, which in turn affect the oral absorption (Tsume et al., 2015). Other more complex models is for example the Biorelevant Gastrointestinal Transfer (BioGIT). It is an open *in vitro* set-up consisting of a gastric, a duodenal and a reservoir compartment. It estimates the apparent drug concentrations of a dosage form administered with a glass of water to fasted adults (Kourentas et al., 2016a). Without any doubt, the most complex multi-compartmental models are the TNO Intestinal Models (TIM). The model TIM-1 simulates the stomach, duodenum, jejunum and ileum, whereas the simplified version tiny-TIM only includes a gastric and an intestinal compartment (Minekus, 2015). The TIM models are a highly biorelevant *in vitro* dissolution model with the potential to target mechanistic questions of disintegration, dissolution, supersaturation, precipitation and absorption *in vivo*. Furthermore, it represents a digestion model and it is widely used for the prediction of food effects (Butler et al., 2019; Verwei et al., 2016). The TIM models mimic exactly the pH-profile throughout the GIT transit, the composition of the gastric and intestinal media (including porcine bile, pancreatin and digestive enzymes), the peristaltic waves and the gastric emptying pattern depending on the feeding condition. The potential of the BioGIT and TIM models to capture the supersaturation and precipitation interplay, as well as the intraluminal concentrations observed *in vivo* for various formulated drug product concepts were reported in several studies (Brouwers et al., 2017; Hens et al., 2016b; Kourentas et al., 2016b, 2016c, 2016d; Van Den Abeele et al., 2016).

1.4 *In vitro* supersaturation and dissolution models

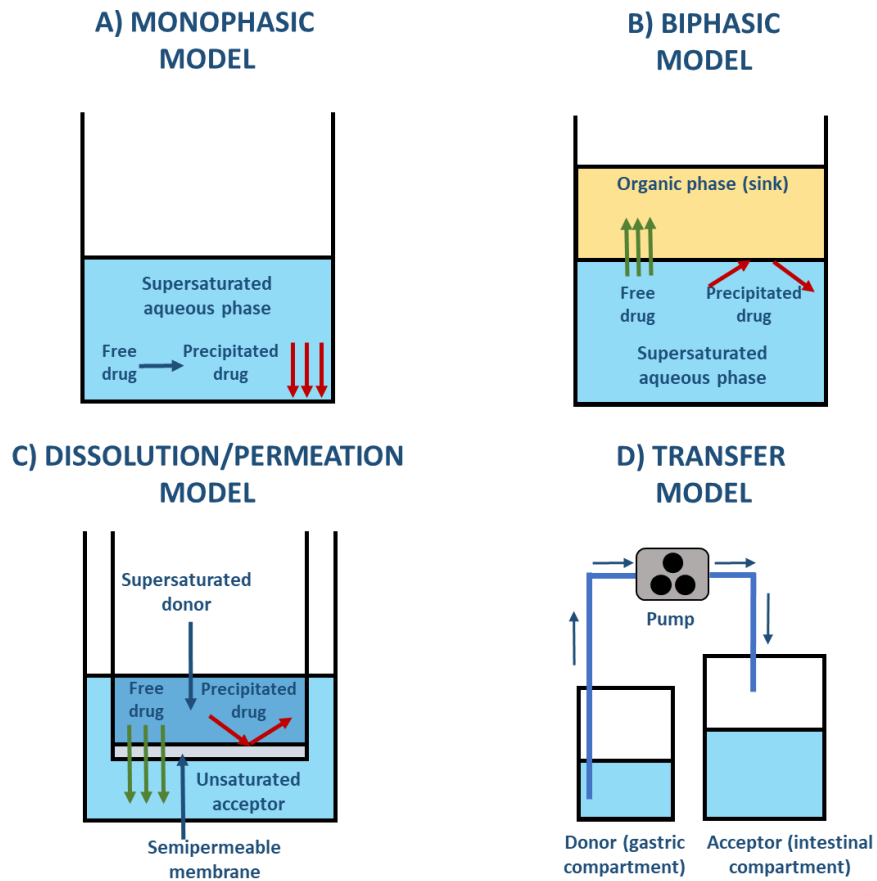


Figure 1.13: Different models applied for the evaluation of supersaturation of formulated drugs. A) Monophasic dissolution B) Biphasic dissolution C) Dissolution/permeation models D) Transfer and multi-compartment models. Adapted from Bevernage et al., 2013.

2 Objective

Despite the large number of publications related to the topic, the fundamental mechanistic understanding of the innate supersaturation behavior of poorly soluble drug molecules (e.g. BCS II), as well as the mechanism of pharmaceutical excipients to enhance and stabilize supersaturated aqueous solutions of poorly soluble compounds, is still only partially understood. The present work targets a deeper understanding of the potential of different polymeric stabilization mechanisms to trigger changes in the oral bioavailability of BCS II molecules, depending on their innate supersaturation behavior. This goal was approached by addressing the supersaturation and solubilization from three perspectives: physicochemical properties, biorelevant *in vitro* dissolution and *in vivo* absorption in a rat model.

A combined evaluation of the three different approaches is expected to facilitate the understanding of the potential and limitations of different stabilization mechanisms to drive changes in the oral exposure of BCS II molecules. Various objectives were defined for each perspective:

Physicochemical properties

- Physicochemical characterization of the selected drug molecules and identification of apparent changes in the ionization equilibria, solubility and lipophilicity in polymeric solutions (thermodynamic perspective). Establishment of a link between the observed changes in equilibrium and particular molecular descriptors, as well as determination of the presence or absence of a polymer concentration-dependent effect.
- Evaluation of the response of drug molecules to the different stabilization mechanisms depending on their innate supersaturation behavior and differentiation between true supersaturation and solubilization.

In vitro (biorelevant)

- Gain a deeper insight in the interplay between drug supersaturation and precipitation from a kinetic perspective under biorelevant conditions.
- Correlate the innate drug supersaturation behavior and the physical state of the precipitating drug form with the kinetic stabilization potential of the polymers.
- Investigation of the polymer stabilization mechanisms potential to facilitate or hinder the partition into an absorptive compartment depending on the physical state of the precipitating drug form.

In vivo (rat)

- Validation or rejection of the hypotheses proposed in both physicochemical and biorelevant *in vitro* dissolution approaches using an *in vivo* rat model.
- Investigation of the response of drug molecules showing different innate supersaturating behaviors to the stabilization in the GI tract and the potential of the stabilization mechanisms to govern changes in the oral absorption and bioavailability.
- Establishment of an *in vitro in vivo* correlation between both approaches to enable a better understanding of the interaction between pharmaceutical excipients and the drug molecules, from a physicochemical and biorelevant perspective.

3 Model

3.1 Drug substance selection

According to the objective of this thesis (see section 2), poorly soluble drugs are in focus to study their supersaturation potential and the impact on enhancing the oral bioavailability. According to the US FDA BCS guidance (FDA/CDER, 2017), a drug substance is considered poorly soluble when the highest available dose is not soluble in 250 mL aqueous media over the entire physiological pH range (pH 1.0 – 6.8). Consequently, molecules sharing this common characteristic were targeted in this work. The drug substance selection was based on several criteria:

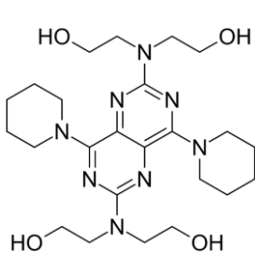
- Presence of at least one weak basic or weak acidic group in the chemical structure of the molecule. This leads to a pH-dependent solubility profile and enables the characterization of its physicochemical properties by means of the methods described in this experimental section (see section 4.2.1).
- Classification as a BCS II drug. This aspect was considered prospectively to the performance of *in vivo* pharmacokinetic experiments to study the real impact of supersaturation and solubilization on the oral bioavailability enhancement. BCS IV molecules would additionally impose a further challenge related to their poor permeability, a fact which is not the target of this work.
- Obtaining a broad spectrum of chemical structures which can represent the chemical space of drug molecules to identify different stabilization mechanisms.

After a first screening, where the suitability of several molecules for the potentiometric physicochemical property determination was evaluated, six drug molecule candidates were selected.

As the Table **3.1 – 3.6** reflect, the selected molecules represent a broad spectrum of chemical structures and physicochemical properties. All of them are commercialized as marketed products and a poor oral bioavailability is known. Consequently, all of them are susceptible to undergo precipitation phenomena in the gastrointestinal tract, a fact that limits the drug fraction accessible for absorption.

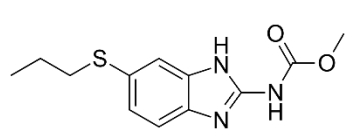
3. MODEL

Table 3.1: Chemical structure, substance information and relevant physicochemical properties of DPD.

Dipyridamole (DPD) 	Drug substance information	IUPAC Name	2-[[2-[bis(2-hydroxyethyl)amino]-4,8-di(piperidin-1-yl)pyrimido[5,4-d]pyrimidin-6-yl]-(2-hydroxyethyl)amino]ethanol	
		Pharmacological information	Manufacturer/Supplier	Swapnroop Drugs and Pharmaceuticals, Aurangabad, India
			Batch Number	DPM/022/09/15
	Pharmacological group		Phosphodiesterase inhibitor ⁽¹⁾	
	Physicochemical information	Therapeutical application	Anticoagulant and prevention of angina ⁽¹⁾	
		Dose strength(s) [mg]	25, 50, 75 and 200 (extended release) ⁽¹⁾	
		MW [g/mol]	504.63 ⁽¹⁾	
		Acid / base	Weak base ⁽²⁾	
		$pK_a(s)$	6.59 ⁽²⁾	
		LogS	-2.7 ⁽³⁾	
LogP		1.52 ⁽³⁾		
BCS Class		II ^(4,5)		
Hydrogen Acceptor Count		12 ⁽²⁾		
Hydrogen Donor Count	4 ⁽²⁾			
PSA [Å ²]	145.44 ⁽²⁾			
Oral BA	11 – 44 % ⁽⁶⁾			

⁽¹⁾ (Wishart et al., 2018); ⁽²⁾ ChemAxon database; ⁽³⁾ ALOGPS database; ⁽⁴⁾ (Butler and Dressman, 2010) ; ⁽⁵⁾ (Tsume et al., 2017) ⁽⁶⁾(Terhaag et al., 1986)

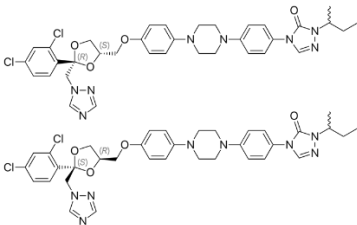
Table 3.2: Chemical structure, substance information and relevant physicochemical properties of ABZ.

Albendazole (ABZ) 	Drug substance information	IUPAC Name	Methyl-[6-(propylsulfanyl)-1H-benzimidazol-2-yl]carbamate	
		Pharmacological information	Manufacturer/Supplier	Fluka Analytical
			Batch Number	MKBR9649V
	Pharmacological group		Tubulin polymerization inhibitor ⁽¹⁾	
	Physicochemical information	Therapeutical application	Anthelmintic ⁽¹⁾	
		Dose strength(s) [mg]	200, 400 ⁽¹⁾	
		MW [g/mol]	265.33 ⁽¹⁾	
		Acid / base	Weak base, weak acid ⁽²⁾	
		$pK_a(s)$	4.27 (B), 9.51 (A) ⁽²⁾	
		LogS	-4.1 ⁽³⁾	
LogP		3.22 ⁽³⁾		
BCS Class		II ⁽⁴⁾		
Hydrogen Acceptor Count		3 ⁽²⁾		
Hydrogen Donor Count	2 ⁽²⁾			
PSA [Å ²]	67.01 ⁽²⁾			
Oral BA	1 – 5 % in humans ⁽⁵⁾			

⁽¹⁾ (Wishart et al., 2018) ⁽²⁾ ChemAxon database; ⁽³⁾ ALOGPS database; ⁽⁴⁾(Lindenberg et al., 2004); ⁽⁵⁾ (Dayan, 2003)

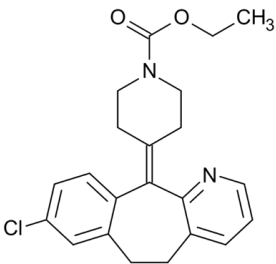
3.1 Drug substance selection

Table 3.3: Chemical structure, substance information and relevant physicochemical properties of ITZ.

Itraconazole (ITZ) 	Drug substance information	IUPAC Name	1-(butan-2-yl)-4-[4-[4-(4-[(2R,4S)-2-(2,4-dichlorophenyl)-2-[(1H-1,2,4-triazol-1-yl)methyl]-1,3-dioxolan-4-yl]methoxy)phenyl]piperazin-1-yl]phenyl]-4,5-dihydro-1H-1,2,4-triazol-5-on	
		Pharmacological information	Manufacturer/Supplier	SRIS Pharmaceuticals, Hyderabad, India
			Batch Number	ITC/1509133
	Pharmacological group		14 α -demethylase inhibitor ⁽¹⁾	
	Physicochemical information	Therapeutical application	Antifungal agent ⁽¹⁾	
		Dose strength(s) [mg]	100 and 200 ⁽¹⁾	
		MW [g/mol]	705.63 ⁽¹⁾	
		Acid / base	Weak base ⁽²⁾	
		pK _a (s)	3.91 ⁽²⁾	
		LogS	-4.9 ⁽³⁾	
LogP		5.48 ⁽³⁾		
BCS Class		II ⁽⁴⁾		
Hydrogen Acceptor Count		9 ⁽²⁾		
Hydrogen Donor Count	0 ⁽²⁾			
PSA [Å ²]	100.79 ⁽²⁾			
Oral BA	55% (oral solution) ⁽⁵⁾			

⁽¹⁾ (Wishart et al., 2018); ⁽²⁾ ChemAxon database; ⁽³⁾ ALOGPS database; ⁽⁴⁾ (Wu and Benet, 2005) ⁽⁵⁾ (Buchanan et al., 2007)

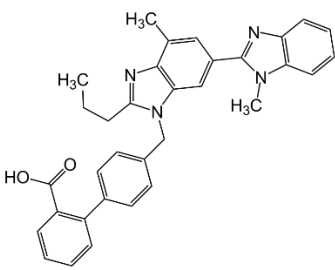
Table 3.4: Chemical structure, substance information and relevant physicochemical properties of LTD.

Loratadine (LTD) 	Drug substance information	IUPAC Name	ethyl 4-{13-chloro-4-azatricyclo[9.4.0.0 ^{3,8}]pentadeca-1(11),3(8),4,6,12,14-hexaen-2-ylidene}piperidine-1-carboxylate	
		Pharmacological information	Manufacturer/Supplier	SRIS Pharmaceuticals, Hyderabad, India
			Batch Number	LRHB5183
	Pharmacological group		Second generation antihistamine ⁽¹⁾	
	Physicochemical information	Therapeutical application	Allergic rhinitis ⁽¹⁾	
		Dose strength(s) [mg]	10 and 5 (extended release formulation with pseudoephedrine sulphate) ⁽¹⁾	
		MW [g/mol]	382.88 ⁽¹⁾	
		Acid / base	Weak base ⁽²⁾	
		pK _a (s)	4.33 ⁽²⁾	
		LogS	-4.5 ⁽³⁾	
LogP		4.8 ⁽³⁾		
BCS Class		I ⁽⁴⁾ / II ^(5,6)		
Hydrogen Acceptor Count		2 ⁽²⁾		
Hydrogen Donor Count	0 ⁽²⁾			
PSA [Å ²]	42.43 ⁽²⁾			
Oral BA	40% ⁽⁷⁾			

⁽¹⁾ (Wishart et al., 2018); ⁽²⁾ ChemAxon database; ⁽³⁾ ALOGPS database; ⁽⁴⁾ (Ramirez et al., 2010); ⁽⁵⁾ (Desai et al., 2019); ⁽⁶⁾ (Khan et al., 2004) ⁽⁷⁾ (Madhav and Kishan, 2018)

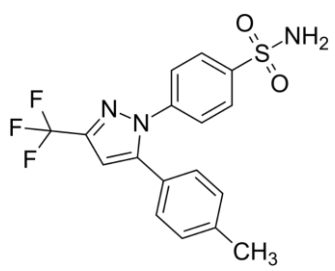
3. MODEL

Table 3.5: Chemical structure, substance information and relevant physicochemical properties of TLM.

Telmisartan (TLM) 	Drug substance information	IUPAC Name	2-([4-methyl-6-(1-methyl-1H-1,3-benzodiazol-2-yl)-2-propyl-1H-1,3-benzodiazol-1-yl]methyl)phenyl)benzoic acid
		Manufacturer/Supplier	SRIS Pharmaceuticals, Hyderabad, India
		Batch Number	PDTEL1507002
	Pharmacological information	Pharmacological group	Angiotensin II receptor antagonist ⁽¹⁾
		Therapeutic application	Treatment of hypertension ⁽¹⁾
		Dose strength(s) [mg]	20, 40 and 80 (several combined formulations with hydrochlorothiazide) ⁽¹⁾
	Physicochemical information	MW [g/mol]	514.62 ⁽¹⁾
		Acid / base	Zwitterion ⁽²⁾
		pK _a (s)	3.06 (B), 4.39 (A), 6.04 (B) ⁽²⁾
		LogS	-5.2 ⁽³⁾
		LogP	6.66 ⁽³⁾
		BCS Class	II ⁽⁴⁾
		Hydrogen Acceptor Count	4 ⁽²⁾
Hydrogen Donor Count		1 ⁽²⁾	
PSA [Å ²]		72.94 ⁽²⁾	
Oral BA	43 % ⁽⁵⁾		

⁽¹⁾ (Wishart et al., 2018); ⁽²⁾ ChemAxon database; ⁽³⁾ ALOGPS database; ⁽⁴⁾ (Park et al., 2013); ⁽⁵⁾ (Wienen et al., 2000)

Table 3.6: Chemical structure, substance information and relevant physicochemical properties of Celecoxib.

Celecoxib (CLX) 	Drug substance information	IUPAC Name	4-[5-(4-methylphenyl)-3-(trifluoromethyl)-1H-pyrazol-1-yl]benzene-1-sulfonamide
		Manufacturer/Supplier	Swapnroop Drugs and Pharmaceuticals, Aurangabad, India
		Batch Number	N/A
	Pharmacological information	Pharmacological group	Selective COX-II inhibitor ⁽¹⁾
		Therapeutic application	Treatment of inflammatory diseases ⁽¹⁾
		Dose strength(s) [mg]	100 and 200 ⁽¹⁾
	Physicochemical information	MW [g/mol]	381.37 ⁽¹⁾
		Acid / base	Weak acid ⁽²⁾
		pK _a (s)	10.7 ⁽²⁾
		LogS	-4.9 ⁽³⁾
		LogP	3.99 ⁽³⁾
		BCS Class	II ⁽⁴⁾
		Hydrogen Acceptor Count	3 ⁽²⁾
Hydrogen Donor Count		1 ⁽²⁾	
PSA [Å ²]		77.98 ⁽²⁾	
Oral BA	40 % (capsule) ⁽⁵⁾		

⁽¹⁾ (Wishart et al., 2018); ⁽²⁾ ChemAxon database; ⁽³⁾ ALOGPS database; ⁽⁴⁾ (Kleberg et al., 2010); ⁽⁵⁾ (Shakeel et al., 2008)

3.2 Pharmaceutical excipients selection

The benefits associated to ASDs in terms of dissolution and precipitation have been extensively reported (Alonzo et al., 2011; Baghel et al., 2016; Van den Mooter, 2012). Nevertheless, the pure effect polymeric excipients as solubility / dissolution rate / supersaturation enhancers and precipitation inhibitor more rarely addressed.

The three pharmaceutical excipients selected in this work were water-soluble polymers. The rationale for their selection was their ability to stabilize and interact with the selected API molecules through a variety of mechanisms and chemical structures. The three selected polymers were:

- Vinylpyrrolidone-vinyl acetate copolymer (Kollidon VA64, KVA64)
- Methylcellulose derivative (Methocel A4C, MA4C)
- Polyvinyl caprolactam-polyvinyl acetate-polyethylene glycol graft copolymer (Soluplus, SOL)

3.2.1 Vinylpyrrolidone-vinyl acetate copolymer (Kollidon VA64, KVA64)

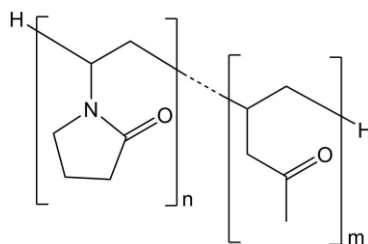


Figure 3.1: Chemical structure of the KVA64 monomers

Kollidon VA64 (copovidone, KVA64) (Figure 3.1) is a supersaturating and solubilizing agent in which vinylpyrrolidone and vinylacetate are randomly copolymerized in a 6:4 ratio (Reintjes, 2011) and it is manufactured by BASF SE (Ludwigshafen, Germany) through spray drying. It is an almost white free-flowing powder with a characteristic odor. The particle size distribution of the standard grade is within the range 50-250 μm with a medium particle size of around 100 μm . KVA64 is highly soluble in almost any hydrophilic solvent like water and several alcohols such as methanol, ethanol and isopropanol, but also in other organic solvents such as methylene chloride and chloroform. KVA64 has a MW range of 45,000 – 70,000 g/mol and K-value of 25.5 – 30.8. The K-value value is a dimensionless number closely related to the inherent viscosity (Schenck et al., 1979).

KVA64 is widely used as a binder in direct compression and wet granulation techniques. Furthermore, it can be used as a film-coating agent together with other polymers. Its ability to enhance the solubility of many APIs is related to the formation of water-soluble complexes between the polymer and drug molecules. The formation of water-soluble complexes might be at least partially related to the high extent of hydrogen acceptors in the KVA64 structure. It facilitates the formation of H-bond interactions with API molecules rich in H-donors (Xu and Dai,

3. MODEL

2013b). This characteristic might enhance the dissolution rate and solubility of poorly soluble drugs, as well as hinder or delay drug precipitation. Some challenging drug molecules were successfully formulated as an ASD with KVA64, including ITZ, which showed a 10-fold increase in its dissolution rate in 0.1 M HCl compared to the crystalline powder (Reintjes, 2011). Additionally, some formulations were successfully commercialized, such as Kaletra[®], a KVA64-based ASD including the API combination ritonavir and lopinavir for the treatment of HIV infections (Klein et al., 2007; Olmo et al., 2008).

3.2.2 Methycellulose derivative Methocel A4C (MA4C)

Methocel A4C (MA4C) (Figure 3.2) is a cellulose ether derivative manufactured by DuPont de Nemours (Michigan, USA) and supplied by Colorcon Ltd (Kent, UK). Several grades of Methocel are available for food and pharmaceutical applications. The polymer grades differ in their degree of methoxyl and hydroxypropoxyl substitution, as well as in their molecular weight and chain length, factors that directly affect their viscosity and hydration properties.

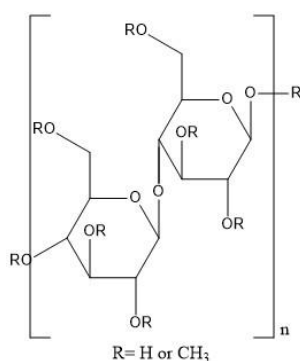


Figure 3.2: Chemical structure of the MA4C monomers

Methocel cellulose ether products dissolve in cold water and in certain organic solvents by swelling and subsequent hydration. The chemical structure enables the formation of a gel colloidal solution, a property from which food and pharmaceutical industries take advantage.

Methocel A4C is commercialized as an essentially odorless and tasteless white powder. It is a water-soluble, high purity, non-ionic cellulose ether having a 27 – 31.5 % methoxyl substitution. Unlike other Methocel grades, it shows a low viscosity in the range of 320 – 480 mPa·s (2% in water at 20°C)(Dow Chemical, 2013). It is used as a thickener, binder and film former. Despite its solubility in cold water, it must be dispersed first to prevent lumping, which results from incomplete wetting of the individual powder particles.

The viscosity of an aqueous Methocel solution is proportional to the molecular weight or chain length of the product. In the specific case of MA4C, the viscosity is 400 mPa·s (2% solution at 20°C in water). The molecular weight of the product has minor impact on the incipient gelation temperature (specific temperature at which bulk thermal gelation occurs), as well as the

strength of the gel. In the case of Methocel A products, with a methoxyl substitution degree between 27 – 31.5% and independent of their chain length, the gelation temperature of a 2% solution is approximately 47 °C (Dow Chemical, 2013).

The main interest of Methocel A4C in this work, is related to its ability to hinder or delay the drug nucleation and crystal growth after supersaturation occurs. In accordance with the Stokes-Einstein law for diffusion in solution (Miller and Walker, 1924), the formation of a low to moderate viscous solution reduces the molecular mobility and diffusion of the drug molecules in colloidal solution, thus preventing or limiting the clustering and nucleation phenomena and consequently hindering the crystal growth. Through this approach, the drug can be maintained in solution over a longer time frame. Besides, the formation of intermolecular interactions with drug molecules such as hydrophobic interactions could be a further contribution factor to the stabilization of the supersaturated state of the drug in solution (Chevillard and Axelos, 1997; Xu and Dai, 2013b).

3.2.3 Polyvinyl caprolactam-polyvinyl acetate-polyethylene glycol graft copolymer (Soluplus, SOL)

Soluplus (SOL) is a graft copolymer with an amphiphilic chemical structure, enabling the formation polymeric micelles in aqueous solution. From a chemical point of view, SOL is composed of a PEG 6000 hydrophilic backbone (13%) with one or two side chains of vinyl acetate (30%), randomly copolymerized with vinyl caprolactam (57%) (Figure 3.3). Due to this amphiphilic structure, the polymer adopts a singular conformation in aqueous solution orienting the lipophilic side chains to the inner core of the micelles, while the hydrophilic backbone remains oriented to the outer phase, directly in contact with the aqueous medium.

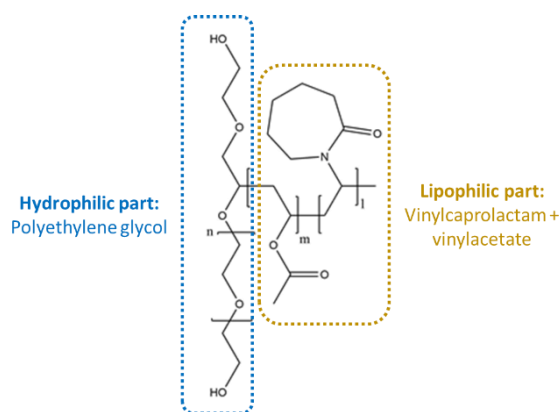


Figure 3.3: Chemical structure of the graft copolymer SOL. Its amphiphilic character can be understood from the presence of both a hydrophilic and lipophilic part within its chemical structure.

3. MODEL

Originally, this polymeric solubilizer was developed for solid solutions. However, due to its bifunctional character, it possesses the ability to act as a matrix polymer for solid solutions and at the same time is able to solubilize poorly soluble drug molecules in aqueous media.

The molecular weight of SOL was determined by gel permeation chromatography and showed an average value of 118,000 g/mol. Besides, as it was firstly developed for solid solutions, it has a low glass transition temperature (T_g) of 70 °C to enable extrudability at lower temperatures compared to other polymers. Furthermore, due to its amphiphilic structure and to the ability to form polymeric micelles, it also has a detectable critical micelle concentration (CMC = 7.6 mg/L), much lower than for other classical low-molecular weight surfactants (Djuric, 2011).

SOL can successfully solubilize lipophilic drug molecules with various chemical structures and therapeutic applications (Djuric, 2011). Its use as a binder or in a simple suspension resulted in an increased intrinsic/ saturation solubility for a vast variety of drugs. In some cases, the solubility was enhanced up to one hundred-fold such as for danazol, estradiol and fenofibrate (Linn et al., 2012). However, due to the successful solubilization of a vast variety of actives, a preference for specific chemical structures could not be identified.

Additionally, to improve the low solubility of drug molecules and to increase their respective low bioavailability (Buch et al., 2009), SOL has been successfully used as a polymeric matrix to amorphize drugs in the hot-melt extrusion process in order to subsequently improve the drug release. As an example, crystalline Itraconazole was amorphously embedded into a SOL matrix. The *in vitro* dissolution studies revealed not just an increased dissolution rate and drug solubility, but also an enhanced increased oral bioavailability *in vivo* (Djuric, 2011).

In the present work, SOL has been successfully applied as a solubilizing excipient in aqueous solution. Nevertheless, it cannot be considered as a universal approach to solve poor bioavailability issues, since micellar solubilization in general compromised the oral bioavailability in certain cases (Poelma et al., 1990, 1991), and solubilization approaches were reported to limit the permeation of drugs through biological membranes (Frank et al., 2012). The lipophilicity of the drug and the degree of stabilization through the formation of specific or unspecific interactions in the inner lipophilic core might play a decisive role on the liberation of solubilized species to enable their permeation through biological membranes.

3.3 Part I: Physicochemical properties of poorly soluble drugs in polymeric solutions and their relationship with supersaturation and solubilization

In this section the supersaturation and solubilization effect were evaluated from a physicochemical point of view. By investigating the apparent shifts observed in the physicochemical properties of the drug molecules (ionization, solubility and lipophilicity) in polymeric solutions, different supersaturation and solubility enhancement mechanisms are elucidated. Therefore, it is the first fundamental step to investigate the potential of supersaturation and solubilization under *in vitro* biorelevant models and under *in vivo* conditions.

3.3.1 Study on the ionization of poorly soluble drug molecules under supersaturation and solubilization conditions

The study of the ionization properties of a molecule as a function of pH is essential to understand the molecule's behavior in the gastrointestinal tract and to determine potential factors that might limit its BA in early-stage drug product development. Furthermore, the influence of pharmaceutical excipients, especially those having an amphiphilic structure to solubilize dissolved species of the drug, might apparently change the ionization constant(s) and $pK_a(s)$, respectively. These apparent shifts in ionization can be indicative for certain physicochemical changes in the system that will be discussed briefly in this chapter and in the section 5.1.1. The appearance of shifts in acid-base equilibria in a colloidal solution related to pharmaceutical excipients is commonly known, as it was already described three decades ago (El Seoud, 1989). Following the solubilization of an acid or a base within the core of an organized surfactant assembly (e.g. aqueous micelle, vesicle, ...), it was proposed that the apparent shift in the ionization equilibrium might be attributed to several factors, such as a change in the properties of the bulk solvent and of the interfacial region (e.g. changes in the microscopic polarity), as well as the perturbation of the acid-base equilibrium by the electrostatic field effect of the charged interface. Later, further studies focused on the apparent shifts in proteolytic equilibria of several sartan-like molecules depending on the nature of the pharmaceutical excipient used (anionic, cationic or non-ionic) (Grujić et al., 2016). The obtained results indicated apparent pK_a shifts (pK_a^{app}) caused by the formation of electrostatic interactions between the ionized micelles and the ionizable groups of the sartans, as well as due to the interactions of the drugs with the hydrophilic palisade layer. These apparent ionization changes potentially influence the intestinal absorption and thus, the oral BA.

Previous findings shed light on potential interaction mechanisms between polymer and drug molecules in the presence of supersaturation and solubilization. However, the underlying stabilization mechanisms are not fully understood (Xu and Dai, 2013b). The determination of these interactions requires the combination of advanced spectroscopic and calorimetric technologies such as Dosy-NMR or isothermic titration calorimetry (ITC). The nature and strength of the intermolecular interaction will affect the accuracy and the reliability of the applied techniques. Other methodologies such as X-ray diffraction, differential scanning calorimetry, raman spectroscopy, fourier transformation infrared spectroscopy, polarized light microscopy, scanning electron microscopy and atomic force microscopy had previously contributed to the elucidation of possible stabilization mechanisms (Douroumis and Fahr, 2007; Edwards et al., 2013; Gao et al., 2009a; Morgen et al., 2012; Palermo et al., 2012; Verma et al., 2009; Yamashita et al., 2003; Zimmermann et al., 2009). In this study, the establishment of drug/polymer interactions, which induce changes in the fraction of molecularly dissolved drug

3. MODEL

molecules, were indirectly evaluated by investigating the changes occurring in the ionization equilibria as a function of the polymer concentration.

3.3.1.1 UV-metric pK_a titration

Due to its simplicity and low amount of required sample, the UV-metric pK_a determination (Box and Comer, 2008) was selected as reference method to investigate potential apparent shifts in the ionization properties of the drug molecules. The importance of this investigation in the present study is to differentiate between supersaturating and solubilizing stabilization mechanisms, as it will be in detail discussed within this section. Briefly, while pure supersaturation constitutes a metastable state in which the drug in solution is molecularly dissolved, solubilization strategies are often associated to complexation or micellization and can therefore affect the fraction of species participating in the ionization equilibria.

The UV-light absorption ($\lambda = 230 - 400$ nm) of many drug molecules can be used to determine their ionization characteristics and pK_a s. UV-light absorption is a property of molecules that have two or more conjugated double bonds within their chemical structure (chromophore). In those cases, in which a molecule has an ionizable group within the chromophore or close to it (3-4 bond lengths), the change in the ionization state will lead to a different molar extinction coefficient (MEC). Therefore, when the entire amount of the drug is dissolved, a shift in the absorption profile related to a pH-change can be assumed as a response to the ionization.

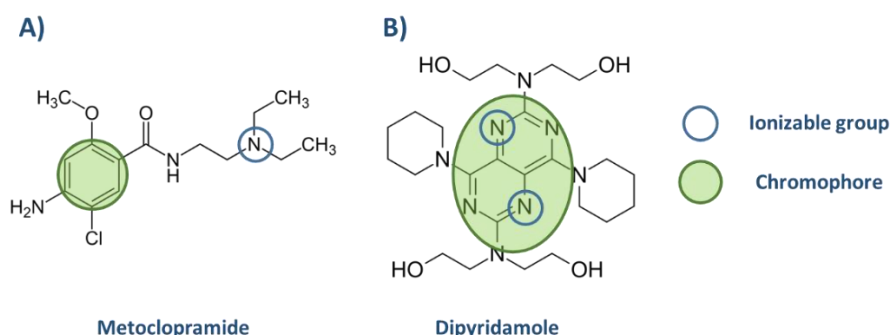


Figure 3.4: A) The ionization center of metoclopramide is four atoms from an aromatic chromophore and ionization may not affect the UV-absorbance spectrum. B) The ionization centers of dipyrizidamole are next to a chromophore and ionization will likely change the absorbance spectrum. Adapted from SiriusT3 instructions manual (Sirius Analytical Instruments Ltd., 2013).

In Figure 3.4, metoclopramide (A) is not suitable for the UV-metric method as the ionization center is too remote from the aromatic conjugated bonds system. Thus, no shifts in the MEC due to a change in ionization is expected. On the contrary, a molecule like dipyrizidamole (B) has ionizable groups within the aromatic double bond system, causing a shift in the MEC when the ionization state of the molecules is changed.

The UV-metric pK_a determination was performed by using the principles of the multiwavelength spectrophotometric determination and target factor analysis (TFA) (Allen et al., 1998) (Box et al., 2003). The method applied in this study was based on similar principles but differed in the experimental setting, as it was incorporated in the novel Pion inForm apparatus (Pion Inc. (UK) Ltd., Forest Row, UK) (Box et al., 2017; Comer, 2014). The Pion inForm incorporates a built-in UV

dip probe (Figure 3.5) made of solarization-resistant quartz fibers and they are connected to a diode array spectrophotometer with a deuterium lamp. The UV-light generated by the deuterium lamp passes through the probe for approximately 1 second per time point. Due to a small mirror built in at the edge of the window, that defines the pathlength of the probe, the unabsorbed light fraction is then reflected to the diode array detector (DAD) through the quartz fibers. A more detailed scheme of the spectroscopic UV-vis system is depicted in the Figure 3.18 and Figure 3.19.

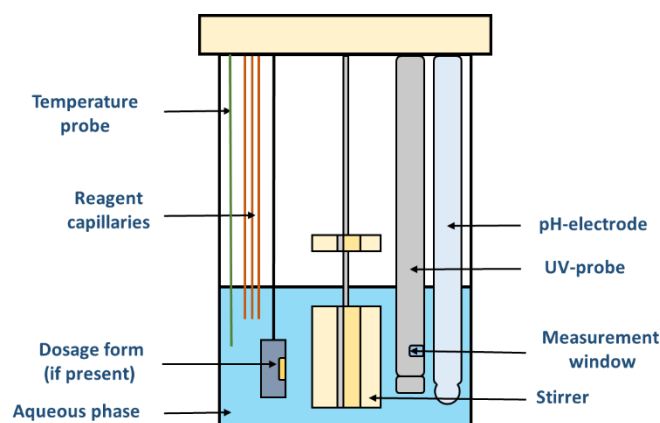


Figure 3.5: Scheme of the Pion inForm probe vessel. UV-metric pK_a determinations are performed in the measurement window by means of the UV-probe. Adapted from Comer et al., 2014.

An evaluation of all absorbance data is performed according to the Lambert-Beer Law:

$$A = c * a * b \quad (\text{Equation 16})$$

- A : Absorbance in absorbance units [AU]
- c : Concentration [mM]
- a : Molar Extinction Coefficient [$\text{mM}^{-1} * \text{mm}^{-1}$]
- b : Path Length [mm]

Regarding the UV-spectra at each pH-value, the changes in the absorbance and molar absorption profile can be recorded during a titration measurement. It results in a spectral data- vs. pH-profile from which an absorbance change vs. pH for each wavelength can be translated (Figure 3.6). Subsequently, by means of the statistical method target factor analysis (TFA), the pK_a - value(s) for a drug molecule can be determined from the pool of spectral data. The TFA describes the variability of measured variables (pH, λ , absorbance and species) derived from a lower number of altered variables during the experiment, which cannot be directly measured (concentrations and ϵ).

3. MODEL

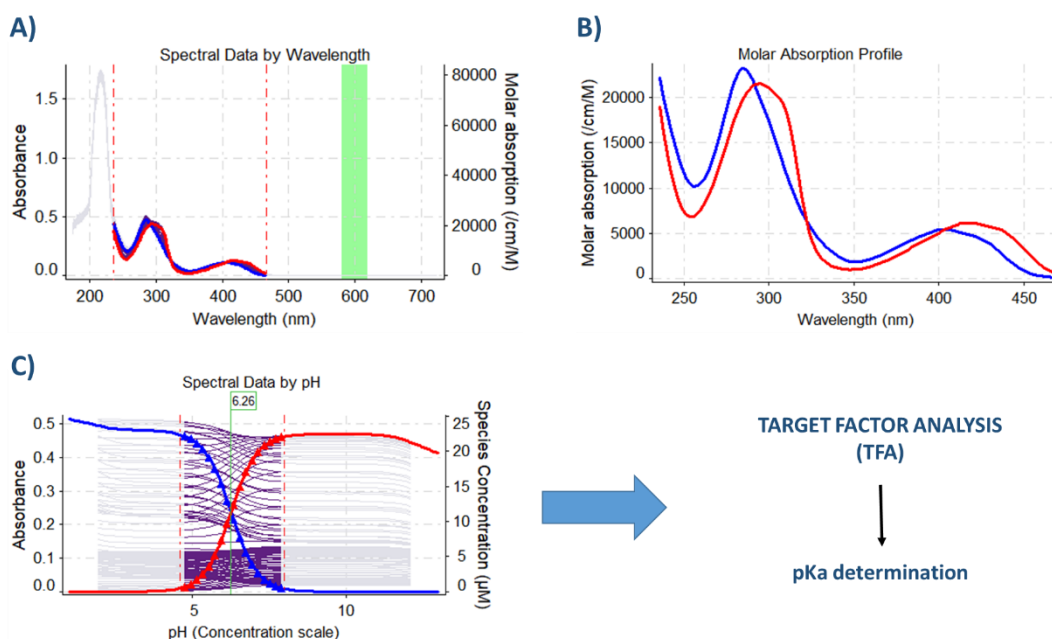


Figure 3.6: Exemplary a UV-metric pK_a determination for Dipyrindamole in 0.15 M NaCl. **A)** Spectral data by wavelength profile. **B)** Molar absorption profile. **C)** Spectral data by pH profile. The blue curves represent the protonated base (BH^+), while the red curves correspond to the neutral base (B^0). Adapted from data generated in the this study.

3.3.1.1.1 UV-metric pK_a determination under the influence of a cosolvent

Special attention must be paid to avoid drug precipitation during pK_a determination. A precipitation event would shift the baseline and the spectra of the drug in solution. Thus, it creates interferences and a proper pK_a determination is impeded. Precipitation can be easily detected by means of the incorporated UV-dip probe coupled to the DAD. It monitors the absorbance at a single wavelength ($\lambda = 500$ nm in this work) in the visible range during the full assay, at which the drug in solution does not absorb UV-light. When the entire drug sample is dissolved and a clear solution appears, the absorbance at a non-absorptive wavelength should be close to zero and a correct baseline is obtained. When precipitation occurs, suspended particles scatter light, causing a sharp increase in absorbance at non-absorptive wavelengths. This finding is interpreted as precipitation, when a threshold of 0.1 AU at the selected wavelength is exceeded (Figure 3.7).

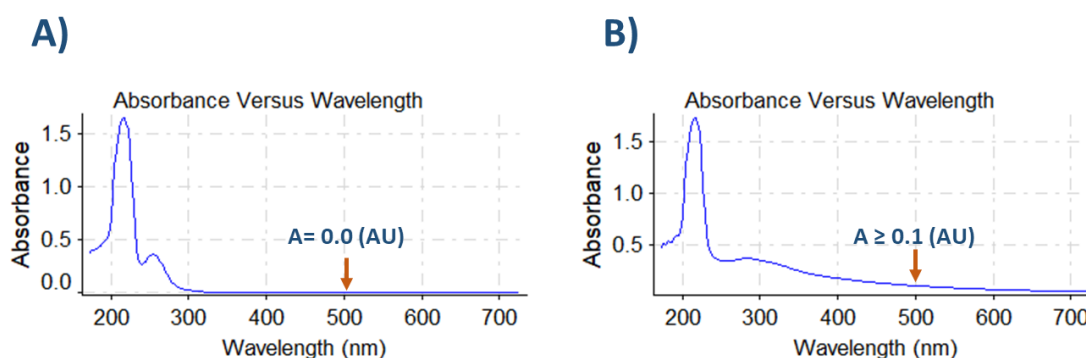


Figure 3.7: Exemplary, Itraconazole UV-spectra before (A) and after (B) precipitation. Adapted from data generated in this work.

One way to overcome this issue involves the use of a water-miscible cosolvent in which the solubility of the drug is increased. For practical reasons 80% methanol, with an adjusted ionic strength to the medium used (0.15 M NaCl), was selected. The main difference between this approach and a normal pK_a titration is the obtained apparent shift in the pK_a , leading to an apparent dissociation constant (p_sK_a). These shifts occur due to a lower dielectric constant (ϵ) when using cosolvents. A fact that partially limits the ionization of the drug in solution. As a result, the obtained shifts are causally related to the fraction of cosolvent in solution. When several titrations at different cosolvent ratios were performed, a proportional shift from the original pK_a value can be obtained for each cosolvent ratio. Consequently, by means of a simple Yasuda-Shedlovsky extrapolation (Avdeef et al., 1999; Takács-Novák et al., 1997), the $pK_a(s)$ of the drug molecule in pure water can be calculated. The pioneers of this method, Yasuda and Shedlovsky, described in their work the relation between the apparent shifts and the cosolvent ratios (Shedlovsky, 1962; Yasuda, 1959). Remarkably, the direction of the shift will depend on the nature of the ionizable group:

- Acidic pK_a s increase
- Basic pK_a s decrease
- In the case of ampholytes or zwitterions, both shifts will be observed as a function of the considered group

The direction of the shift can be explained by the changes in the equilibria between the acid and base, as defined in the Henderson-Hasselbach equation (Avdeef et al., 1993). These changes are related to the different ϵ and ionization of the molecule in a binary mixture (solvent and cosolvent).

The p_sK_a is determined by using the TFA procedure for each methanol-water mixture. The changes in the apparent dissociation constant for each cosolvent ratio are plotted against the invert of the dielectric constant. The aqueous pK_a is then extrapolated by using the Yasuda-Shedlovsky method and the y-axis-intercept of the linear plot from Equation 17.

$$y = a + bx \quad (\text{Equation 17A})$$

$$p_sK_a + \log[H_2O] = a + b/\epsilon \rightarrow a = p_sK_a + \log[H_2O] - b/\epsilon \quad (\text{Equation 17B})$$

$$\text{Assuming that } [H_2O] = 55.55 \text{ M} = 55.55 \text{ mol/L} \rightarrow \log(55.55) \approx 1.75 \quad (\text{Equation 17C})$$

$$pK_a = a - 1.75 \quad (\text{Equation 17D})$$

In Equation 17, p_sK_a is the negative logarithm of the apparent dissociation constant of the molecule in the binary mixture, ϵ is the dielectric constant of the medium, a is the y-axis-intercept and b is the slope. In Figure 3.8, two linear plots of the Yasuda-Shedlovsky extrapolation are shown as an example.

3. MODEL

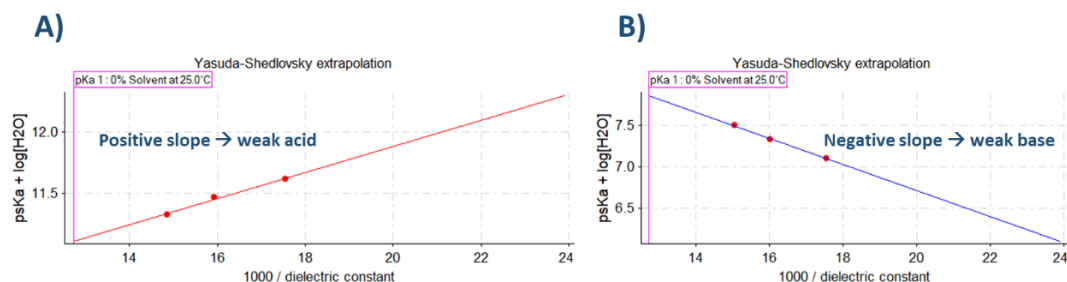


Figure 3.8: Exemplary, the Yasuda-Shedlovsky extrapolation for the weak acid celecoxib (A) and for the weak base dipyrindamole (B). Adapted from data generated in this work.

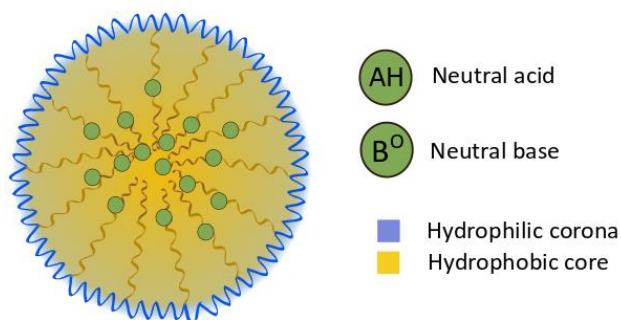
3.3.1.1.2 Differentiation between solubilizing and non-solubilizing drug-polymer combinations by means of the apparent shifts in the ionization properties

In general, as discussed in the sections 1.2 and 1.4, the nature of solubilization approaches is based on micellization, complexation or cosolvency effects. These involve the establishment of strong interactions between the drug molecules and pharmaceutical excipients to increase the fraction of apparently dissolved drug (not “truly” molecularly dissolved), which is associated with an increase in the thermodynamic solubility in equilibrium conditions. In this sense, the solubilization approaches potentially decrease the “truly” molecularly dissolved drug fraction and shift the acid-base equilibria established in aqueous solution. On the other side, the supersaturation is per definition a metastable state in which the drug is molecularly dissolved, and therefore, it does not induce changes in the acid-base equilibria. As a result, the pK_a values remain constant when just supersaturation effects but not solubilization is present.

In this sense, the appearance of pK_a^{app} values was associated with solubilization events, where a polymer concentration dependent effect was present. At the same time, the absence of changes in the ionization and pK_a with increasing polymer concentrations could be attributed to supersaturation events. However, the absence of changes in the ionization equilibria can similarly indicate a complete absence of stabilization. This will be further investigated and confirmed under the kinetic approach followed in the section 5.2.

The solubilization of drug molecules by micellization in the case of the amphiphilic graft copolymer SOL, as well as the formation of polymer/ drug intermolecular interactions in the presence of KVA64 and MA4C is graphically depicted in the Figure 3.9.

A) Polymeric micelle



B) Linear polymer

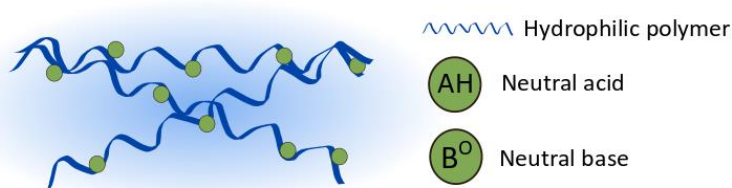
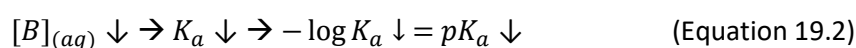
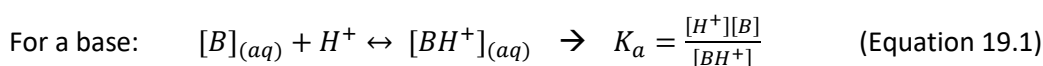
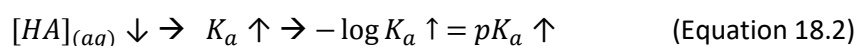
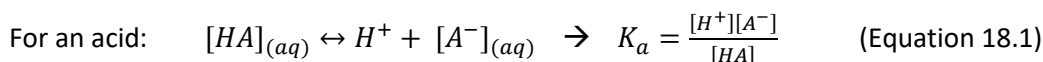


Figure 3.9: **A)** Incorporation of drug molecules in the lipophilic core of a micelle. This phenomenon corresponds to the main stabilization mechanism of SOL. **B)** Establishment of intermolecular interactions between drug molecules and linear polymers, likely applicable for KVA64 and MA4C. Both mechanisms have the potential to cause shifts in the ionization equilibria and conduct to an apparent pK_a value.

The changes in the acid-base equilibria established are mainly attributed to the decrease in the fraction of molecularly dissolved neutral species, independently of the behavior as a weak acid (AH) or as a weak base (B^o). This induces an apparent increase in the pK_a of acidic drug molecules (Equations 18.1 and 18.2) and an apparent decrease for basic drug molecules (Equations 19.1 and 19.2).

In aqueous medium:



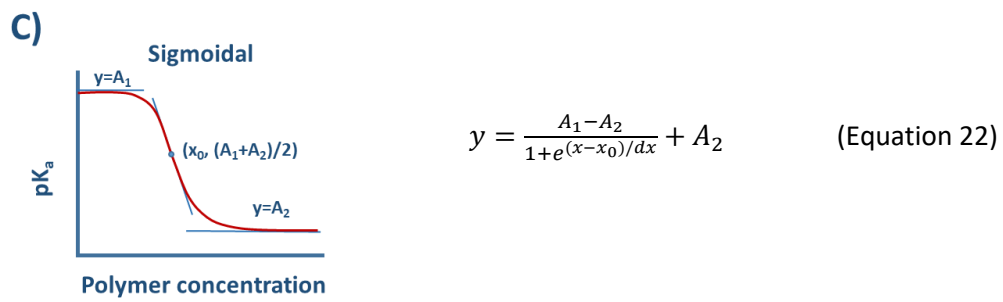
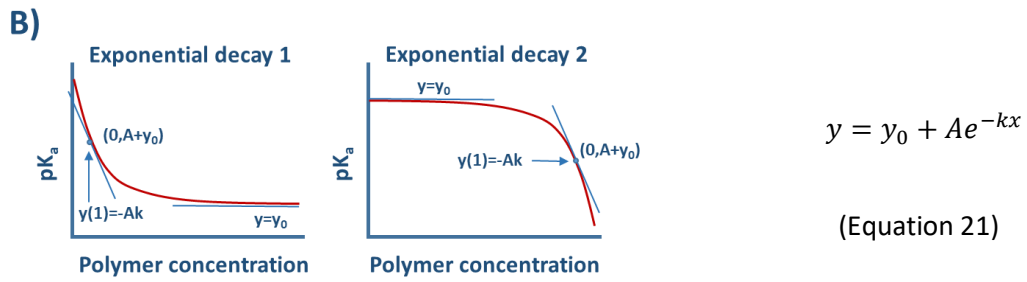
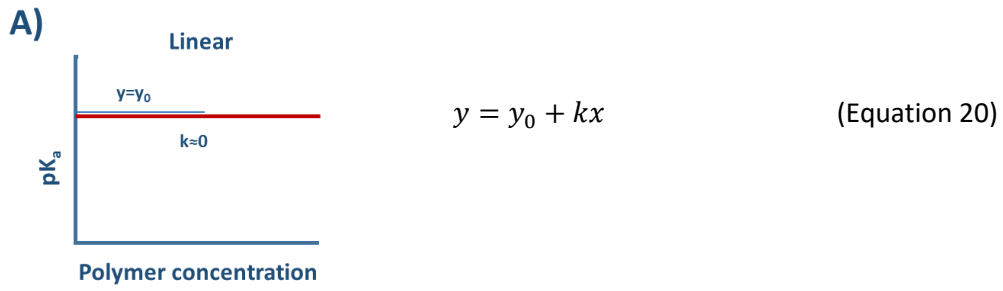
In the case of **ampholyte or zwitterion** drug molecules, which have acidic and basic ionizable groups, the direction of the shift is likely related to the nature of the ionizable group involved in the establishment of a certain equilibrium.

3. MODEL

As a result of the presence or absence of solubilization effects and of the changes produced in the ionization equilibria (Equations 18 and 19), three mathematical trends were identified to describe the relationship established between the ionization (expressed as the pK_a) and the polymer concentration. These relationships define in the present study the so called pK_a curve and were identified to be linear (Equation 20) or exponential (Equation 21) in most of the cases. Exceptionally, a clear sigmoidal relationship (Equation 22) was identified in few cases. Similar to the rate of reaction observed for enzymes as a function of the substrate concentration, the changes in the ionization equilibria as a function of the polymer concentration, showed similar dependencies. In the case of enzymes and substrates, a classical exponential Michaelis-Menten kinetic (Michaelis and Menten, 1913) is observed for simple enzymes, while a sigmoidal kinetic is observed for allosteric enzymes (Herve, 1989). Both exponential and sigmoidal relationships were mostly associated with a solubilization effect, while the linear trend was indicative for the absence of solubilization. Nevertheless, as the linear trend suggested no changes in the ionization equilibria, this is compatible with a supersaturation effect or with a lack of stabilization.

- Linear (Equation 20). This trend was often indicative for an absence of changes in the ionization equilibria. The slope (k) of this linear trend was close to 0 and no significant changes in the pK_a values were identified. As a result, this mathematical trend suggested an absence of solubilization through micellization or complexation.
- Exponential (Equation 21). The establishment of an exponential trend between the pK_a and the polymer concentration indicated significant changes in the ionization equilibria, as well as a polymer concentration-dependent effect. Two curve fits were identified in this case:
 - Exponential decay 1 (plateau $< pK_a$ for weak bases, plateau $> pK_a$ for weak acids). This trend was characterized by a positive decay constant (k) which achieved a real polymer concentration dependency due to a continuous shift in the ionization equilibria with increasing polymer concentration and it is associated to a solubilization effect. For comparative purposes, the decay constant was considered as an indicative parameter for the extent of the interaction between polymer and drug.
 - Exponential decay 2 (plateau = pK_a of the pure drug molecule). This trend showed a negative decay constant (k). No changes in the ionization equilibria were found at low polymer concentrations but when higher polymer concentrations were applied (0.250 % w/V). This was attributed to a polymeric molar excess which causes steric hindrance for the accessibility of the drug molecules in solution to participate in the ionization equilibria. Furthermore, changes in the overall viscosity of the system could limit the accessibility of neutral species to participate in acid-base equilibria and therefore induce apparent shift in the ionization.
- Sigmoidal (Equation 22). This trend was very rarely observed and indicated a lack of changes in the ionization properties at low polymer concentrations, followed by a real polymer concentration-dependent effect. This behavior is similar to the kinetic reaction of allosteric enzymes which have a regulatory site and an active site (Herve, 1989). In allosteric enzymes, the interaction established between a modulator with the regulatory site induces a conformational change and facilitates the interaction of the substrate with the active site of the enzymes. In this work, a clear sigmoidal relationship was only

observed for the combination ABZ/ KVA64. Possible explanations for the sigmoidal behavior will be discussed within this chapter.



3. MODEL

3.3.2 Solubility and solubility enhancement

3.3.2.1 CheqSol method

The CheqSol (Chasing equilibrium Solubility) method (Box et al., 2009, 2006; Stuart and Box, 2005a), which is incorporated in the Pion inForm platform, was applied to assess the pH-dependent solubility profile of the selected BCS II drugs. By tracking the changes in the kinetic and intrinsic solubility of the drug molecules in polymeric solutions, the potential of these excipients as precipitation inhibitors or solubilizing agents can be additionally assessed and complemented to the UV-metric pK_a determinations. In this sense, the CheqSol evaluations represent the central part of this thesis, as it enables a direct investigation of the polymers potential to enhance the solubility of the drug molecules from a kinetic and thermodynamic perspective

Compared to other traditional solubility determination methods (e.g. shaking flask method) (Veseli et al., 2019), the present approach shows several advantages, which allow a deeper understanding and insight into the supersaturation ability of the pure drug molecules. A solubility determination in the presence of water-soluble pharmaceutical excipients (e.g. supersaturating polymers) is also feasible in most of the cases. Amongst others, the most remarkable advantages of the CheqSol method include:

- Allows the investigation of the pH-dependent solubility profile for ionizable compounds. The method is built in as a potentiometric titration by the addition of predefined acid or base aliquots. A resulting pH-dependent drug solubility profile can be determined. The pH-dependent solubility can play *in vivo* a decisive role, especially for weak bases. Due to their low pK_a value, they (partially) dissolve in the stomach and may later precipitate in the upper small intestine.
- Differentiation between molecules which have an innate supersaturation ability in solution (chasers, slow precipitators) and compounds which do not possess this behavior (non-chasers, fast precipitators) in the absence of excipients (Comer, 2010). For this purpose, not just the intrinsic solubility (equilibrium solubility at a pH where the API is present in its fully neutral state) but also the kinetic solubility is determined. The potential differences in kinetic and equilibrium solubility categorize the behavior of the drug molecule into non-chaser or chaser.
- Reaches faster the drug equilibrium state in solution, thus shortening the time required for the solubility determination, when compared to other traditional methods (e.g. shake-flask method).
- Determines the amorphous solubility in those cases, in which the drug precipitates as an amorphous form, thus serving as an indicator for liquid-liquid phase separation (LLPS) (Comer et al., 2014).

Simultaneously, the suitability of the CheqSol method strongly depends on the physicochemical properties of the drug and several requirements must be fulfilled to enable a reliable measurement:

- Lack of applicability for neutral compounds. Neutral BCS II compounds (e.g. griseofulvin) have a fully neutral charge in the entire pH range and a respective low solubility, which impedes an initial dissolution of the sample followed by a pH-dependent precipitation. This fact disables the determination of kinetic and intrinsic solubility.

- Limited applicability for compounds with an extremely low kinetic and intrinsic solubility. The accuracy of the method relies on the detection of potentiometric changes in solution. These changes are not detectable for molecules with an extremely low aqueous solubility. As an example, the solubility of the extremely poor soluble drug itraconazole (ITZ) cannot be determined under these experimental conditions.
- Limited applicability for compounds with an extremely low dissolution rate. The drug must dissolve under a fast stirring rate (≈ 300 rpm) within few minutes in a pH, where its dissolution is favored from a thermodynamic and physicochemical point of view. In those cases, in which the slow dissolution rate causes an initial turbidity at the beginning of the measurement, the generated turbidity might be misinterpreted as an immediate precipitation. As a result, an error in the determination of kinetic and intrinsic solubility will occur.

The CheqSol method is basically a potentiometric acid/base titration solubility determination procedure (Avdeef and Berger, 2001) in which the amount of neutral and ionized drug in solution is identified by means of the *Charge and Mass Balance Equations*. These are extensively described in literature (Stuart and Box, 2005a) and they are directly related to the also well-known Henderson-Hasselbach equation (Avdeef, 2007; Hasselbalch, 1916; Völgyi et al., 2010).

As introduced, two different types of behaviors can be detected under the CheqSol method for poorly soluble drug molecules, when considering their supersaturation ability in solution: chaser vs. non-chaser.

On the one hand, those drug molecules that supersaturate by themselves in response to a pH shift, have a larger kinetic solubility than intrinsic solubility and tend to quickly recrystallize. These molecules are also defined as chasers (Comer, 2010). In general, the crystalline state is thermodynamically favored for a chaser molecule. In accordance with the organized arrangement of a crystal lattice, they tend to have low entropy. Consequently, a high activation energy is needed to achieve nucleation (Brouwers et al., 2009) with relatively slow crystallization rates. As a result, the phenomenon of supersaturation is favored. It was previously reported that a strong inverse dependency between the extent of supersaturation and the crystallization rate exists (Lindfors et al., 2008). The use of polymers might trigger a delay of the nucleation, as well as the inhibition of the crystal growth by several mechanisms, thus a supersaturation effect is obtained.

On the other hand, molecules that do not possess the ability to supersaturate by themselves without the help of pharmaceutical excipients, tend to show identical kinetic and intrinsic solubility values. This class of molecules are known as non-chasers, since compared to the chasers, they do not chase the equilibrium once they have precipitated.

It was observed that non-chasers do not show a supersaturation ability because they initially precipitate as a liquid phase which recrystallizes very slowly or does not recrystallize during the CheqSol determination (Comer et al., 2014). As introduced in the section 1.2, this phenomenon was previously described by the term "Liquid-Liquid Phase Separation" (LLPS) (Veesler et al., 2003) and is applicable to most of the non-chaser molecules. For non-chasers, the LLPS is considered as a metastable amorphous state. It possesses no long-range order and is consequently favored from an entropic point of view, showing a higher free energy as the crystalline form. The LLPS is a rapidly occurring phenomenon (Veesler et al., 2003). Due to the high free energy of the drug-rich liquid droplets, the driving force to crystallization is high. Nevertheless, the drug liquid phase owns the LLPS solubility until it is completely converted to the less energetic crystalline form (Comer et al., 2014). Since the formation of the crystalline

3. MODEL

form from a LLPS system is a kinetic process, the oral bioavailability might be unaffected, if the conversion can be controlled by means of pharmaceutical excipients. Potentially, no further stabilization is needed when LLPS occurs, since this phenomenon is enough to trigger oral absorption as a result of the extremely slow crystallization rates.

In some cases with LLPS, the recrystallization might occur in a faster manner (minutes), which makes it detectable for the CheqSol determination. In this context, the study previously performed by Hsieh et al. (Hsieh et al., 2012) showed for ketoconazole an initial precipitation through LLPS, followed by a kinetic crystallization into a 20-fold lower soluble form. Accordingly, even though it might be challenging to enhance the solubility of an amorphous form, the inhibition of the crystallization might serve as stabilization principle for enhanced-solubility formulations (Ilevbare and Taylor, 2013; Ilevbare et al., 2013a).

Considering all these aspects, the differentiation between the supersaturation and precipitation behavior of chaser and non-chaser molecules by means of the CheqSol method, represents the basis to further understand the potential of the polymers to enhance the oral absorption of the poorly soluble drugs.

3.3.2.1.1 Solubility determination by means of potentiometric titration: chasers vs non-chasers

The determination of the kinetic solubility involves the precipitation of the analyte in solution. In this way, the method requires a prior dissolution of a certain amount of sample (in most of the cases 10 – 20 mg in approximately 40 mL of medium) that can be detected potentiometrically and UV-metrically. A normal CheqSol experiment follows the experimental sequence depicted in Figure 3.10A.

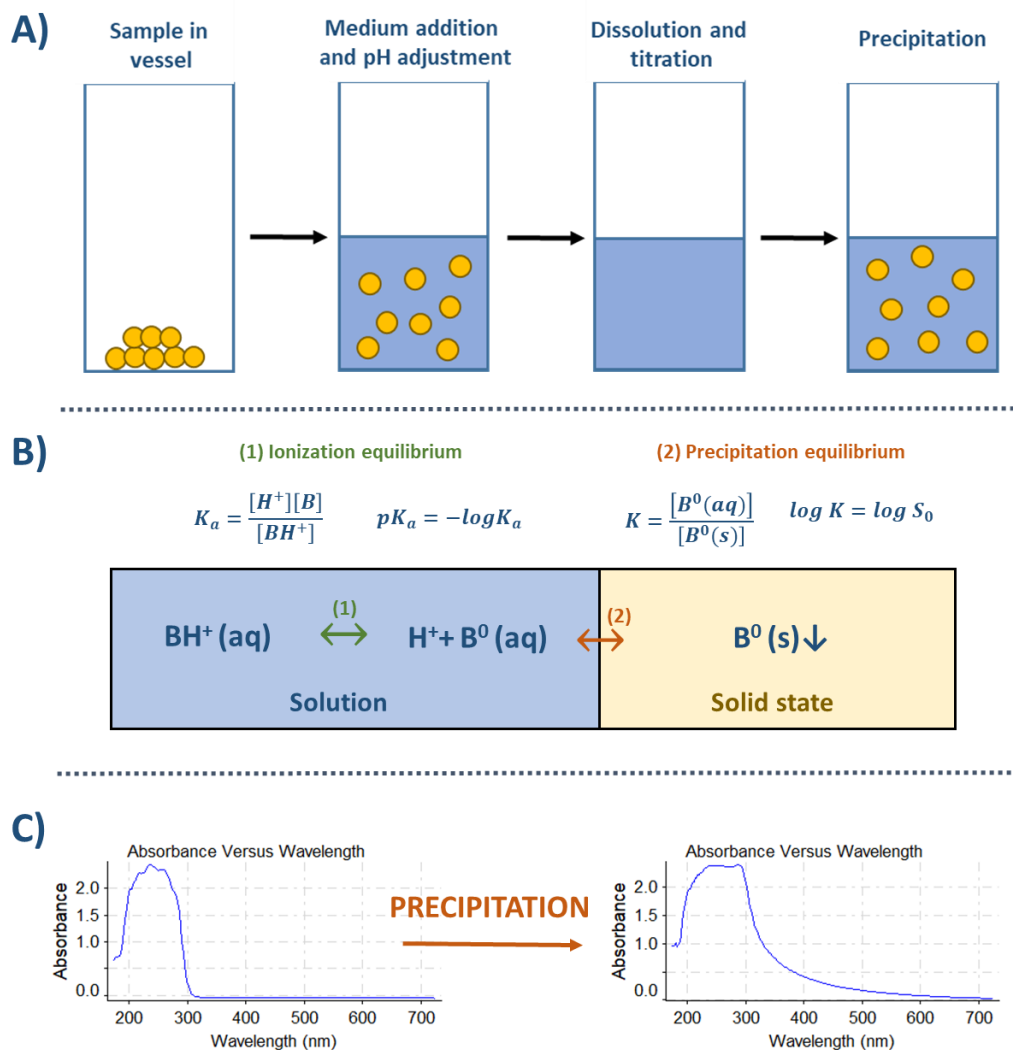
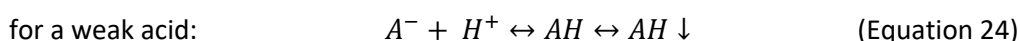
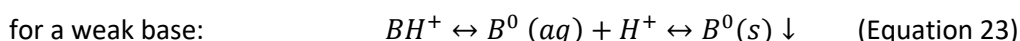


Figure 3.10: **A)** Initial experimental sequence of a CheqSol experiment. **B)** Ionization and precipitation equilibria in solution for a weak base molecule. **C)** UV-metric precipitation detection

- A) Dissolution. The sample (powder or highly concentrated aliquot of the analyte) is pre-dissolved in 0.15 M NaCl at a high stirring rate (300 rpm) for 2 minutes at a pH, which favors dissolution due to the generation of the mainly ionized drug.
- B) Titration. With increasing pH for a weak base and decreasing pH for a weak acid, the drug converts from its ionized form to its unionized form. It causes a change in the molecular charge, which approximates to neutral and eventually leads to precipitation (Figure 3.10B). In this way, the titration enables the establishment of an ionization equilibrium, as defined by the equations 23 and 24.

3. MODEL

- C) Precipitation. The precipitation is easily recorded by means of UV-spectroscopy (Figure 3.10C). When the sample is completely dissolved, no light is scattered at non-absorptive wavelengths. After precipitation, scattering occurs due to the presence of nucleation and crystal growth phenomena in the sample medium. Similar to the UV-metric pK_a determination, potential precipitation was identified at 500 nm, if the absorbance threshold of 0.1 AU was exceeded. When precipitation is first detected, the kinetic solubility is calculated potentiometrically from the concentration of neutral substance (B or AH) in solution. At this point, the solubility of the molecule ($\log S_0$) is equivalent to the precipitation constant ($\log K$, Figure 3.10B).



Depending on the supersaturation ability of the compound, the assay design and sequence will vary after precipitation:

- For chasers, compounds with a supersaturation ability, the kinetic solubility differs from intrinsic solubility. Thus, the intrinsic solubility will be determined by means of the “crossing points”, following the *CheqSol method* (Box et al., 2009).
- For non-chasers, compounds without supersaturation behavior, kinetic and intrinsic solubility are identical. In this case, the precipitation points are fitted to a precipitation profile by means of the *curve fitting method* (Box et al., 2009).

In both cases, the precipitation can be clearly analyzed through a shift in the theoretical ionization profile of the drug by using the potentiometric *Bjerrum curve* (Figure 3.11). The *Bjerrum curve* represents the average number of bound H^+ per mole of molecule vs. pH. The shift in the ionization profile is causally related to an apparent deviation in the ionization constant caused by the precipitation event. Molecules with a very low solubility undergo larger shifts in the ionization constant than molecules with a higher solubility, since the solubility and the extent of the shift are inversely connected.

A *Bjerrum curve* is automatically calculated from pH, pK_a and intrinsic solubility and it comprises two different graphs:

- **Solution Bjerrum curve (ionization profile)**. Represents an ionizable sample that is in solution across the entire pH range.
- **Precipitation Bjerrum Graph (precipitation profile)**. Represents a sample when precipitation occurs. Solution and precipitate are in equilibrium.

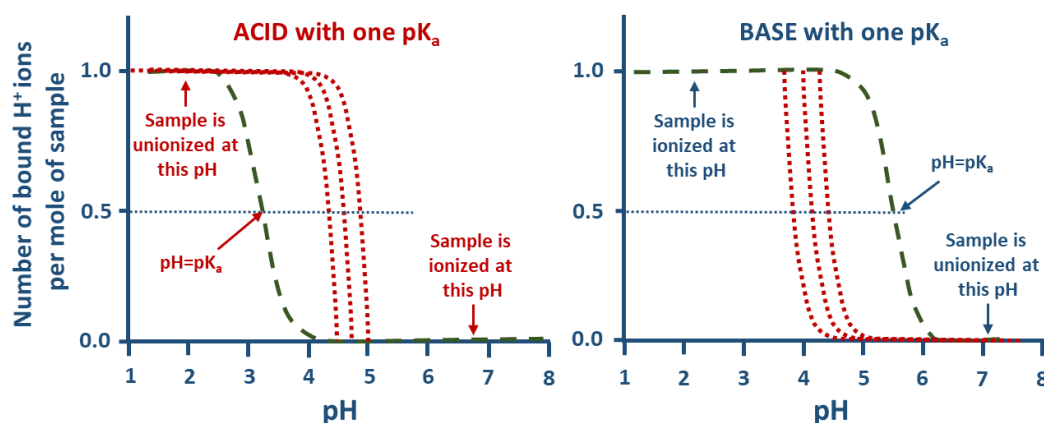


Figure 3.11: Solution (green) and precipitation (red) Bjerrum curves obtained in a CheqSol experiment for a weak acid (left) and for a weak base (right). A shift from the theoretical ionization profile represented by the solution Bjerrum curve indicates a precipitation event. The extent of the shift is inversely related to the solubility value. Adapted from "Introduction to pH-metric solubility measurement" (Sirius Analytical Instruments, 2009a)

Depending on the supersaturation ability of a compound, all the precipitation points may fall in a single Precipitation Bjerrum Graph when the kinetic and equilibrium precipitation graphs are identical (non-chasers) (Figure 3.12A). Contrary, the first precipitation point differs from the equilibrium precipitation points curve, when supersaturation is achieved in the case of chasers (Figure 3.12B).

As above mentioned, this different behavior will govern the method applied for the solubility determination:

- Chasers → *Cheqsol method*. The chaser system is supersaturated after precipitation occurs. Consequently, the potentiometric method titrates the system back into the direction of the original pH, with the aim of subsaturating the solution. Therefore, the equilibrium is reached in a rapid and reproducible way (Figure 3.12A). This is in accordance with the behavior of a chaser drug, since it possesses supersaturation ability and the kinetic solubility is higher than the intrinsic solubility. Thus, the equilibrium precipitation graph is shifted when compared to the kinetic precipitation graph.
- Non-chasers → *Curve fitting method*. When the sample first precipitates, the equilibrium is already reached and thus, there is no need to fluctuate the system between the supersaturated and subsaturated state (Figure 3.12B). The potentiometric method assumes that a system is equilibrated when there is no change in the pH over time ($dpH/dt=0$) (Figure 3.13).

3. MODEL

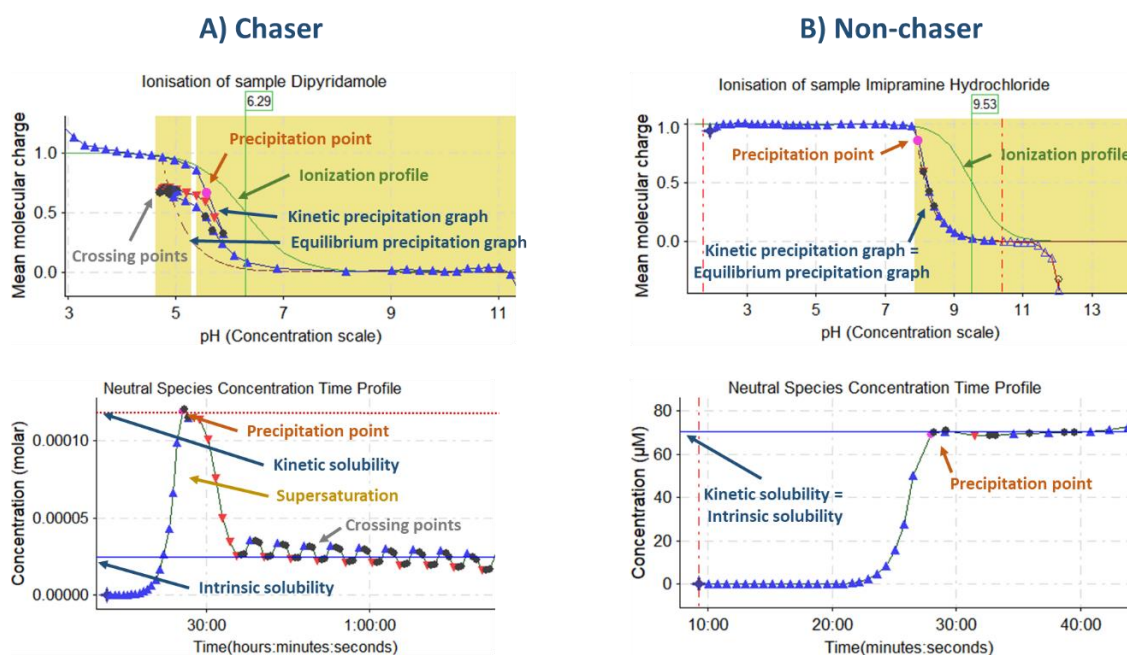


Figure 3.12: Exemplary, an experimental course of two CheqSol experiments (top) and neutral species concentration profiles (bottom) for a chaser molecule (**dipyridamole, A**) and for a non-chaser molecule (**imipramine, B**). The kinetic and equilibrium precipitation graphs are identical for a non-chaser due to the absence of supersaturation and contrary to a chaser molecule. Adapted from data generated within this work.

The slope, which defines the direction of the pH change over time (dpH/dt) (Figure 3.13), allows the method to easily recognize if the neutral species of the drug are in a supersaturated state (excess neutral species in solution) or subsaturated state (excess undissolved neutral species). At the mid-point between both states, the concentration of neutral species is in equilibrium. Referring to the previously described procedure (Figure 3.12), the method will always *chase the equilibrium* of the neutral species, independently from the current state of the system (supersaturated or subsaturated).

The direction of the dpH/dt depends on the physicochemical properties of the drug and the pH, which directly influence the ionization, supersaturation and precipitation behavior of the drug. As it can be understood from the equation 23 and from the equilibria described in the Figure 3.10B, when a weak base precipitates, protons are liberated to the medium and the pH drops. The system is supersaturated. On the contrary, when a weak base gets dissolved, protons are taken from the medium and pH increases. The system is subsaturated (Table 3.7).

For a weak acid, the experiment would follow a similar pattern to chase the equilibrium. The only remarkable difference would reside on the direction of the titration and the inverted addition of titrants to supersaturate and subsaturate the sample, when compared to a weak base (Table 3.7).

Table 3.7: Fluctuation of a weak base and weak acid between the supersaturated/ subsaturated state and involved pH changes and events.

Compound	State	dpH/dt	Event
Base	Subsaturated	> 0	Dissolution
	Supersaturated	< 0	Precipitation
Acid	Subsaturated	< 0	Dissolution
	Supersaturated	> 0	Precipitation

The chase of the equilibrium will continue until a dpH/dt vs. time graph can be drawn, from which an intrinsic solubility can be extrapolated by means of the *Charge and Mass Balance equations* (Stuart and Box, 2005b). In this graph, the constant fluctuation of the system between supersaturated and subsaturated state enables the calculation of the so-called *crossing points* at those times where the $dpH/dt=0$. At these points, the sample is at equilibrium, since no precipitation or dissolution occur (Figure 3.13). In general, 20 crossing points are collected to calculate a mean intrinsic solubility.

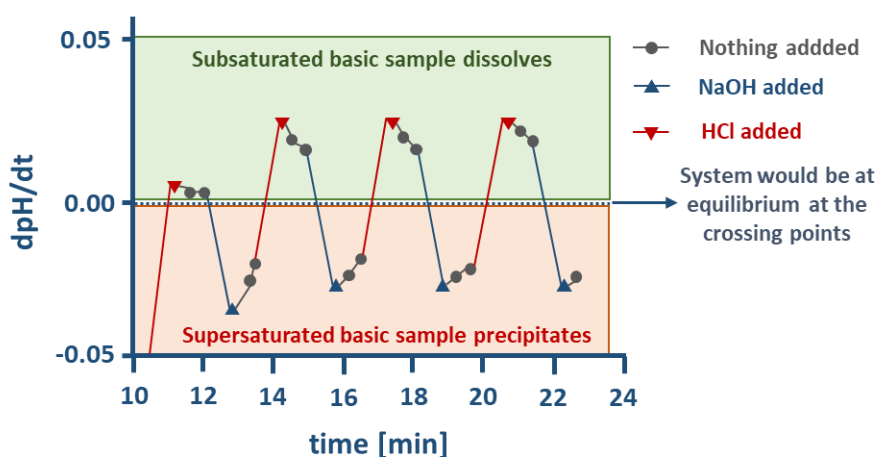


Figure 3.13: Crossing point graph for a weak base. The intrinsic solubility is calculated at the points where $dpH/dt=0$. Adapted from "Introduction to pH-metric solubility measurement" (Sirius Analytical Instruments, 2009a).

3.3.2.2 Shaking flask method

As described in section 3.3.2.1, one of the disadvantages of the CheqSol method is related to its lack of accuracy for extremely poorly soluble drugs. For the cases of albendazole (ABZ) and itraconazole (ITZ), the intrinsic solubility of these drug molecules was determined by means of the shaking flask method (Avdeef et al., 2016; Veseli et al., 2019). Furthermore, the present turbidity in certain colloidal solutions (especially in the presence of SOL) impeded in some cases a proper determination of the precipitation point by means of the CheqSol method. Consequently, the solubility enhancement achieved through SOL for loratadine (LTD) and telmisartan (TLM) was additionally determined by the shaking flask method.

3. MODEL

3.3.3 Lipophilicity: Log*P* and Log*D*

The lipophilicity of the pure drug molecules was investigated in the present study in order to obtain a deeper understanding on the mechanistic stabilization of the drug molecules in SOL solutions. In this sense, the Log*P* can affect the extent of solubilization within the SOL micelles and therefore, it is an important physicochemical property to investigate (see section 5.1.4.2.2)

3.3.3.1 Chromatographic method

The chromatographic approach is based on the work performed by Donovan and Pescatore (Donovan and Pescatore, 2002) and was selected as the reference methodology to evaluate the lipophilicity of the drug molecules in equilibrium. The simplicity of this method lies on the retention time determination from the analytes of interest within a methanol “cocktail”. The “cocktail” includes the internal standards toluene and triphenylene (Figure 3.14), from which their lipophilicity values are already known.

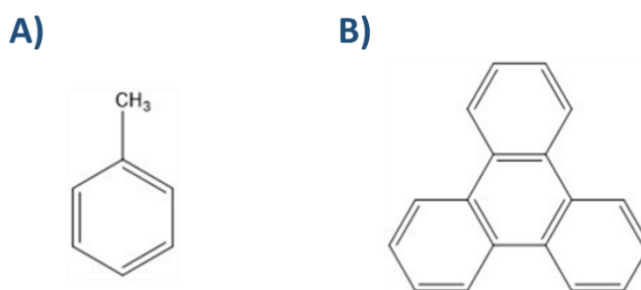


Figure 3.14: Chemical structures of the internal standards used for the chromatographic method: toluene (A, Log*P*= 2.72) and triphenylene (B, Log*P*= 5.49) (Donovan and Pescatore, 2002).

Based on the linear correlation between the retention times and Log*P*, the Log*P* of an unknown molecule can be calculated by substitution of the Log*P* from both standards and the retention times from the three molecules, as defined by the Equation 25:

$$\text{Log}P = \left(\frac{\log P_1 - \log P_2}{t_1 - t_2} \right) t_R + \left(\frac{t_1 \log P_2 - t_2 \log P_1}{t_1 - t_2} \right) \quad (\text{Equation 25})$$

Simplified to

$$\text{Log}P = \frac{(\log P_1 - \log P_2)t_R + t_1 \log P_2 - t_2 \log P_1}{t_1 - t_2} \quad (\text{Equation 25B})$$

with toluene as compound 1 and triphenylene as compound 2:

$$\text{Log}P_{\text{unknown}} = \frac{(\log P_{\text{tol}} - \log P_{\text{triph}})t_{\text{unknown}} + t_{\text{tol}} \log P_{\text{triph}} - t_{\text{triph}} \log P_{\text{tol}}}{t_{\text{tol}} - t_{\text{triph}}} \quad (\text{Equation 25C})$$

Despite the accuracy of this method, the main disadvantage is that the determination of apparent changes in the lipophilicity of drug molecules due to the influence of pharmaceutical excipients is not feasible. The large molecular size of the water-soluble polymers used would

immediately block the stationary phase, leading to a shift in the retention times and thus, compromising the reliability of the method. Accordingly, the influence of the selected polymers on the lipophilicity was investigated from a kinetic perspective by means of a water/octanol biphasic system (see section 4.2.2.1.3). Furthermore, TLM was characterized by a pH-metric titration method because the chromatographic approach was infeasible.

3.3.3.2 pH-metric titration

The pH-metric titration follows the potentiometric method and it is incorporated in the Pion SiriusT3 platform (Pion Inc. (UK) Ltd., Forest Row, UK). The method is based on the shift of the ionization curve of a molecule depending on its lipophilicity in the presence of a second organic phase (Avdeef, 1992; Slater et al., 1994). By means of a refinement procedure, the experimental data were fitted into a calculated apparent titration curve, which differed from the real ionization profile. Thus, for a reliable measurement, a previous accurate pK_a determination in the same system is mandatory. Once the fit was performed, the $\text{Log}P$ and the lipophilicity vs. pH can be calculated. Titrations from $\text{pH} \approx 3$ to $\text{pH} \approx 11$ were conducted in triplicate at different organic/ aqueous solvent ratios.

The pH-metric titration has several advantages when compared to other available methods:

- It does not require $\text{Log}P$ standards.
- It measures partition in a two-phase system, similarly to the shaking flask method but faster (1.5 – 2 hours instead of 48 – 72 hours).
- It is an independent reference method (Lombardo et al., 2001) and it is directly validated with reference to pH electrode calibration and titrant standardization.
- It allows the determination of the entire lipophilicity profile ($\text{Log}D$ and $\text{Log}P$) as a function of the pH.

At the same time, it presents some disadvantages:

- In general, potentiometric methods are inaccurate below pH 3 or above pH 11.
- Lack of applicability for extremely lipophilic weak bases and weak acids. The shifts obtained from the ionization profile under the influence of a second organic phase is often too large and the apparent pK_a s shifts to pH where the potentiometric method loses its accuracy. Thus, this method was only applied in this thesis to TLM.

According to Le Châtelier's principle (Le Chatelier, 1888), for an ionizable molecule in a biphasic system, two different equilibria are established. The first equilibrium refers to its dissociation into ionized and neutral species (Figure 3.15A, equation 26). The second is related to the equilibrium between the fraction of species that partition into the organic phase and the fraction that remains in the aqueous phase (Figure 3.15B, equation 27). The partition equilibrium disturbs the pK_a equilibrium, shifting consequently the pK_a to a new apparent value (p_oK_a). The $\text{Log}P$ is consequently directly proportional to the shift in the pK_a .

$$\text{Equilibrium 1:} \quad pK_a = \text{Log} \frac{[XH^+]}{[H^+][X^0]} \quad (\text{Equation 26})$$

$$\text{Equilibrium 2:} \quad \text{Log}P = \text{Log} \frac{[X^0]_{oct}}{[X^0]_{aq}} \quad (\text{Equation 27})$$

3. MODEL

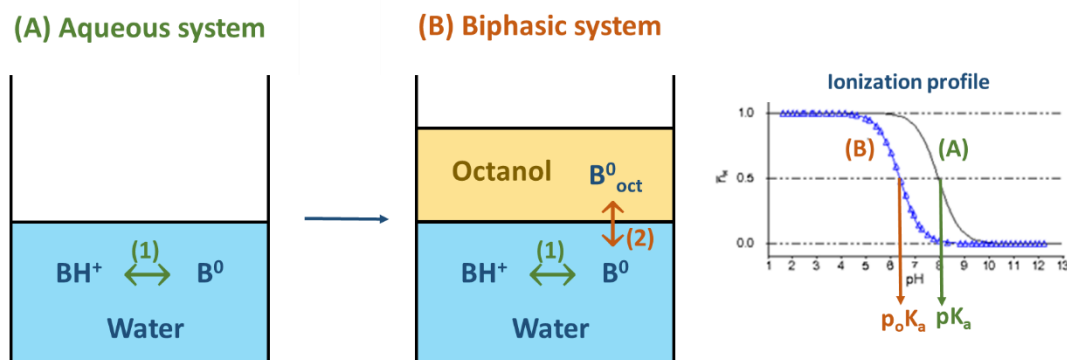


Figure 3.15: Equilibria established for a monoprotic weak base in an aqueous (A) and biphasic (B) systems and its influence on the aqueous ionization profile. Adapted from "Introduction to pH-metric LogP measurement" (Sirius Analytical Instruments, 2009b).

Based on the ionization properties of a molecule, the equation to calculate the partition coefficient P from pK_a shift will vary. The degree of complexity depends mainly on the number of ionizable groups and it increases when several different contributing groups are present in one molecule (Avdeef, 1992). The Equation 23 and 24 show the relationship established for a monoprotic weak acid and weak base, respectively.

- Acid with one pK_a :
$$P = \frac{10^{(p_oK_a - pK_a)} - 1}{r} \quad \text{(Equation 28)}$$

- Base with one pK_a :
$$P = \frac{10^{-(p_oK_a - pK_a)} - 1}{r} \quad \text{(Equation 29)}$$

The p_oK_a is the apparent pK_a in the biphasic system and r is the ratio between the volume of octanol and the volume of water. In those cases in which both volumes are equal, then $\text{Log}P \approx |pK_a - p_oK_a|$

As it can be deduced from the above equations, the direction of the shift from the ionization curve will depend on the nature of the chemical group causing the shift. For an acid, the $[AH]$ will decrease in the aqueous medium, causing a shift of the pK_o to higher values. On the contrary, for a base, the $[B^0]$ decreases due to the partition to the organic phase, causing an apparent shift of the ionization profile to lower pH values. These shifts are in accordance with the Henderson-Hasselbach equilibria, similarly to the previously described Yasuda-Shedlovsky extrapolation (Equation 17, Figure 3.8).

Through the performance of three different titrations at different octanol:water ratios, the lipophilicity profile of the molecule can be calculated when using the protonation constant, the partition coefficient (when the considered group is fully neutral) and the distribution coefficient (when the same group is fully ionized). Depending on the protonation degree of the group, which will be calculated from the $[H^+]$, the distribution coefficient will vary with the pH (Avdeef, 1996).

Example

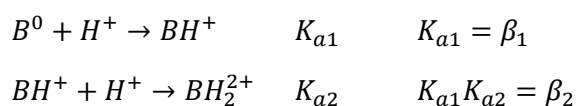
- Monoprotic base:
$$D = \frac{P^0 + P^1[H^+]K_a}{1 + [H^+]K_a} \quad (\text{Equation 30})$$

K_a is the ionization constant, P^0 is the partition coefficient of the fully neutral weak base and P^1 is the distribution coefficient of the fully ionized weak base.

- General equation:

$$D = \frac{P^0 + [H^+]\beta_1 P^1 + [H^+]^2 \beta_2 P^2 + \dots}{1 + [H^+]\beta_1 + [H^+]^2 \beta_2 + \dots} \quad (\text{Equation 31})$$

Two protonation constants define the ionization degree of the molecule presenting more than one ionizable group:



K is the protonation constant, β is the cumulative protonation constant, P^0 is the partition coefficient of the fully neutral weak base, P^1 is the distribution coefficient of the first fully ionized weak base (BH^+) and P^2 is the distribution coefficient of the second fully ionized weak base (BH_2^{2+})

In the case of ampholyte or zwitterionic molecules such as TLM, the special physicochemical properties related to the presence of both basic and acidic groups in the chemical structure, will lead to a particular Bjerrum profile in the presence of an organic solvent. The shifts from the theoretical ionization profile will take place in both directions (Figure 3.16A). This will condition the shape of the lipophilicity profile which tends to be bell-shaped for ampholytes (acid $pK_a >$ basic pK_a) and for zwitterions (acid $pK_a <$ basic pK_a) (Figure 3.16B).

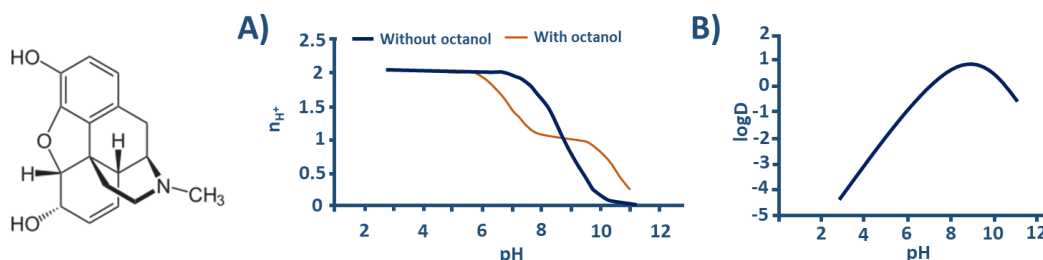


Figure 3.16: A) Ionization profile (Bjerrum curve) in aqueous solution of the ampholyte molecule morphine (base, $pK_a = 8.17$; acid, $pK_a = 9.26$) without (blue curve) and with (red curve) the presence of an octanol phase; **B)** Lipophilicity profile of morphine vs. pH. Adapted from "Introduction to pH-metric LogP measurement" (Sirius Analytical Instruments, 2009).

3. MODEL

In spite of the validation of the pH-metric titration by comparing it to previously published shake flask data (Comer et al., 1995; Slater et al., 1994; Takács-Novák and Avdeef, 1996), the applicability of the method is very limited for extremely lipophilic weak bases or weak acids. A challenge that caused errors in the determination of the $\text{Log}P$ and lipophilicity profile from most of the drugs used in this work. An exception was TLM for which a determination of the lipophilicity of the pure drug was feasible. Additionally, the lipophilicity of the molecule under supersaturating conditions in the presence of water-soluble polymers, could be investigated.

3.4 Part II: *In vitro* evaluation of the supersaturation and solubilization potential to enhance oral bioavailability.

3.4.1 Monophasic and Biphasic Dissolution Tests (MDTs and BDTs)

This section focuses on an *in vitro* kinetic investigation of the polymers potential to stabilize the poorly soluble drugs in solution by means of supersaturation and solubilization, as well as to enhance their partition into an organic phase simulating an absorptive compartment. With this purpose, the fasted gastrointestinal conditions are simulated as described within this chapter.

3.4.1.1 Apparatus design

All dissolution tests carried out in the current study were performed with the help of the novel Pion inForm system following the GI dissolution approach described by Gravestock and co-workers (Gravestock et al., 2011) with slight variations. As described in literature (Comer et al., 2014), the Pion inForm is a fully automated USP II-like dissolution apparatus with the potential to simulate biorelevant GIT conditions. The dissolution vessels used were cylindrical shaped glasses (diameter = 8.0 cm; height = 12.0 cm) (Figure 3.17). A proper hydrodynamic is ensured by means of two built in stirring paddles for the aqueous and organic phases (Figure 3.17 B1). The aqueous phase paddle has a diameter of 3.0 cm and a height of 4.0 cm. The organic phase paddle has a diameter of 3.0 cm and a height of 1.0 cm. Additionally, a pH electrode (Figure 3.17 B7) monitors the pH during the entire experiment, thus acting as an input signal to drive the addition of acid and base titrants when needed. The vessel incorporates a thermometer and it is placed on a Peltier block device to monitor and maintain a constant temperature. The different reagents are added automatically into the beaker by means of fine capillaries (Figure 3.17 B3) built into a ceramic block. For each reagent, the dispense system includes a plunger pump to load and dispense the reagent individually.

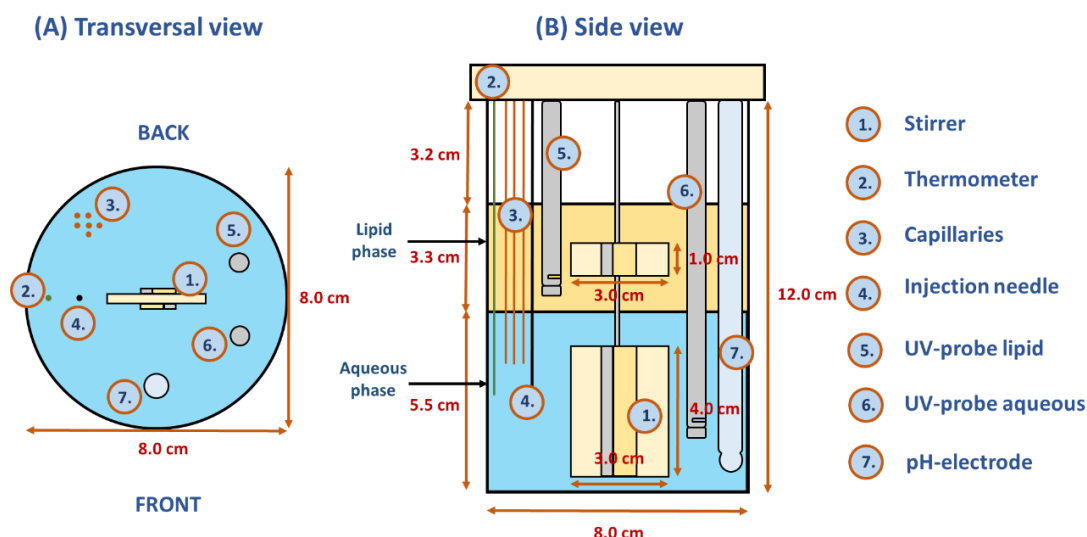


Figure 3.17: Schematic illustration of the dissolution vessel incorporated in the Pion inForm model. **A)** Transversal section showing the position of each spare part in the model. **B)** Side view reflecting two phases (aqueous and octanol) and the dimensions of the stirring paddles (1) and vessel. Volume of aqueous phase = 50 mL; volume of octanol phase = 30 mL.

3. MODEL

The different reagents include:

- 0.15 M NaCl. Medium.
- 0.5 M NaOH and 0.5 M HCl. Titrants to adjust pH.
- 0.1 M phosphate acetate buffer. Added in the form of a 4 mL aliquote to the aqueous phase.
- 1-octanol. Used only for the BDT. Due to the partial miscibility of 1-octanol with water, both phases were saturated with each other prior the experiment.
- Polymeric and API stock solutions were placed in an autosampler module and they were automatically added into the beaker by means of an injection needle (volume 5 – 4000 μL) (Figure 3.17 B4)

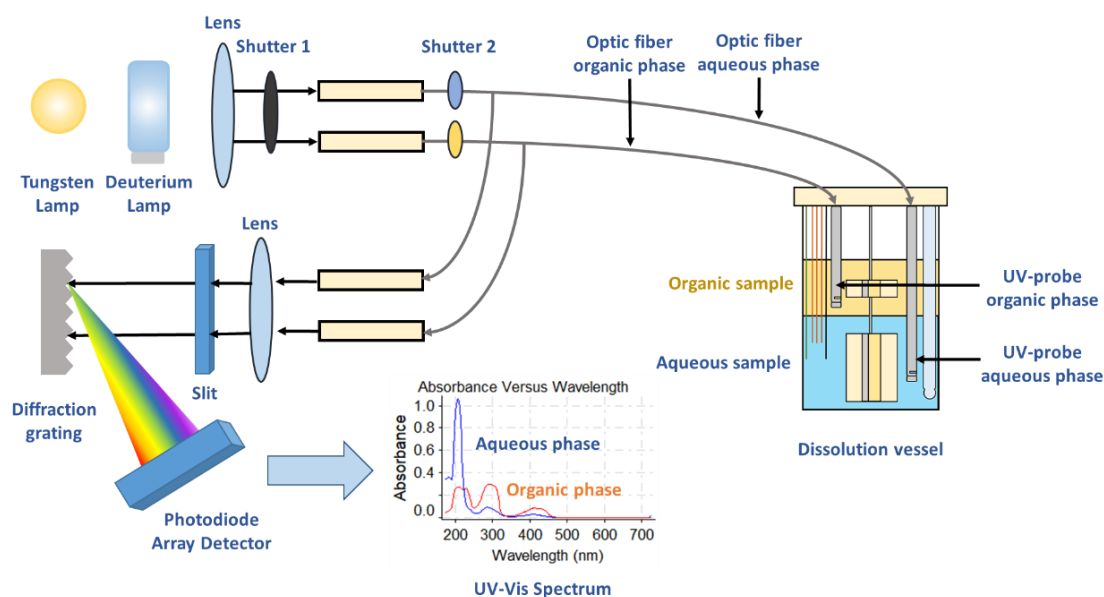


Figure 3.18: Schematic representation of UV-Vis bichannel spectroscopic system incorporated in the Pion inForm device. Adapted from Lu. et al, 2003.

Quantification is performed by means of *in situ* UV-Vis spectroscopy. The spectrometer used incorporates a Tungsten-Vis lamp and a Shimadzu UV- deuterium lamp (Figure 3.18). The UV- and Vis-light is merged and transferred through two Hellma UV-Vis immersion probes (Figure 3.17 B5, B6) made of optic fiber material. As shown in the figure, one probe quantifies the dissolved drug in the aqueous phase, while the second is immersed in the octanol phase, when present. The light transfer is controlled by two shutters (Figure 3.18). The position of the shutter blend 1 controls the light from the lamp into the optic fiber. The shutter blend 2 switches between both optic fibers, enabling the quantification in both phases if necessary. Each UV-Vis immersion probe incorporates a measurement window (Figure 3.19), whose path length can be adjusted depending on the molar extinction coefficients (MEC) and concentration range needed for each drug molecule. At the end of each measurement window, a small mirror reflects the transmitted light into a diffraction grating (polychromator). Subsequently, the diffracted light reaches a photodiode array detector (PDA), where the light intensity is converted into the absorbance signal for each wavelength and time point.

Due to the turbidity originated in a dissolution vessel, UV-fiber optic probes are not as accurate as an offline HPLC determination but have shown their usefulness and simplicity in *in situ* quantification (Chen and Brown, 1994; Josefson et al., 1988; Lu et al., 2003). Concretely, Chen and Brown reported the use of several optical fibers and a PDA spectrometer to track multiple dissolution vessels. The quantification principle used in all MDT and BDT experiments is similar as the one applied by Chen and Brown, as reflected in Figure 3.18.

In general, Tyndall and Rayleigh scattering phenomena in the aqueous phase are associated to turbidity due to precipitation events or the formation of nanostructures under the presence of certain pharmaceutical excipients (Kraemer and Dexter, 1927; Young, 1981) (Figure 3.19B). The Tyndall effect is the light scattering by particles in a colloid or in a very fine suspension and is observed when the particles ranges between 40 and 900 nm (below or near the wavelengths of visible light, 400 – 750 nm) in a light-transmitting medium, such as an aqueous solution. Rayleigh scattering is the light-scattering of far smaller particles than the visible light wavelength (roughly below 40 nm). Owing to the larger particle sizes involved, Tyndall scattering is much more intense than Rayleigh scattering. These two scattering effects cause a shift in baseline at non-absorptive wavelengths and a deformation of the obtained UV-Vis spectra, as described in the section 3.3.1.1 (Figure 3.7). This may cause an overestimation of the fractions of drug dissolved (Figure 3.20A). To solve this problem, the software inForm Refine 1.4.0.0 (Sirius Analytical Instruments Ltd., Forest Row, UK) incorporates a Tyndall-Rayleigh scattering correction tool that subtracts the scattered light from the spectra. With this purpose, the scattering correction is applied in a 20-40 nm range of the electromagnetic spectrum in which the baseline should be 0. At the same time, the selected wavelength should be as close as possible to the absorption peak (Figure 3.20B). Finally, the obtained corrected spectrum fits to the standard measurements performed in the MEC calibration.

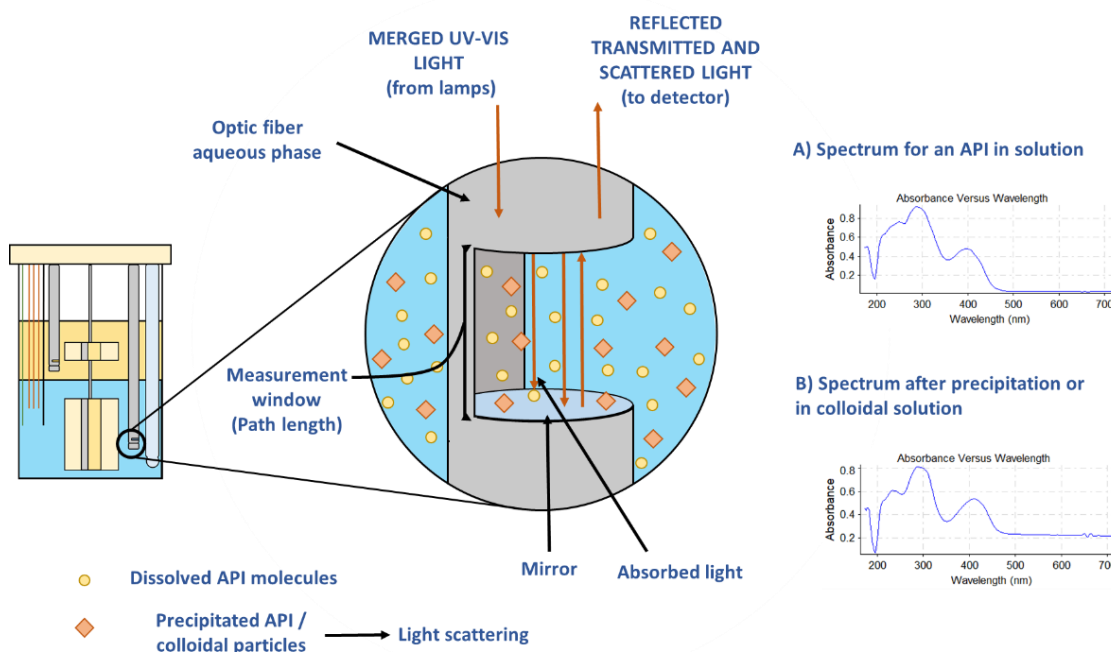


Figure 3.19: Schematic representation of a UV-Vis immersion probe and its function. **A)** Spectrum from a drug molecule in solution. **B)** Scattered spectrum after precipitation or in colloidal solution.

3. MODEL

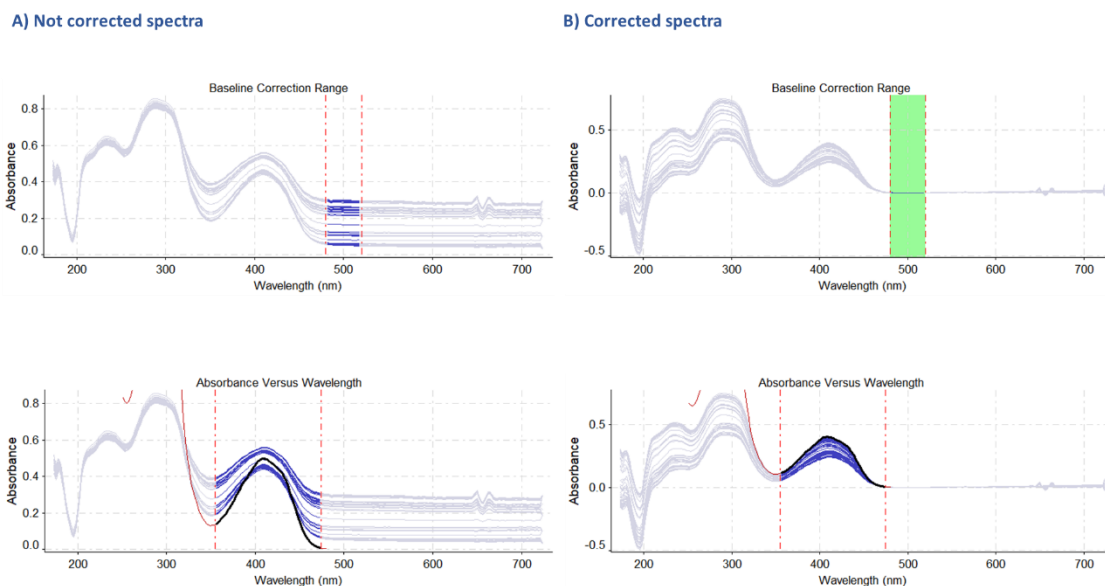


Figure 3.20: **A)** Non-corrected spectra for a precipitated Dipyridamole sample. The black spectrum represents a standard spectrum from the calibration curve. **B)** Corrected spectra after applying the Tyndall-Rayleigh scattering correction tool between 480 – 520 nm (top). The corrected dissolution spectra fit in this case with the standard spectra (bottom).

3.4.1.1.1 Experimental design

All dissolution tests were designed to simulate the pH shift under physiological conditions in the fasted state of a human GI tract (Asare-Addo et al., 2011; Koziolok et al., 2015a). The dissolution test was based on previous work from Gravestock *et al.* (Gravestock et al., 2011) including slight variations in the vessel geometry and further experimental conditions of the miniaturized model. In contrast to the work performed by Gravestock *et al.*, where the intrinsic dissolution rate (IDR) of different compacts was determined, the present work intends to evaluate *in vitro* the potential of supersaturation to delay precipitation in the GIT and to estimate BA changes *in vivo*. In this way, 4 pH intervals were defined to represent the gastric and the small intestinal transit. The Figure 3.21 shows a schematic comparison of the *in vitro* dissolution test and *in vivo* conditions. Briefly, the first pH interval (pH 1.2, duration = 15 min) corresponds to a fasted human stomach. A subsequent buffering to pH 5.5, pH 6.8 and pH 7.4 (45 minutes each) mimics the pH conditions of the duodenum, jejunum and ileum, respectively.

The time of each *in vitro* pH-intervals do not correlate with the *in vivo* transit time of the GIT segments, as reflected in the Figure 3.21. This deviation in time was applied to shorten the duration of the entire experiment. Due to the experimental purpose to differentiate between suitable and non-suitable drug-polymer combinations in terms of solubility enhancement and precipitation inhibition and to correlate them with supersaturation and solubilization mechanisms, a time reduction was favored over the precise imitation of *in vivo* conditions.

The administration of the drug molecules as a stock solution in DMSO instead of a solid dosage form, together with the high solubility of almost all selected drugs at low pH values, justifies the shortening of the first pH interval compared to the *in vivo* gastric transit times. The selection of similar length intervals (45 minutes) for the different intestinal pH-sectors, was applied to investigate the potential of the supersaturation in each gastrointestinal segment, independent of the real transit time.

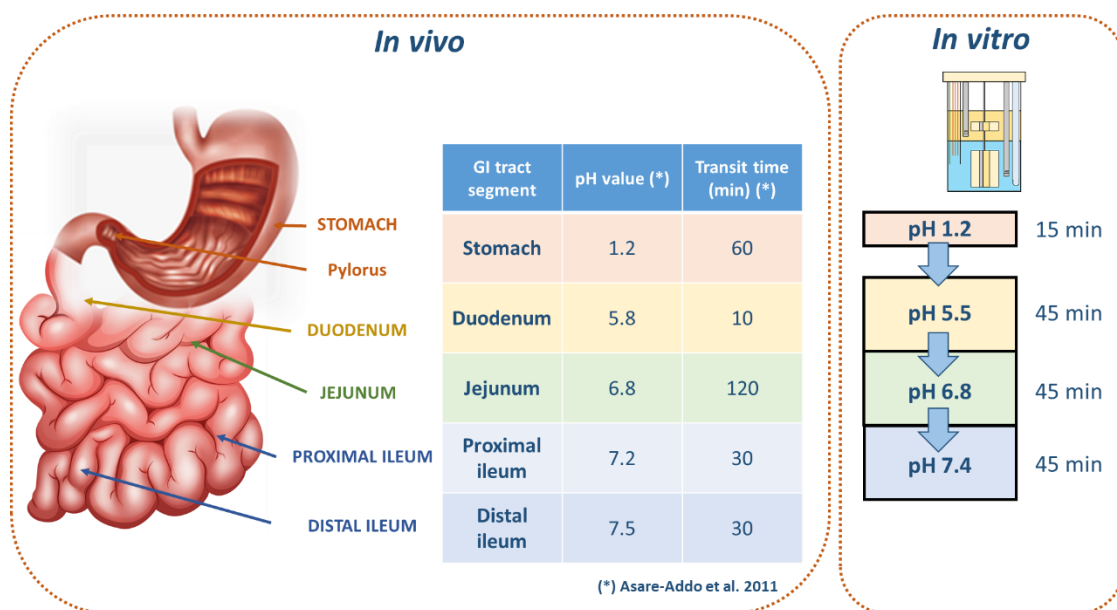


Figure 3.21: *In vitro* gastrointestinal dissolution approach (right) compared to *in vivo* physiological fasted conditions in the gastrointestinal tract (left). The pH sectors *in vitro* intend to simulate the different gastrointestinal segments.

3.4.2 Particle size distribution analysis

The particle size distribution analysis was accomplished with the aim of further investigating the potential of the polymers as precipitation crystal growth inhibitors. The offline characterization of precipitates was evaluated by means of laser diffraction spectrometry (LDS) or dynamic light scattering (DLS), depending on the size of the particle population obtained. In this work, the characterization was conducted after test end. Nevertheless, the precipitation and crystal growth phenomena are governed by kinetic processes (Brouwers et al., 2009) and should (when possible) be also investigated from a kinetic point of view.

3.4.2.1 Particle size analysis via Laser diffraction

Laser diffraction is a light scattering method applied for particle size distribution (PSD) analysis in the range from submicron to millimeter scale. This principle is based on the interaction between a laser beam and a particle population which is mathematically described by the Fraunhofer diffraction (Boer et al., 1987) and Mie scattering (Mie, 1908) theories. Normally, a single spherical particle produces a typical ring structure diffraction pattern. The diffraction pattern of a specimen and its intensity depend on the particle amount and size, respectively. In general, large particles generate small diffraction angles, while small particles produced larger diffraction angles with a monochromatic laser beam.

Several phenomena take place when a laser beam interacts with a particle. Amongst other, absorption, reflection, refraction and diffraction (Figure 3.22). The diffraction occurs when a wave encounters an obstacle (particle) or slit, resulting into the bending of these waves around the corners of this obstacle or through an aperture.

3. MODEL

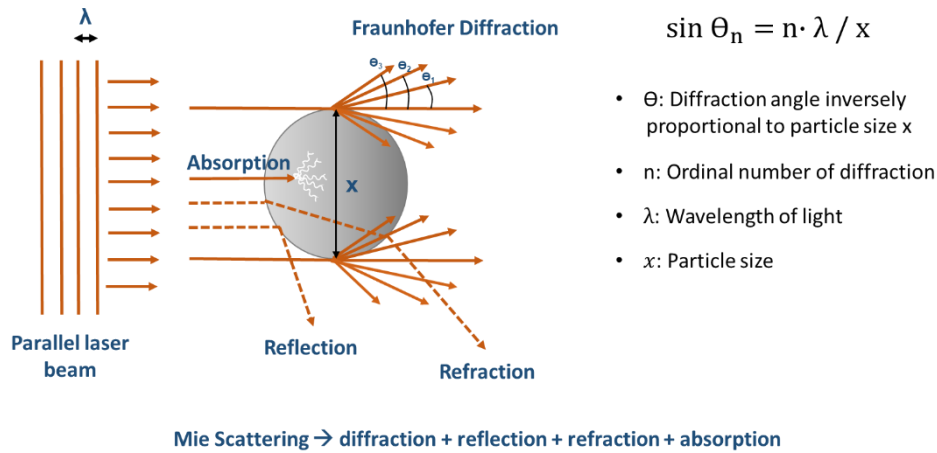


Figure 3.22: Schematic representation of Fraunhofer Diffraction Diffraction and Mie Scattering phenomena. Adapted from Sympatec GmbH Website (Clausthal-Zellerfeld, Germany)(Sympatec GmbH)

The Fraunhofer theory (Boer et al., 1987) considers just the diffraction at the contour of the particle in the near-forward direction, while the reflection, refraction and absorption terms are excluded. The Fraunhofer approximation is applicable to particle populations composed by different particle shapes and materials. Under these conditions, the particle sizes obtained under laser diffraction correspond to the equivalent diameter of a spherical particle with identical diffraction pattern. For a population with different particle sizes, a superposition of the diffraction patterns will occur as long as the diffraction between particles is negligible. In order to convert the diffraction patterns obtained into a PSD, the inversion process is accomplished by means of the Phillips-Twomey algorithm (Kenneth Wolfenbarger and Seinfeld, 1990; Phillips, 1962; Twomey, 1963).

The d_{10} , d_{50} and d_{90} indicate the particle diameters where the portion of particles are smaller than 10%, 50% and 90% of all particles, respectively (Hu et al., 2002; Lefebvre and McDonell, 2017). Similarly, the span index is used to describe the polydispersity in a given particle size distribution and is defined by the Equation 32.

$$Span = d_{90} - d_{10} / d_{50} \quad (\text{Equation 32})$$

3.4.2.2 Dynamic Light Scattering (DLS) / Photon Correlation Spectroscopy (PCS)

Dynamic Light Scattering (DLS) uses the principle of random changes in the intensity of scattered light from a suspension or colloidal solution. This effect is observed due to the Brownian motion, a stochastic motion of particles induced by random collisions with neighboring molecules (Chandrasekhar, 1943). The investigated particle samples are suspended in a solvent, whose molecules are much smaller than the considered particles. The bombardment of solvent molecules on the particles produces incessant particle movements in random directions within the solvent (Rudin and Choi, 2012). In this way, at equilibrium, the average velocity of the particles over infinite time is zero since the particles are moving in all directions with identical probability. This random particle motion is modelled by the Stokes-Einstein equation (Equation 28) (Einstein, 1905; Smoluchowski, 1906), which connects the diffusion coefficient measured by dynamic light scattering to particle size.

$$D_h = \frac{k_B T}{3\pi\eta D_t} \quad (\text{Equation 33})$$

D_h is the hydrodynamic diameter [nm], D_t is the translational diffusion coefficient (determined by DLS), k_B is the Boltzmann's constant [J/K], T is the temperature [K], η is the dynamic viscosity [$\text{N}\cdot\text{s}/\text{m}^2$]

Since D_h , which corresponds to a spherical particle which is diffusing similarly to the particle under investigation, is temperature and viscosity-dependent, both parameters must be kept constant during measurement. In general, the velocity of the Brownian motion is defined by the translational diffusion coefficient (D_t). It is inversely related to the particle size (large particles = lower Brownian motion/ smaller particles = faster Brownian motion). Furthermore, D_t depends on the surface structure and on the ionic strength, as well as the type of ions present in the mixture.

The extent in Brownian motion is transferred into PSD using a correlation function by means of several algorithms applying the Stokes-Einstein equation (Equation 33). Finally, a particle size population is defined by:

- Z-average (Z_D). Defined as the intensity weighed mean diameter derived from a cumulant analysis. This parameter is very sensitive to the presence of aggregates or contaminants, according to the inherent intensity weighing.
- PDI. A dimensionless measure of the broadness of the size distribution calculated from a cumulant analysis. This factor typically ranges between 0 – 1. A value > 1 can be considered as an indicator for an extremely polydisperse sample that may not be suitable for DLS determination. A sample achieving a DLS of < 0.2 is assumed to be monodisperse.

3.4.3 Polarized Light Microscopy

Polarized Light Microscopy (PLM) was applied to investigate the physical state of the precipitates (amorphous vs. crystalline particles), to evaluate their shape and to confirm the PSD obtained under laser diffraction. Due to the use of visible light, only precipitates in the micron range can be analyzed.

PLM uses a polarizing filter (polarizer) which generates a light beam vibrating in a single plane. When this polarized light is transmitted through a birefringent sample (crystalline, anisotropic), that has not the identical optical properties in all directions, to the second filter (analyzer), the rays do not cancel each other when they are recombined (described as *out-of-phase*). This is translated as an interference of colors that shows bright colorful samples under a dark background, which is mainly observed for crystalline specimen. On the other side, when polarized light is transmitted through a sample which has identical optical properties in all directions (amorphous, isotropic), the rays formed are *in phase* with each other, as they travel at the same speed rate through the substance. As a result, a destructive interference in the analyzer takes place, canceling the rays so that no samples can be seen under a cross polar set up.

3. MODEL

3.5 Part III: Supersaturation and solubilization in the gastrointestinal tract and its relevance for oral bioavailability: an *in vitro* vs. *in vivo* approach

Following the investigation of the supersaturated state from a physicochemical and *in vitro* biorelevant point of view, the validation of the hypotheses established in the above-mentioned approaches (see sections 3.3 and 3.4) was performed by transferring three case studies (celecoxib, telmisartan and itraconazole) into an *in vivo* model. These drug molecules were selected based on the relevance of the results obtained in the physicochemical and *in vitro* biorelevant approaches. In accordance with the goals established in the present work, the selection was accomplished on the aim of demonstrating the broad spectrum of effects that the supersaturation and solubilization of drug molecules can cause in the GI tract, as well as their influence on the oral absorption and BA.

With the aim of highlighting the potential predictive power of the biphasic dissolution test (BDT) approach and its ability to establish *in vitro in vivo* correlations (IVIVC), the BDT was additionally performed with the inclusion of biorelevant surfactants, thus generating a simulated intestinal fluid (SIF). The potential of the supersaturation effect to conduct changes in the partition of drugs into the organic phase was mathematically compared to the changes produced in the oral BA using Sprague-Dawley male albino rats as an *in vivo* model. This rodent model was preferred to mice according to an easier handling and to the broad establishment of this strain in the field of oral bioavailability investigations.

3.5.1 Blood extraction and quantification

In general, the extraction of drug molecules and their metabolites from the blood samples (Figure 3.23) involved the precipitation of water-soluble proteins and other components by means of metal salts. This was followed by a stepwise extraction of the drug molecules with organic solvents and subsequent solvent evaporation under nitrogen stream. A reconstitution with a mobile phase solvent, followed by centrifugation and filtration, completed the extraction procedure. The extraction procedure was based on previously published and validated methods, as described in detail within the section 4.2.3. For each drug molecule, the procedure differed in terms of the metal salts and organic solvents used. In general, the extraction was directly performed from blood samples and not from plasma in order to avoid the sedimentation of the drug fraction bounded to the red blood cells.

3.5 Part II: Supersaturation and solubilization in the gastrointestinal tract

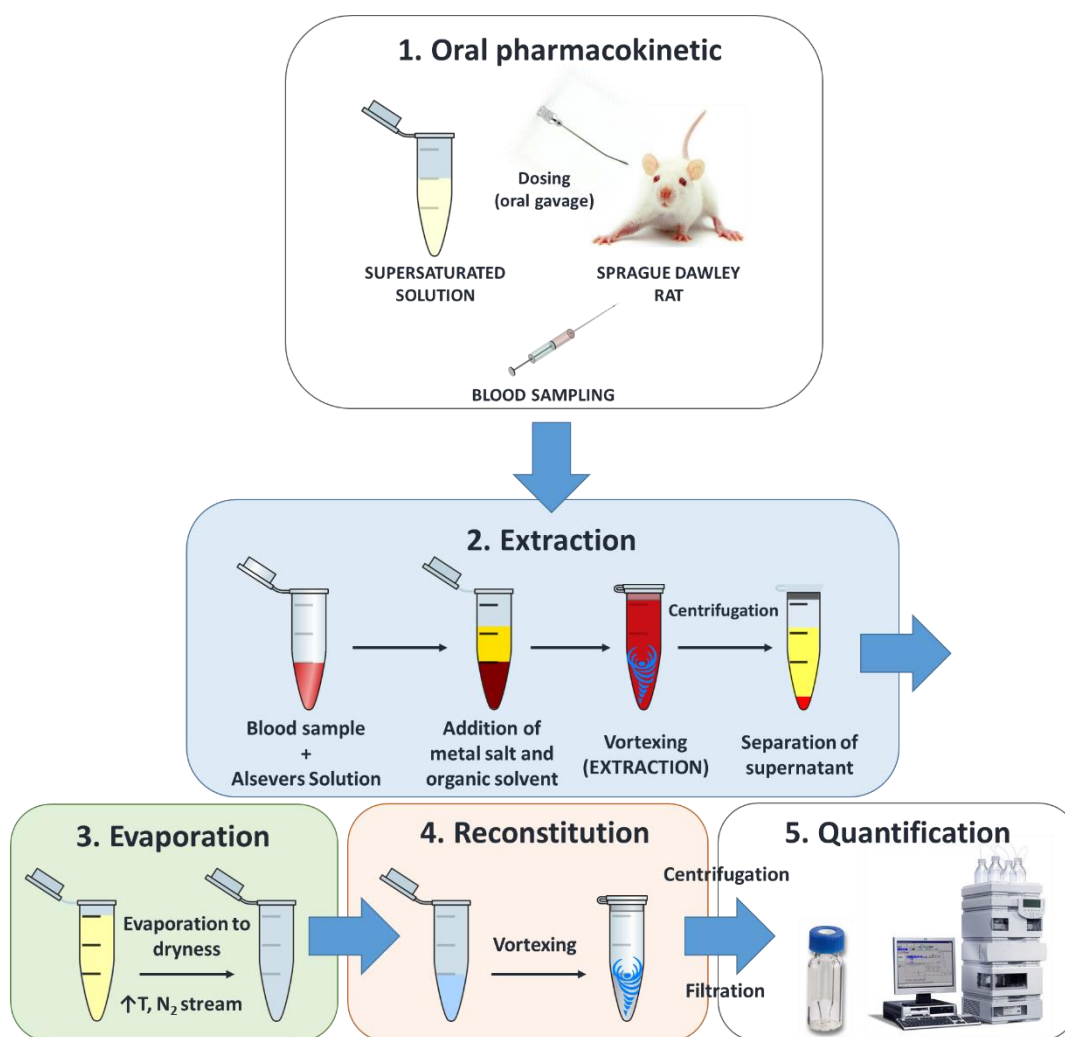


Figure 3.23: General blood sample preparation procedure. The extraction was performed by means of vigorous vortexing in the presence of organic solvents. Subsequently this was evaporated to dryness and reconstituted with mobile phase upon quantification.

3.5.2 Pharmacokinetic parameter calculation

Different pharmacokinetic (PK) parameters were calculated using the Kinetica 7.0 software. The obtained PK profiles were fitted to an extravasal mono-compartmental model and the pharmacokinetic parameters area under the curve (AUC), maximum concentration (C_{max}), maximum concentration time (t_{max}), elimination constant (K_e), half-life ($t_{1/2}$) and mean residence time (MRT) were calculated.

3. MODEL

3.5.3 Deconvolution and IVIVC calculation

At the final step, to evaluate the ability of the biphasic dissolution approach to act as a biopharmaceutical *in vitro* tool to predict oral BA, an IVIVC was established between the *in vitro* % fractions of drug partitioned into the organic phase and the % fractions of drug absorbed *in vivo* (

Figure 3.24). With this purpose, a Wagner-Nelson deconvolution (Margolskee et al., 2015; Wagner and Nelson, 1964) was performed using the obtained *in vivo* pharmacokinetic profiles to calculate the fractions of absorbed drug. The resulting absorption curves were fitted to an exponential Box-Lucas function (Equation 34). Subsequently, as described by the US FDA Guidance for Industry for the elaboration of IVIVC (FDA, 1997), a time scaling factor was estimated by the means of a Levy Plot (Cardot and Davit, 2012) to make *in vitro* and *in vivo* data (partition in the organic phase and oral absorption, respectively) superimposable. A single time scaling factor was calculated for all formulations of each drug, so that the obtained IVIVC became quantitatively comparable. Finally, the % fraction absorbed *in vivo* was calculated using the previously determined time scaling factor and it was correlated to the *in vitro* % fraction partitioned into the octanol absorptive compartment using numerical regression. The slope of the obtained correlation, as well as the coefficients of determination (R^2) were used to evaluate the accuracy of the prediction. *In vivo* relative bioavailabilities (BA_{rel}) were taken into consideration for the calculation of the time scaling factor and for the establishment of the IVIVC.

$$y = a(1 - e^{-bx}) \quad \text{(Equation 34)}$$

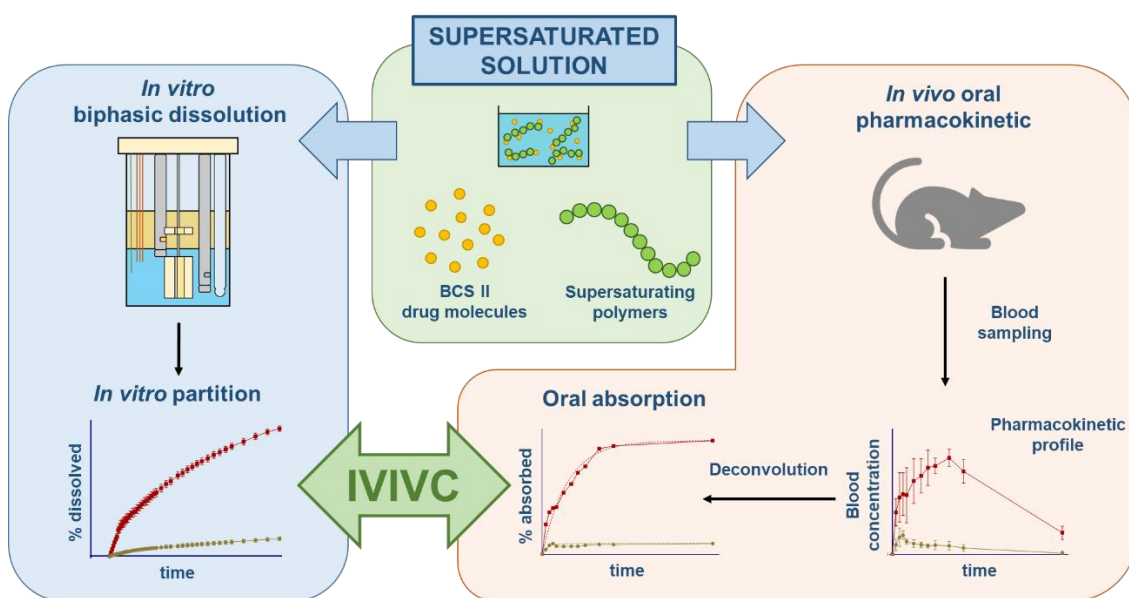


Figure 3.24: Schematic representation of the *in vitro* and *in vivo* approaches accomplished, including the establishment of an IVIVC between the drug fraction partitioned *in vitro* and absorbed *in vivo*.

4 Experimental

4.1 Materials

4.1.1 Equipment

Table 4.1: Devices used for all experiments

DEVICE NAME	TYPE	MANUFACTURER/SUPPLIER
Analytical balance	AG 204	Mettler Toledo GmbH, Gießen, Germany
Analytical balance	Extend ED224S	Sartorius Lab Instruments GmbH & Co. KG, Goettingen, Germany
Centrifuge	Centrifuge 5804 R	Eppendorf Vertrieb Deutschland GmbH, Wesseling-Berzdorf, Germany
Centrifuge	Universal 320 R	Andreas Hettich GmbH & Co. KG, Tuttlingen, Germany
Cuvettes	Silica glass	Hellma Analytics, Müllheim, Germany
Drying oven	UNB 200	Memmert GmbH & Co. KG, Schwabach, Germany
Eppendorf tubes	Eppendorf safelock tubes 1.5 / 2 mL	Eppendorf Vertrieb Deutschland GmbH, Wesseling-Berzdorf, Germany
HPLC Photodiode Array Detector	Waters 996	Waters Corporation, Milford, Massachusetts, USA
HPLC System 1	Alliance 2695 Separations module	Waters Corporation, Milford, Massachusetts, USA
HPLC System 2	Agilent 1220 Infinity	Agilent Technologies GmbH, Bensheim, Germany
Laboratory balance	PB5001-S	Mettler Toledo GmbH, Gießen, Germany
Laser diffraction system	Helos/KF	Sympatec GmbH, Clausthal-Zellerfeld, Germany
Magnetic stirrer and heating plate	MSH basic Yellow Line	IKA-Werke GmbH & Co. KG, Staufen, Germany
Magnetic stirrer and heating plate	IKA Combimag RCH	IKA-Werke GmbH & Co. KG, Staufen, Germany

4. EXPERIMENTAL

Magnetic stirrer and heating plate	RCT standard safety control	IKA-Werke GmbH & Co. KG, Staufen, Germany
Microscope camera	QImaging MicroPublisher 5.0 RTV Camera	QImaging, Surrey, British Columbia, Canada
Nanoparticle analyzer	nanoPartica SZ-100	Horiba Jobin Yvon GmbH, Bensheim, Germany
pH-meter	Inolab pH 720	Xylem Analytics Germany GmbH & Co. KG, WTW, Weilheim, Germany
Pion inForm		Pion Inc (UK) Ltd., Forest Row, East Sussex, UK
Pipette	500-5000 µL; 100-1000 µL; 10-100 µL; 2-20 µL	Eppendorf Vertrieb Deutschland GmbH, Wesseling-Berzdorf, Germany
Polarized Light Microscope	Leica DM2700 M	Leica Camera AG, Leitz-Park GmbH, Wetzlar, Germany
Rotary evaporator	Laborota 4000 efficient	Heidolph Instruments GmbH & Co. KG, Swabach, Germany
Sample concentrator	Techne Dri-Block DB 3A	Bibby Scientific, Staffordshire, UK
Shaking water bath	1083	GFL Gesellschaft für Labortechnik GmbH, Burgwedel, Germany
Pion SiriusT3		Pion Inc (UK) Ltd., Forest Row, East Sussex, UK
Sprague-Dawley rats	Sprague-Dawley male albino rats (250 - 300 g)	Janvier Labs (Le Genest-Saint-Isle, France)
UV-Vis Spectrophotometer	Agilent 8453	Agilent Technologies GmbH, Bensheim, Germany
Vortex mixer	Vibrofix VF1 Electronix	Janke & Kunkel GmbH & Co. KG IKA-Werk, Staufen, Germany
Water purification system	Elga Purelab Ultra IO MK2 system	Elga Labwater (High Wycombe, UK)

4.1.2 Excipients and chemicals

Table 4.2: Chemicals and excipients used for all experiments

CHEMICAL / EXCIPIENT	LOT NR.	MANUFACTURER/SUPPLIER
Acetonitrile for HPLC LC-MS grade	Several Lots.	VWR Chemicals, Fontenay-sous-Bois, France
Alsever's solution	RNBG3860	Sigma Aldrich Co Ltd, Irvine, UK
Dimethylsulfoxide	BCBG6914V	Sigma-Aldrich Chemie GmbH, Taufkirchen, Germany
Di-sodium hydrogen phosphate di-hydrate (Na ₂ HPO ₄ ·2H ₂ O)	K42147380 113	Merck KGaA, Darmstadt, Germany
Hydrochloric acid (0.1 N)	Several Lots.	Sigma-Aldrich Chemie GmbH, Taufkirchen, Germany
Hydrochloric acid (0.5 N)	Several Lots.	Carl Roth GmbH & Co. KG, Karlsruhe, Germany
Lecithin, refined	N23C070	ThermoFisher (Kandel) GmbH, Karlsruhe, Germany
Methanol (AnalaR NORMAPUR)	15J290518	VWR Chemicals, Fontenay-sous-Bois, France
Methanol, ≥ 99.8% HPLC grade	Several Lots.	VWR Chemicals, Fontenay-sous-Bois, France
Methocel A4C Premium Methylcellulose (MA4C)	DT360478	Colorcon, Kent, UK
Nitrogen	--	University of Bonn, Bonn, Germany
Nitrogen	--	University of Bourgogne Franche-Comté, Besançon, France
1-Octanol, 99%	Several Lots.	ThermoFisher (Kandel) GmbH, Karlsruhe, Germany
Orion™ pH 7.0 Buffer	VV1	Thermo Scientific
Polyvinyl caprolactam-polyvinyl acetate-polyethylene glycol graft copolymer (Soluplus, SOL)	500071	BASF SE, Ludwigshafen, Germany
Potassium chloride for Analysis (EMSURE®)	Several Lots.	Merck KGaA, Darmstadt, Germany
Potassium dihydrogen phosphate ≥ 98%, Ph. Eur.	Several Lots.	Carl Roth GmbH & Co. KG, Karlsruhe, Germany
Purified water	--	Millipore water purification system, University of Bonn, Bonn, Germany
Purified water	--	Elga Purelab Ultra IO MK2 purification system, University of Bourgogne Franche-Comté, Besançon, France
Sodium acetate trihydrate	SZBE078AV	Sigma-Aldrich Chemie GmbH, Taufkirchen, Germany

4. EXPERIMENTAL

Sodium chloride p.A.	Several Lots.	neoFroXX GmbH, Einhausen, Germany
Sodium hydroxide concentrate, 1.0 mol, FIXANAL	Several Lots.	Sigma-Aldrich Chemie GmbH, Taufkirchen, Germany
Sodium hydroxide	SZBF2850V	Sigma-Aldrich Chemie GmbH, Taufkirchen, Germany
Sodium phosphate monobasic monohydrate	BCBL5442V	Sigma-Aldrich Chemie GmbH, Taufkirchen, Germany
Sodium taurocholate hydrate, 96%	N02C026	ThermoFisher (Kandel) GmbH, Karlsruhe, Germany
Toluene	SZBF2710V	Sigma-Aldrich Chemie GmbH, Taufkirchen, Germany
Triphenylene	LC10004V	Supelco, Bellefonte, PA, USA
Vinylpyrrolidone-vinyl acetate copolymer (Kollidon VA64, KVA64)	004638; 801328; 409777	BASF SE, Ludwigshafen, Germany

4.1.3 Drug substance and formulation

Table 4.3: Drug substances and formulation used

DRUG SUBSTANCE / FORMULATION	LOT NR.	MANUFACTURER/SUPPLIER
Albendazole (ABZ)	MKBR9649V	Sigma-Aldrich Chemie GmbH, Taufkirchen, Germany
Candesartan (CDS)	CDS/1393910	Swapnroop drugs and pharmaceuticals, Maharashtra, India
Celecoxib (CLX)	CEL/16010032	Swapnroop drugs and pharmaceuticals, Maharashtra, India
Dipyridamole (DPD)	DPM/022/09/15	Swapnroop Drugs and Pharmaceuticals, Aurangabad, India
Hydroxyitraconazole 100 µg/mL in methanol (OH-ITZ)	FN09281502	Sigma-Aldrich Inc., St. Louis, MO, USA
Itraconazole (ITZ)	ITC/1509133	SRIS Pharmaceuticals, Hyderabad, India
Ketoconazole, 98% (KTZ)	M09A019	ThermoFisher (Kandel) GmbH, Karlsruhe, Germany
Loratadine (LTD)	LRHB5183	SRIS Pharmaceuticals, Hyderabad, India
Phenytoin (PHY)	PB/07/16	JPN Pharma PVT Ltd, Maharashtra, India
Telmisartan (TLM)	PDTEL1507002	SRIS Pharmaceuticals, Hyderabad, India
Sporanox® 100 mg capsules	HDL8N01	Janssen-Cilag GmbH, Neuss, Germany

4.2 Experimental conditions

4.2.1 Part I: Physicochemical properties of poorly soluble API in colloidal solutions and their relationship with supersaturation and oral bioavailability

4.2.1.1 UV-metric pK_a titration

For all tested drugs, pK_a s were determined by means of the UV-metric method. Experiments were designed as a multiset, for each of which three titrations were performed in different methanol/water mixtures. If feasible, cosolvent ratios of 50, 40 and 30% v/v were applied to not compromise the linearity of the method. Solely for those drugs which precipitated at a certain point of the experiment, cosolvent ratios up to 60% v/v were used. Depending on the physicochemical properties of the drug molecules used, titrations were performed from low to high pH (weak bases) or from high to low (weak acids). 0.5 M HCl and 0.5 M NaOH were used as titrants. Following a predefined experimental protocol, medium (NaCl 0.15 M) and cosolvent (methanol 80%) were automatically added to the test vessel. To evaluate the influence of water-soluble polymers on the ionization of poorly soluble drugs, the excipients were pre-dissolved in 0.15 M NaCl as a 2.5% (w/V) stock solution and aliquots were automatically pipetted into the medium to achieve polymer concentrations of 0.031, 0.062, 0.125 and 0.250% w/V prior to the addition of the drug. Subsequently, 100 μ L from a 10 mM stock solution of the drug in DMSO were added and stirred at 300 rpm and 25 °C during the entire measurement. A UV-spectrum was recorded at each pH point to ensure the reliability of the TFA outcome. The pK_a values and apparent pK_a (p_sK_a) were plotted as a function of the polymer concentration to identify potential interaction mechanisms as a response to supersaturation and/or solubilization.

4.2.1.2 Solubility determination by means of potentiometric titration

15-20 mg of drug powder was weighed into the Pion inForm glass beaker and this was placed into the autosampler to schedule subsequent measurements. 40 mL of medium (0.15 M NaCl) was automatically added into the beaker. Aliquots of the polymeric stock solution (2.5% w/V) were automatically added to the medium prior to the beginning of the experiment to achieve the desired polymer concentration of 0.031, 0.062, 0.125 and 0.250 %w/V. For all weak bases, as well as for the zwitterionic drug telmisartan (TLM), the pH was adjusted to 2.0 by means of 0.5 M HCl. For the weak acid celecoxib (CLX), the pH was initially adjusted to pH 12.0 to allow a complete drug dissolution. The dissolution segment was in all cases 2 minutes at 300 rpm. Subsequently, the titration was performed with 0.5 NaOH or 0.5 M HCl, respectively until the drug first precipitated. The precipitation point was recorded UV-metrically and, depending on the behavior of the sample (chaser or non-chaser), the crossing point or the curve fitting method was applied. Stirring was kept constant at 300 rpm and the temperature was set to 25 °C by means of a thermometer and a Peltier device system during the entire measurement. The pH was constantly controlled by means of an inForm pH electrode and provided the dpH/dt . The evaluation of the data was performed manually by means of the inForm software (Sirius Analytical Instruments Ltd., Forest Row, UK, version 1.4.0.0). Following the refinement of the data, the kinetic and intrinsic solubility, as well as the pH-dependent solubility profile were calculated.

4. EXPERIMENTAL

4.2.1.3 Solubility determination by means of shaking flask method

Following the European Pharmacopoeia (Ph. Eur.) 8th edition guidelines for itraconazole (ITZ) and albendazole (ABZ) solubility determinations, a pH 6.8 KH₂PO₄ / Na₂HPO₄ buffer (ionic strength= 0.05 M) was prepared. In the case of telmisartan, a pH 5.5 KH₂PO₄ buffer (ionic strength= 0.05 M) was selected, according to its zwitterionic nature and the respective low solubility in the pH range of approximately 5 – 5.5. In the case of LTD, the solubility was determined in both media.

All KVA64, MA4C and SOL polymeric solutions were prepared in the required buffer at a concentration of 2.5% (w/V) by stirring overnight at 25°C and 250 rpm. Aliquots of the polymeric stock solutions were pipetted into Erlenmeyer flasks and diluted with the respective buffer to achieve the desired polymer concentrations of 0.031, 0.062, 0.125 and 0.250 % w/V. Subsequently, and following the solvent shift method (Warren et al., 2010; Yamashita et al., 2011), the drugs were transferred into the polymeric solutions as aliquots of highly concentrated stock solutions in DMSO. The target concentration was 0.2 mg/mL for ABZ and ITZ, 0.16 mg/mL for TLM and 0.04 mg/mL for LTD. The drug concentrations were based on the therapeutic doses (when possible the highest available dose) divided by 250 mL, following a previously reported protocol in the literature (Qiu et al., 2009). Nevertheless, the variation in drug concentration should not affect the thermodynamic solubility value as long as non-sink conditions were generated. The final volume was in all cases 20 mL. For comparison, the solubility of the pure drug in the buffer was additionally measured and all determinations were performed in triplicate.

The prepared supersaturated solutions were shaken in a 1083 shaking water bath (GFL Gesellschaft für Labortechnik GmbH, Burgwedel, Germany) at 25 °C for 72 hours. After this time, it was assumed that equilibrium conditions were reached and the concentration of drug in solution represents the intrinsic solubility. The samples were subsequently filtered through a 25 mm 0.45 µm cellulose acetate membrane syringe filter and quantified by means of liquid chromatography in an Alliance 2695 Separations module (Water corporation, Milford, Massachusetts, USA), using a C₁₈ 250 x 4.6 mm Lichrospher 100 RP 18-5 µm EC column and a 10 x 4 mm Lichrospher 100 RP 18-5 µm EC precolumn (Chromatographie Service GmbH, Langerwehe, Germany) as stationary phase.

For ABZ and ITZ, the isocratic chromatographic method described by Miller (Miller et al., 2008a) was applied to prepare the calibration curves. Absorbance was recorded at 260 nm for ABZ and 235 nm for ITZ, according to their maximum absorbance wavelengths (λ_{max}) under these chromatographic conditions. ITZ achieved an elution time of 16.9 minutes, while ABZ was eluted at 4.9 minutes. The samples were not further diluted prior to injection and the injection volume was 100 µL in all cases.

TLM samples were quantified using the same chromatographic system and stationary phase. The mobile phase and chromatographic method were selected based on a previous publication (Sengupta et al., 2017). The calibration curve and quantification were performed by using the absorbance signal at 298 nm and the injection volume was 100 µL. Under these chromatographic conditions, TLM eluted at 5.8 minutes.

Due to technical reasons, LTD samples were not quantified by means of liquid chromatography but directly by UV spectroscopy by using an Agilent 8453 UV-vis spectrophotometer (Agilent

4.2 Experimental conditions

Technologies GmbH, Bensheim, Germany). The calibration curves for quantification were performed at 244 nm, corresponding to the λ_{max} value.

4.2.1.4 Lipophilicity determination: chromatographic method

A Waters 2695 Separation Module coupled with a Waters 996 Photodiode Array Detector was used. Aligned with the described method (Donovan and Pescatore, 2002), a 20x 4.0 mm, 5 μ m 250 Armstrong pore size, ODP-50 cartridge column (Supelco, distributed by Sigma-Aldrich) was selected as stationary phase due to its highly retentive capacity for lipophilic compounds. A linear gradient of 10 – 100% methanol in 10 minutes was used as mobile phase at a 1.50 mL/min flow rate. This chromatographic condition gave a linear relationship between the retention times and literature $\text{Log}P_{ow}$ ($\text{Log}P$ coefficient in octanol-water) of the drug used.

To ensure the presence of the drug molecules' neutral form to avoid interactions with the stationary phase, the aqueous mobile phase was composed of a 0.01 M Na_2HPO_4 buffer, adjusted to a certain pH with 0.1 M NaOH or 0.1 M HCl and finally filtered through a 0.2 μ m pore size cellulose acetate filter membrane under vacuum. Depending on the ionization properties of the molecules, pH values were adjusted to 10.0 (DPD, LTD and ITZ) or 8.0 (ABZ and CLX). Due to the zwitterionic behavior of TLM, the chromatographic lipophilicity determination method was unfeasible, since there is no pH value in which the molecule is fully neutral. For all other drugs analyzed under the chromatographic method, samples were prepared at a concentration of 1 mg/mL (except for ITZ: 0.33 mg/mL) in a methanol cocktail containing two internal standards (IS):

- Toluene: 2 mL →
 - Triphenylene: 20.0 mg →
- Diluted to 200 mL with Methanol**

5 μ L from each sample was injected into the system. The analyte and the two IS were eluted at different retention times following the chromatographic protocol described above. The selection of the two standards is related to their lipophilicity: toluene is a very low lipophilic molecule, while triphenylene presents an extremely lipophilic structure (Figure 3.14).

4.2.1.5 Rheological characterization

For the rheological characterization, a water-cooled RotoVisco RV1 of Thermo Fisher (Karlsruhe, Germany), equipped with a double gap cylinder geometry DG43 (DIN 53544), was used. As a measuring method, the following procedure was performed for all experiments:

1. Constant rotational ramp from a shear rate of 100 s^{-1} to 3000 s^{-1} in 180 seconds
2. A constant shear rate of 3000 s^{-1} for 30 seconds
3. Constant rotational ramp from a shear rate of 3000 s^{-1} to 100 s^{-1} in 180 seconds

To compare the measured viscosity for all samples at measuring conditions, which led to a valuable result due to the applied shear rate, the listed viscosity is the measured viscosity at a shear rate of 500 s^{-1} .

4. EXPERIMENTAL

4.2.2 Part II: *In vitro* evaluation of the supersaturation and solubilization potential to enhance oral bioavailability

4.2.2.1 Monophasic and biphasic dissolution tests

4.2.2.1.1 Polymer and API stock solutions preparation

Polymeric stock solutions were prepared in the experimental medium (0.15 M NaCl) and were stirred overnight at 300 rpm at room temperature. A concentration of 3.125% (w/V) was selected for SOL and KVA64 stock solutions. In the case of MA4C, a 1.25% (w/V) concentration was used. A higher concentrated solution would result in an increased viscosity, which would impede later a proper administration into the system. The preparation of the MA4C stock solution was based on the Colorcon guidelines for the preparation of Methocel™ aqueous solutions (Colorcon, 2009). Through the addition of polymeric solution aliquots (Table 4.4) into the test medium, the identical polymer concentrations were targeted as for the UV-metric pK_a and solubility determinations (sections 4.2.1.1 and 4.2.1.2).

The drugs were added as a DMSO stock solution following the described solvent shift method in section 1.4.1. The total DMSO fraction in the total volume of the aqueous phase was $\leq 1\%$ to prevent artifacts on the solubility of the APIs.

4.2.2.1.2 Pretests

The aqueous medium selected to perform *in vitro* dissolution tests was 0.15 M NaCl (26 mL), buffered with 4 mL of a 0.1 M acetate-phosphate buffer. The initial volume of 0.15 M NaCl varied, depending on the desired polymer concentration. Driven by the addition of 10 mL of 0.5 M HCl, the pH was automatically adjusted to the initial pH 1.2. At this time point, if needed, the addition of certain aliquots of the polymeric stock solutions was performed automatically (Table 4.4) for KVA64 and SOL by means of the injection needle (Figure 3.17B4). Due to the higher viscosity of the MA4C stock solution, these aliquots were manually added prior the start of the test. By adding the polymer before the drug, a pre-dissolution of the polymer was ensured to evaluate its potential on the drug in terms supersaturation and precipitation inhibition. Subsequently, the drug stock solution was automatically added into the medium (Table 4.5). Prior the beginning of the gastric phase (pH 1.2), the total volume was always 40 mL.

Table 4.4: Polymer stock solution aliquots administered to MDT and BDT.

Polymer	Concentration Stock Solution (%w/V)	Volume stock solution (μ L)	Target concentration (%w/V)	Final aqueous phase volume (mL)
None (Ref)	0	0	0	50
KVA64	3.125	500	0.031	50
		1000	0.062	
		2000	0.125	
		4000	0.250	
MA4C	1.25	1250	0.031	50
		2500	0.062	
		5000	0.125	
		10000	0.250	
SOL	3.125	500	0.031	50
		1000	0.062	
		2000	0.125	
		4000	0.250	

3. EXPERIMENTAL

Table 4.5: Therapeutic doses, biorelevant concentrations and preparation of API stock solutions in DMSO.

API	Therapeutical dose (mg)	Dose / 250 mL (mg/mL)	Concentration Stock solution (mg/mL)	Volume stock solution (µL)	DMSO Concentration (% V/V)	API (mg)	Target concentration (mg/mL)	Final volume aqueous phase (mL)	Path length (mm)
DPD	75	0.3	50	400	0.8	20	0.4	50	1
ABZ	100	0.4	20	500	1	10	0.2	50	1
ITZ	100	0.4	20	500	1	10	0.2	50	1
LTD	10	0.04	20	100	0.2	2	0.04	50	20
TLM	40	0.16	15	535	1.07	8	0.16	50	1
CLX	100	0.4	40	250	0.5	10	0.2	50	1

4. EXPERIMENTAL

4.2.2.1.3 Test and parameters investigated

After the gastric phase (pH 1.2), 10 mL of 0.5 M NaOH was automatically added to obtain pH 5.5 and simulate the upper small intestine (duodenum). By the addition of small base aliquots, the pH was subsequently adjusted to mimic the jejunum and ileum without exceeding an aqueous phase volume of 50 – 51 mL.

For all BDT experiments, 30 mL of 1-octanol were automatically dispensed right after the first pH shift (pH 1.1 → pH 5.5) (Figure 4.1B). The organic phase acted as a sink absorptive compartment during the 3 final pH sectors and represented the absorption through enterocytes throughout the small intestine into the portal vein and passing to systemic circulation. The partition kinetics into the octanol phase are mainly driven by the fraction of drug dissolved or solubilized in the aqueous phase and thus accessible for partition, as well as by the lipophilicity of the compound. This approach potentially simulates the absorption through passive diffusion and consequently, it is an *in vitro* model suitable to investigate whether the supersaturation and solubilization improve the oral bioavailability *in vivo* (Pestieau and Evrard, 2017).

To evaluate the effectiveness of the water-soluble polymers in terms of supersaturation and partition enhancement, several parameters were investigated (Figure 4.1):

- Monophasic dissolution tests (MDT, Figure 4.1A)
 - Area under the curve (AUC). Defines the fraction of drug dissolved or solubilized in the intestinal precipitation test phase. It was used to compare the extent of supersaturation in the aqueous phase achieved by the polymer in comparison to the pure drug. It is calculated as the sum of the areas obtained for each time interval throughout the test (Equation 35) The AUC was calculated by the GraphPad Prism 8 software (GraphPad Software, San Diego, CA, USA), following the trapezoidal rule (Tallarida and Murray, 1987)
 - Average precipitation rate (dC/dt). It defines indirectly the ability of the polymers to act as precipitation or crystal growth inhibitors. The average precipitation rate was calculated by dividing the concentration difference (dC) occurring in a defined time frame (dt) (Equation 36).
 - Precipitation time (t_p). When the drug precipitates during the full length of the intestinal phase, the precipitation time equals the total length of the three intestinal intervals (pH 5.5, 6.8 and 7.4 period → 135 minutes). Otherwise, the t_p was equal to the time difference between the beginning of the pH 5.5 intestinal phase and the time at which the drug fully precipitated (concentration in solution ≈ 0 $\mu\text{g/mL}$)
 - Particle size distribution (PSD). Conducted as offline measurement after test end by means of laser diffractometry or dynamic light scattering (DLS) to investigate potential precipitation and crystal growth inhibition by the polymers.
 - Physical state characterization of precipitates (crystalline/ amorphous) by means of offline Polarized Light Microscopy (PLM) after test end.
- Biphasic dissolution tests (BDT, Figure 4.1B)
 - Area under the curve aqueous phase (AUC_{aq}). Defined as the fraction of drug dissolved during the precipitation period in the aqueous phase. Represents an indicator of supersaturation and describes the fraction of drug “accessible” to partition into the organic compartment.

3. EXPERIMENTAL

- Area under the curve organic phase (AUC_{oc}). Defined as the fraction of drug partitioned during the precipitation period into the organic phase. Represents the fraction of drug bioavailable *in vivo*.
- Partition rate (PR). Represents the speed at which the drug partitions into the organic phase. It is affected by the polymer used and its ability to supersaturate the drug in solution. At the same time, it can be decelerated due to specific or unspecific interactions between the polymer and drug molecules which can be attributed to solubilization. The partition rate was calculated in $\mu\text{g/mL/min}$ by fitting the BDT results to a first order kinetic, similar to the Noyes-Whitney equation (Dokoumetzidis and Macheras, 2006; Noyes and Whitney, 1897). This fitting tool is incorporated in the inForm Refine 1.4.0.0 software.

$$AUC = \sum_{i=0}^n \frac{1}{2} (C_{n-1} + C_n)(t_n - t_{n-1}) \quad (\text{Equation 35})$$

$$dC/dt = \frac{(C_0 - C_p)}{(t_p - t_0)} \quad (\text{Equation 36})$$

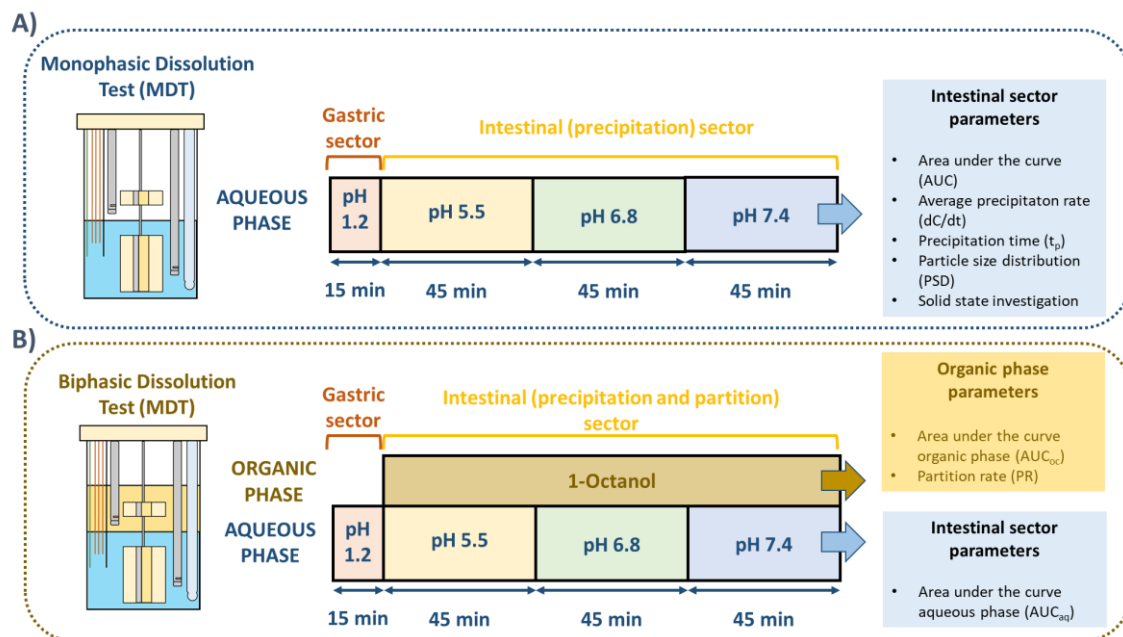


Figure 4.1: Schematic representation of the MDT (A) and BDT (B) approach designs and the parameters calculated from the experimental results.

4.2.2.2 Particle size analysis via laser diffraction

Particle Size Distribution determinations were performed on a Helos/KF Laser diffraction sensor manufactured by Sympatec GmbH (Clausthal-Zellerfeld, Germany). The system produces a laser beam with a diameter of 26 mm and incorporates a Fourier lens (focal length adjusted to 100 mm, 200 mm or 500 mm, depending on the obtained PSD). Since precipitation from a

4. EXPERIMENTAL

supersaturated solution is kinetically controlled and it depends on the experimental conditions, irregular sized and shaped particles were obtained and the Mie theory could not be applied. Therefore, the PSDs were determined by the Fraunhofer theory. 10 ml samples from the MDT were diluted with 30 mL of similar buffer medium (pH 7.4) to prevent redissolution or further precipitation of the particles. The sample (40 mL) was transferred into a 50 mL quartz cuvette with an optical path of 20 mm, especially designed for suspensions. The quartz cuvette was positioned on a dispersing unit, perpendicular to the laser beam (angle: 0°). The homogenization of the sample during measurement was performed by a PTFE-coated magnetic stirrer. Due to the fragility of the precipitated particles, stirring rate was set to a low speed (100 rpm) to ensure a proper homogenization but also avoiding particle breakage. The data collection and evaluation were performed by the software Windox 3.4 (Sympatec GmbH, Clausthal-Zellerfeld, Germany) to calculate the PSD, median PS (d_{50}) and the span value.

4.2.2.3 Dynamic light scattering (DLS)/ Photon correlation spectroscopy (PCS)

Turbid samples obtained from MDT (end point, $t = 150$ minutes), for which PSD determinations under laser diffraction conditions was not feasible, were analyzed by means of DLS. 10 mL of these samples were transferred to 15 mL Falcon tubes and centrifuged for 5 minutes at 4500 rpm, 25 °C and 1 mL of the supernatant was immediately transferred to a PTFE cuvette to determine the PSD. Determinations were performed in a nanoPartica SZ-100 nanoparticle analyzer (Horiba Jobin Yvon GmbH, Bensheim, Germany) using a diode pumped, frequency doubled laser as light source ($\lambda = 532$ nm, 10 mW) and photomultiplier tubes as a detector. The system had a particle size measuring range of 0.3 nm to 8 μm and was operated at a 173° measurement angle without sample dilution. Each measurement was composed of 10 single determinations at 25 °C (room temperature) or 37 °C (physiological temperature). If saturation of the detector occurred by an excessive amount of particles, the samples were diluted in NaCl 0.15 M and PSDs were detected by means of the side detector (90° measurement angle).

Samples with a PDI ≤ 0.2 were considered to follow a monodisperse distribution. No changes in viscosity of the colloidal solutions were found for all containing SOL and KVA64 samples, compared to pure water. In the case of MA4C, the viscosity was taken into consideration, as it is inversely related to the hydrodynamic diameter as described by the Stokes-Einstein equation (Equation 33).

4.2.2.4 Polarized light microscopy (PLM)

Micrographs were taken by means of a Leica DM2700 M polarized light microscope (Leica Camera AG, Leitz-Park GmbH, Wetzlar, Germany) equipped with a QImaging MicroPublisher 5.0 RTV camera (QImaging, Surrey, British Columbia, Canada). Lighting of the samples is performed with a universal white light (4500 K) LED illumination with a fully integrated power supply. The system incorporates a Koehler condenser to ensure a Koehler illumination of the sample (even illumination and absence of the light source filaments in the resulting image) when the transmitted light mode is applied. N plan series achromatic objectives were built into the microscope to allow 10x, 20x and 50x magnifications of the samples, multiplied by the ocular magnification factor (10x). For each sample magnification, a calibration was performed by means of a microscope calibration slide and a calibration tool incorporated in the software.

Following these calibrations, a size determination was enabled for each analyzed precipitate sample.

To differentiate between crystalline and amorphous precipitates, polarized light was used. Following the *crossed polars transmitted light* mode, both polarizer and analyzer were perpendicularly positioned (90° angle) to each other. To allow the birefringence observation (when present), the sample stage was rotated to 45° angle position in relation to the polarizers. In this way, the maximum brightness could be ensured.

The suspensions in aqueous medium from the MDT (after test end, 150 minutes) were shortly homogenized by slight shaking to ensure a representative sample when a small amount was withdrawn to be placed on a glass slide. A coverslip was added and the sample was finally mounted on the circular rotating stage and analyzed at various magnifications, starting from 100x and following with 200x and 500x. Under these settings, the morphology of the precipitates, as well as the particle size distribution were confirmed (for particles in the micron range). More importantly, the differentiation between crystalline and amorphous precipitates was performed. This supported in many cases the understanding of the obtained MDT results. For those cases in which the amount of particles in suspension was too large, samples were diluted accordingly with pH 7.4 0.15 M NaCl.

Micrographs were recorded using a QCapture Pro 7 Software (QImaging, Surrey, British Columbia, Canada). The software was also applied to adjust the white-balance of the images by selecting an auto white-balance modus. Similarly, the color balance and brightness were adjusted in those cases where this was necessary.

4.2.3 Part III: Supersaturation and solubilization in the gastrointestinal tract and its relevance for oral bioavailability: an *in vitro* vs. *in vivo* approach

4.2.3.1 *In vitro* biphasic dissolution tests (BDT)

In vitro BDTs were carried out simulating biorelevant GI tract conditions by means of the fully automated Pion inForm instrument (Figure 3.17), following a similar experimental setup as for the previously described BDT (Figure 4.1B). To differentiate the normal BDT approach from the biorelevant version, the fasted state simulated intestinal fluid (FaSSIF) BDT will be referred as FaSSIF-BDT. The medium of the gastric pH interval was maintained, a 0.1 M HCl solution in 0.15 NaCl (36 mL) and 4 mL of a 0.1 M phosphate-acetate buffer. The concentrations of the surfactants sodium-taurocholate (NaTC) and lecithin were maintained at the identical level as for the FaSSIF Version 2 (FaSSIF-V2) (Fuchs and Dressman, 2014; Jantratid and Dressman, 2009). Following the procedure described by Denninger and co-workers (Denninger et al., 2020), NaTC (272.3 mg) and lecithin (26.0 mg) were solubilized in 1100 µL demineralized water. At the end of the gastric pH interval, 333 µL of the surfactant concentrate were added to simulate the composition of the upper intestinal milieu. Finally, the pH was adjusted to 5.5 by the addition of 10 mL of 0.5 M NaOH, and subsequently readjusted to pH 6.8 and 7.4 with the same titrant. The volume of the aqueous phase during the three intestinal pH intervals was kept constant in the range of 50.5 ± 0.5 mL.

4. EXPERIMENTAL

Due to the partial miscibility of the aqueous phase with 1-octanol (Denninger et al., 2020), both solvents were saturated within each other prior measurement. 30 mL of saturated 1-octanol were added to the dissolution vessel prior to the start of the pH 5.5 interval. All other experimental parameters such as stirring rate, T and quantification were adjusted as described in the section 4.2.2.1. In those cases, in which the absorbance signal was scattered due to the presence of precipitated particles in the aqueous medium, the signal was corrected manually by means of the incorporated Tyndall-Rayleigh scattering correction tool (Figure 3.20), as previously described in the literature (Colombo et al., 2017).

The target concentrations for CLX, TLM and ITZ in the aqueous phase were 0.2, 0.16 and 0.2 mg/mL, respectively. These were selected based on the highest available dose divided by 250 mL, which allowed a proper quantification and correction of the absorbance signals under the described experimental conditions. The polymer concentration for all trials was 0.031 % w/V, corresponding to a polymer/drug ratio (w/w) of 1.55 for CLX and ITZ, and 1.94 for TLM. Following the extensively reported solvent-shift method (section 1.4.1), the drug was added prior to the beginning of the test as a concentrated stock solution in DMSO to the 0.1 M HCl medium where the polymer had been previously dissolved following the schema described in the Table 4.4 and Table 4.5.

4.2.3.2 *In vivo* pharmacokinetics

All animal experiments were performed in accordance with the Guide for the Care and Use of Laboratory Animals (Institute for Laboratory Animal Research, National Research Council, 2010). *In vivo* PK studies were conducted at the University of Bourgogne Franche-Comté (Besançon, France) in compliance with the French legislation and European Community Guidelines on animal experimentation under the project “Project Exp An N2 EA4267 2015-2020”, previously supervised and accepted by the ethical committee CEBEA 58. 200 g Sprague Dawley male albino rats were acclimatized to laboratory conditions for one week in a ventilated room at 22°C and 45% relative humidity with a 12 hours light/ 12 hours darkness cycle, preceding the start of the experiments. Food and water were supplied *ad libitum*.

Sprague Dawley rats were maintained in fasted conditions with free access to water for 12 h prior to the start of the experiments. The water-soluble polymers were initially dissolved in a 0.1 M HCl solution and the drugs were dissolved in DMSO as highly concentrated stock solutions with the help of ultrasonication, as previously performed *in vivo* in other studies (Strindberg et al., 2020). Right before administration, a small fraction of the drug stock solution was transferred into the polymeric solution, thus generating a partially supersaturated solution, which had the identical polymer/ drug ratio (1.55 for CLX and ITZ, and 1.94 for TLM, w/w) as for the *in vitro* experiments. For comparison, the identical procedure was performed for the pure drug, transferring the aliquots of the DMSO stock solution into 0.1 HCl medium without polymer. In all cases, doses of 30, 16 and 30 mg/kg weight for CLX, TLM and ITZ respectively, were orally administered (n=4) to 250 – 350 g rats using a gastric gavage tube. The doses were selected based on the sensitivity of the analytical method, so that low drug fractions absorbed into the blood stream could be subsequently quantified. Blood samples were withdrawn at predefined time points (0, 0.5, 1, 1.5, 2, 3, 4, 5, 6, 8, 10 and 24 h) from the caudal vein and diluted at similar volume ratios (1:1) with Alsevers solution, immediately weighed, vortexed and refrigerated at 4°C for further extraction and analysis on the same day.

4.2.3.3 Extraction and quantification of CLX

The extraction of CLX and its metabolites from blood samples was performed following the method validated by Ma et al. (Ma et al., 2015) with slight variations. Briefly, a „salting-out liquid-liquid extraction“ (Kole et al., 2011) was carried out with the purpose of making the blood sample immiscible with the organic solvent. 5 μL of the internal standard phenytoin (PHY) stock solution in methanol was first added to the refrigerated blood sample to generate a PHY concentration of 2000 ng/mL. Subsequently, 50 μL of a saturated NaCl solution was added to the blood sample followed by the addition of 500 μL of acetonitrile (ACN). The mixture was vigorously vortexed for 1 minute and the extraction process was repeated once more. Centrifugation was performed for 15 minutes at 12000 G in a 5804R Centrifuge (Eppendorf Vertrieb Deutschland GmbH, Wesseling-Berzdorf, Germany) and the supernatant was subsequently transferred to a new tube. The organic solvent ACN was evaporated in a Techne Dri-Block DB 3A Sample Concentrator (Bibby Scientific, Staffordshire, UK) at 70 °C under constant nitrogen stream. Samples were reconstituted with 250 μL of the mobile phase, further centrifuged and filtered through a 13 mm 0.45 μm pore diameter PTFE Membrane Syringe Filter. Quantification was achieved by reversed-phase chromatography in an Agilent 1220 Infinity HPLC System coupled with a UV-DAD detector using a C_{18} 250 x 4.6 mm Lichrospher 100 RP 18-5 μm EC column coupled with a 10 x 4 mm Lichrospher 100 RP 18-5 μm EC precolumn (Chromatographie Service GmbH, Langerwehe, Germany). A methanol-water 75:25 (% v/v) eluent in isocratic mode was selected as mobile phase at a flow rate of 1.0 mL/min following the method validated by Baboota and co-workers (Baboota et al., 2007). Injection volumes were kept constant at 100 μL for all samples. Detection was performed at 264.5 nm for CLX and PHY and a sharp peak was obtained for CLX at a retention time of 7.836 ± 0.092 min, while the internal standard PHY was eluted at 3.863 ± 0.110 min. Linear regression analysis showed a good correlation between the responses and CLX:PHY peak ratios in the range of 25 – 3500 ng/mL ($R^2 = 0.9987$). Extraction recoveries of $90.71 \pm 2.13\%$ were achieved.

4.2.3.4 Extraction and quantification of TLM

The extraction of TLM from blood samples was performed as described by Sengupta and co-workers (Sengupta et al., 2017) including slight variations in the method. Candesartan (CDS) was selected as internal standard and 5 μL of a high concentrated CDS aliquot in methanol was added to the blood sample prior to the extraction to achieve a concentration of 1000 ng/mL. Extraction from blood samples was performed in two steps under vigorous vortexing using dichloromethane (DCM) as organic solvent. After centrifugation at 1800 G for 15 minutes, supernatants were separated and evaporated at 40 °C under constant nitrogen stream. Samples were reconstituted with 250 μL of the mobile phase, centrifuged at 1800 G for 10 minutes and filtered through a 13 mm 0.45 μm PTFE Membrane Syringe Filter. The extraction procedure showed a mean recovery rate of $98.12 \pm 1.81\%$. The identical chromatographic system was used as for the CLX samples. The TLM samples were quantified using the method validated by (Wankhede et al., 2007) with slight variations. Elution of the analytes was performed using ACN - 0.05 M KH_2PO_4 buffer adjusted to pH 3.0, 60:40 (% v/v) as mobile phase. Detection was performed at 298.4 nm for both TLM and CDS standard. Sharp peaks were obtained for CDS and TLM at retention times of 3.957 ± 0.001 and 5.532 ± 0.005 minutes, respectively. Linear regression analysis of the TLM/CDS peak ratios showed a good correlation between the responses and concentrations in the range of 25 – 2000 ng / mL ($R^2 = 0.9971$).

4. EXPERIMENTAL

4.2.3.5 Extraction and quantification of ITZ

The extraction of ITZ was performed directly from the blood samples following a “salting-out liquid-liquid extraction”, as it was used for CLX. Ketoconazole (KTZ) was selected as internal standard and 5 μL KTZ stock solution in methanol was added to each blood sample and vortexed to achieve a KTZ concentration of 1000 ng/mL previous to the extraction procedure. Subsequently, 200 μL of a 1 M $\text{H}_3\text{BO}_3\text{-Na}_2\text{CO}_3\text{-KCl}$ buffer solution were added to facilitate the precipitation of blood proteins. The extraction was performed in two steps with tert-butyl-methyl ether (TBME). First, 500 μL of the organic solvent were added into the sample and vigorously vortexed for 1 minute. As next step, 1 further mL of TBME was transferred into the tube and the mixture was vortexed for 2 minutes to enable an efficient extraction of the drug and active metabolites. Subsequently, the samples were centrifuged for 5 minutes at 2000 rpm, allowing the sedimentation of insoluble components and the separation of both phases. The organic phase was transferred to new tubes and evaporated under a constant nitrogen stream at 50 °C. Finally, the samples were reconstituted with 250 μL of mobile phase, vortexed for 1 minute and centrifuged for 15 minutes at 3000 G. Finally, 150 μL of the supernatant were filtered through a 13 mm 0.45 μm PTFE Membrane Syringe Filter and directly transferred into HPLC vials. The extraction procedure showed a mean recovery rate of 93.57 ± 2.61 % for OH-ITZ and 90.55 ± 0.81 % for ITZ. The identical chromatographic system was used as for the CLX and TLM samples. Samples were quantified using the method validated by Miller and co-workers (Miller et al., 2008a) with slight adaptations. Elution of the analytes was performed using ACN - 0.05 M KH_2PO_4 buffer adjusted to pH 6.7, 62:38 (% v/v) as mobile phase. Detection was performed at 264.5 nm for both KTZ, OH-ITZ and ITZ. Sharp peaks were obtained for KTZ, OH-ITZ and ITZ at retention times of 5.965 ± 0.003 , 7.151 ± 0.004 and 16.912 ± 0.009 minutes, respectively. Linear regression analysis of the OH-ITZ/KTZ and ITZ/KTZ peak ratios showed a good correlation between the responses and concentrations in the range of 25 – 2000 and 50 – 2000 ng/mL, respectively. The coefficients of determination R^2 obtained for both calibration curves were 0.9980 and 0.9994, respectively.

5 Results and discussion

5.1 Part I: Physicochemical properties of poorly soluble API in colloidal solutions and the relation to supersaturation and oral bioavailability

5.1.1 Ionization constant and pK_a

The apparent changes in the ionization properties of ionizable drug molecules in the presence of water-soluble polymers were determined by means of UV-metric pK_a titration using cosolvents, as described in the sections 3.3.1.1 and 4.2.1.1. It provided a first differentiation between supersaturating and solubilizing stabilization mechanisms. As introduced within the section 3.3.1.1.2, the solubilization approaches potentially decrease the “truly” molecularly dissolved drug fraction and shift the acid-base equilibria established in aqueous solution. As a result, the shape of the pK_a -curve as a function of the polymer concentration facilitated the understanding of the interaction between the polymer and drug at a molecular level. Exponential and sigmoidal curves were associated to solubilization effects or to a polymer excess causing and steric hindrance. Linear curves with a slope (k) close to 0 indicated the absence of solubilization effects, but for which a supersaturation effect cannot be excluded. The presence or absence of supersaturation will be further investigated and confirmed by using a kinetic approach (see section 5.2).

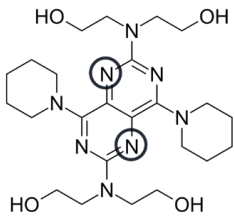
In the present work, four weak bases, one weak acid and one ampholyte drug were investigated, leading to the corresponding pK_a shifts in both directions as a function of the ionizable groups in the respective molecule, as depicted in the Figure 3.8.

Interestingly, for all drugs, the largest shifts in ionization were mainly observed in the presence of SOL (Figure 3.9, Equations 18 and 19). Regarding its amphiphilic structure, a solubilization of the drugs through micellization is highly expected, as demonstrated in the sections 5.1.2, 5.2.1 and 5.2.2. Therefore, changes in the ionization equilibria were associated to the polymer concentration and followed an exponential decay 1 in all cases.

Regarding KVA64 and MA4C, the pK_a shifts were mainly minor. The trends observed were related to specific drug/ polymer combinations, since no mathematical trend was applicable to all drug molecules when using the identical polymer. These observations will be further discussed in more detail and it will be correlated with the overall changes observed in drug solubility and lipophilicity within this chapter.

5. RESULTS AND DISCUSSION

5.1.1.1 Dipyrnidamole

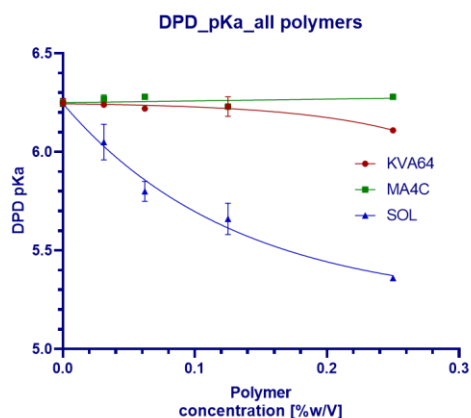
<p>Dipyrnidamole</p>  <p>$pK_a: 6.25 \pm 0.02$ (B)</p>	<p>Phys.-chem. properties</p>	Acid/ base	Weak base
		pK_a	6.25 ± 0.02
		Chemical group involved	Pyrimidine nitrogen (2x)
		H-Donor/H-acceptor count ⁽¹⁾	4 (OH- groups) / 12 (N- atoms)
<p>pK_a shifts present? Best fitting?</p>	KVA64	YES → EXPONENTIAL DECAY 2	
	MA4C	NO → LINEAR	
	SOL	YES → EXPONENTIAL DECAY 1	

⁽¹⁾ ChemAxon database

A)

[Polymer]	0%	0.031 %	0.062 %	0.125 %	0.250 %
KVA64	6.25 ± 0.02	6.24 ± 0.01	6.22 ± 0.00	6.23 ± 0.05	6.11 ± 0.01
MA4C		6.27 ± 0.02	6.28 ± 0.01	6.23 ± 0.01	6.28 ± 0.01
SOL		6.05 ± 0.09	5.80 ± 0.05	5.66 ± 0.08	5.36 ± 0.01

B)



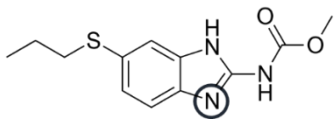
DPD pKa shifts (R^2 , k)				
Fitting		KVA64	MA4C	SOL
Linear	R^2	-	0.999	-
	k	-	0.090	-
Exponential	R^2	0.958	-	0.974
	k	-12.077	-	7.675

Figure 5.1: A) DPD pK_a and apparent pK_a (pK_a^{app}) (green) B) Graphical scheme and curve fit. The R^2 values represent the best fitting for each polymer.

In Figure 5.1, the following observations were made:

- KVA64. The observed exponential decay 2 and the negative decay constant (k) supported a polymeric molar excess at a concentration of 0.250% w/V which limited the accessibility of the drug species to participate in the acid-base equilibria.
- MA4C. The linear trend and the low constant ($k= 0.090$) indicated the absence of changes in the ionization equilibria.
- SOL. The exponential trend and the positive decay constant supported a polymer concentration-dependent solubilization effect.

5.1.1.2 Albendazole

<p style="text-align: center;">Albendazole</p>  <p style="text-align: center;">$pK_a: 4.13 \pm 0.02$ (B)</p>	<p style="text-align: center;">Phys.-chem. properties</p>	<p style="text-align: center;">Acid/base</p>	Ampholyte: Weak base / weak acid (not biorelevant)
		<p style="text-align: center;">pK_a</p>	4.13 ± 0.02 (B) / 9.51 (A)
		<p style="text-align: center;">Chemical group involved</p>	Imidazole nitrogen
	<p style="text-align: center;">H-Donor/H-acceptor count ⁽¹⁾</p>	2 (NH- groups) / 3 (imidazole N and ester group)	
<p style="text-align: center;">pK_a shifts present? Best fitting?</p>	<p style="text-align: center;">KVA64</p>	YES → SIGMOIDAL	
	<p style="text-align: center;">MA4C</p>	NO → LINEAR	
	<p style="text-align: center;">SOL</p>	YES → EXPONENTIAL DECAY 1	

⁽¹⁾ ChemAxon database

A)

[Polymer]	0%	0.031 %	0.062 %	0.125 %	0.250 %
KVA64	4.13 ± 0.02	4.13 ± 0.02	4.12 ± 0.02	4.08 ± 0.00	4.03 ± 0.03
MA4C		4.14 ± 0.03	4.15 ± 0.02	4.13 ± 0.02	4.14 ± 0.02
SOL		3.97 ± 0.01	3.87 ± 0.02	3.72 ± 0.02	3.52 ± 0.03

B)

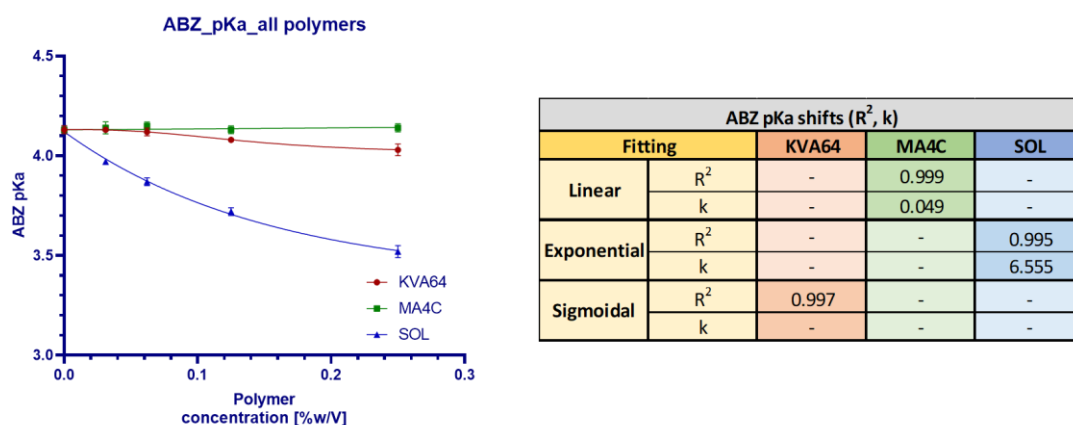


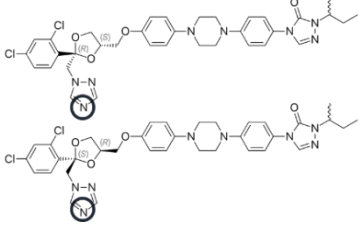
Figure 5.2: A) ABZ pK_a and apparent pK_a (pK_a^{app}) (green) B) Graphical scheme and curve fit. The R^2 values represent the best fitting for each polymer.

In Figure 5.2, the following observations were made:

- KVA64. The sigmoidal trend indicated the absence of changes in the acid-base equilibria at low polymer concentrations, while at higher polymeric concentrations, a concentration-dependent effect was found. The changes in the ionization equilibria were the result of the formation of drug-polymer complexes which reduced the molecularly dissolved drug fraction in the polymeric solution.
- MA4C. The linear trend and the low constant ($k= 0.049$) indicated the absence of changes in the ionization equilibria.
- SOL. The exponential trend and the positive decay constant supported a concentration-dependent solubilization effect through micellization.

5. RESULTS AND DISCUSSION

5.1.1.3 Itraconazole

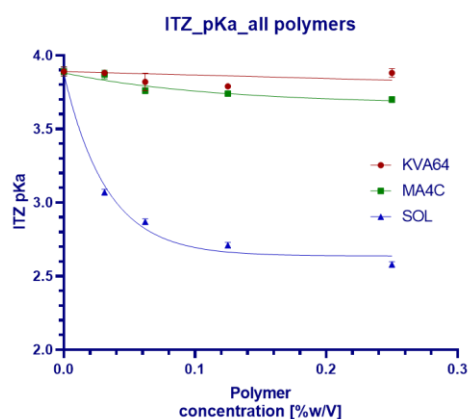
<p style="text-align: center;">Itraconazole</p>  <p style="text-align: center;">pK_a: 3.89 ± 0.03 (B)</p>	Phys.-chem. properties	Acid/ base	Weak base
		pK_a	3.89 ± 0.03
		Chemical group involved	Triazole nitrogen
		H-Donor/H-acceptor count ⁽¹⁾	0 / 9 (heterocyclic amines and carbamide)
pK_a shifts present? Best fitting?	KVA64	NO → LINEAR	
	MA4C	YES → EXPONENTIAL DECAY 1	
	SOL	YES → EXPONENTIAL DECAY 1	

⁽¹⁾ ChemAxon database

A)

[Polymer]	0%	0.031 %	0.062 %	0.125 %	0.250 %
KVA64	3.89 ± 0.03	3.88 ± 0.01	3.82 ± 0.06	3.79 ± 0.01	3.88 ± 0.03
MA4C		3.87 ± 0.03	3.76 ± 0.02	3.74 ± 0.01	3.70 ± 0.02
SOL		3.07 ± 0.02	2.87 ± 0.02	2.71 ± 0.02	2.58 ± 0.02

B)



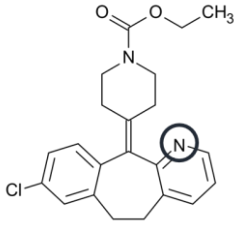
ITZ pKa shifts (R^2 , k)				
Fitting		KVA64	MA4C	SOL
Linear	R^2	0.999	-	-
	k	-0.237	-	-
Exponential	R^2	-	0.839	0.981
	k	-	11.831	30.769

Figure 5.3: A) ITZ pK_a and apparent pK_a (pK_a^{app}) (green) B) Graphical scheme and curve fit. The R^2 values represent the best fitting(s) for each polymer.

In Figure 5.3, the following observations were made:

- KVA64. The linear trend and the low constant ($k = -0.237$) indicated the absence of changes in the ionization equilibria.
- MA4C. The exponential trend and the positive decay constant supported a concentration-dependent effect and the decrease in the molecularly dissolved fraction in solution induced through a solubilization effect.
- SOL. The exponential trend and the large decay constant ($k = 30.769$) supported a concentration-dependent effect, as well as a high solubilization extent through micellization.

5.1.1.4 Loratadine

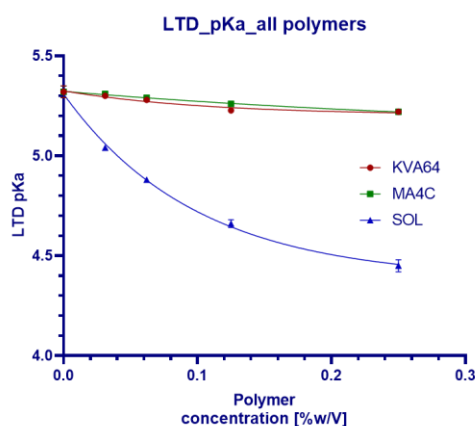
Loratadine  $pK_a: 5.32 \pm 0.03$ (B)		Acid/ base		
		Phys.-chem. properties	pK_a	Weak base
			Chemical group involved	5.32 ± 0.03
			H-Donor/H-acceptor count ⁽¹⁾	Pyridine nitrogen
pK_a shifts present? Best fitting?	KVA64	0 / 2 (heterocyclic amine and carbamide)		
	MA4C	YES → EXPONENTIAL DECAY 1		
	SOL	YES → EXPONENTIAL DECAY 1		

⁽¹⁾ ChemAxon database

A)

[Polymer]	0%	0.031 %	0.062 %	0.125 %	0.250 %
KVA64	5.32 ± 0.03	5.30 ± 0.01	5.28 ± 0.01	5.23 ± 0.01	5.22 ± 0.01
MA4C		5.31 ± 0.01	5.29 ± 0.01	5.26 ± 0.01	5.22 ± 0.01
SOL		5.04 ± 0.01	4.88 ± 0.00	4.66 ± 0.02	4.45 ± 0.03

B)



LTD pKa shifts (R^2 , k)				
Fitting		KVA64	MA4C	SOL
Linear	R^2	-	-	-
	k	-	-	-
Exponential	R^2	0.909	0.991	0.996
	k	9.341	2.769	10.109

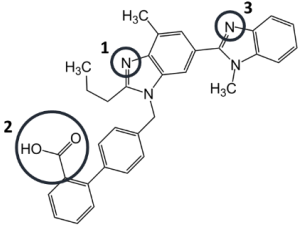
Figure 5.4: A) LTD pK_a and apparent pK_a (pK_a^{app}) (green) B) Graphical scheme and curve fit. The R^2 values represent the best fitting for each polymer.

In Figure 5.4, the following observations were made:

The exponential fitting achieved for LTD in three cases indicated the propensity of the polymers to induce changes in the acid-base equilibria in solution. As reflected in Figure 5.4, the changes in the ionization were much higher when using SOL compared to KVA64 and MA4C. In this sense, the micellization by SOL induced a high reduction in the fraction of molecularly dissolved drug which led to major and polymer concentration-dependent pK_a shifts. The changes in the acid-base equilibria when using KVA64 or MA4C were minor. Therefore, low solubilization extents could be expected in the presence of KVA64 and MA4C, while a higher solubilization was obtained with SOL.

5. RESULTS AND DISCUSSION

5.1.1.5 Telmisartan

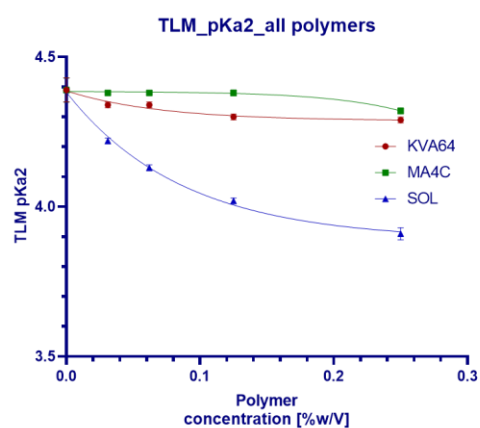
<p>Telmisartan</p>  <p> pK_{a1}: 3.06 ± 0.01 (B) pK_{a2}: 4.39 ± 0.04 (A) pK_{a3}: 6.04 ± 0.00 (B) </p>	Phys.-chem. properties	Acid/ base	Zwitterion	
		pK_a	3.06 ± 0.01 (B), 4.39 ± 0.04 (A), 6.04 ± 0.00 (B)	
		Chemical group involved	Imidazole nitrogens and carboxylic group	
		H-Donor/H-acceptor count ⁽¹⁾	1 (OH- carboxylic group) / 4 (heterocyclic N atoms imidazole rings)	
pK_a shifts present? Best fitting?	KVA64	YES → EXPONENTIAL DECAY 1		
	MA4C	YES → EXPONENTIAL DECAY 2		
	SOL	YES → EXPONENTIAL DECAY 1		

⁽¹⁾ ChemAxon database

A)

TLM	Polymer	0 %	0.031 %	0.062 %	0.125 %	0.250 %
pK_{a1} (Base)	SOL	3.06 ± 0.01	3.07 ± 0.02	3.07 ± 0.02	3.02 ± 0.00	2.99 ± 0.03
	KVA64		3.03 ± 0.01	3.02 ± 0.02	3.01 ± 0.02	3.03 ± 0.01
	MA4C		3.04 ± 0.03	3.05 ± 0.03	3.04 ± 0.02	3.05 ± 0.02
pK_{a2} (Acid)	SOL	4.39 ± 0.04	4.22 ± 0.01	4.13 ± 0.01	4.02 ± 0.01	3.91 ± 0.02
	KVA64		4.34 ± 0.01	4.34 ± 0.01	4.30 ± 0.01	4.29 ± 0.01
	MA4C		4.39 ± 0.00	4.38 ± 0.00	4.38 ± 0.01	4.32 ± 0.01
pK_{a3} (Base)	SOL	6.04 ± 0.00	5.95 ± 0.02	5.92 ± 0.01	5.90 ± 0.01	5.83 ± 0.07
	KVA64		5.86 ± 0.00	5.76 ± 0.01	5.57 ± 0.02	5.42 ± 0.02
	MA4C		6.04 ± 0.00	6.03 ± 0.01	6.04 ± 0.01	5.93 ± 0.00

B)



TLM2 pKa shifts (R^2 , k)				
Fitting		KVA64	MA4C	SOL
Linear	R^2	-	-	-
	k	-	-	-
Exponential	R^2	0.908	0.964	0.993
	k	14.269	-18.031	11.530

Figure 5.5: A) TLM pK_a and apparent pK_a (pK_a^{app}) (green) **B)** Graphical scheme and curve fits. The R^2 values represent the best fitting for each polymer.

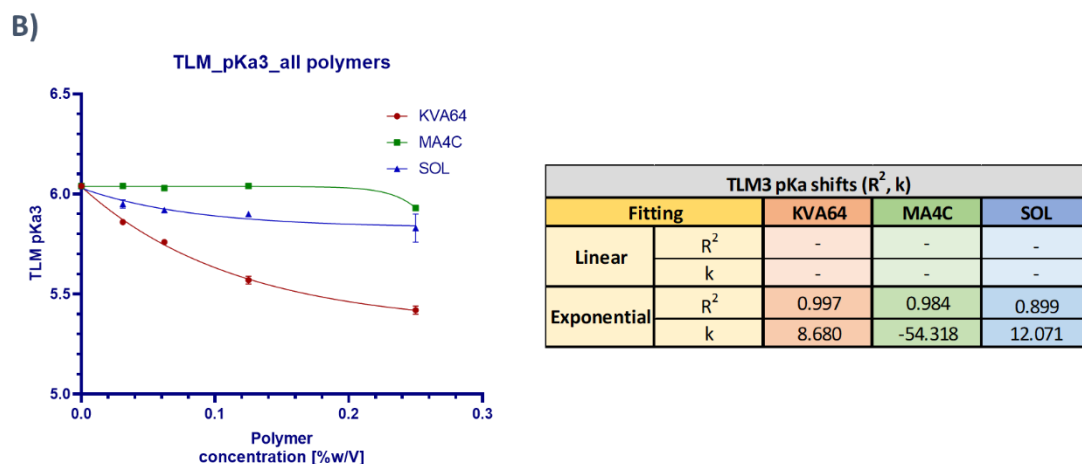
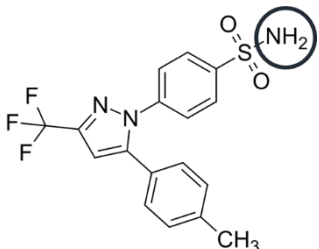


Figure 5.5: A) TLM pKa and apparent pKa (pK_a^{app}) (green) **B)** Graphical scheme and curve fits. The R^2 values represent the best fitting for each polymer.

Due to the specific physicochemical behavior of TLM, several clarifications are needed at this point. According to its zwitterionic chemical structure, the species in solution were always at least partially ionized independently of the pH value. The mean molecular charge (MMC) is a result of the established ionization equilibria of each ionizable group at each pH value. This fact has several implications for the pH-dependent solubility, as well as for the ability to interact with other pharmaceutical excipients in solution. The two weak bases and one weak acid functional group in the TLM chemical structure led to a constantly changing MMC throughout the different pH segments in the GI tract (Table 5.3). As a result of the equilibria established, the molecule had a MMC of +2 in fasted stomach conditions, while this became close to neutral in the upper regions of the small bowel ($pH \approx 5$). It underwent a further anionization in the jejunum and ileum at $pH \geq 5.5$. The obtained shifts for pK_{a1} were very low and these were not fitted to any mathematical model or further discussed. Therefore, no graphical representation was performed for this group. Within the SOL micelles, the ionization obviously affected the extent of solubilization, as the lipophilic SOL core tended to act as a reservoir for neutral molecules. Accordingly, the observed shifts for the carboxylic group (pK_{a2}) are higher (up to 0.48 pH units) than for pK_{a1} and pK_{a3} (up to 0.21 pH units), attributed to the practically neutral MMC of the molecule at $pH = pK_{a2}$. More remarkably, the exponential trend for pK_{a2} and pK_{a3} in the presence of KVA64 suggested the formation of interactions between the polymer and drug molecules and a solubilization effect. It reduced the fraction of molecularly dissolved drug and induced a polymer concentration-dependent effect. The extent of these interactions was high, since the pK_a shifts obtained with KVA64 was the first time higher (up to 0.62 pH units) than for SOL. This special behavior will be a topic of further discussion within this and the next sections. Both pK_a -curves were described well by an exponential decay 1 curve, showing a positive decay constant and a real concentration-dependent effect. The exponential decay 2 fittings characterized by a negative decay constant for MA4C suggested the absence of real a polymer concentration-dependent effect. Instead of that, the shift observed at the highest polymer concentration (0.250% w/v) suggested a molar polymeric excess which caused steric hindrance for the participation of the molecules in the acid-base equilibria. Furthermore, the steric hindrance was related to the increased viscosity in solution (Table 5.4).

5. RESULTS AND DISCUSSION

5.1.1.6 Celecoxib

<p style="text-align: center;">Celecoxib</p>  <p style="text-align: center;">$pK_a: 9.49 \pm 0.03$ (A)</p>	Phys.-chem. properties	Acid/ base	Weak acid
		pK_a	9.49 ± 0.03
		Chemical group involved	Sulfonamide
		H-Donor/H-acceptor count ⁽¹⁾	1 (Sulfonamide H) / 3 (diazole N, sulfonamide N)
pK_a shifts present? Best fitting?	KVA64	NO → LINEAR	
	MA4C	NO → LINEAR	
	SOL	YES → EXPONENTIAL GROWTH	

⁽¹⁾ ChemAxon database

A)

[Polymer]	0%	0.031 %	0.062 %	0.125 %	0.250 %
KVA64	9.49 ± 0.03	9.54 ± 0.05	9.50 ± 0.02	9.47 ± 0.01	9.50 ± 0.01
MA4C		9.47 ± 0.01	9.45 ± 0.02	--	--
SOL		10.13 ± 0.01	10.32 ± 0.02	10.45 ± 0.02	10.75 ± 0.03

B)

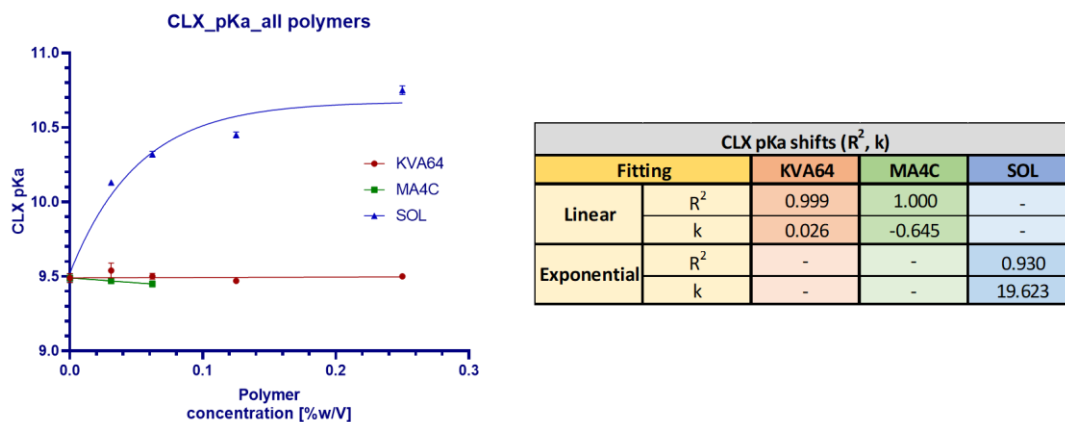


Figure 5.6: A) CLX pK_a and apparent pK_a (pK_a^{app}) (green) B) Graphical scheme and curve fit. The R^2 values represent the best fitting for each polymer.

In Figure 5.6, the following observations were made:

- KVA64. The linear trend and the low constant ($k= 0.026$) indicated the absence of changes in the ionization equilibria.
- MA4C. The linear trend and the low constant ($k= -0.645$) indicated the absence of significant changes in the ionization equilibria.
- SOL. The exponential growth supported the concentration-dependent solubilization through micellization. On the contrary to weak bases, the reduction of molecularly dissolved neutral species induced an apparent increase in the pK_a values, as reflected by the equation 18.

5.1.1.7 pK_a and apparent pK_a fitting

The mathematical fits of the pK_a -curves as a function of the polymer concentration served as an indicator for various interaction mechanisms between the drug and polymer molecules in colloidal solutions. Therefore, the identification of polymer/ drug combinations inducing a decrease in the molecularly dissolved drug fractions and suggesting solubilization events was enabled. The next subsections analyze the different trends identified for each polymer.

5.1.1.7.1 *Kollidon VA64*

KVA64 interacted with all selected drug molecules in a heterogeneous manner and consequently, more than one mathematical trend was applied to fit the pK_a -curve of the respective samples. As a result, various mathematical fit outcomes were obtained (Figure 5.7).

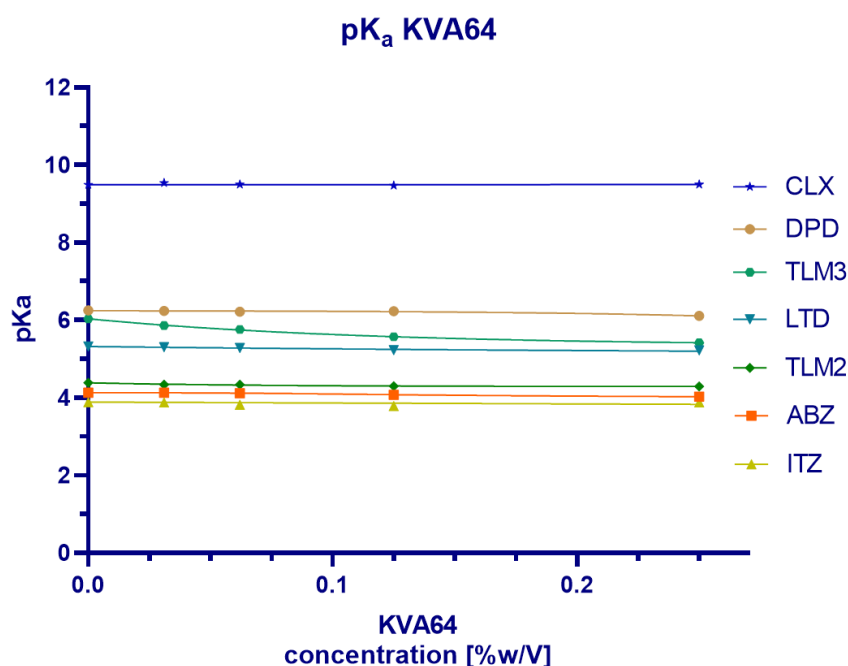
In literature, for PVP derivative polymers, hydrogen bonding was previously identified as a feasible mechanism to hinder nucleation and crystal growth in solution (Balani et al., 2010; Xie et al., 2010; Yani et al., 2011). In the present study, the pK_a -curve progressions indicated H-bond intermolecular interactions between each drug/ KVA64 molecule. In general, molecules, which were strongly enhanced in solubility by KVA64, showed either a sigmoidal (ABZ) or exponential fit (see DPD, ABZ and TLM). Molecules undergoing a lower solubility enhancement such as ITZ or CLX showed a linear relationship, therefore showing a lack of changes in the ionization equilibria. In this way, the trends observed in the pK_a curves were indicative for the extent of aqueous solubility enhancement. The solubility results are compiled in the section 5.1.3 and the potential impact of this observation on oral absorption, will be further discussed in section 5.2.2.

The three previously described mathematical fits (Equations 20, 21 and 22) were applied at the different drug molecules in dependence of their interaction with KVA64:

- **Linear (for ITZ and CLX).** The absence of changes in the ionization equilibria induced a linear trend with very low constant (k). These were observed for the chaser molecule CLX and for the extremely poorly soluble molecule ITZ in the presence of KVA64.
- **Exponential (decay 1 for LTD and TLM/ decay 2 for DPD).**
 - Exponential decay 1. The exponential trend with a positive decay constant suggested a real polymer concentration-dependent effect. This induced a decrease in the fraction of molecularly dissolved drug as a function of the polymer concentration. The decay constant serves as indicative factor for the reduction extent of the molecularly dissolved fraction. As a result, the extent of the changes in the ionization equilibria are a response to the degree of interactions and solubilization. This trend was observed for the non-chaser molecules LTD and TLM.
 - Exponential decay 2. The exponential trend with a negative decay constant indicated the formation of polymeric clusters at high polymer concentrations. The entrapment of drug molecules within these clusters caused steric hindrance (Ma et al., 1996; Xie et al., 2010) that affects the accessibility of these molecules to participate in the acid-base equilibria, thus contributing to a pK_a shift. This trend was observed for the chaser molecule DPD which has 4 H-donor groups prompting to interact with the H-acceptors of KVA64. However, no real concentration-dependent effect was found.

5. RESULTS AND DISCUSSION

- Sigmoidal (for ABZ).** This trend was only observed for the extremely poorly soluble drug molecule ABZ. It determined a lack of changes in the ionization equilibria at low polymer concentrations (0.031 %w/V), followed by a polymer concentration-dependent effect. This was similar to the behavior of allosteric enzymes, where the presence of a regulatory and an active center induce no enzymatic response at low substrate concentrations until a conformational change is induced. After this change, interaction of the substrate with the active center of the enzyme is favored.



Behavior	DRUG	Linear		Exponential		Sigmoidal	
		R ²	k	R ²	k	R ²	k
Chaser	DPD	-	-	0.958	-12077	-	-
	CLX	0.999	0.026	-	-	-	-
Non Chaser	LTD	-	-	0.909	9.341	-	-
	TLM2	-	-	0.908	14.269	-	-
	TLM3	-	-	0.997	8.680	-	-
Extremely poorly soluble	ABZ	-	-	-	-	0.997	-
	ITZ	0.999	-0.237	-	-	-	-

Figure 5.7: *pK_a*-curves for all drug molecules in KVA64 colloidal solutions and their mathematical fit (*R*² and constant, when applicable). The linear trend assumes no changes in the acid-base equilibria, while the exponential and sigmoidal fit indicate changes attributed to solubilization as a function of the polymer concentration.

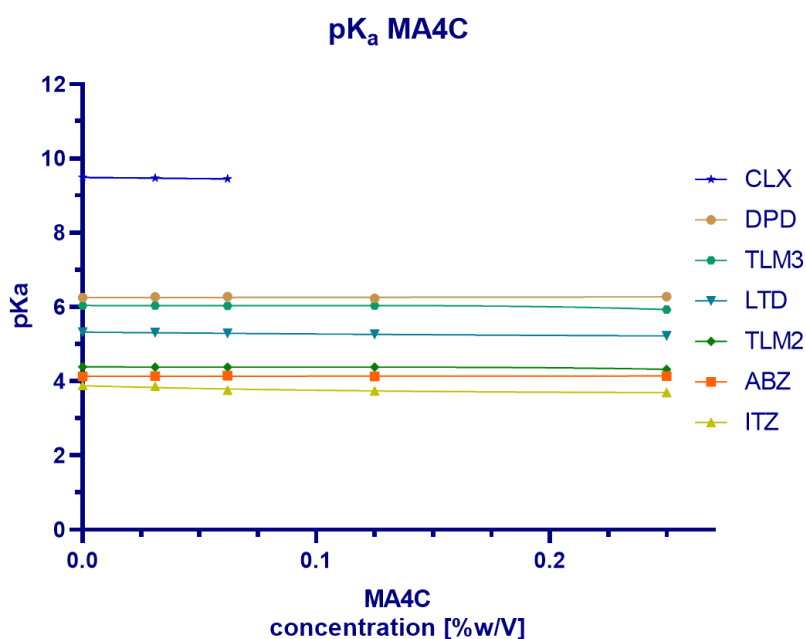
5.1.1.7.2 Methocel A4C

As introduced in the section 3.3.1.1.2 (Equations 20 and 21), two mathematical fits were identified for the drug molecules as a function of the MA4C polymer concentration (Figure 5.8):

- Linear (for DPD, CLX and ABZ).** The chaser molecules DPD and CLX, as well as the extremely poorly soluble drug ABZ, showed a linear relationship between *pK_a* and an increasing polymer concentration. Additionally, a low constant (*k*) was obtained, which

supported the absence of changes in the ionization equilibria and the absence of solubilization.

- **Exponential (decay 1 for LTD and ITZ/ decay 2 for TLM).** This behavior was observed for the non-chaser molecules LTD and TLM and for the extremely poorly soluble molecule ITZ. At the same time, the decay constant defined differences in the type of interaction established between these molecules and MA4C.
 - **Exponential decay 1.** The positive decay constants ($k > 0$) for LTD and ITZ indicated a polymer concentration-dependent effect. In this case, the shifts in the acid-base equilibria, occurring as a function of the polymer concentration, were associated to the formation of hydrophobic interactions and to a solubilization effect. The formation of hydrophobic interactions between different Methocel grades with a high methoxyl substitution and lipophilic drug molecules was described in previous publications (Xu and Dai, 2013b) Similarly, a dependency of the hydrophobicity of the polymer on the stabilization degree at similar viscosity was observed (Bi et al., 2011).
 - **Exponential decay 2.** The negative decay constants for two TLM functional groups (TLM2 and TLM3) supported the theory of an entrapment of the drug molecules within polymeric clusters at a large polymer concentration (0.250 %w/V). This was attributed to a viscosity increase, as reported for cellulose derivatives in the literature (Dow, 2013).



Behavior	DRUG	Linear		Exponential	
		R ²	k	R ²	k
Chaser	DPD	0.999	0.090	-	-
	CLX	1.000	-0.645	-	-
Non Chaser	LTD	-	-	0.991	2.769
	TLM2	-	-	0.964	-18.031
	TLM3	-	-	0.984	-54.318
Extremely poorly soluble	ABZ	0.999	0.049	-	-
	ITZ	-	-	0.839	11.831

Figure 5.8: pK_a-curves for all drug molecules in MA4C colloidal solutions and their mathematical fit (R² and constant, when applicable). The linear trend assumed no changes in the acid-base equilibria, while the exponential fit indicates changes as a function of the polymer concentration.

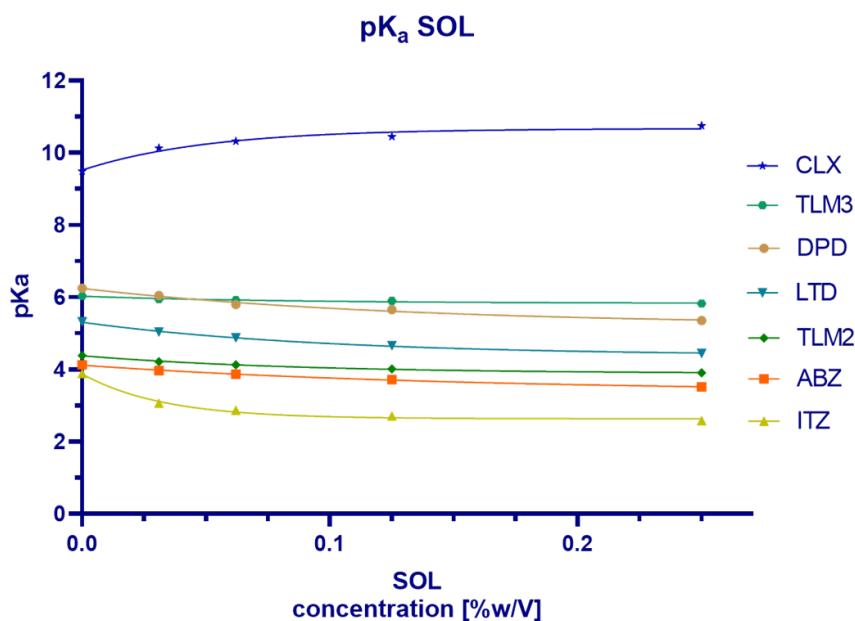
5. RESULTS AND DISCUSSION

The presence of a linear fit in the pK_a -curves for the chasers (DPD, CLX) and ABZ indicated the absence of changes in the ionization equilibria as a function of the polymer concentration. Therefore, the molecularly dissolved fraction remained unchanged and no solubilization effects occurred. Nevertheless, the exponential trends observed for the non-chaser molecules LTD and TLM, as well as ITZ indicated a reduction of the molecularly dissolved drug fraction due to a viscosity increase and subsequent entrapment within polymeric clusters (TLM, exponential decay 2) or due to the formation of hydrophobic interactions as a function of the polymer concentration (LTD and ITZ, exponential decay 1). From a kinetic perspective, the presence of a supersaturating effect could not be excluded, especially for the chaser molecules (DPD, CLX) and ABZ. This fact played an important role for the investigation in the sections 5.1.2 and 5.2.

5.1.1.7.3 *Soluplus*

The solubilization effect induced by SOL clearly shifted the acid-base equilibria of all drug molecules as a function of the polymer concentration. This effect was in good accordance with literature which generally reported shifts in the ionization equilibria when using surfactants (El Seoud, 1989; Grujić et al., 2016). These pK_a -shifts depended heavily on the polymer concentration used and led to an exponential profile in all cases (Figure 5.9). The exponential fit 1 showed a positive constant for all 6 drug molecules, confirming the existence of a concentration-dependent effect. The decay constant not only determined the presence, but also the extent of solubilization. The direction of the shift depended on the nature of the ionizable group in the drug molecule, as reflected by the equations 18 and 19. These observations supported a micellization effect, which might hinder oral absorption as it was proposed in general for solubilization approaches (Figure 3.9). Accordingly, the solubilization enhancement by SOL could be (partially) irreversible in dependence of the nature and strength of the interactions established between the drug molecules and the polyvinylcaprolactam and polyvinylacetate groups of the lipophilic core (Pudlas et al., 2015).

Employing the micellization assumption, the extent of internalization is proportional to the lipophilicity of the drug molecule and determines the decay constant value (Figure 5.9). Further correlations were established between the observed pK_a -shifts, the lipophilicity and the extent of internalization (Figure 5.24). At a first glance, it can be noted that the obtained pK_a -shifts for the high lipophilic ITZ are much higher (up to 1.31 pH units) than for other less lipophilic molecules, where much lower shifts (e.g. 0.61 pH units for ABZ at a similar polymer-drug molar ratio) were obtained.



Behavior	DRUG	Linear		Exponential	
		R ²	k	R ²	k
Chaser	DPD	-	-	0.974	7.675
	CLX	-	-	0.930	19.623
Non Chaser	LTD	-	-	0.996	10.109
	TLM2	-	-	0.964	11.530
	TLM3	-	-	0.899	12.071
Extremely poorly soluble	ABZ	-	-	0.995	6.555
	ITZ	-	-	0.981	30.769

Figure 5.9: pK_a-curves for all drug molecules in SOL colloidal solutions and their mathematical fit (R² and constant, when applicable). The exponential fit indicated changes in the acid-base equilibria as a function of the polymer concentration in all cases.

5.1.2 Lipophilicity: LogP and LogD

5.1.2.1 Chromatographic method

The chromatographic method proved to be suitable for the LogP determination of all drug molecules (DPD, CLX, LTD, ABZ and ITZ), except for the zwitterionic TLM. The LogP values helped to establish several correlations and to further explain the underlying stabilization mechanisms in aqueous solution, as it will be discussed in the sections 5.1.3 and 5.1.4. The measured LogP values for the drug molecules are listed in Table 5.1.

5. RESULTS AND DISCUSSION

Table 5.1: LogP values determined by the chromatographic method described by Donovan and Pescatore (index (*) determines values taken from Donovan and Pescatore, 2002).

COMPOUND	RT (min)	LogP
Toluene (I.S. 1)	8.28	2.72 (*)
Triphenylene (I.S. 2)	12.35	5.49 (*)
DPD	8.20	2.66
ABZ	8.57	2.92
ITZ	11.24	4.73
LTD	9.88	3.81
TLM	--	--
CLX	8.24	2.69

5.1.2.2 pH-metric titration method

In the case of TLM, the pH-metric method enabled the determination of the TLM lipophilicity profile within the pH range of 3 – 11 for the pure drug, as well as in polymeric solutions. Due to the zwitterionic behavior of TLM, the calculated values corresponded to the logarithmic value of the distribution coefficient (D) between octanol and water ($\text{Log}D_{ow}$) at $\text{pH} \approx 7.4$, as introduced in the section 3.3.3. In the polymeric solutions (polymer concentration: 0.031 – 0.250 % w/V) lower $\text{Log}D_{ow}$ values were found (range: 3.06 – 2.67), compared to the pure drug ($\text{Log}D_{ow}$: 3.22) (Table 5.2). The decrease in $\text{Log}D_{ow}$ determined a change in the distribution equilibria and it indicated the formation of stable interactions between the drug and polymer in aqueous solution. These were attributed to a solubilization effect and to a decrease in the molecularly dissolved drug fraction, which in turn can influence the apparent lipophilicity of the TLM molecules and their partition into the octanol layer.

Table 5.2: Distribution coefficient in octanol-water ($\text{Log}D_{ow}$) at pH 7.4 for TLM with or without KVA64, MA4C and SOL.

Polymer [%w/V]	Log D_{ow} (pH 7.4)		
	KVA64	MA4C	SOL
0		3.22	
0.031	3.06	--	2.90
0.062	3.03	2.93	2.95
0.125	2.88	2.90	2.85
0.250	2.92	2.88	2.67

5.1.3 Solubility and solubility enhancement

The fundament of this work is based on the ability of the polymers to enhance the aqueous solubility of the selected drug molecules from a kinetic or a thermodynamic perspective. Thus, the solubility determination is one of the key parameters investigated in the present study, as introduced in the section 3.3.2.

Independently from the drug molecule used, the extent of stabilization observed in kinetic and intrinsic solubility mainly depended on the nature and concentration of the polymer applied. In general, an enhancement in the intrinsic solubility of drugs under the CheqSol method was associated with an inhibition or delay of precipitation events, mainly triggered by supersaturation. This caused a shift from chaser into non-chaser behavior. Furthermore, the kinetic or intrinsic solubility enhancement up to values considerably exceeding the kinetic solubility of the pure drug was associated with a solubilization effect.

For a facilitated understanding, the results are grouped into sections according to the drug's supersaturation behaviors: chaser vs. non-chaser vs. extremely poorly soluble drugs.

5.1.3.1 Chaser molecules

5.1.3.1.1 Dipyridamole

In accordance with previously published results (Hsieh et al., 2012), dipyridamole showed a chaser behavior. Under potentiometric titration from low to high pH, it exhibited an extensive degree of supersaturation (ratio between kinetic and intrinsic solubility). Related to its weak basic behavior ($pK_a = 6.25 \pm 0.02$), precipitation was detected first under non-sink conditions at a $pH = 5.61 \pm 0.02$. At this point, the concentration of drug dissolved in solution was $69.99 \pm 3.65 \mu\text{g/mL}$ (Figure 5.10). Following this determination, the system was brought to equilibrium conditions, enabling the determination of an intrinsic solubility of $14.42 \pm 0.86 \mu\text{g/mL}$. Consequently, a supersaturation ratio of 4.86 ± 0.20 -fold was obtained.

As already highlighted, the stabilization of a chaser molecule in solution is favored, compared to a non-chaser molecule. Under this context, the three polymers tested showed a positive effect as crystal growth inhibitors, as they converted the chaser behavior into a non-chaser one, as shown in the Figure 5.10. Nevertheless, the kinetic solubility of DPD remained similar (range 55 – 80 $\mu\text{g/mL}$) in almost all cases, except for the solubilization approach through SOL. This highlights that despite of inhibiting or delaying crystal growth, KVA64 and MA4C were not able to completely prevent DPD nucleation. Nevertheless, the shift into a non-chaser behavior is already an indicator for a positive kinetic stabilization from which the drug could benefit *in vivo*.

KVA64. The formation of H-bonds between polymer and drug molecules was proposed as a crystal growth inhibition mechanism (Balani et al., 2010; Xie et al., 2010; Yani et al., 2011). In this case, the interactions established between the 4 H-donor in DPD functional groups and the acceptors groups in KVA64, were responsible for the increased intrinsic solubility. Remarkably, only minor differences in solubility were observed as a function of the polymer concentration remaining the intrinsic and kinetic solubility values in the range 60 – 70 $\mu\text{g/mL}$. It indicated that the adsorption of the polymer molecules to the crystal lattice is sufficient to inhibit or delay the crystal growth at low polymer concentrations, as already observed for bicalutamide (Lindfors et al., 2008). At the highest polymer concentration applied (0.250 % w/V), the behavior shifted back into a chaser molecule and the intrinsic solubility decreased up to $\approx 50 \mu\text{g/mL}$. At this concentration, a remarkable shift of the pK_a value led to an exponential decay 2 function (Figure 5.1). Under these conditions, a molar polymeric excess is responsible for the entrapment

5. RESULTS AND DISCUSSION

of drug molecules in polymeric clusters, causing this shift. Additionally, the polymer excess could render the accessibility of the H-bond acceptor groups of the polymer for intramolecular interactions (Trasi and Taylor, 2012), which could be involved in the change to a chaser behavior when a high polymer concentration is applied.

MA4C. The increased viscosity in MA4C colloidal solutions was a contributing factor for the limited precipitation and enhanced intrinsic solubility, compared to the pure drug. The kinetic and intrinsic solubility values remained in this case in the range 40 - 55 $\mu\text{g}/\text{mL}$. A shift into a non-chaser behavior took place at all MA4C concentrations applied and led to a positive kinetic stabilization. Previous works proposed that the crystal growth rate was directly proportional to the diffusion rate of a particular compound in a given medium (Brouwers et al., 2009). Thus, when the molecular mobility was reduced, both the nucleation and crystal growth rates decreased. Similarly, the absence of a polymer concentration-dependent effect indicated that a low to moderate viscosity was sufficient to partially hinder the crystal growth.

SOL. The intrinsic and kinetic solubility of DPD was directly related to the polymer concentration applied. The DPD kinetic solubility reached values of up to 120 $\mu\text{g}/\text{mL}$ at the highest polymer concentration. This effect corresponded to the definition of solubilization: as long as a sufficient drug concentration in the medium was obtained, an increasing SOL concentration enhanced the kinetic and intrinsic solubility of the drug by means of micellization. The solubilization effect inhibited the nucleation and crystal growth, and therefore increased the solubility of the drug. The observation was in accordance with the previously obtained pK_a shifts and exponential curve (Figure 5.1).

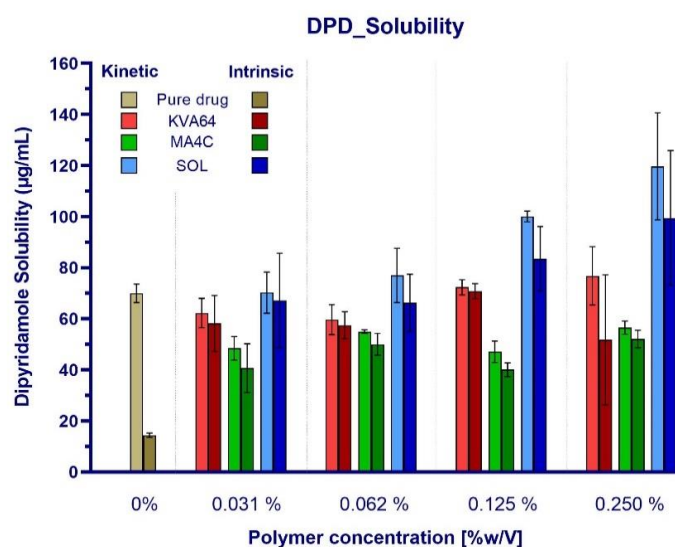


Figure 5.10: Kinetic and intrinsic dipyridamole solubility determined in 0.15 M NaCl by means of the CheqSol method in a Pion inForm platform. Titrations were performed in triplicate from low to high pH using 0.5 M NaOH and 0.5 M HCl as titrants.

5.1.3.1.2 Celecoxib

Due to the behavior as a weak acid, the potentiometric titration was performed from high to low pH, contrarily to the other tested drugs. Under these experimental conditions, CLX first precipitated at a pH of 9.91 ± 0.12 and showed a chaser behavior. This was determined by a kinetic solubility of $35.176 \pm 2.635 \mu\text{g}/\text{mL}$ and an intrinsic solubility of $13.150 \pm 1.412 \mu\text{g}/\text{mL}$.

Based on its innate supersaturation ability, the suitability of the polymers to act as crystal growth inhibitors was evaluated. Apparently, the polymer addition could not prevent or delay the

nucleation, as the first precipitation event was directly detected at a pH close to 10. Despite this fact, KVA64 and MA4C showed a positive effect as crystal growth inhibitors, as they shifted the chaser behavior into a non-chaser, independently of the polymer concentration applied (Figure 5.11).

KVA64. Driven by the presence of only one H-donor group in CLX chemical structure and the behavior as a chaser molecule, the H-bond interactions established between KVA64 and CLX were responsible for the crystal growth inhibition. Thus, a change to non-chaser properties was obtained and kinetic stabilization in colloidal solution occurred, reflected as an increase in the intrinsic solubility up to 30 $\mu\text{g}/\text{mL}$. However, and on the contrary to DPD, which also showed the shift from chaser into non-chaser behavior, no positive polymer concentration-dependent effect was achieved. The solubility values decreased up to 20 $\mu\text{g}/\text{mL}$ at a polymer concentration of 0.125 %w/V. Remarkably, the pK_a -curve showed no relevant pK_a -shift in the presence of KVA64 (Figure 5.6) and did not indicate a solubilization effect. Contributing factors to the observed negative polymer concentration-dependent effect were mainly steric hindrance or the self-association of the polymer molecules, thus limiting the accessibility of CLX to interact with the acceptor groups of KVA64. Given the fact that the kinetic and intrinsic solubility of the drug in KVA64 solutions did not exceed the kinetic solubility of the pure drug, no solubilization effect was found. As a result, the main stabilization mechanism was a supersaturation effect achieved by crystal growth inhibition.

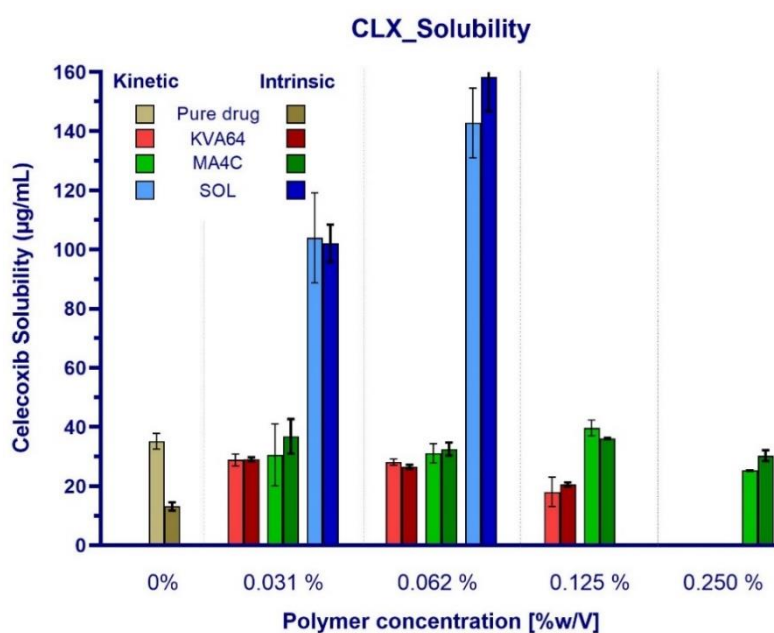


Figure 5.11: Kinetic and intrinsic celecoxib solubility determined in 0.15 M NaCl by means of the CheqSol method in a Pion inForm platform. Titrations were performed in triplicate from high to low pH using 0.5 M NaOH and 0.5 M HCl as titrants.

MA4C. Supporting the observations from other authors (DiNunzio et al., 2008; Gao et al., 2009a; Usui et al., 1997), the highly increased viscosity impacted negatively the crystal growth and resulted into an increased intrinsic solubility (range: 30 - 40 $\mu\text{g}/\text{mL}$). However, high polymer concentrations (0.250% w/v) slightly reduced the solubility compared to lower concentrations (0.031 – 0.125% w/v), which is in good accordance with other authors (Bevernage et al., 2011; Dai et al., 2008; Guzmán et al., 2007b). This observation might be attributed to an entrapment of CLX species within a MA4C polymeric cluster, a problem that seems to be generalized for all

5. RESULTS AND DISCUSSION

drugs tested. Nevertheless, in all cases, a kinetic stabilization was achieved, as reflected by the similar kinetic and intrinsic solubility in MA4C colloidal solutions. Similar to KVA64, the linear trend of the pK_a -curve (Figure 5.6) additionally supported the absence of a solubilization effect.

SOL. The determinations performed by means of the CheqSol® method up to a concentration of 0.062% w/v reported an increase in the kinetic and intrinsic solubility up to values in the range 140 – 160 $\mu\text{g}/\text{mL}$ (Figure 5.11). Homayouni et al. similarly reported a positive solubilization effect of CLX when formulated with SOL (Homayouni et al., 2014, 2015). Based on these findings and the exponential pK_a -curve (Figure 5.6), a polymer concentration-dependent effect was found (Figure 5.11)

5.1.3.2 Non-chaser molecules

5.1.3.2.1 Loratadine

Loratadine (LTD) was classified as a non-chaser molecule. The pure drug showed no supersaturation tendency under potentiometric titration from low to high pH, according to its kinetic and intrinsic solubility ($10.8 \pm 0.53 \mu\text{g}/\text{mL}$ and $10.54 \pm 0.49 \mu\text{g}/\text{mL}$), respectively. These values were in line with previous findings, where the phenomenon of LLPS was similarly observed (Hsieh et al., 2012). Following its precipitation from an acidic solution, LTD appeared to precipitate as an amorphous liquid form. As previously mentioned, the improvement of the kinetic and intrinsic solubility for non-chaser molecules can be challenging.

KVA64 and MA4C. The absence of H-donors and the presence of only 2 H-acceptor groups within LTD's chemical structure limited the establishment of intermolecular interactions with the polymers KVA64 and MA4C. As a result, only a minor increase in LTD's solubility was measured as a function of KVA64 and MA4C concentration (Figure 5.12). However, regarding the precipitation of the drug into a higher energetic state by means of LLPS (Hsieh et al., 2012), the adsorption of polymer to the drug molecule surface was facilitated. A fact which is in good accordance with the obtained exponential decay fit for the pK_a (Figure 5.4). Consequently, the observations suggested a minimal solubilization effect. Even when the polymers did not significantly enhance the solubility of the amorphous precipitated drug form, they were able to prevent or at least partially hinder its crystallization. This was additionally confirmed by means of the shaking flask approach after 48 hours of stabilization (results not shown).

SOL. An investigation of the influence of SOL on LTD solubility was not feasible by means of the CheqSol method due to high turbidity. Consequently, this was determined by means of the shaking flask method at pH 6.8, at which the intrinsic solubility was determined. The results were further compared to the intrinsic solubility of the pure drug in the identical medium after 48 hours for equilibration. As expected, the initial LLPS observed in the CheqSol method was turned into crystallization of the drug and the formation of a less soluble form was obtained ($2.45 \pm 0.04 \mu\text{g}/\text{mL}$) (Figure 5.12). With the identical approach, the solubilization of LTD by means of SOL was similarly confirmed and intrinsic solubility values of up to $\approx 95 \mu\text{g}/\text{mL}$ were obtained. A polymer concentration-dependent effect, as it was previously predicted by the pK_a -curve (Figure 5.4), was demonstrated.

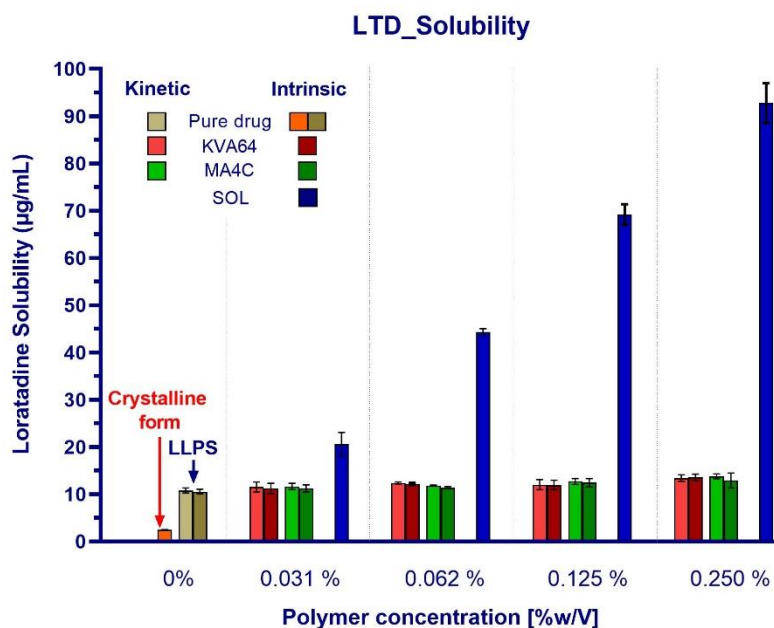


Figure 5.12: Kinetic and intrinsic loratadine solubility determined in 0.15 M NaCl by means of the CheqSol method in a Pion inForm platform for the pure drug (LLPS), KVA64 and MA4C. Titrations were performed in triplicate from low to high pH using 0.5 M NaOH and 0.5 M HCl as titrants. The determination of the intrinsic solubility for the crystalline form and in the presence of SOL was performed by means of a shaking flask method over 48 h in a pH 6.8 KH_2PO_4 buffer at 37°C. The dissolved drug concentration was subsequently quantified by means of HPLC ($n=3$).

5.1.3.2.2 Telmisartan

Under the selected potentiometric titration conditions, the drug dissolved easily at acidic pH and precipitated when the medium was titrated with 0.5 M NaOH. The solubility vs. pH-profile had an inversed-bell shape, showing its minimum at pH 5.0, while it increased in both acidic and basic directions (Figure 5.13). As previously discussed, telmisartan (TLM) is a molecule with three ionizable functional groups (Figure 5.5) and as a result of the ionization interplay the MMC at $\text{pH} \approx 5.0$ is close to 0 (Table 5.3). Thus, the ionization equilibria are much more complex and its solubility changes constantly in the different segments of the GI tract. Even minimal changes in the pH value can generate high shifts in TLM solubility. Nevertheless, the molecule is a zwitterion and consequently, it is not fully neutral at any pH value. Similar to LTD, TLM was unable to supersaturate by itself and behaved partially like a non-chaser molecule. The term “partially” refers to the fact that the kinetic solubility ($9.21 \pm 5.75 \mu\text{g/mL}$) was lower than the intrinsic solubility ($17.14 \pm 1.63 \mu\text{g/mL}$). This observation did not properly fit to the definition of a non-chaser. The main cause for this finding was related to the amorphous TLM precipitation by means of LLPS (Figure 5.46). Due to the zwitterionic behavior, the amorphous form could easily re-dissolve as a response to the pH and ionization ($\text{pH} \neq 5.0$) and as a result, the intrinsic solubility was higher than the kinetic solubility. A quick re-dissolution would not be favored if the drug precipitated in its lower energetic and entropic crystalline form. This initial precipitation by LLPS was further supported by shaking flask experiments over 48 h at pH 5.0, in which the amorphous form crystallized into an approximately 50-fold less soluble form (Figure 5.14). The influence of KVA64 and MA4C on TLM was investigated by means of the CheqSol method. On the contrary to LTD, for which the intrinsic and kinetic solubility was not highly enhanced due to LLPS

5. RESULTS AND DISCUSSION

phenomena, the TLM results contradicted the general belief that the solubility of non-chaser molecules cannot be improved.

KVA64. KVA64 induced an enhancement in the kinetic and intrinsic solubility values of TLM and showed a polymer concentration-dependent effect (Figure 5.14). With this, the function of the polymer molecules as a solubilizing agent was confirmed. Surprisingly, the non-chaser behavior was even shifted into a chaser at high polymer concentrations, an observation which was not made in any other case studied in this thesis. As a consequence, an enhanced kinetic solubility up to 85 $\mu\text{g/mL}$ was obtained. Additionally, the crystallization of the amorphous form was impeded at least during the length of the CheqSol assay (1.5 h). For TLM-KVA64, the solubilization effect was attributed to the formation of stable H-bond interactions between the H-donor carboxylic group in TLM and the H-acceptor groups in KVA64. Supporting these findings, the exponential decay in the pK_a -curves already suggested a solubilization effect of KVA64 for TLM (Figure 5.5). An exponential decay of this extent was not observed for any other drug molecule in the presence of KVA64.

MA4C. The stabilization achieved by MA4C was again attributed to the increased viscosity. The effectiveness of the polymer as crystallization inhibitor was demonstrated and it maintained the amorphous form during the test. However, an entrapment of the drug molecules within the polymeric cluster led to a maximum solubility at a polymer concentration of 0.062% w/v (kinetic solubility \approx intrinsic solubility = 31 $\mu\text{g/mL}$), while a decrease in TLM solubility was observed at higher polymer concentrations (Figure 5.14). As a result, the pK_a -curve showed an exponential decay 2 trend with a negative decay constant (Figure 5.5), associated with the entrapment of the drug molecules within polymeric clusters at high polymer concentrations.

SOL. Similarly to LTD, the turbidity obtained at different SOL concentrations impeded a Cheqsol solubility determination. Generally, this was unfeasible for LTD and TLM which precipitated by LLPS. This suggested that non-chaser molecules precipitation in this form generated very turbid colloidal solutions, even when the drug is fully solubilized. Accordingly, the equilibrium solubility of the TLM crystalline form was determined by means of the shaking flask method at pH 5.0 after 48 hours with different SOL concentrations. The equilibrium solubility of the crystalline TLM form at low SOL concentrations (0.031 and 0.062 %w/v) did not exceeded the solubility of the amorphous form (17 $\mu\text{g/mL}$) generated after the LLPS. However, in all cases, the crystalline solubility of the pure TLM (0.16 $\mu\text{g/mL}$) was exceeded, thus showing a positive solubilization effect and reaching solubility values of up to 80 $\mu\text{g/mL}$ (Figure 5.14). This was in accordance with the exponential decay applied to the pK_a -curve (Figure 5.5), where a positive concentration dependent solubilization effect was observed.

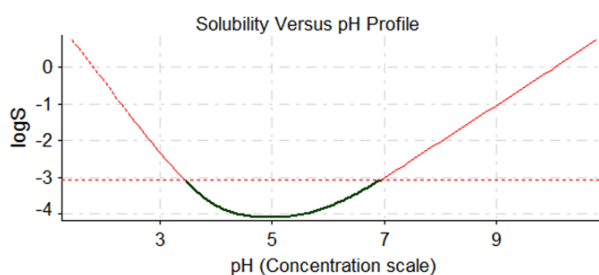
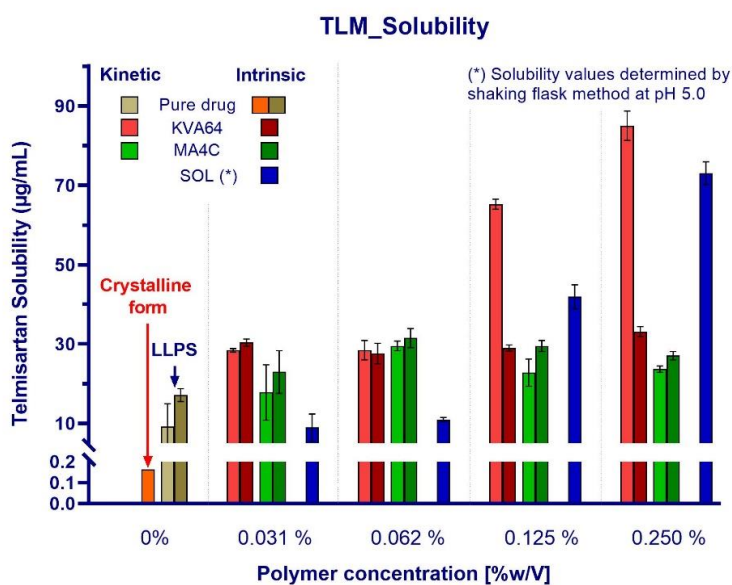


Figure 5.13: TLM pH-dependent solubility profile of the amorphous form. The inverted bell-shaped curve corresponds to a zwitterionic molecule.

Table 5.3: Approximate ionization state and mean molecular charge (MMC) of TLM molecules throughout the different gastrointestinal tract segments as a function of the pH.

pH value	Ionizable group			Mean molecular charge	Solubility
	Base 1 (pKa = 3.06)	Acid 2 (pKa = 4.39)	Base 3 (pKa = 6.04)		
	Charge	Charge	Charge		
pH = 1.0	1	0	1	2	++
pH = 4.0	0,25	-0,4	1	0.85	+
pH = 5.0	0	-0,8	0.9	0.1	-
pH = 7.0	0	-1	0	-1	+

**Figure 5.14:** Kinetic and intrinsic telmisartan solubility determined in 0.15 M NaCl by means of the CheqSol method in a Pion inForm platform for the pure drug (LLPS), KVA64 and MA4C. Titrations were performed in triplicate from low to high pH using 0.5 M NaOH and 0.5 M HCl as titrants. The determination of the intrinsic solubility for the crystalline form with SOL were performed by means of a shaking flask method over 48 h in a pH 5.0 KH_2PO_4 buffer at 37°C. The dissolved drug concentration was subsequently quantified by means of HPLC (n=3).

5. RESULTS AND DISCUSSION

5.1.3.3 Extremely poorly soluble molecules

5.1.3.3.1 *Albendazole*

The extremely poor aqueous solubility of Albendazole (ABZ) made the potentiometric titration unfeasible, as the method cannot properly record the dpH/dt slope. Furthermore, due to the poor dissolution rate of the crystalline drug, the required initial dissolution of 15 – 20 mg of the drug within a few minutes, imposed a challenge even at pH 1. Therefore, the determination failed by the means of the CheqSol method. Alternatively, the shaking flask method was applied. The solubility measured under these conditions was equivalent to the theoretical intrinsic solubility identified by the CheqSol method, since it was determined in a pH 6.8 buffer, in which the charge of the molecule is fully neutral. Unfortunately, the shaking flask determination impeded the investigation of the chaser/non chaser behavior. However, due to the reported extremely low solubility and dissolution rate of the crystalline drug, it was expected to behave as a non-chaser molecule but with a fast crystallization rate. The experimental solubility of crystalline albendazole was extremely low (14.77 ± 3.25 ng/mL) (Figure 5.15). The applied polymers proved in many cases to act as solubility enhancers.

KVA64. It showed an up to approximately 200-fold enhancement factor and therefore proved to be the most effective of the three polymers in equilibrium conditions (Figure 5.15). Since the drug solubility was determined in equilibrium conditions (≈ 3 $\mu\text{g/mL}$), a strong solubilization was considered as the main stabilization mechanism in solution. Nevertheless, no polymer concentration-dependent effect was observed. This observation suggested that the molar ratio at the lowest polymer concentration saturated the 2 H-donor functional groups in ABZ, responsible for the intermolecular interactions with the H-acceptor groups in KVA64. As a result, an increase in polymer concentration did not lead to a further stabilization due to the lack of free groups within the drug molecules to establish more intermolecular interactions. The high solubility enhancement factors observed (Figure 5.15) were attributed to the low M_w of ABZ (265.33 g/mol) and its simple chemical structure. This facilitated the establishment of intermolecular interactions with the H-acceptor groups of KVA64 due to a low steric hindrance. The sigmoidal pK_a -curve supported the observed solubilization effect as a function of the polymer concentration (Figure 5.2).

MA4C. Surprisingly, the extent of ABZ solubility enhancement achieved by MA4C was much more limited (2 – 4-fold) than observed for the other drugs and all solubility values remained in the ng/mL range (30 – 60 ng/mL). However, a more remarkable polymer concentration-dependent effect was found, since the increased viscosity limited the crystallization. Furthermore, the linear trend observed in the pK_a -curve (Figure 5.2) did not suggest the presence of a strong solubilization effect, as it was confirmed by the shaking flask solubility determination.

SOL. By using SOL, an exponential effect on ABZ solubility (Figure 5.15) was observed. The low solubilization effect (2-fold) achieved by the lowest polymer concentration (0.031% w/v) was attributed to the conformation stability between ABZ and SOL, as this can affect the bonding interaction between both molecules (Fule and Amin, 2014a, 2014b; Kaur et al., 2019). The results suggested that the lowest polymer concentration applied was unable to achieve a stable conformation, while this was favored at higher polymer concentrations (≥ 0.062 % w/v) and the ABZ solubility reached values of up to 8 $\mu\text{g/mL}$ at the highest polymer concentration. The results are in accordance with the exponential decay 1 obtained in the pK_a -curve, where a solubilization effect was suggested (Figure 5.2).

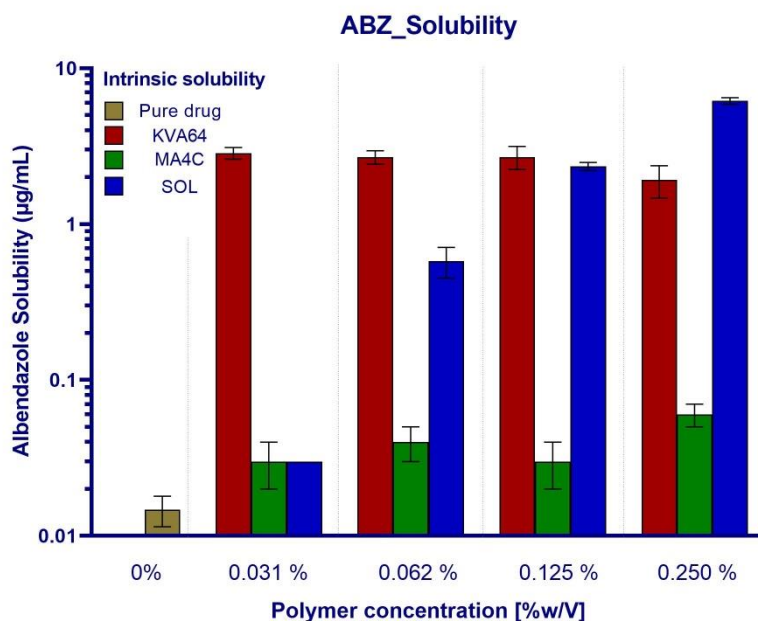


Figure 5.15: Intrinsic albendazole solubility determined by means of a shaking flask method over 48 h in a pH 6.8 KH_2PO_4 (ionic strength: 0.05 M) buffer at 37°C. Concentrations dissolved were subsequently quantified by means of HPLC ($n=3$).

5.1.3.3.2 Itraconazole

Similar to ABZ, the extremely poor aqueous solubility of the crystalline ITZ impeded a solubility determination by means of the CheqSol method. Consequently, the traditional shaking flask method was applied. In terms of solubility, ITZ is one of the most challenging drug molecules that reached the market. Unfortunately, the solubility determination of the pure crystalline ITZ was unfeasible as the concentrations of drug dissolved at pH 6.8 were below the limit of detection (LOD) and limit of quantification (LOQ). However, previous works reported an aqueous intrinsic solubility of approximately 1 ng/mL (Van Speybroeck et al., 2010b). In equilibrium conditions, MA4C and SOL showed a polymer concentration-dependent solubilization effect, while this was not obtained for KVA64.

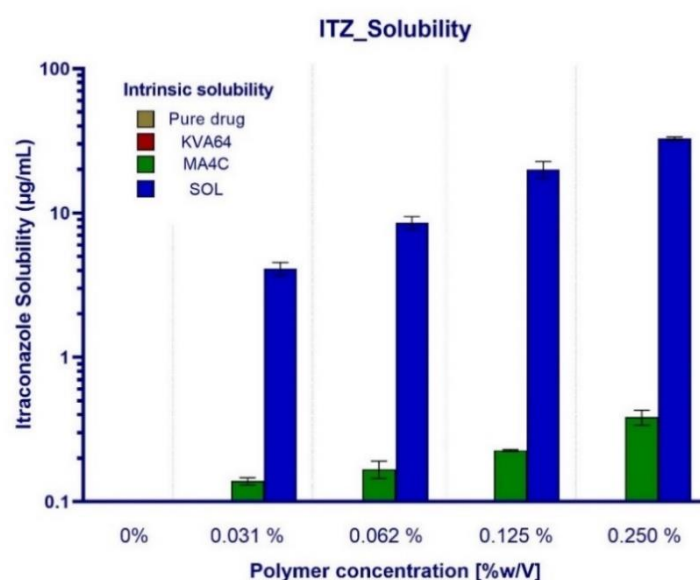
KVA64. A complete lack of thermodynamic stabilization at all KVA64 concentrations was determined (5.16). This can be explained by the absence of H-donor groups within the chemical structure of ITZ, which disabled the formation of H-bond interactions in aqueous solution. The absence of interactions correlated with the linear trend observed in the pK_a -curve, where no significant changes in the ionization and no solubilization effect were detected (Figure 5.3).

MA4C. ITZ benefited from the increased viscosity of the colloidal solution, favoring the equilibrium solubility of the drug at pH 6.8. Compared to the aqueous solubility determined by Speybroeck and co-workers (1 ng/mL), MA4C achieved solubility enhancement ratios in the range of 100 – 300-fold. Furthermore, despite the lack of linearity, a polymer concentration-dependent effect was found (5.16). The formation of hydrophobic interactions with MA4C, as previously proposed for cellulose derivatives (Bi et al., 2011), was considered as an additional contributing factor to the solubilization effect achieved in aqueous solution. The solubilization was supported by the exponential decay 1 observed in the pK_a -curve (Figure 5.3).

SOL. The high solubilizing capacity of SOL and the lipophilicity of ITZ resulted in a very suitable combination in terms of solubility enhancement and clearly showed a polymer concentration-

5. RESULTS AND DISCUSSION

dependent effect (5.16). Considering the previously reported aqueous solubility of the crystalline ITZ, the solubility enhancement ratios were in the range of approximately 3,000 – 30,000-fold. This effect was directly related to the extremely lipophilic structure of ITZ, undergoing the solubilization path as a mechanism to avoid precipitation. This trend was already predicted by the pK_a -curve, at which a clear exponential decay was observed (Figure 5.3). According to the solubility of ITZ in SOL-based polymeric matrices (Bochmann et al., 2016), the combination was investigated in several works focusing on the manufacturing of ITZ ASDs in a SOL matrix (Albadarin et al., 2017; Davis et al., 2017; Thiry et al., 2017).



5.16. *Intrinsic itraconazole solubility determined by means of a shaking flask method over 48 h in a pH 6.8 KH_2PO_4 (ionic strength: 0.05 M) buffer at 37°C. Concentrations dissolved were subsequently quantified by means of HPLC (n=3).*

5.1.3.4 Solubility enhancement as a function of the innate supersaturation behavior

In general, regarding the innate supersaturation capacity and the type/ degree of interaction with the polymer, three different categories of drugs molecules were identified:

- Chaser molecules (DPD and CLX). These molecules were able to supersaturate in solution and slowly precipitated in a crystalline form with lower energy and entropy. In all cases, the polymers achieved a positive effect as crystal growth inhibitors. Therefore, the kinetic and intrinsic solubility in colloidal solutions were similar, but the intrinsic solubility differed from the pure drug molecules. The kinetic stabilization with KVA64 and MA4C was attributed to a supersaturation effect, which did not reduce the molecularly dissolved drug fraction. This observation was supported by the linear trends of the pK_a curves (Figure 5.1, Figure 5.6) for DPD and CLX, respectively.
- Non-chaser molecules (LTD and TLM). The absence of an innate supersaturation ability was related to the initial precipitation as an amorphous form through the LLPS phenomena. The amorphous precipitates were stable in solution during the length of the experiment. The amorphous precipitate was in a high energetic and entropic state. Therefore, a supersaturation effect was more challenging than for chaser molecules. At the same time, non-chasers appeared to be more suitable to form stable interactions with the polymers at a molecular level, which contributed to a solubilization effect in all

cases. Supporting the solubilization effect, all pK_a -curves showed an exponential trend independently of the polymer used (Figure 5.4, Figure 5.5).

- Extremely poorly soluble molecules. The CheqSol method was not feasible for these drug molecules (ABZ and ITZ). Therefore, their innate supersaturation behavior could not be investigated. However, owing to their immediate crystallization, the drugs had characteristics of chasers and of non-chasers. On the one hand, they precipitated in a crystalline form, a characteristic of chaser molecules. On the other hand, the precipitation occurred so fast that if a supersaturation was present, it only lasted for a very short time (seconds). Due to their extremely poor intrinsic solubility, these molecules achieved the highest solubility enhancement factors in colloidal solution. In this sense, the polymers proved their effectiveness as crystal growth inhibitors and solubility enhancers. In many cases (e.g. ABZ/KVA64 and ITZ/MA4C), the establishment of specific interactions between polymer and drug molecules, induced polymer concentration-dependent effects which correlated with the exponential decays of the pK_a -curves. In further cases (ABZ/MA4C and ITZ/KVA64), no thermodynamic stabilization associated to a solubilization occurred, supported by the identified linear pK_a -curves. As a result, the variety of effects observed for these molecules depended heavily on the specific drug-polymer combination.

All drug molecules showed the ability to undergo solubilization through SOL at a lower or higher extent. The lipophilic character of all selected model drugs triggered the micellization of the drug molecules within the lipophilic micelles and determined the extent of solubilization, as it will be further discussed in the section 5.1.4.2.

5. RESULTS AND DISCUSSION

5.1.3.5 Solubility enhancement mechanisms

5.1.3.5.1 Kollidon VA64

As it was discussed in the literature, one of the main mechanisms driving the supersaturation stabilization by PVP-based polymers, is the formation of intermolecular H-bond interactions with the drug (Xu and Dai, 2013b). The ability to form these bonds was related to the H-donors and H-acceptors count within the molecules. KVA64 has only H-acceptor groups within its chemical structure and consequently can only interact with H-donor groups of a drug. Hence, the degree of interaction is related to the H-donor count of the drug but also it depends on the nature of the groups involved, showing different bond energies (0.2 – 40 kcal/mol) (Steiner, 2002). More importantly, at similar drug-polymer molar ratios (approximately 50:1), the solubility enhancement factor for the intrinsic solubility was proportional to the H-donors count of the drug molecules and a linear correlation ($R^2 = 0.9969$) was established (Figure 5.16).

Remarkably, no effects or a very low solubility enhancement factor was observed for those molecules lacking H-donor atoms (ITZ and LTD) (Figure 5.17, Figure 5.12). Thus, the formation of H-bond interactions between drug molecules and KVA64 was unfeasible. In the case for TLM and CLX, only one H-donor atom, enhanced the intrinsic solubility by approximately 1.6-fold. The 4 H-donor atoms of DPD considerably increased the intrinsic solubility in KVA64 colloidal solution (3.6-fold). These results support the formation of H-bond interactions as an important supersaturation mechanism with the ability to enhance not only the kinetic, but also the intrinsic solubility of poorly soluble drugs.

It is worth mentioning, that ABZ did not fit to this rule and a much higher solubility enhancement factor was observed (130-fold at a similar drug:polymer molar ratio (50:1)) although only 2 H-donor groups are present in its structure. Due to its low M_w and linear structure, which reduces steric hindrance, interactions with the polymer and the adsorption of the polymer onto the crystal surface were facilitated (Xie et al., 2010).

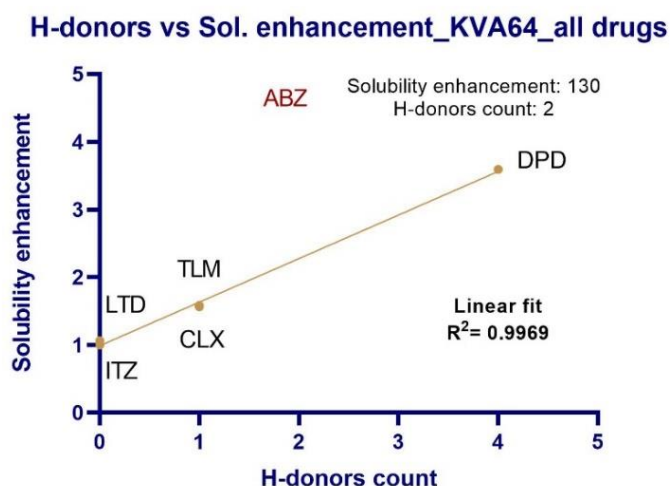


Figure 5.17: Linear relationship between the H-donor count within the drug molecules and the solubility enhancement factor in KVA64 colloidal solution (\approx molar ratio drug:polymer, 50:1).

5.1.3.5.2 Methocel A4C

Considering the gel-like properties of cellulose derivatives, such as Methocel A4C, the increased medium viscosity is one of the main impact factors for stabilizing the supersaturated state of poorly soluble drugs in solution (DiNunzio et al., 2008; Gao et al., 2009b; Usui et al., 1997). Only MA4C caused a significant viscosity increase in 0.15 M NaCl, which followed a linear relationship with the polymer concentration ($R^2= 0.9961$) (Table 5.4, Figure 5.18). The low viscosity increase observed for SOL and KVA64 was not significant.

The increased viscosity facilitated a supersaturation stabilization and precipitation inhibition. It reduced the molecular mobility within the medium and partially hindered nucleation and crystal growth (Xu and Dai, 2013b). This is again in good accordance with the spring and parachute model proposed by Guzman (Guzmán et al., 2004), in which the polymer delays precipitation. Using MA4C, an enhanced solubility was determined for all drug molecules tested but no direct relationship between the viscosity and solubility enhancement factor could be made. No significant polymer concentration-dependent effect was found and high polymer concentrations (0.125 and 0.250 % w/V) induced a decrease in the solubility. The formation of polymeric clusters at higher polymer concentrations were counterproductive for the drug solubility due to steric hindrance. Additionally, a counterproductive effect on the solubility with increasing viscosity was described in previous works for other polymers (Bevernage et al., 2011; Dai et al., 2008; Guzmán et al., 2007b).

Table 5.4: Viscosity values in (mPa*s) determined for KVA64, MA4C and SOL colloidal solutions in 0.15 M NaCl at a shear rate of 500 s⁻¹. A significant increase was observed for MA4C.

Polymer Concentration [% w/V]	KVA64		MA4C		SOL	
	Mean	SD	Mean	SD	Mean	SD
0.000	1.363	0.151	1.363	0.151	1.363	0.151
0.031	1.383	0.135	1.443	0.146	1.353	0.143
0.100	1.347	0.193	1.827	0.165	1.268	0.157
0.250	1.416	0.161	2.651	0.167	1.443	0.143

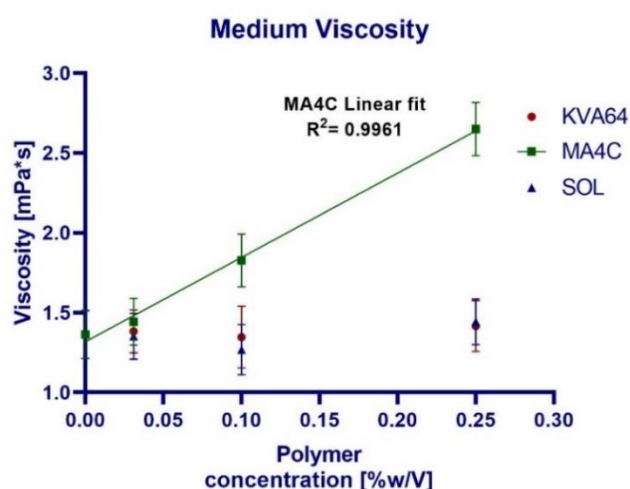


Figure 5.18: Linear concentration-dependent viscosity increase for MA4C colloidal solutions.

5. RESULTS AND DISCUSSION

5.1.3.5.3 *Soluplus*

The importance of the $\text{Log}P$ value in the formulation of lipid-based systems was already topic of discussion (Pouton, 2000). Considering the amphiphilic character of SOL, some similarities were found when formulating poorly soluble drugs with this polymer. The solubilization by SOL is driven by the incorporation of neutral drug molecules in the lipophilic core of the SOL-micelles, as shown in the Figure 3.9. Given the lipophilic nature of the core, the extent of solubilization mainly depends on the lipophilicity of the drug molecule. Under this assumption, high lipophilic molecules undergo a higher solubilization than low lipophilic molecules.

The correlation between the lipophilicity, expressed as partition coefficient P , with the extent of solubility enhancement showed an exponential relationship (Figure 5.19), thus supporting the above-mentioned theory. The trends were fitted to an exponential growth equation for each polymer concentration. The relationship established between the lipophilicity and solubility clearly indicated that the solubilization extent is minor for middle-lipophilic molecules (5-10-fold for DPD and CLX, $\text{Log}P$: 2.66 and 2.69, respectively) when compared to extremely lipophilic molecules such as ITZ (5,000 – 30,000-fold, $\text{Log}P$: 4.73). In this sense, the extremely low solubility of high lipophilic molecules increased the solubilization potential.

Despite the exponential trend observed, 2 out of the 6 tested molecules did not fit to this rule:

- ABZ. The low molecular weight weak base did not fit previously to the H-donor rule of KVA64 (Figure 5.17). Furthermore, it had not an extremely high $\text{Log}P$ value (2.92), compared to the other tested drugs. Despite this fact, it was extremely low soluble in aqueous medium (14.77 ± 3.25 ng/mL), a fact that triggered the solubilization by the SOL-micelles. In principle, it is rare that a molecule with a $\text{Log}P$ of 2.92 is extremely low soluble. In this case, other molecular descriptors can play a decisive role and limit the aqueous solubility. Under this assumption, the validity of the proposed relationship between the lipophilicity and the extent of solubilization could be limited to certain drug molecules.
- TLM. The complex ionization interplay for SOL-TLM (Table 5.3) influenced the extent of micellization. Besides, as the molecule is always partially ionized, it does not properly present a $\text{Log}P$ value and could not therefore be measured by means of the described chromatographic method (section 3.3.3.1). Instead, a $\text{Log}D$ of 3.22 at pH 7.4 was measured by means of the potentiometric determination (section 3.3.3.2). The value agreed with previously published results (Wienen et al., 2000). Nevertheless, the relation between the D value and the extent of solubilization did not fit to the proposed theory either, as solubilization extents ranged around 3,000 – 4000-fold (Figure 5.19). The precipitation of the drug as an amorphous form through LLPS was considered to additionally facilitate its solubilization within the polymeric micelles. Due to all these reasons, the relationship below did not appear to be suitable for a molecule like TLM with such a unique physicochemical behavior.

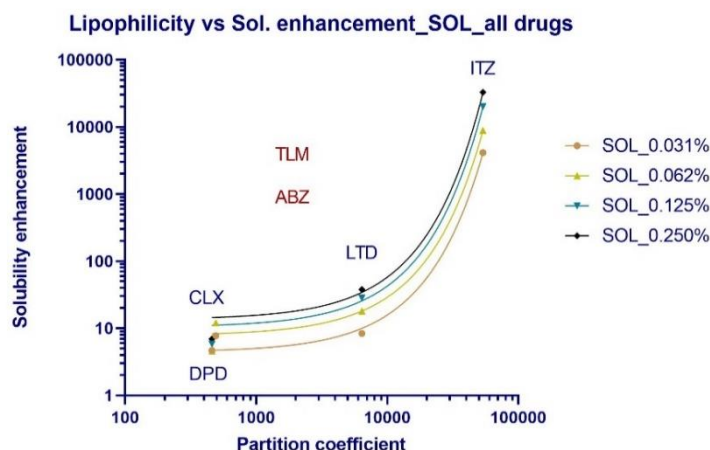


Figure 5.19: Exponential relationship between the SOL solubility enhancement factor and the partition coefficient. ABZ and TLM did not fit to the rule. TLM is a zwitterionic molecule and consequently its lipophilicity was not determined by means of the chromatographic method, but by potentiometric titration.

5.1.4 General physicochemical evaluation and underlying stabilization mechanisms

5.1.4.1 Relationship between pK_a shifts and solubility enhancement

The relationship between the pK_a -curves and the solubility facilitated the understanding of the previously proposed stabilization mechanisms (section 5.1.3.5) and the likeliness of solubilization. In the following, this is discussed for each investigated polymer.

5.1.4.1.1 Kollidon VA64

As previously discussed (Figure 5.17), the formation of intermolecular H-bond interactions drove the stabilization of poorly soluble drug molecules in KVA64 colloidal solution. At similar drug-polymer molar ratios, the H-donor count played an important role in the extent of stabilization achieved.

As proposed in the section 5.1.1, only the exponential decay 1 pK_a -curves were directly associated to a polymer concentration-dependent solubilization effect. The Figure 5.20A, indicated the absence of a correlation between the pK_a -curve and the solubility for the chaser molecules DPD and CLX, as well as for the extremely poorly soluble molecules ABZ and ITZ. For these molecules, either a linear (ITZ and CLX), an exponential decay 2 (DPD) or a sigmoidal (ABZ) pK_a -curve was obtained. Due to the absence of a real solubilization effect for these drug molecules, no relationship could be established between the solubility values and the apparent shifts in the pK_a (when present).

The non-chaser molecules LTD and TLM, which precipitated by means of LLPS, had exponential decay 1 pK_a -curves (Figure 5.4, Figure 5.5) in KVA64 solutions. It suggested a solubilization effect attributed to intermolecular interactions of an H-bonding nature in the case of TLM (1 H-Donor) and of other nature in the case of LTD (no H-Donor). The exponential shifts in the acid-base equilibria for TLM were related to an increase in its kinetic solubility (Figure 5.14). Furthermore,

5. RESULTS AND DISCUSSION

linear relationships were found between the pK_a and solubility curves, for the amorphous form (Figure 5.20A), as well as for the stable crystalline form (Figure 5.20B). For the non-chaser molecules, it confirmed a polymer concentration-dependent solubilization effect, which was not present for the chasers or for the extremely poorly soluble drugs.

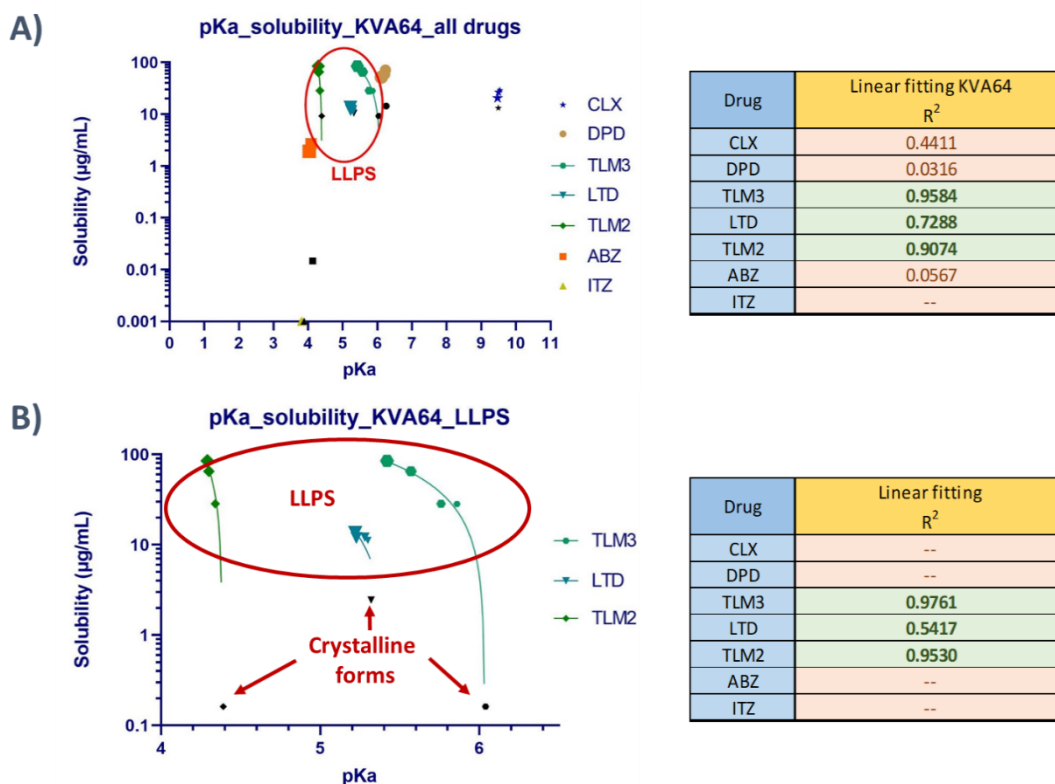


Figure 5.20: Relationship between the pK_a -curve and the solubility for all drugs in KVA64 colloidal solutions. **A)** An absence of a linear relationship (or other mathematical correlation) is observed for the chaser and extremely poorly soluble drugs. A linear relationship is observed for non-chaser molecules precipitating through LLPS. Black symbols represent the solubility of the amorphous form after precipitation. **B)** Linear relationship established for non-chaser molecules precipitating through LLPS. The black symbols represent the solubility of the crystalline form. The size of the colored symbols indicates an increasing polymer concentration.

5.1.4.1.2 Methocel A4C

The viscosity increase was considered as the main stabilization mechanism in MA4C colloidal solutions (Figure 5.18). At the same time, the formation of hydrophobic intermolecular interactions cannot be excluded as a solubilization mechanism. While for the chaser molecules, as well as for ABZ and TLM, only a supersaturation effect attributed to the viscosity increase could be detected, ITZ and LTD underwent a solubilization effect in MA4C solutions (see section 5.1.3). For the first group of molecules (chasers, ABZ and TLM) a linear or an exponential decay 2 pK_a -curve was measured. In the case of ITZ and LTD, an exponential decay 1 indicated the presence of a polymer concentration-dependent effect (Figure 5.8). As a result of the solubilization effect obtained for ITZ and LTD, a linear relationship was established between the pK_a -curves and the solubility (Figure 5.21). The solubilization effect responsible for the linear relationship between the pK_a and solubility curves was associated to the formation of

hydrophobic interactions, as it has been elucidated in previous works for cellulose derivate polymers (Gao et al., 2009b; Ilevbare et al., 2013b; Tian et al., 2007). Both ITZ and LTD molecules are very lipophilic (LogP: 3.81 for LTD and 4.73 for ITZ) and therefore, susceptible to establish hydrophobic interactions with MA4C. The absence of a polymer concentration-dependent solubilization effect for the chasers, ABZ and TLM was responsible for the lack of relationship between the pK_a and the solubility curves (Figure 5.21). Instead of that, the plot reflected a cluster of points for the drug in colloidal solution (colored points) and a lower solubility for the pure drug (black points).

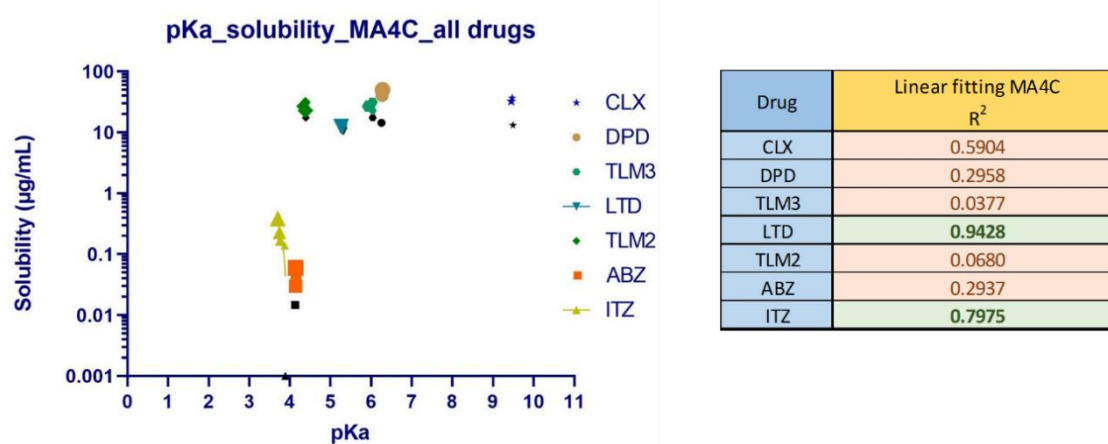


Figure 5.21: Relationship between the pK_a -curve and the solubility for all drugs in MA4C colloidal solutions. An absence of a linear relationship (or other mathematical correlation) is observed for almost all drugs, indicating the absence of intermolecular interactions and postulating the viscosity increase as the main supersaturation stabilization mechanism. The linear trend observed for LTD and ITZ supports the establishment of hydrophobic intermolecular interactions between both drugs with the MA4C monomers. The black symbols represent the intrinsic solubility of the form originated after precipitation. The size of the colored symbols indicates an increasing polymer concentration.

5.1.4.1.3 Soluplus

An exponential decay 1 progression was determined for the pK_a -curves in SOL solution (Figure 5.9). High pK_a shifts, even at the lowest applied polymer concentration (0.031% w/V), indicated its high solubilization potential and its ability to avoid precipitation from a thermodynamic perspective. As a result, SOL showed an exponential relationship between the pK_a -curve and the solubility for all drug molecules (Figure 5.22). The high R^2 coefficients of determination established between the pK_a and solubility curves confirmed the decrease of the molecularly dissolved drug fraction by means of micellization. The extents of solubilization and the shift in the pK_a heavily depended on the drug molecule used, as reflected in the plot (Figure 5.22).

5. RESULTS AND DISCUSSION

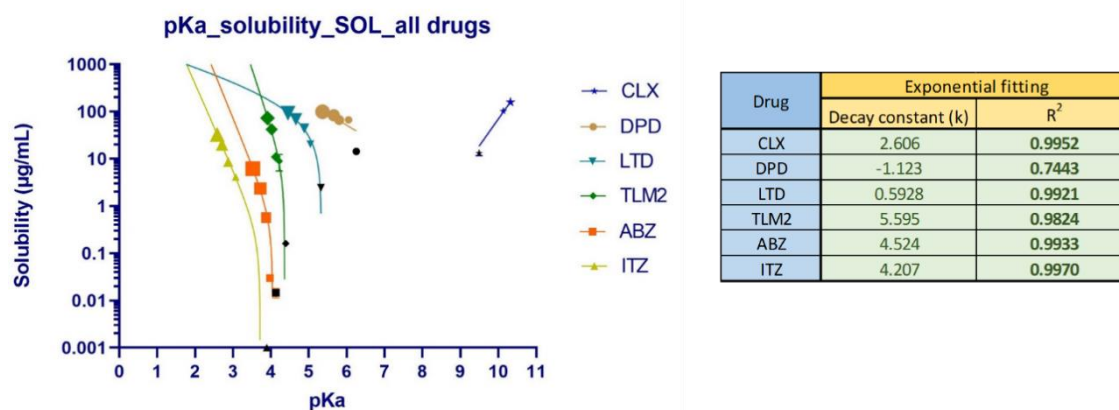


Figure 5.22: Relationship between the pK_a -curve and the solubility for all drugs in SOL colloidal solutions. An exponential trend was observed in all cases, supporting the relationship between the pK_a -shifts and the extent of solubilization. The black symbols represent the intrinsic solubility of the stable crystalline form. The size of the colored symbols indicates an increasing polymer concentration.

5.1.4.2 Relationship between the SOL pK_a -shifts and other physicochemical properties

Following the previously established relationship between the pK_a and solubility curves with a polymer concentration-dependent effect (Figure 5.22) and the influence of the $\text{Log}P$ on the extent of solubilization (Figure 5.19), a correlation between the pK_a shifts and the $\text{Log}P$ was investigated. The validation whether the drug lipophilicity triggers micellization and induces changes in the acid-base equilibria, which are the result of a solubilization effect, was in focus.

The plot established between $\text{Log}P$ ($\text{Log}D$ pH 7.4 for TLM) of each drug molecule and their respective pK_a -shifts indicated an exponential relationship ($R^2 = 0.9632$) for the lowest SOL concentration applied (0.031% w/V) (Figure 5.23). This goes hand in hand with the type of model for the pK_a -curves (exponential decay, Figure 5.9) and the exponential increase of the solubility enhancement ratios as a function of the $\text{Log}P$ (Figure 5.19). However, with increasing SOL concentration, the exponential relationship could no longer be applied and the R^2 values of the fitting decreased (Figure 5.23). Therefore, the lipophilicity partially explains the pK_a -shifts and the solubilization effect for weak basic molecules, but other physicochemical properties such as molecular weight, polar surface area and the total number of H-donors and acceptors can play an important role, too.

The weak acid molecule CLX ($\text{Log}P$: 2.692) did not fit to the described relationship (Figure 5.23). Despite a similar lipophilicity to DPD, the pK_a -shifts observed for CLX were much higher (0.64 – 1.26). Therefore, at similar $\text{Log}P$, the degree of solubilization and its translation into pK_a -shifts might be different for basic and acidic molecules and consequently, it should be regarded separately.

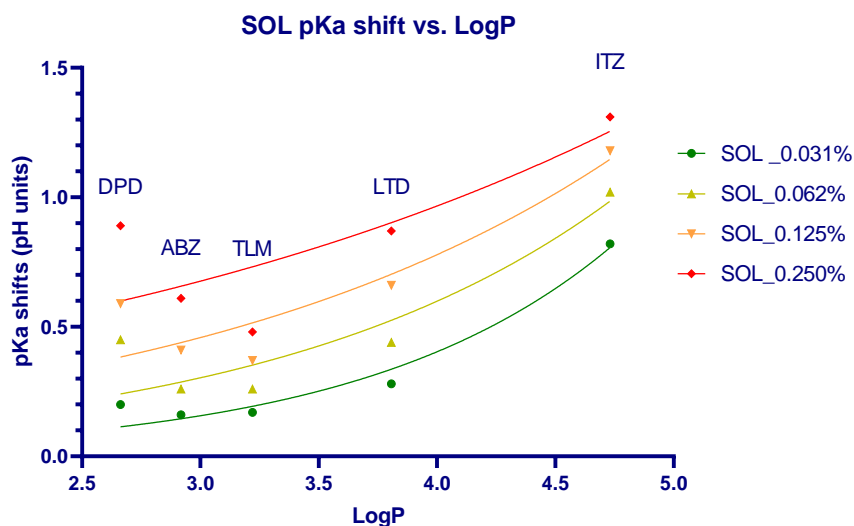


Figure 5.23: Exponential relationship established between the pK_a shifts (pH units) and the LogP values for the molecules investigated within this work. The green curve presents a coefficient of determination $R^2 = 0.9632$. This decreases at increasing polymer concentrations.

The absence of a general direct relationship between the pK_a -shifts and solubility enhancement factors for all drug molecules (Figure 5.22) highlighted the importance of the lipophilicity of the drug molecules as a third contributing factor to the solubilization (Figure 5.23). Nevertheless, a nearly exponential relationship between the pK_a -shifts and the solubility enhancement factors were observed separately for each drug molecule investigated (2D plot Figure 5.24, Table 5.5). The growth constant indicated the degree of change in the solubility with increasing polymer concentrations as a function of the pK_a -shifts.

The relationship between the three physicochemical properties (pK_a , solubility and lipophilicity) was considered in the 3D plot in Figure 5.24. In this plot, two regions (A and B) were identified. In region A, lower lipophilic molecules were clustered which are less susceptible for solubilization, such as DPD or CLX (chaser molecules). The region B corresponds to higher lipophilic molecules, for which higher solubilization effects and higher pK_a -shifts were measured, like for ITZ. In between both regions, the non-chasers LTD and TLM, as well as ABZ were found. Despite the absence of a complete correlation, a connection between pK_a -shifts, lipophilicity and the solubilization extents was recognized. The missing complete correlation is an indicator for additional molecular descriptors or physicochemical properties involved in the internalization of neutral species within the SOL-polymeric micelles.

5. RESULTS AND DISCUSSION

Table 5.5: Parameters obtained for the exponential relationship between the pK_a -shifts and the solubility enhancement ratios for the drug molecules in SOL colloidal solutions. The growth constant indicated the degree of change in the solubility with increasing polymer concentrations as a function of the pK_a -shifts.

Drug	Exponential fitting	
	Growth constant (k)	R ²
ITZ	4.242	0.9965
TLM	6.690	0.9715
ABZ	5.811	0.9827
LTD	2.009	0.9515
CLX	2.308	1.0000*
DPD	0.6542	0.8842

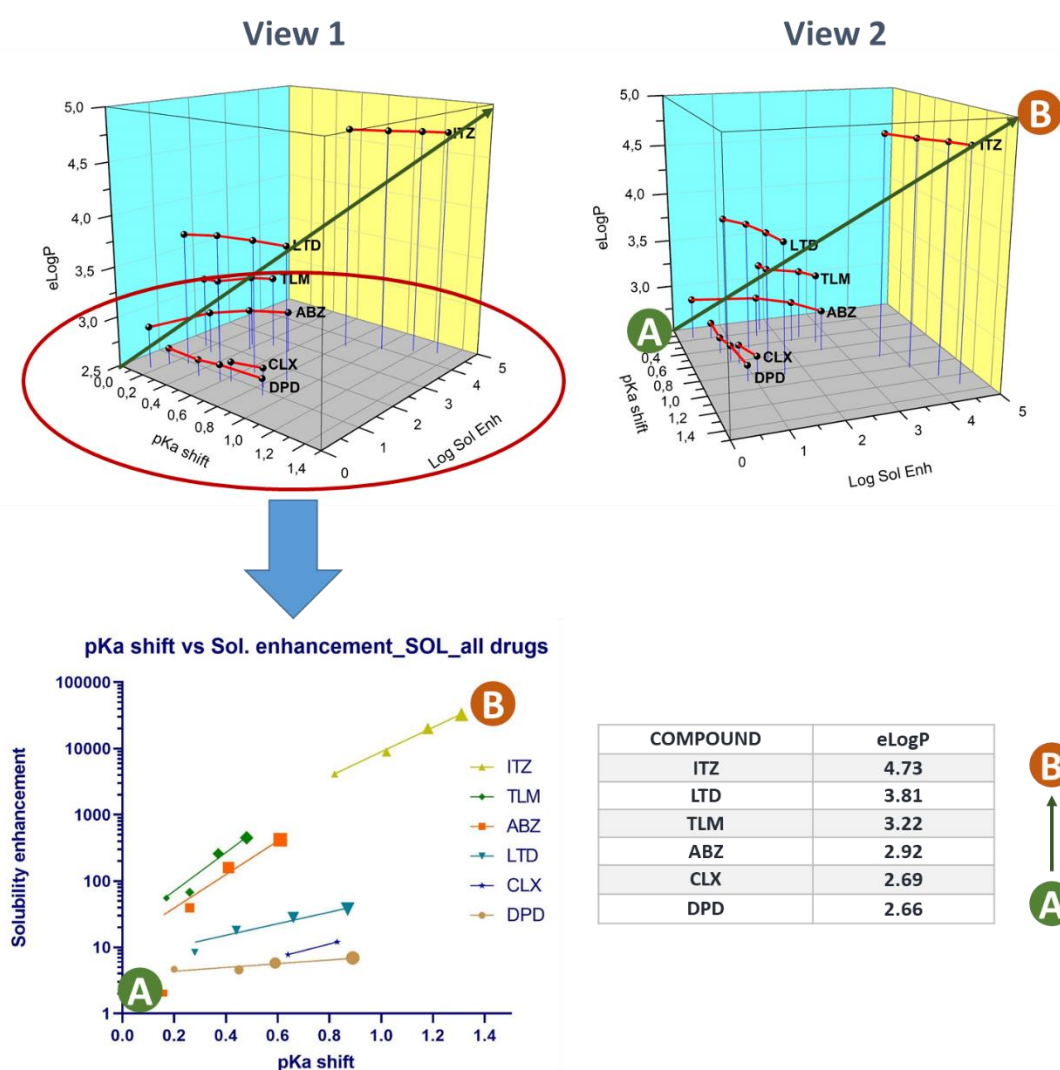


Figure 5.24: Trend between pK_a -shifts, solubility enhancement ratios and $eLogP$ in SOL colloidal solutions. The right 3D plot shows the presence of two regions for low lipophilic molecules with low degrees of solubilization (**A**) and high lipophilic molecules with a higher degree in solubilization (**B**). The green arrow describes the connection between pK_a -shifts, solubility enhancement ratios and $LogP$. The size of the colored symbols indicated an increasing polymer concentration.

5.1.5 Conclusion

The physicochemical characterization of poorly soluble drug in polymeric solutions provided an important insight in the supersaturation and solubilization at a molecular level. These investigations facilitated the elucidation of the different supersaturation mechanisms achieved by the selected polymers, as well as a clear differentiation between supersaturating and solubilizing drug-polymer combinations.

First of all, the UV-metric pK_a -determination was suitable to detect changes in the ionization equilibria induced by variations in the molecularly dissolved drug fraction due to solubilization effects. Strong complexation, micellization or generally steric hindrance were limiting factors for the participation in this ionization equilibrium. Based on the assumption that only the molecularly dissolved fraction is accessible for absorption (Buckley et al., 2013), the presence of a pK_a -shift might be indicative for an impeded drug permeation through biological membranes caused by the addition of stabilizing polymers.

The CheqSol method enabled the differentiation between compounds showing an innate supersaturation ability (chasers, DPD and CLX) and compounds which did not supersaturate (non-chasers, LTD and TLM). Furthermore, the intrinsic solubility of extremely poorly soluble molecules (ABZ and ITZ) was characterized by means of the shaking flask method.

The main stabilization mechanisms of the three polymers used were identified. For KVA64, a linear relationship between the intrinsic solubility and the H-donor count of the drugs was found at similar drug/polymer molar ratios (Figure 5.17). The formation of H-bond interactions, as previously proposed (Xu and Dai, 2013b), was considered as the main stabilization mechanism for this polymer. For MA4C, an increased medium viscosity caused by the general gelling behavior of cellulose derivatives was observed (Figure 5.18). Although this was considered as its main stabilization mechanism to limit precipitation, the contribution of other mechanisms, such as the formation of hydrophobic interactions with highly lipophilic molecules like LTD and ITZ, could not be excluded. For SOL, a clear solubilization effect caused by micellization was identified for all drugs (Figure 5.22). The extent of solubilization by SOL depended on the drug lipophilicity (Figure 5.19), as well as on the polymer concentration applied.

For chasers (DPD and CLX), which precipitated into the crystalline form, KVA64 and MA4C polymers had a positive effect as crystal growth inhibitors (Figure 5.10, Figure 5.11), induced by a supersaturation effect as indicated by linear pK_a -curves (Figure 5.1, Figure 5.6). For non-chasers (LTD and TLM), which precipitated as an amorphous form by means of LLPS (Comer et al., 2014) certain solubilization extents were observed (Figure 5.12, Figure 5.14). The exponential pK_a -curves obtained for all non-chaser drugs were indicator for polymer concentration-dependent solubilization effects by the formation of intermolecular interactions or complexation (Figure 5.4, Figure 5.5). This was attributed to the higher energetic state of the precipitating form when compared to chaser molecules. For the extremely poorly soluble ABZ and ITZ, the improvement of intrinsic solubility depended on specific drug-polymer interactions. The exponential decays in pK_a -curves suggested the formation of intermolecular interactions for ABZ/KVA64 and ITZ/MA4C (Figure 5.2, Figure 5.3) and a solubilization effect in colloidal solutions was obtained (Figure 5.15, Figure 5.17). For the other combinations (ABZ/MA4C and ITZ/KVA64), no solubilization effect occurred.

5. RESULTS AND DISCUSSION

5.2 Part II: *In vitro* evaluation of the interplay between supersaturation and partition by means of a biorelevant gastrointestinal dissolution tests.

Complementing the first part of this thesis, where the supersaturation and solubilization were characterized from a physicochemical and thermodynamic perspective, the second part focused on an *in vitro* kinetic investigation of the supersaturation and solubilization potential under biorelevant conditions.

The combination of the thermodynamic and kinetic approaches allowed a more detailed investigation on the biorelevant interplay between supersaturation, precipitation and partition *in vitro*. Therefore, it differentiated between suitable drug-polymer combinations, which maintained the supersaturated state and can facilitate the oral absorption by passive diffusion *in vivo*, and drug-polymer combinations for which the solubilization effect impedes permeation. Relevant aspects, including the precipitation time or the physical state of the precipitating form, which affect the bioaccessibility and bioavailability of poorly soluble drugs *in vivo*, were investigated *in vitro* by two biorelevant approaches:

- investigation of water-soluble polymers to potentially influence the supersaturation/solubilization and precipitation interplay (monophasic approach)
- and the supersaturation potential to enhance oral absorption (biphasic approach).

5.2.1 Monophasic dissolution test (MDT)

The monophasic dissolution test was used to investigate the ability of polymers to stabilize the supersaturation or solubilization under simulated biorelevant conditions. Contrary to the biphasic approach, it only focused on potential effects of the polymers as precipitation inhibitors. In this way, it set the basis for the biphasic approach (section 5.2.2), as it enabled the differentiation between stabilizing polymer/drug combinations and those with very limited stabilization effects. As described in the section 4.2.2.1.3, the parameters area under the curve (AUC), precipitation time (t_p) and average precipitation rate (dC/dt) were calculated from the dissolution results to evaluate the efficacy of the polymers as precipitation inhibitors.

Additionally, the particle size distribution (PSD) and the physical state of these precipitated particles were analyzed after the end of the test by means of laser diffraction spectrometry (LDS)/ dynamic light scattering (DLS) and polarized light microscopy (PLM).

5.2.1.1 Chaser molecules

5.2.1.1.1 Dipyridamole

According to DPD's ionization constant ($pK_a = 6.25 \pm 0.02$), a pH-dependent solubility was expected within the different regions of the GI tract. It led to two separate precipitation events for the pure drug and in combination with the supersaturating polymers KVA64 and MA4C. These precipitation events differed between 1) pH interval 5.5 and 2) pH interval 6.8 – 7.4 (Figure 5.25A-C). The fastest precipitation rates, induced by the specific ionization properties of DPD, occurred after buffering the aqueous phase from pH 1.1 to pH 5.5 (Figure 5.27A).

KVA64. The precipitation inhibition for DPD was minor (Figure 5.25B). Consequently, no significant deceleration in the precipitation rate was observed (Figure 5.27A,B) and the AUC

values remained in a very similar range as for the pure drug (Figure 5.26). Initially, a higher kinetic stabilization was expected due to an adsorption of KVA64 to the DPD crystals, as it was shown for other PVP derivatives and drug combinations (Ma et al., 1996; Xie et al., 2010).

MA4C. The viscosity increase in MA4C colloidal solutions (up to 2.6 mPa*s) showed a positive concentration-dependent effect as precipitation inhibition mechanism at pH 5.5 (Figure 5.25C). However, this effect was not maintained at pH 6.8 or 7.4. Remarkably, higher degrees of supersaturation ($\approx 400 \mu\text{g/mL}$ of DPD) at pH 5.5 induced faster initial precipitation after buffering to pH 6.8, caused by an increased chemical potential (μ) (Brouwers et al., 2009). Nevertheless, this was followed by a further re-dissolution and precipitation of the drug in the pH 6.8 period (Figure 5.25C).

SOL. The solubilization approach through SOL proved to be the most effective as precipitation inhibitor (Figure 5.25D). It considerably limited or completely hindered the crystal growth by means of the internalization of neutral species in the SOL-micelles and maintained between 90 – 100% of the drug in solution over the full length of the test. Therefore, a deceleration of the dC/dt or a completely absence of precipitation in some replicates was observed, which was in turn responsible for the high standard deviation in t_p and dC/dt (Figure 5.27A,B).

The potential of KVA64 and MA4C as supersaturating excipients was similarly demonstrated by the MDT and correlated with the CheqSol observations (Figure 5.10) and the pK_a -curves (Figure 5.1) which suggested the absence of solubilization.

The MDT did not consider the *in vivo* presence of an absorptive compartment and consequently, it did not address intestinal absorption. As a result, an overestimation of the dC/dt in the GI lumen might occur (Dai, 2010; O'Dwyer et al., 2019). Despite this fact, the MDT proved to be a useful and a simple approach to differentiate between suitable and unsuitable drug-excipient combinations in terms of stabilization and crystal growth inhibition.

5. RESULTS AND DISCUSSION

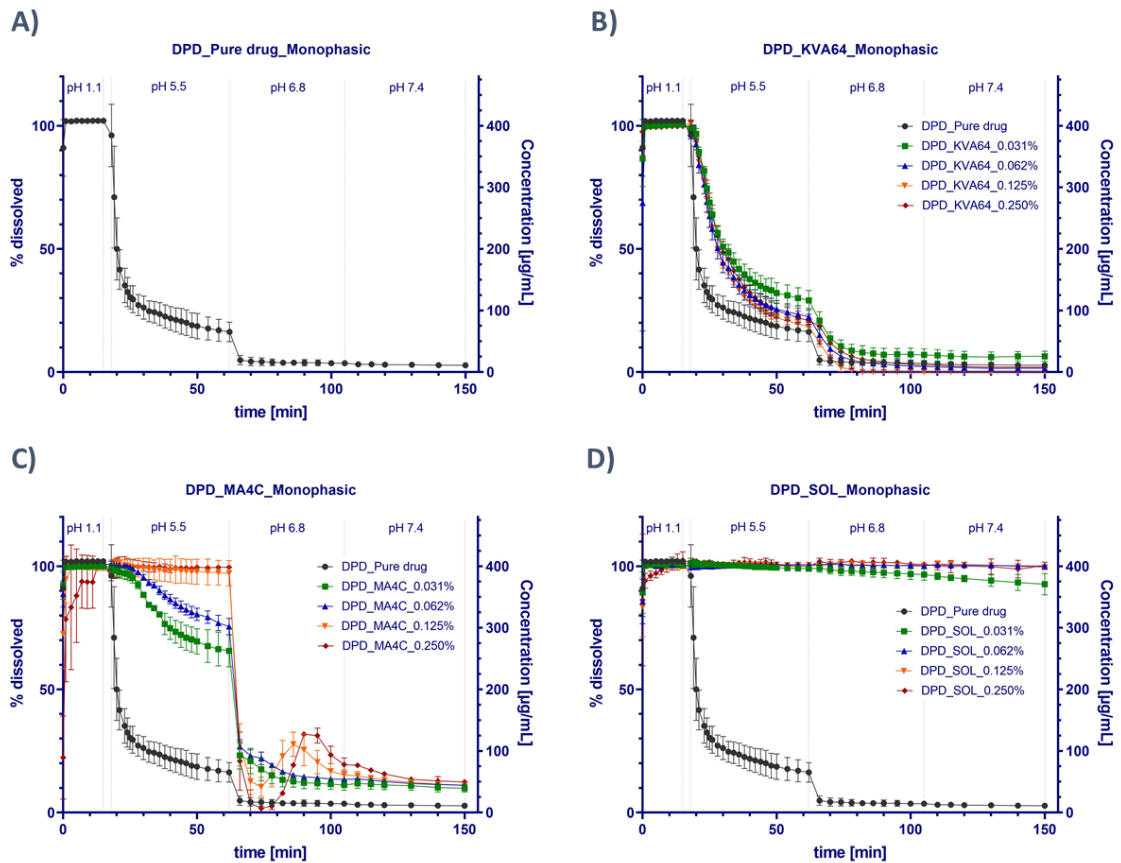


Figure 5.25: DPD monophasic dissolution tests (Mean \pm SD, $n=3$) in NaCl 0.15 M. **A)** Pure drug, **B)** KVA64, **C)** MA4C, **D)** SOL. The poor solubility of the pure drug under small intestinal conditions, as well as the stabilization achieved through the polymeric colloidal solutions is highlighted.

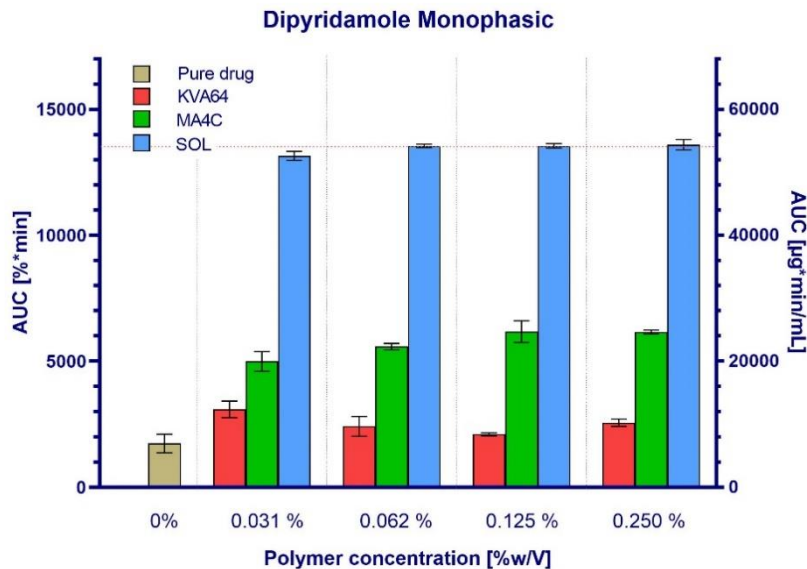


Figure 5.26: DPD comparative AUCs obtained from the precipitation phase (pH 5.5 – pH 7.4) in the MDT approach (Mean \pm SD, $n=3$). The red dotted line represents 100% of dissolved drug during the precipitation phase, corresponding to 13500 %*min (left y-axis) or 54000 $\mu\text{g} \cdot \text{min}/\text{mL}$ (right y-axis).

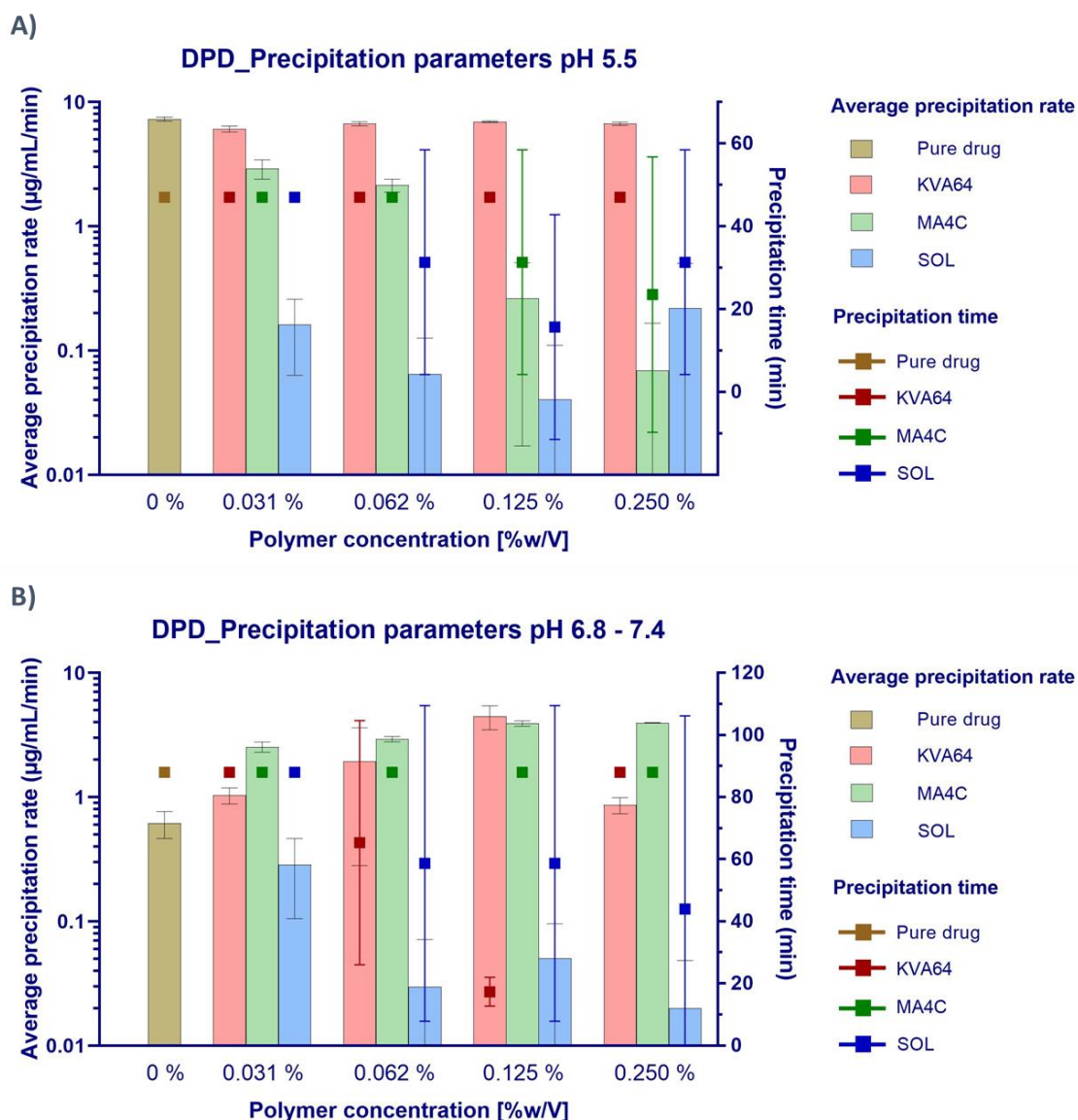


Figure 5.27: Comparative DPD average precipitation rates (left y-axis) and precipitation times (right y-axis) (Mean \pm SD, $n=3$) at pH 5.5 (A) and at pH 6.8-7.4 (B). High SD in the precipitation times indicated the absence of precipitation or the presence of very low precipitation rates during the experiment in some cases.

Dipyridamole particle size distribution

The MDTs revealed a positive stabilization of DPD in solution by the three stabilizing polymers (Figure 5.25). However, extensive precipitation still occurred in all KVA64 and MA4C polymeric solutions. Even when the precipitate PSD is the result of a complex kinetic process, which should be analyzed *in situ*, only an offline endpoint determination was feasible. Therefore, no kinetic changes in the PSD over time were determined and only the effect of the polymers to the final PSD (pH 7.4) will be discussed in this section.

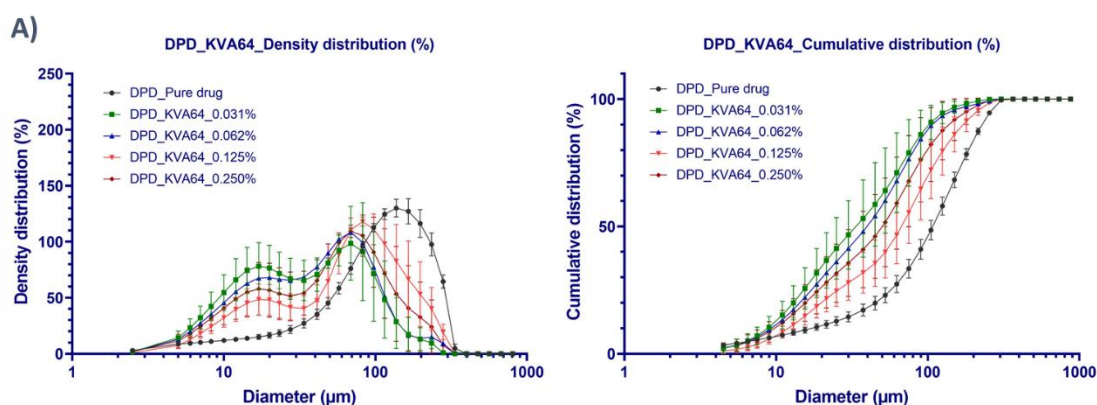
5. RESULTS AND DISCUSSION

Pure DPD microcrystals showed a broad monomodal distribution with d_{10} , d_{50} and d_{90} of 17.63, 108.08 and 229.14 μm , respectively (Figure 5.31A). Besides, it achieved a span-value of 1.96, indicating a broad distribution of the particles (Figure 5.28A, left). The pure DPD precipitates were needle-shaped (Figure 5.28B), which contributed to the broad distribution observed. In dependence of the precipitate orientation in the measuring device, it either detected the long height or the short width of the needles.

KVA64. Despite the minor stabilization of DPD in solution, KVA64 was effective as crystal growth inhibitor and changed the obtained PSDs into bimodal distributions at all polymer concentrations (Figure 5.28A, left). Compared to pure DPD, KVA64 decreased the average diameter of the DPD particles as a function of decreased polymer concentration (Figure 5.31A). As reflected in the PSDs and micrographs, the adsorption of the polymer molecules to the DPD crystal lattice limited the crystal growth (Figure 5.28B). At the same time, the shape of the particles remained unaffected and the PSDs became broader due to the shift into a bimodal distribution.

MA4C. Despite the positive kinetic stabilization effect by different MA4C concentrations at pH 5.5 (Figure 5.25C), the drug precipitation was not hindered in neutral medium. Surprisingly, the PSDs of precipitates and pure drug were similar (Figure 5.29A). Compared to the pure drug, due to a lower fraction of smaller particles in the colloidal solution, the broadness of the PSDs seemed to decrease at all polymer concentrations, as reflected by the span-values (Figure 5.31A). Furthermore, needle-shaped crystals were similarly observed in MA4C as for KVA64 colloidal solutions (Figure 5.29B).

SOL. According to the micellization of DPD by SOL, the PSDs were in the nano-range (Figure 5.30A). These nanoparticles should not be considered as precipitated drug, but as the vehicle where the drug molecules are apparently dissolved. The Z-average values were in the range of 179 to 247 nm and tended to increase as a function of polymer concentration (except for 0.250% w/V), similarly to the polydispersity indexes (PDI) (Figure 5.31B). The results showed a monodisperse nanoparticle distribution for the two lowest polymer concentrations (0.031 – 0.062 % w/V), since a PDI < 0.2 was obtained. This was not the case for SOL concentrations \geq 0.125 % w/V. Remarkably, 24 h after the end of the MDT, a cluster of crystalline microparticles was observed under PLM for the 0.031% colloidal solution (Figure 5.30B). This was not obtained at higher concentrations. These results supported the stability of the SOL-solubilization approach as a suitable mechanism to avoid the precipitation of DPD.



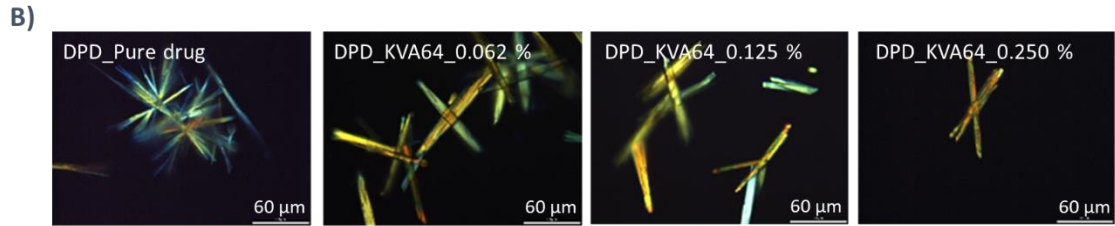


Figure 5.28: Comparative particle analysis for DPD_KVA64. **A)** Particle size distributions obtained by laser diffractometry (Mean \pm SD, $n=3$). **B)** Micrographs obtained by PLM in a transmitted light modus (500x). The presence of needle-shaped crystals was characteristic in all cases.

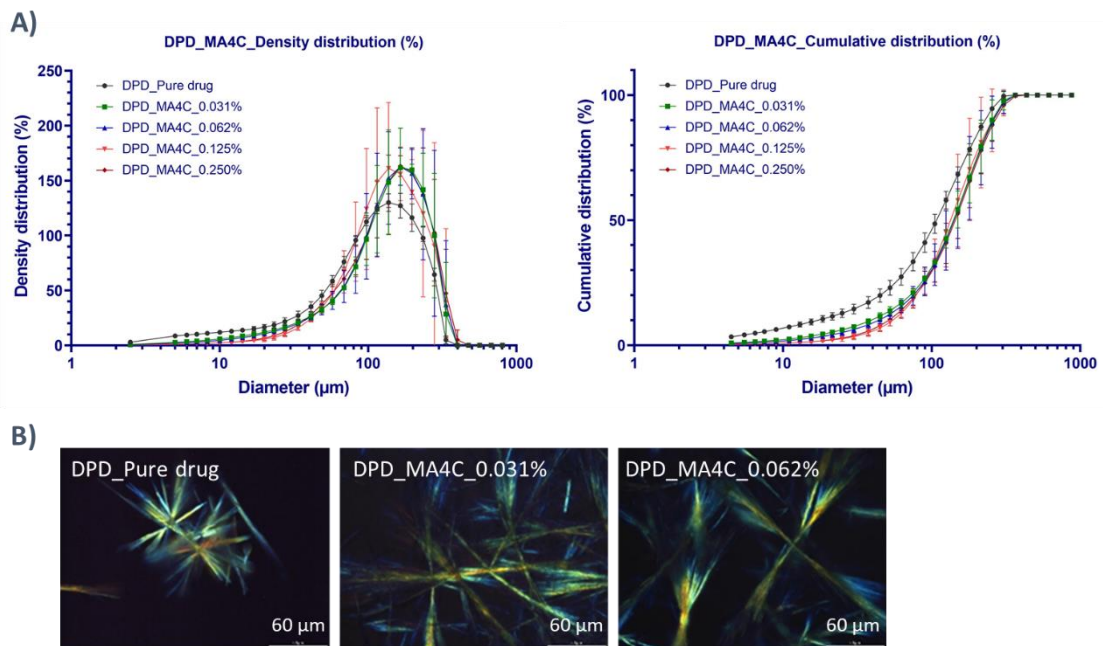
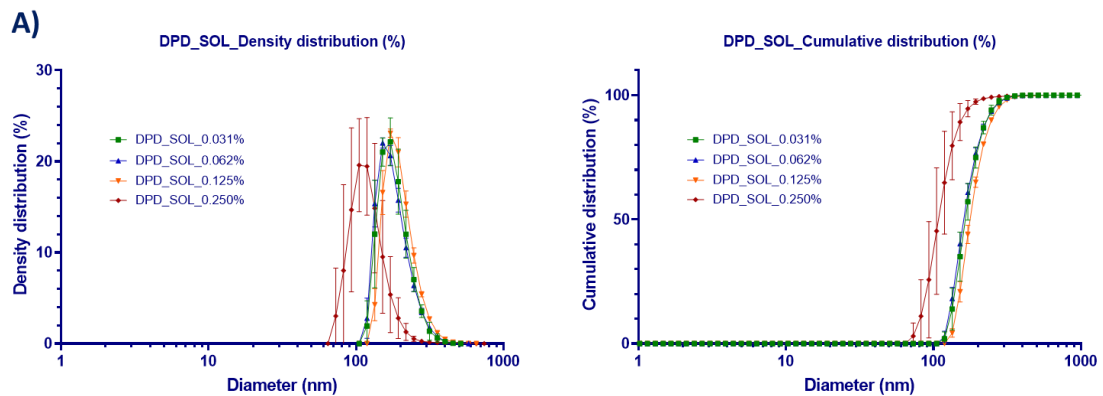


Figure 5.29: Comparative particle analysis for DPD_MA4C. **A)** Particle size distributions obtained by laser diffractometry (Mean \pm SD, $n=3$). **B)** Micrographs obtained by PLM in a transmitted light modus (500x). DPD crystals formed in MA4C colloidal solutions tended to be more filamentary than for the pure drug.



5. RESULTS AND DISCUSSION

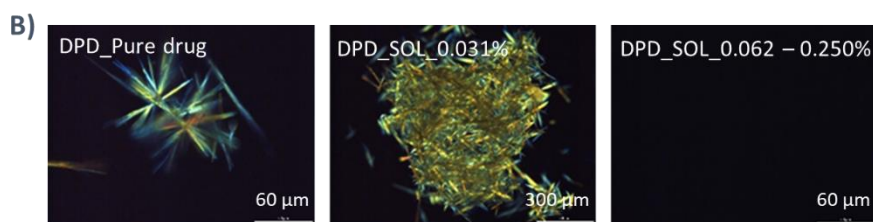


Figure 5.30: Comparative particle analysis for DPD_SOL. **A)** Particle size distributions obtained by dynamic light scattering (Mean \pm SD, $n=3$). **B)** Micrographs obtained by PLM in a transmitted light modus (500x, 100x and 500x, respectively). Agglomerates of DPD precipitates were observed at the lowest concentration applied at 24 h after test end. This was not observed at higher polymeric concentrations.

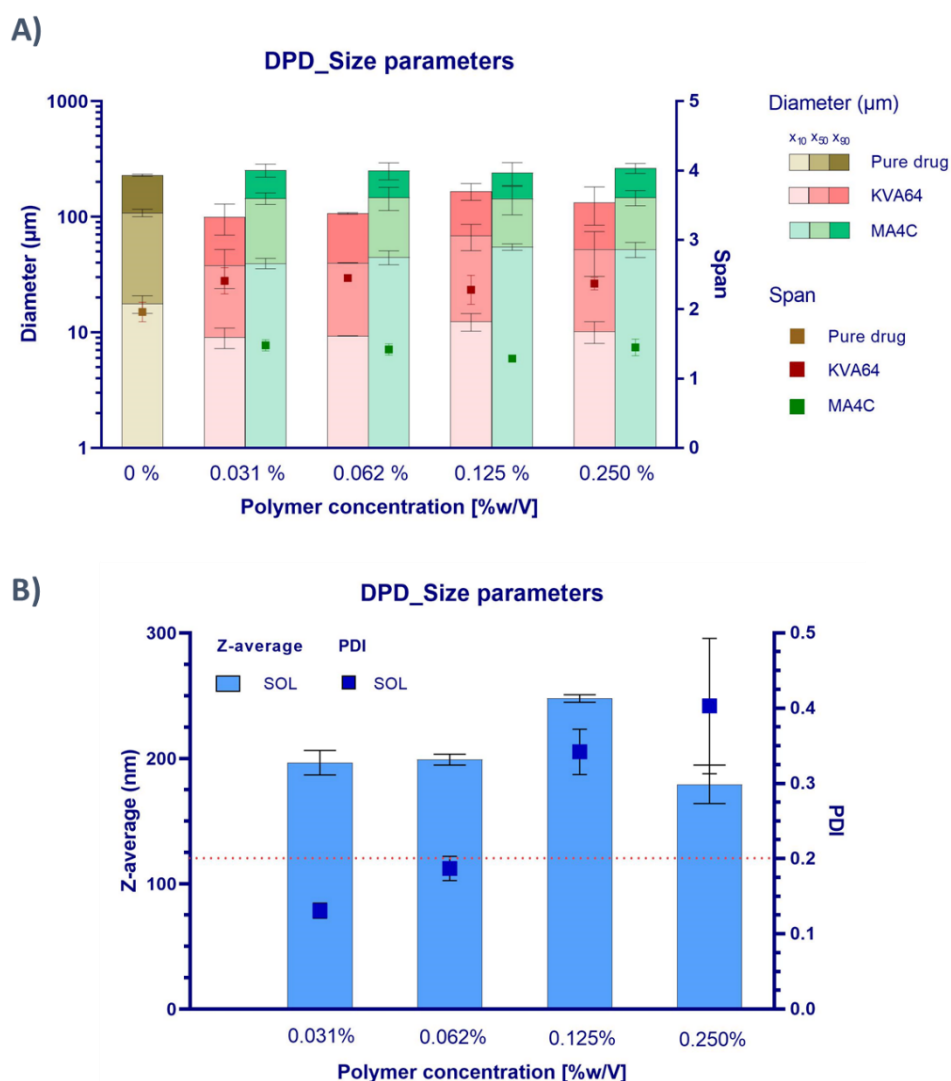


Figure 5.31: Comparative DPD particle size parameters. **A)** Size diameters (left y-axis) and span-values (right y-axis) (Mean \pm SD, $n=3$) for DPD particles formed by the pure drug and in KVA64 and MA4C colloidal solutions. **B)** Z-average values (left y-axis) and polydispersity indices (right y-axis) for DPD-SOL nanoparticles. The red dotted line, referred to the right y-axis, indicating the PDI limit of monomodal dispersed particle population.

5.2.1.1.2 *Celecoxib*

Due to the CLX specific physicochemical properties (weak acid, $pK_a = 9.49 \pm 0.03$), the drug showed a poor solubility throughout the entire pH-range used in the MDT. The high amount of the neutral CLX form in gastric and intestinal conditions is one of the main reasons for its low oral bioavailability (Celebrex[®] capsule: 40%)(Shakeel et al., 2008). Due to the experimental setup in the MDT, following the solvent shift method, a short time of supersaturation for the pure drug in the gastric pH interval was seen (Figure 5.32A). This short supersaturation time of 10-15 minutes was followed by precipitation to the saturation solubility ($\approx 20 \mu\text{g/mL}$) (Figure 5.11). The stabilization of this short supersaturation period can therefore become a suitable approach to enhance its oral bioavailability. An average $dC/dt = 0.263 \pm 0.09 \mu\text{g/mL/min}$ was measured, as well as a $t_p = 135 \text{ min}$. In the case of polymer addition, all three polymers achieved high extent of stabilization of CLX in colloidal solution.

KVA64 and MA4C. The polymers KVA64 and MA4C induced an extensive supersaturation effect, especially in the intestinal period and reached drug concentrations in the range of 125 – 175 $\mu\text{g/mL}$ (Figure 5.32B,C). According to the pure drug (Figure 5.32A), this effect cannot be explained by CLX physicochemical properties (e.g. weak acid), since the CLX molecules remain in their neutral form during all GI tract conditions. The innate supersaturation ability of CLX (which is additionally favored in polymeric colloidal solutions) might be one of the key points to understand these observations. More importantly, CLX clearly precipitated in colloidal solutions as nanoparticles (Figure 5.36) in the amorphous form, which was confirmed by the absence of birefringence under PLM. The amorphous state of the particles was indicative for a controlled precipitation with hindered or delayed nucleation and crystallization phenomena. Furthermore, the precipitation in this highly energetic amorphous form facilitated the re-dissolution of the drug when thermodynamically favored conditions (e.g. volume addition during buffering to pH 5.5) were given. The high extent of supersaturation and the additional precipitation inhibition during this intestinal pH period for CLX under the influence of KVA64 or MA4C was not comparable to the other investigated weak bases and ampholyte molecules. Especially in KVA64 colloidal solutions, independently of the dissolution extent in the gastric phase, similar supersaturation levels were reached in the subsequent intestinal conditions (Figure 5.32B). The absence of a polymer concentration-dependent effect was related to the saturation of the interaction points between CLX and KVA64 already at low polymer concentrations, since CLX only possesses 1 H-donor atom (hydrogen from sulfonamide group).

In the case of MA4C colloidal solutions, identical dissolution rates to KVA64 colloidal solutions were observed in the gastric phase, independent of the polymer concentration applied. However, higher polymer concentrations (0.125 % w/v) achieved a lower stabilization during the intestinal pH period and showed CLX concentrations of 150 $\mu\text{g/mL}$ in solution, while lower polymer concentrations maintained the CLX concentration at around 170 $\mu\text{g/mL}$ (Figure 5.32C).

In comparison to the results of the other drug molecules, the high extent of CLX supersaturation in the intestinal period made the occurring precipitation negligible for all KVA64 and MA4C colloidal solutions (Figure 5.32B,C). Overall, compared to the pure drug, the supersaturation effect for CLX was maintained in solution during the entire test (135 minutes, intestinal period). It supported the shift from chaser into a non-chaser behavior of CLX prior observed in the CheqSol determination (Figure 5.11).

5. RESULTS AND DISCUSSION

SOL. The positive solubilization effect for CLX-SOL colloidal solutions was confirmed from a thermodynamic perspective in the CheqSol approach (Figure 5.11). From a kinetic point of view, the solubilization was further supported by the MDTs at different polymer concentrations with a clear polymer concentration-dependent effect. At the lowest polymer concentration (0.031 % w/V), only a minor solubilization was observed with a CLX concentration of approximately 50 $\mu\text{g/mL}$ at test end (Figure 5.32D). Thus, the equilibrium solubility ($\approx 100 \mu\text{g/mL}$ in the CheqSol method) was not reached and the drug kept dissolving. When higher polymer concentrations ≥ 0.062 % w/V were applied, the entire drug fraction used was solubilized and a CLX concentration of 200 $\mu\text{g/mL}$ during the entire experiment was achieved (Figure 5.32D). It highlighted the extensive solubilization potential of SOL for CLX. As expected, the lipophilicity of CLX and the high fraction of the neutral CLX form over the entire experiment favored the solubilization.

To sum up, CLX was successfully stabilized in solution through a variety of mechanisms (intermolecular interactions, viscosity increase and solubilization), as it was clearly reflected by the AUCs of the dissolved drug (Figure 5.33). Considering the poor solubility of the pure drug throughout the GIT and its stabilization by three different mechanisms, it made CLX suitable as chaser model drug to test under *in vivo* conditions. Based on the BDT results (discussed in the section 5.2.2), the suitability of CLX to be tested under an *in vivo* approach will be further evaluated.

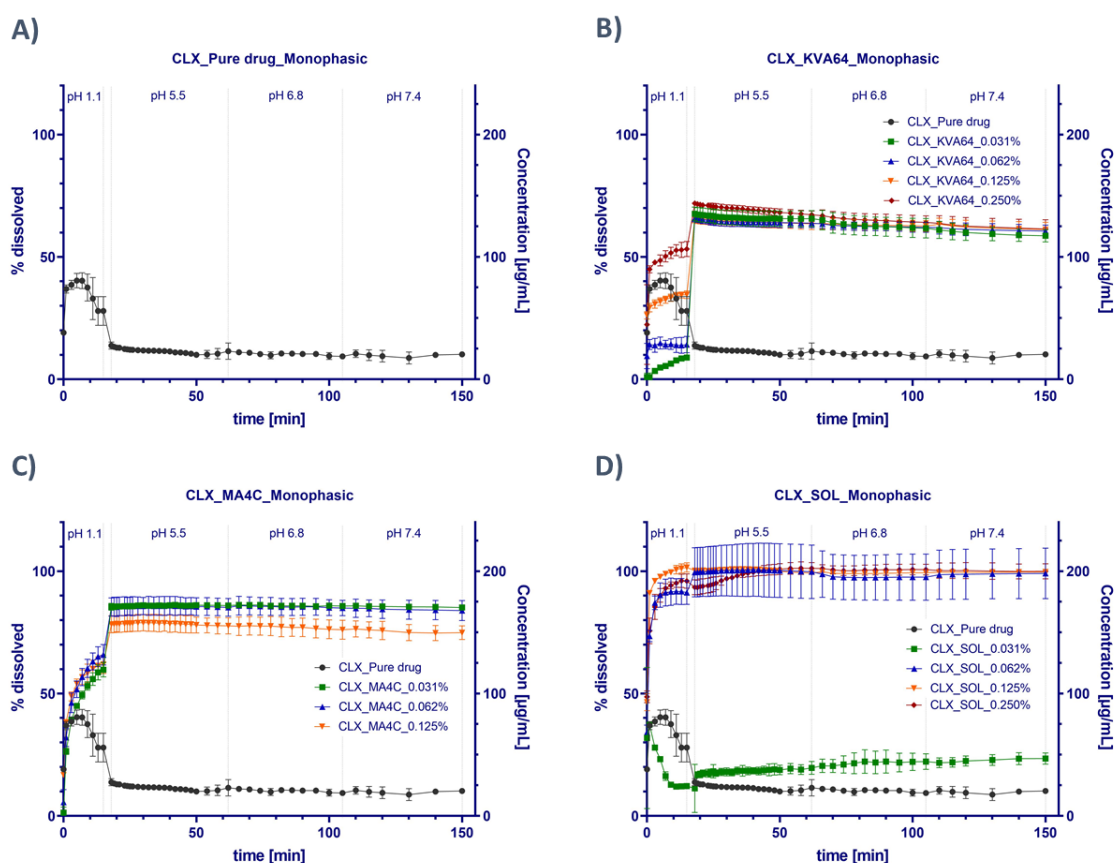


Figure 5.32: CLX monophasic dissolution tests (Mean \pm SD, $n=3$) in NaCl 0.15 M with a poor solubility of the pure drug in the entire GIT pH range. **A)** Pure drug, **B)** KVA64, **C)** MA4C, **D)** SOL. The high stabilization in colloidal solutions highlighted the potential of the supersaturation and solubilization mechanisms to enhance its oral bioavailability.

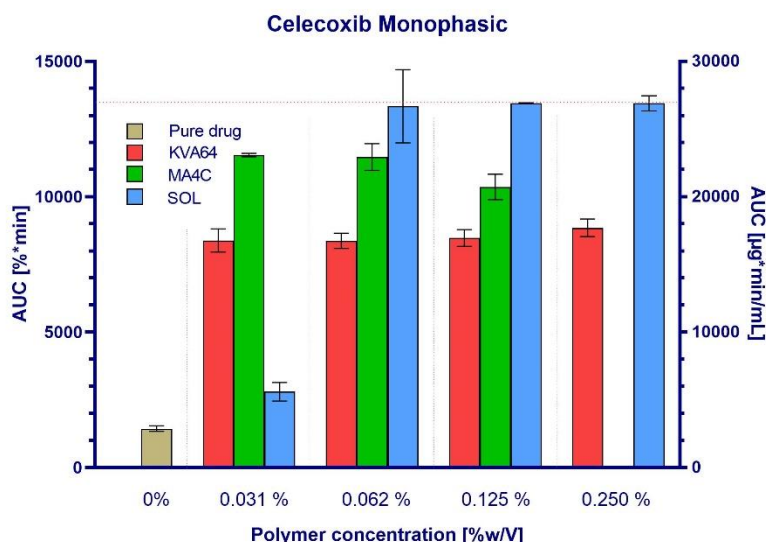


Figure 5.33: CLX comparative AUCs obtained from the precipitation phase (pH 5.5 – pH 7.4) in the MDT approach (Mean \pm SD, n=3). The red dotted line represents 100% of dissolved drug during the precipitation phase, corresponding to 13500 %*min (left y-axis) or 27000 $\mu\text{g}^*\text{min}/\text{mL}$ (right y-axis).

Celecoxib particle size distribution

Similar to DPD, needle-shaped CLX crystals with a length of 20 – 60 μm and a width of 5 – 10 μm were determined by PLM for the pure drug (Figure 5.34). Regarding the high extent of supersaturation and solubilization in colloidal polymeric solutions, no structures or particles were identified in the micron-range by means of PLM. Thus, the formation of needle-shaped crystals was clearly hindered, which indicated an interference of the supersaturation and solubilization mechanisms with the nucleation and crystal growth phenomena. Nevertheless, the turbidity of the generated colloidal solutions indicated the presence of nanostructures in all cases. This was confirmed by means of DLS (Figure 5.35A-C).



Figure 5.34: Micrographs obtained by PLM in a transmitted light modus at different magnifications (100x, 200x and 500x, respectively). The precipitation of pure CLX as needle-shaped microcrystals was confirmed.

5. RESULTS AND DISCUSSION

KVA64. Since all KVA64 concentrations achieved a similar degree of stabilization without any concentration-dependent effect, similar PSDs for all samples were obtained (Figure 5.35A). The Z-average ranged between 145 nm and 175 nm (Figure 5.36) and no trend in PDI was observed. The PDI was always below 0.2, indicating a monomodal distribution of the nanoparticles formed.

MA4C. For MA4C under MDT conditions, a slightly negative concentration-dependent effect was found (Figure 5.32C). Unfortunately, and probably due to the presence of particle aggregates, a determination of the PSD was not feasible at higher polymer concentrations (0.125 and 0.250% w/V). However, some trends could be detected. In general, higher polymer concentrations increased the Z-average up to values around 250 nm (Figure 5.35B, Figure 5.36), which was in good accordance with the MDT results (Figure 5.32C), where a decrease in the supersaturation extent was achieved by increasing the polymer concentration. The high viscosity and the gelling properties of MA4C can slightly favor the aggregation of particles at high polymer concentrations. Furthermore, the particle distribution switched from monodisperse (PDI approx. 0.2) to a polydisperse distribution (PDI approx. 0.3) at a polymer concentration of 0.062 % w/V.

SOL. The SOL-solubilization effect on CLX was confirmed. All determined PSDs in a polymeric concentration range of 0.031 – 0.125% w/V showed a Z-average close to 200 nm and no trend was recognized (Figure 5.35C, Figure 5.36). Nevertheless, the PDI values depended on the polymer concentration used. The particles followed a monomodal distribution in a polymer range between 0.031 – 0.062% w/V. At higher polymer concentrations, the PDI increased similarly to the DPD-SOL polymeric micelles (Figure 5.31B). The higher polymer concentrations might facilitate the formation of heterogeneous micelles, causing broader PSDs. Surprisingly, the average particle size distribution at a SOL concentration of 0.031% did not differ from the other polymer concentrations (Figure 5.32D). Despite the lower extent of solubilization at 0.031% SOL, the polymeric micelles with their surface-active properties might still limit the crystal growth and maintain the precipitated drug in a higher energetic amorphous form.

In conclusion, the CLX stabilization in colloidal solutions led to a clear decrease in PSD. The original precipitation kinetics of the pure drug reflected its chaser behavior and contributed to the formation of large crystalline needle-shaped particles. In polymeric colloidal solutions, the high extent of supersaturation limited the particle growth in all cases. The particles formed remained in the nanometer range and likely in a higher energetic amorphous form. These observations supported the suitability of CLX as a model drug to investigate the impact of supersaturation and solubilization in the GI tract on oral BA.

5.2 Part II: *In vitro* evaluation of supersaturation and solubilization

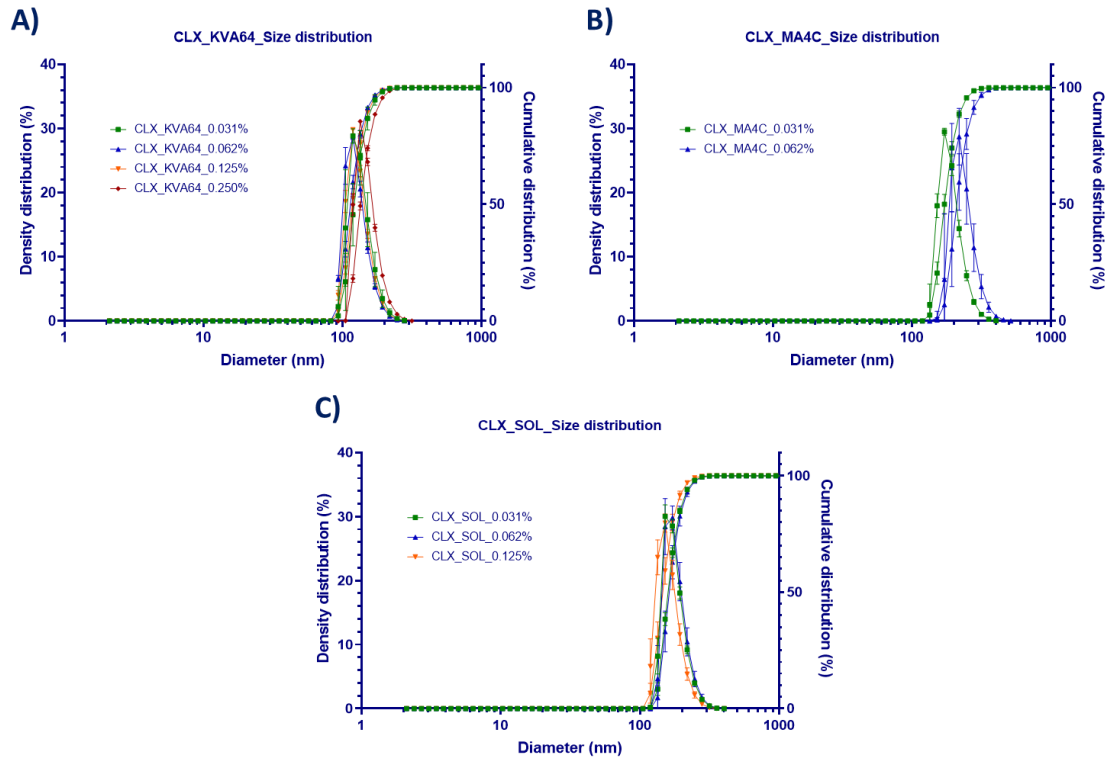


Figure 5.35: CLX density and cumulative particle size distributions in KVA64 (A), MA4C (B) and SOL (C) colloidal solutions determined by dynamic light scattering (Mean \pm SD, $n=3$).

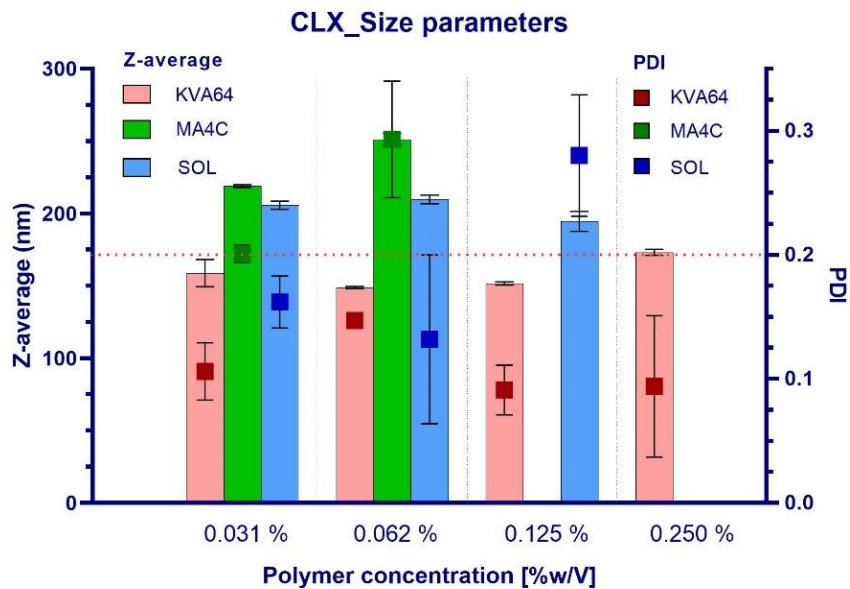


Figure 5.36: Comparative CLX particle size parameters. Z-average (left y-axis) and polydispersity indices (right y-axis) for KVA64, MA4C and SOL colloidal solutions. The red dotted line, referred to the right y-axis, indicating the PDI limit of monomodal dispersed particle population.

5. RESULTS AND DISCUSSION

5.2.1.2 Non chaser molecules

5.2.1.2.1 Loratadine

The identified non-chaser molecule Loratadine (LTD) tended to initially precipitate by means of LLPS as a liquid “amorphous” form (Hsieh et al., 2012). The MDT results clearly showed a high precipitation of the pure drug, when the solution was buffered to pH 5.5 (Figure 5.37A), which was already expected from its physicochemical behavior (weak base, $pK_a = 5.32 \pm 0.03$). Subsequently, the drug partially re-dissolved up to concentrations of 15 $\mu\text{g}/\text{mL}$, which was close to the kinetic and intrinsic solubility of the liquid amorphous form previously determined (Figure 5.12). The quick re-dissolution supported again the presence of a LLPS event. Even though the amorphous form appeared to be kinetically stable over the entire CheqSol experiment (ca. 50 minutes), the MDT indicated the stability of the amorphous form over a longer time frame (135 minutes). Consequently, no crystallization can be expected during the GI transit.

The physicochemical characterization showed only a minor solubilization effect by KVA64 and MA4C (Figure 5.12), which was attributed to the generation of the highly energetic amorphous form in solution.

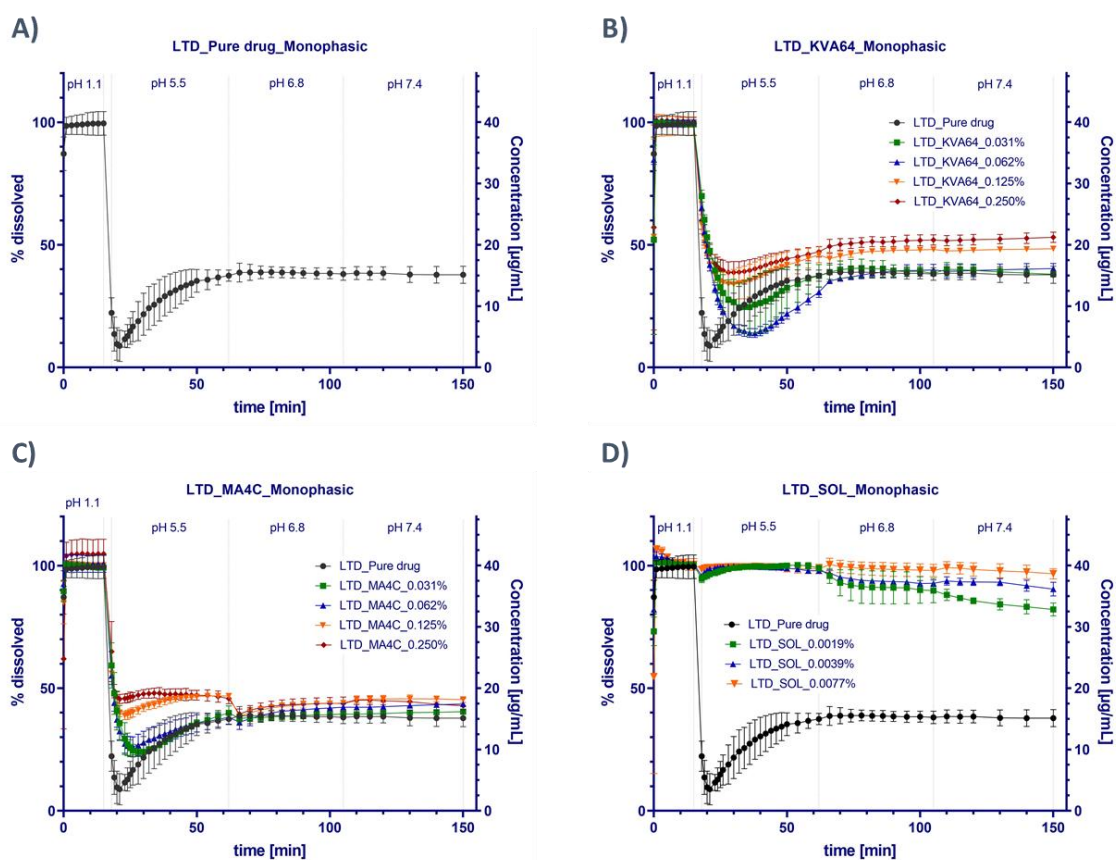


Figure 5.37: LTD monophasic dissolution tests (Mean \pm SD, $n=3$) in NaCl 0.15 M. **A)** Pure drug, **B)** KVA64, **C)** MA4C, **D)** SOL. The poor solubility of the pure drug under small intestinal conditions, as well as the stabilization achieved through the polymeric colloidal solutions is highlighted.

KVA64 and MA4C. KVA64 and MA4C initially limited the precipitation during MDT (Figure 5.37B,C). At the same time, a positive polymer concentration-dependent effect was identified for both polymers. This correlated with the pK_a -curves, which were previously fitted to exponential decay 1 models for KVA64 and MA4C (Figure 5.4) and indicated a slight solubilization effect. Nevertheless, the plateaus reached in all cases in the MDT were very close to the pure drug (15 $\mu\text{g}/\text{mL}$) and therefore, their function as solubility enhancers was limited. Therefore, the average dC/dt values minor differed in KVA64 and MA4C colloidal solutions when compared to the pure drug (Figure 5.38). This observation was related to the challenge in solubility enhancement of the precipitated amorphous form.

SOL. Owing to the low biorelevant concentrations used for LTD (40 $\mu\text{g}/\text{mL}$) and due to analytical reasons, the SOL concentrations were reduced to 16 – 4-fold (0.0019, 0.0039 and 0.0077 % w/V, respectively). All SOL concentrations used were above the previously reported critical micellar concentration of SOL (CMC = 7.6 mg/L) (Djuric, 2011) and consequently, its solubilization capacity was maintained. Therefore, the MDT showed in all cases a high extent of solubilization (Figure 5.37D) and a strong deceleration of the average dC/dt , accordingly (Figure 5.38). The t_p values remained unaffected at all SOL concentrations (135 min), as none of them impeded the precipitation of LTD.

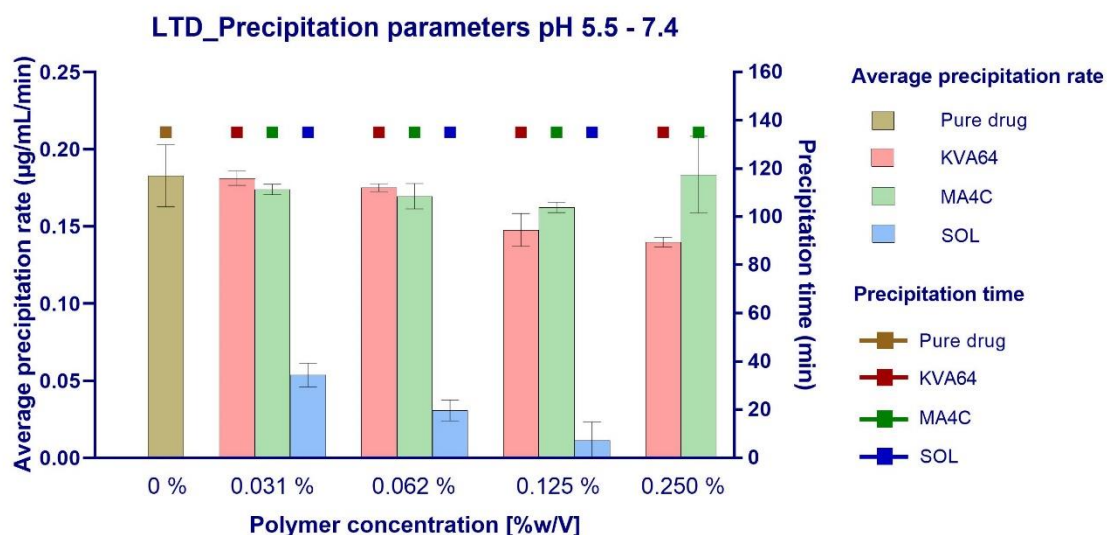


Figure 5.38: Comparative LTD average precipitation rates (left y-axis) and precipitation times (right y-axis) (Mean \pm SD, $n=3$) for the pH period 5.5 – 7.4.

All in all, the kinetic MDT stabilization results were in good accordance with the physicochemical predictions established by the prior solubility test (Figure 5.12). From a kinetic point of view, KVA64 and MA4C did not considerably enhance the solubility of the LTD amorphous precipitate, generated by LLPS, but they limited the initial precipitation extent (Figure 5.37B,C). The suitability of both polymers as crystallization inhibitors could not be evaluated under this approach, as the pure drug did not recrystallize during the experiment.

The micellization by SOL proved again its effectiveness to maintain the LTD molecules apparently dissolved and to limit the precipitation. The overall extent of stabilization was depicted for all polymers in the Figure 5.39.

5. RESULTS AND DISCUSSION

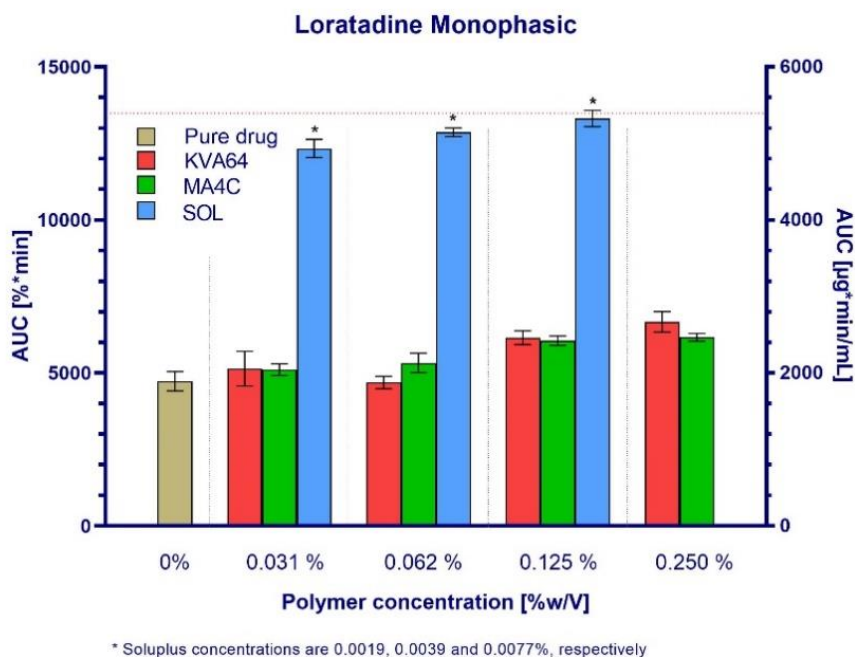


Figure 5.39: LTD comparative AUCs obtained from the precipitation phase (pH 5.5 – pH 7.4) in the MDT approach (Mean \pm SD, n=3). The red dotted line represents 100% of drug dissolved over the full length of the precipitation phase, corresponding to 13500 %*min (left y-axis) or 5400 $\mu\text{g}^*\text{min}/\text{mL}$ (right y-axis)

Loratadine particle size distribution

Due to the low LTD target concentrations in MDT and the precipitation of LTD by LLPS, a particle size investigation was only applicable for SOL colloidal solutions, for which the size of the polymeric micelles was investigated.

The DLS measurements confirmed the solubilization of LTD by SOL. Even at very low SOL concentrations (0.0019 – 0.0077% w/V), narrow PSDs in the nanometer range were detected. The Z-average was between 218 and 250 nm and tended to increase as a function of the polymer concentration, which was attributed to a higher solubilization of LTD species. Additionally, the PDIs shifted from ≤ 0.2 , indicative for a monomodal distribution at low polymer concentration (0.0019 and 0.0039 % w/V), to values of approx. 0.35 at higher polymer concentration (0.0077 % w/V) (Figure 5.40A, B). The higher PDI with increasing polymer concentrations correlated with the observations from other drug molecules such as DPD, CLX or TLM in the presence of SOL.

The PLM evaluation of all polymeric solutions after MDT test end confirmed the precipitation of LTD as a liquid amorphous form, as no birefringence was detected (Figure 5.41A). This also determined the stability of the amorphous precipitate over the entire test and indicated that LTD was unlikely to crystallize during GI transit. However, at 24 h after MDT test end, the microscopic investigation of the samples revealed the presence of crystalline structures, especially for the pure drug and in KVA64 colloidal solutions (Figure 5.41B). At the same time, the crystals observed under PLM in MA4C colloidal solutions were much smaller, thus indicating a better suitability of MA4C as crystallization inhibitor than KVA64. No crystalline structures were found in SOL colloidal solutions, supporting the irreversible character of the SOL solubilization approach.

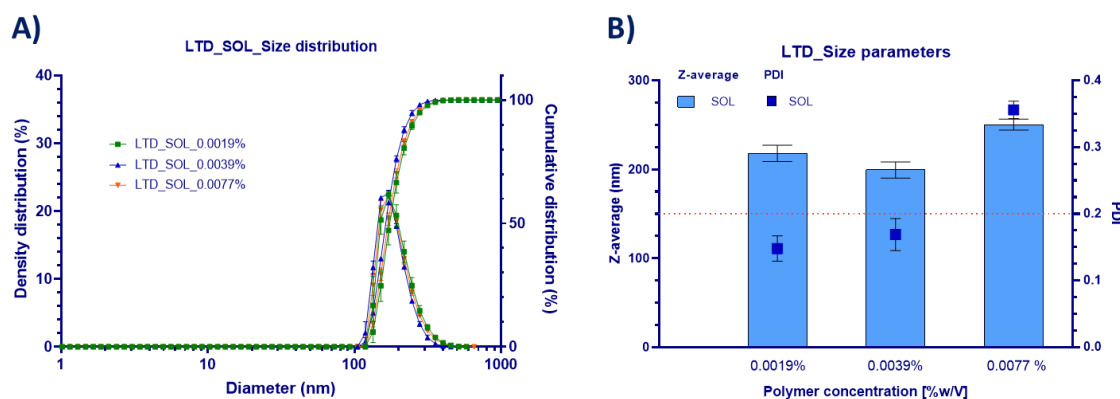


Figure 5.40: **A)** LTD particle size distributions obtained in SOL colloidal solution. **B)** Size parameters of LTD in SOL colloidal solutions. No particle size distributions or parameters could be determined for LTD in KVA64 or MA4C colloidal solutions.

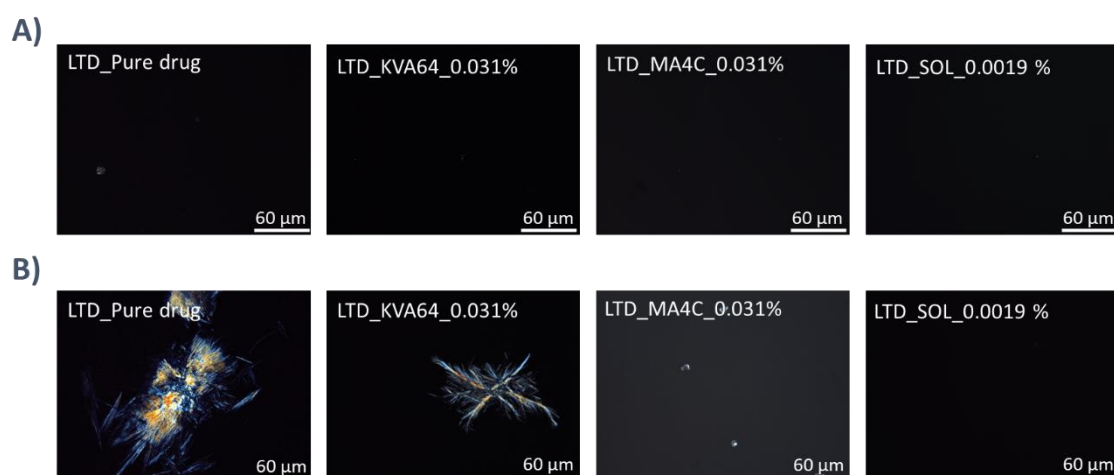


Figure 5.41: Micrographs obtained by PLM (500x) in a transmitted light modus for LTD pure drug and colloidal solutions **A)** The absence of crystalline precipitates supported the precipitation of LTD by means of LLPS and the stability of the amorphous form until the end of the test. **B)** The investigation of the identical samples at 24 hours after the MDT test end revealed the presence of crystals for the pure drug, KVA64 and MA4C samples.

5.2.1.2.2 Telmisartan

The complex interplay between the dissolution, supersaturation and precipitation phenomena of TLM was confirmed by means of the MDT approach. Due to the 3 ionizable groups of TLM, the constant change in ionization (Figure 5.5) and equilibrium solubility led to an inverted-bell shape solubility in the biorelevant pH range with a minimum at pH 5.0 (Figure 5.13). Additionally, TLM as a non-chaser precipitated as amorphous form in solution (Figure 5.46) by means of LLPS and similar to LTD.

The TLM characteristic solubility curve and its amorphous precipitation behavior (non-chaser behavior) were of major importance for solubility enhancement strategies, since the liquid amorphous precipitate easily re-dissolved at a thermodynamically favored pH change. One thermodynamically favored condition for TLM was the neutralization of the pH in the small intestine, as previously investigated (Koziolek et al., 2015b). The simulated transfer of the TLM

5. RESULTS AND DISCUSSION

drug molecules from the duodenum (pH \approx 5.0 – 5.5) into the jejunum and ileum (pH 6.8 – 7.4) creates a negative MMC, as shown in Table 5.3, which favored the re-dissolution of TLM molecules. Accordingly, only the stabilization of TLM in the upper regions of the small intestine was needed. Thus, two different MDT setups were carried out: the first setup investigated solely the potential stabilization under a thermodynamically unfavored condition (pH 5.5, 135 min) following a gastric phase (Figure 5.42A,B). The second setup additionally examined the re-dissolution occurring in the jejunum and ileum (Figure 5.44A,B), following a similar experimental procedure as for the other drug molecules used (Figure 4.1A). Due to analytical reasons, the tests were carried out for KVA64 and MA4C colloidal solutions only, as the high turbidity generated under SOL disabled an *in situ* quantification.

Under the first setup, the pure drug immediately precipitated after buffering the medium to pH 5.5. Remarkably, a complete precipitation occurred in 3 minutes. Thus, a fast initial precipitation rate was obtained (Figure 5.43) caused by an increased chemical potential (μ). However, and similar to LTD, the LLPS clearly favored a partial re-dissolution of TLM after 5 – 10 minutes (Figure 5.42) to level at a dissolved TLM concentration of approx. 25 $\mu\text{g}/\text{mL}$. This was slightly higher than the previous determined intrinsic solubility of the amorphous form at pH 5.0 (Figure 5.14). It was in good accordance with the CheqSol solubility determination, in which the kinetic solubility was lower than the intrinsic solubility.

The potential of KVA64 and MA4C to enhance the TLM solubility in the upper regions of the small intestine was confirmed in the MDT (Figure 5.42A,B). The presence of interaction between drug and polymer molecules, when the drug precipitates as a highly energetic amorphous form, was in good accordance with the exponential trends observed in the pK_a -curves (Figure 5.5B), which suggested especially for KVA64 a solubilization effect. In the MDT, this was reflected by a polymer concentration-dependent stabilization by both polymers (Figure 5.42A,B).

KVA64. Remarkably the shift of TLM from a non-chaser behavior into a chaser behavior, identified by the CheqSol approach, was also found in MDT with a kinetic perspective (Figure 5.42A). In this sense, the pure drug and the lowest KVA64 concentration showed a high initial precipitation within 3 minutes (Figure 5.43), followed by a re-dissolution of the drug up to a concentration of 145 $\mu\text{g}/\text{mL}$. At higher polymer concentrations (\geq 0.062 % w/V), the initial precipitation was more limited but continued over the entire test time, resembling to a chaser behavior. The precipitation rates appeared to be governed by first-order (KVA64) kinetic processes which can be attributed to the formation of intermolecular H-bond interactions.

MA4C. TLM precipitation in MA4C colloidal solutions was minor compared to KVA64 and a concentration-dependent effect was also detected (Figure 5.42B) and appeared to be governed by zero-order kinetic processes. The increased viscosity, as well as a facilitated interaction between TLM and MA4C molecules might limit the initial extent of precipitation by LLPS and maintained LTD concentrations in solution in the range between 105 – 140 $\mu\text{g}/\text{mL}$.

5.2 Part II: *In vitro* evaluation of supersaturation and solubilization

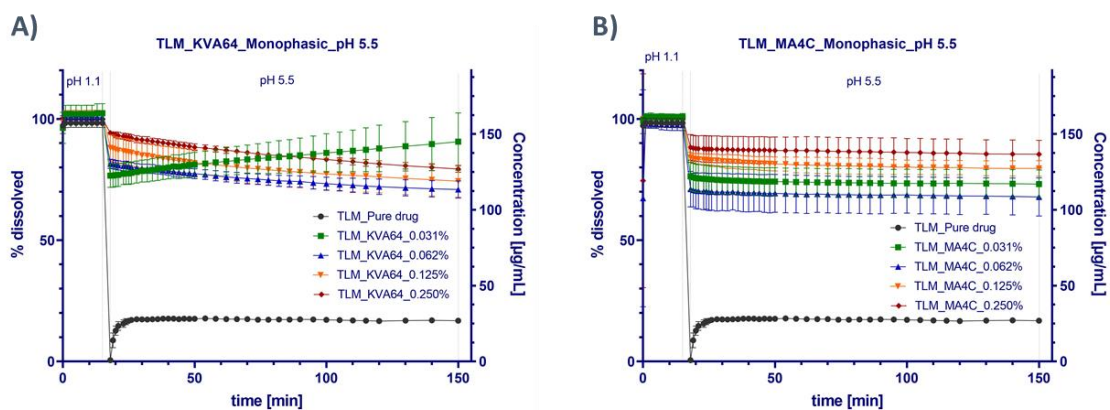


Figure 5.42: TLM monophasic dissolution tests (Mean \pm SD, $n=3$) at pH 5.5 in NaCl 0.15 M. **A)** KVA64, **B)** MA4C. The precipitated pure drug partially re-dissolves due to its precipitation as an amorphous solid. The poor solubility of the pure drug at this pH is overcome in KVA64 and MA4C colloidal solutions.

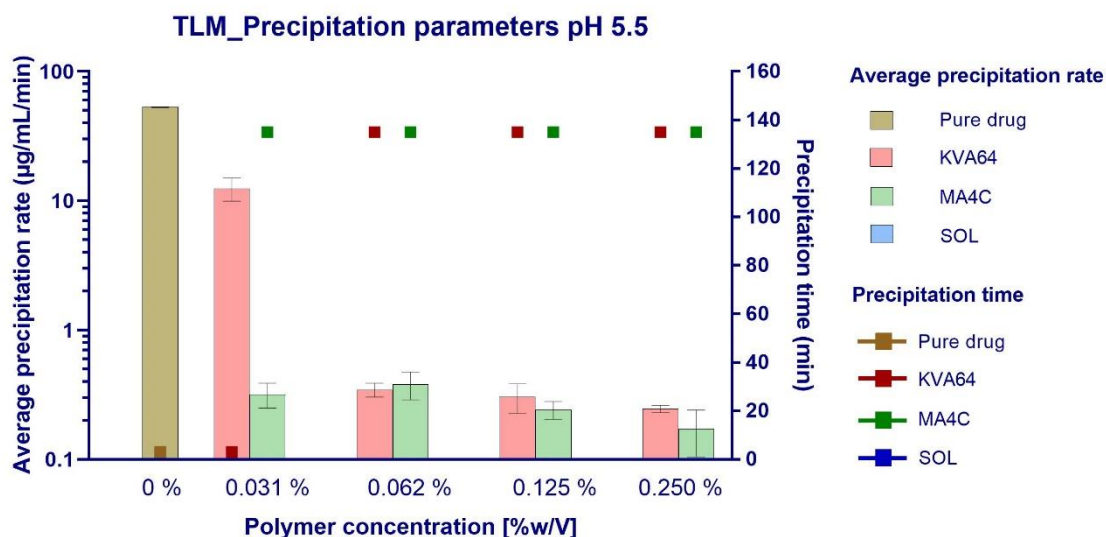


Figure 5.43: Comparative TLM average precipitation rates (left y-axis) and precipitation times (right y-axis) (Mean \pm SD, $n=3$) for the pH 5.5.

When the physiological pH-shift in the small intestine is considered, a completely different scenario was drawn. The amorphous precipitate of the pure drug showed the ability to completely re-dissolve when the system was buffered to pH 6.8 (Figure 5.44). In KVA64 and MA4C colloidal solutions, a similar trend was expected and therefore, the precipitation inhibition effect of KVA64 and MA4C became only important in the pH 5.5 period (Figure 5.44A,B). Regarding the constant pH-gradient in the small intestine, the benefit achieved by the polymers in terms of initial precipitation inhibition might be irrelevant for the oral absorption. In this sense, when considering the 3 pH periods, the overall benefit of the polymers might be minor, as it was shown in Figure 5.45.

5. RESULTS AND DISCUSSION

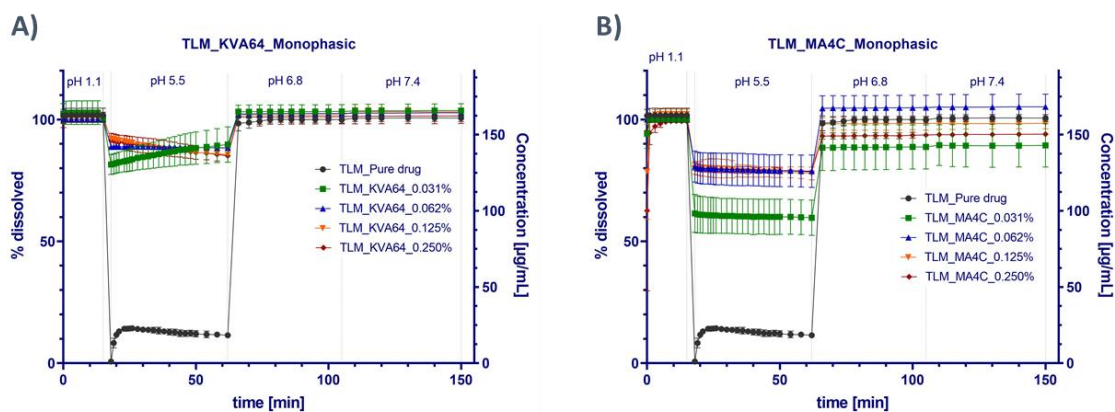


Figure 5.44: TLM monophasic dissolution tests (Mean \pm SD, $n=3$) in NaCl 0.15 M. **A)** KVA64, **B)** MA4C. The re-dissolution at pH 6.8 of the previously precipitated TLM caused by a change in the ionization state of the molecules.

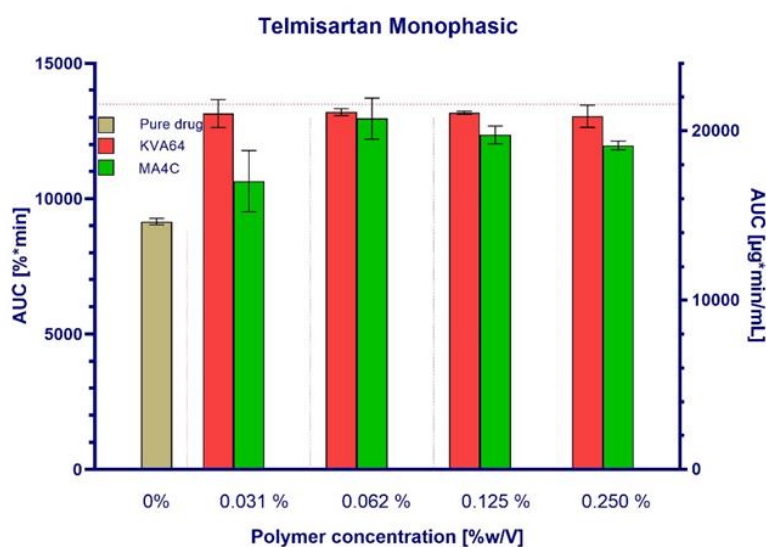


Figure 5.45: TLM comparative AUCs obtained from the precipitation periods (pH 5.5 – pH 7.4) in the MDT approach (Mean \pm SD, $n=3$). The red dotted line represents 100% of dissolved drug during the entire precipitation phase, corresponding to 13500 %*min (left y-axis) or 21600 $\mu\text{g}^*\text{min}/\text{mL}$ (right y-axis).

Telmisartan particle size distribution

Due to the characteristic behavior of TLM in solution and according to its ionization properties, the PSD was measured for samples withdrawn at the end of the pH 5.5 period. An observation of the pure drug samples under PLM revealed no birefringence (Figure 5.46B) and consequently, the drug was amorphous (Figure 5.46). Therefore, TLM might initially precipitate by means of LLPS and subsequently form clusters of amorphous material during MDT. A further investigation of these samples by means of laser diffraction showed a particle distribution in the low micrometer range with a d_{10} , d_{50} and d_{90} of 3.38, 8.35 and 17.51 μm , respectively. A span value of 1.69 indicated a relatively broad distribution of the particles with respect to the d_{50} (Table 5.6, Figure 5.47A). Remarkably, one part of the pure drug particles was in the nanometer range and could not be measured by laser diffraction.

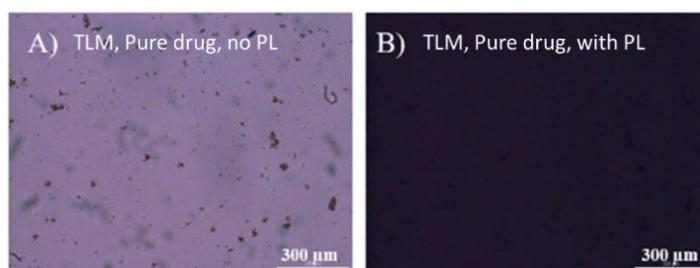


Figure 5.46: Micrographs obtained for TLM pure drug (100x). A) Without polarized light B) With polarized light. The absence of birefringence under polarized light indicated the amorphous character of the precipitated particles.

Table 5.6: TLM pure drug size diameters and span-value determined by laser diffraction at pH 5.5.

Pure drug	d_{10} (μm)	d_{50} (μm)	d_{90} (μm)	SPAN
	3.38	8.35	17.51	1.69

The PSDs of TLM in the polymeric colloidal solutions reflected the positive effect of the polymers as precipitation inhibitors. All distributions were in the nanometer range and were determined by DLS (Figure 5.47B-D).

KVA64. The positive concentration-dependent effect observed for KVA64 considerably impeded the precipitation after buffering the system to pH 5.5 (Figure 5.42A). In this way, the polymer concentration was inversely related to the initial precipitation step, as well as to the Z-average (250 – 175 nm) and PDI (0.2 – 0.1) (Figure 5.48). In all cases, a monomodal distribution was obtained, except for the lowest polymer concentration (0.031% w/V), where re-dissolution phenomena occurred.

MA4C. An inverted trend was observed for MA4C colloidal solutions. Despite the positive effect in terms of stabilization, the Z-average and PDI increased as a function of the polymer concentration, reaching values of 425 nm and 0.3, respectively. As previously proposed for CLX, the gelling properties of MA4C might favor the aggregation of particles and in turn increase the broadness of the size distribution and Z-average, as well as the broadness of the distribution (Figure 5.47C, Figure 5.48).

SOL. Despite the lack of stabilization and precipitation data for the combination TLM/SOL, several conclusions were withdrawn from the PSDs (Figure 5.47D). A In the MDT, the micelle size detected by DLS was inversely related to the polymer concentration in solution (Figure 5.48). Here, a higher degree of internalization of TLM species within the lipophilic cores at low polymeric concentrations (0.031 – 0.062 % w/V) was suggested, leading to a lower a fraction of larger micelles (100 – 200 nm). Conversely, when an excess of micelles was present in the medium, the drug was solubilized within a higher fraction of smaller micelles (\approx 75 nm). Worth mentioning, all micelle populations followed a monomodal distribution with a PDI \leq 0.1, which decreased as a function of increased polymer concentration (Figure 5.48).

5. RESULTS AND DISCUSSION

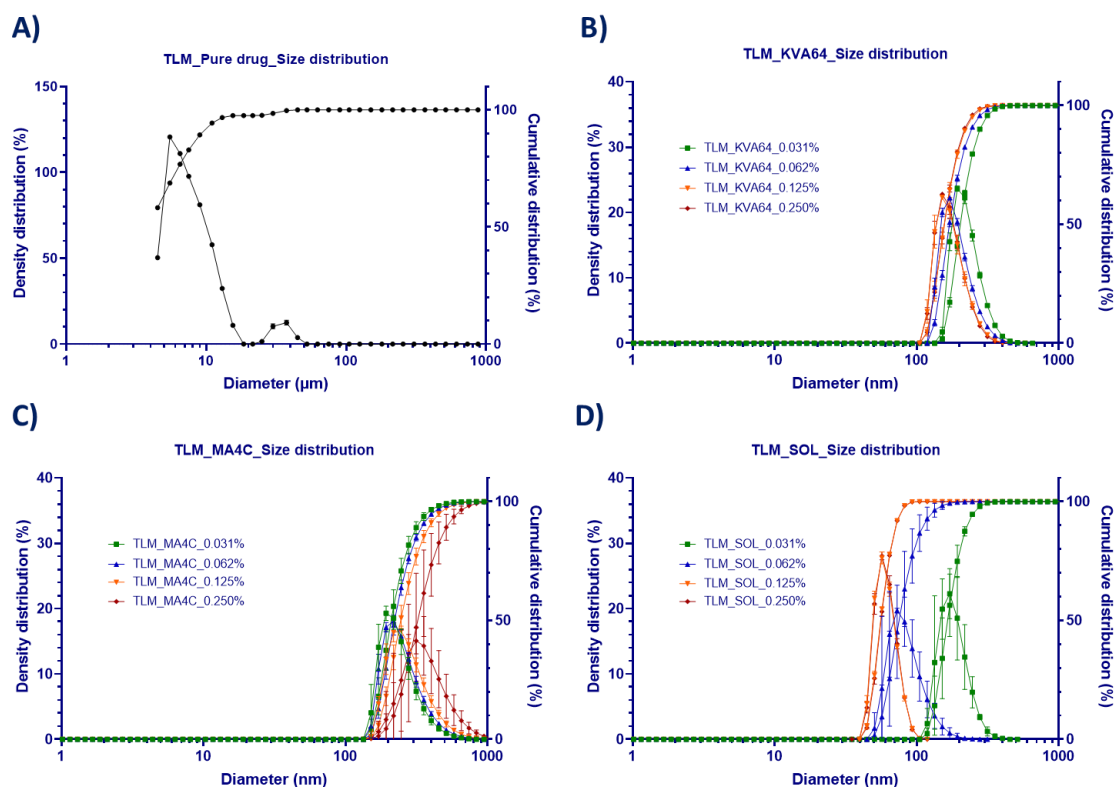


Figure 5.47: A) TLM pure drug particle size distributions determined at pH 5.5 by laser diffractometry. TLM particle size distributions in KVA64 (B), MA4C (C) and SOL (D) colloidal solutions determined by dynamic light scattering (Mean \pm SD, $n=3$).

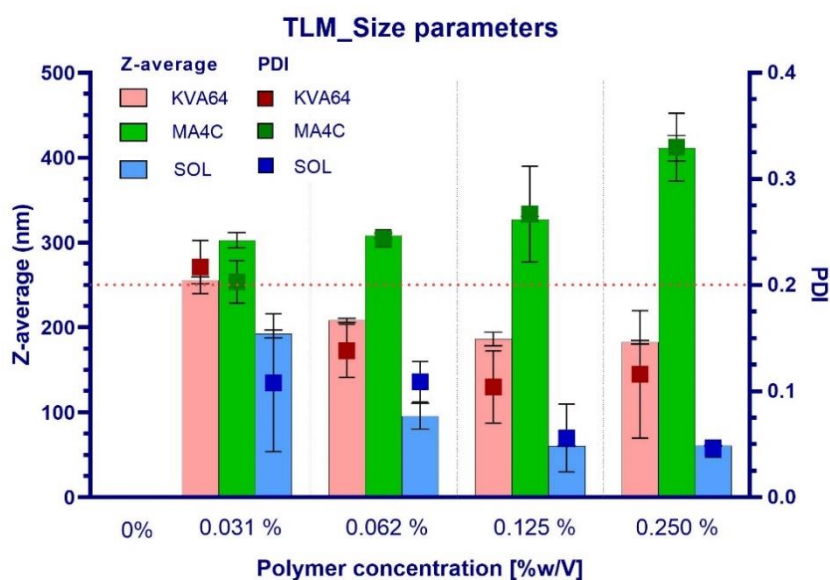


Figure 5.48: Comparative TLM particle size parameters. Z-average values (left y-axis) and polydispersity indexes (right y-axis) for KVA64, MA4C and SOL colloidal solutions. The red dotted line, referred to the right y-axis, indicated the PDI limit of monomodal dispersed particle population.

5.2.1.3 Extremely poorly soluble molecules

5.2.1.3.1 *Albendazole*

According to its weak basic character ($pK_a = 4.13 \pm 0.02$), ABZ showed a moderate solubility under gastric conditions and the target ABZ concentration (200 $\mu\text{g}/\text{mL}$) remained fully dissolved over the entire pH 1.1 period in MDT. For the pure drug, the deionization of the species in solution at pH 5.5 caused an immediate and complete precipitation right after the pH shift (Figure 5.49A), which might explain its poor oral BA (Lindenberg et al., 2004). Nevertheless, the potential of supersaturation to enhance ABZ intestinal absorption was confirmed *in vivo* in a rat model after intraduodenal administration of drug suspensions (Higashino et al., 2014).

The polymers already demonstrated their potential to enhance ABZ intrinsic solubility from a thermodynamic perspective (Figure 5.15). In all cases, the kinetic MDT approach showed also a positive polymeric effect on the precipitation kinetics, thus increasing t_p and decreasing dC/dt (Figure 5.51).

KVA64. Copovidone was the most effective polymer to maintain ABZ in solution over the entire test time (Figure 5.49B). A positive concentration-dependent effect was observed in the MDT, having a maximum effect (concentration range in the intestinal period: 110 – 60 $\mu\text{g}/\text{mL}$) at a polymer concentration of 0.125% w/V. The highest polymer concentration (0.250 % w/V) had a lower effect on the crystal growth due to a polymeric molar excess that partially hindered the interaction with the drug molecules (Figure 5.49B). Remarkably, a similar effect for the highest polymer concentration was observed for the intrinsic solubility (Figure 5.15). The high stabilization extent by KVA64 was attributed to a high interaction with ABZ molecules and low steric hindrance, due to the low ABZ M_w (265.33 g/mol). Furthermore, the benzol ring in the chemical structure of ABZ might have a polarizable character, which could facilitate the formation of interactions with the KVA64 monomers and contribute to the supersaturation found in MDT. From a thermodynamic perspective, a solubilization effect of ABZ in KVA64 solution was confirmed by the sigmoidal pK_a -curve (Figure 5.2), as well as by the up to 200-fold increased solubility enhancement factors for ABZ (Figure 5.15). ABZ was the only drug molecule that did not fit to the proposed H-donor rule in the section 5.1.3.5.1 and the experimental solubility considerably exceeded the prediction proposed by this rule (Figure. 5.17).

MA4C and SOL. Both polymers led to lower stabilization extent than KVA64 (Figure 5.49C,D). Although the initial precipitation inhibition was higher than for KVA64, a complete precipitation at $t_p \approx 60 - 70$ min was obtained (MA4C, Figure 5.49C and SOL, Figure 5.49D). Consequently, the average dC/dt was much faster than for KVA64 (Figure 5.51).

This minor kinetically driven effect was previously determined in equilibrium conditions by means of the shaking flask method (Figure 5.15), where MA4C and SOL only minor enhanced the ABZ solubility at low polymer concentrations. In the case of MA4C, the linear pK_a -curve did not suggest a solubilization effect (Figure 5.2). However, this did not exclude the possibility of a kinetic stabilization by means of supersaturation, as shown in the Figure 5.49C.

In the case of SOL, although a positive solubilization effect was observed by means of the shaking flask method (solubility enhancement ratios $\approx 2 - 700$ -fold) the highest ABZ concentrations achieved were between 1 – 7 $\mu\text{g}/\text{mL}$ (Figure 5.15). The quantification of these low ABZ concentrations in a highly turbid SOL-medium, by means of the fiber optic in the MDT approach, was challenging. As a result, although the SOL profiles might indicate a complete precipitation (Figure 5.49D), very low ABZ fractions could be solubilized within the SOL micelles.

5. RESULTS AND DISCUSSION

In general, all polymers investigated showed an ABZ stabilization potential from a kinetic perspective in the MDT (Figure 5.50). The extent of stabilization for ABZ, strongly depended on the polymer used.

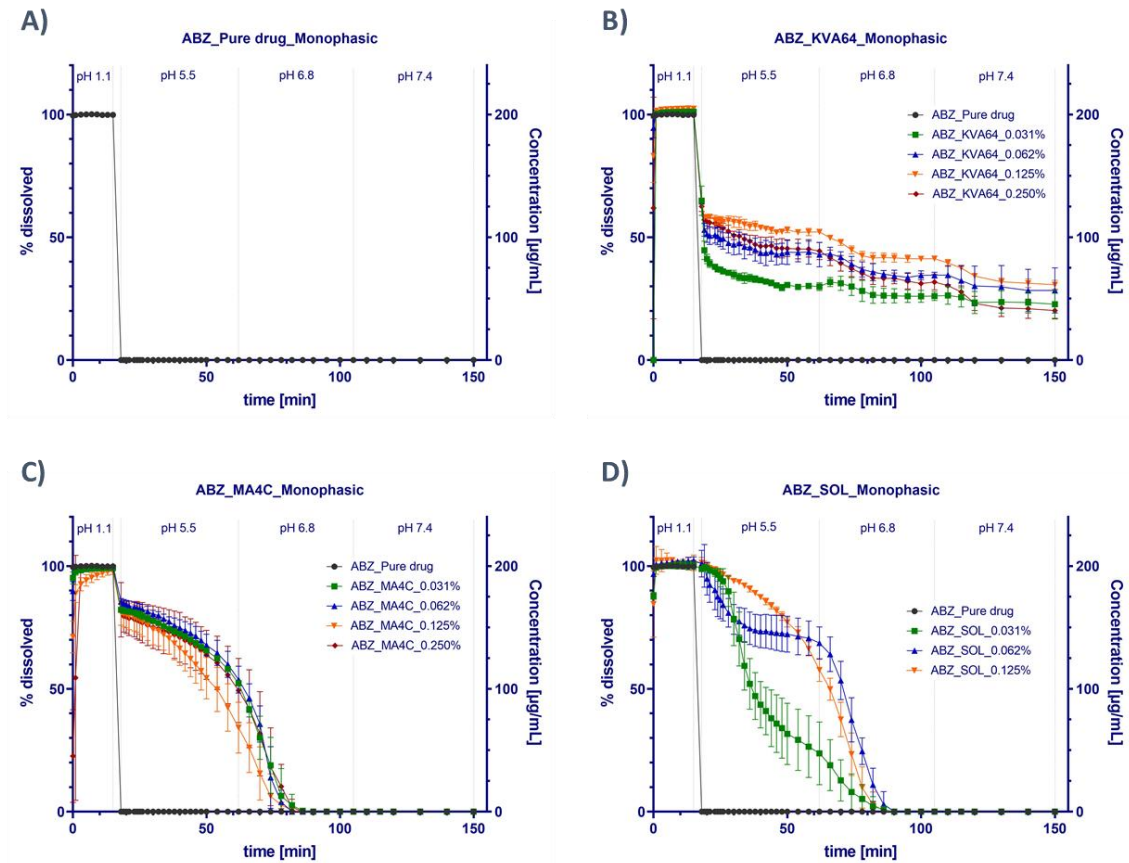


Figure 5.49: ABZ monophasic dissolution tests (Mean \pm SD, $n=3$) in NaCl 0.15 M. **A)** Pure drug, **B)** KVA64, **C)** MA4C, **D)** SOL. The extremely poor solubility of the pure drug under small intestinal conditions, as well as the stabilization achieved by the polymeric colloidal solutions is highlighted.

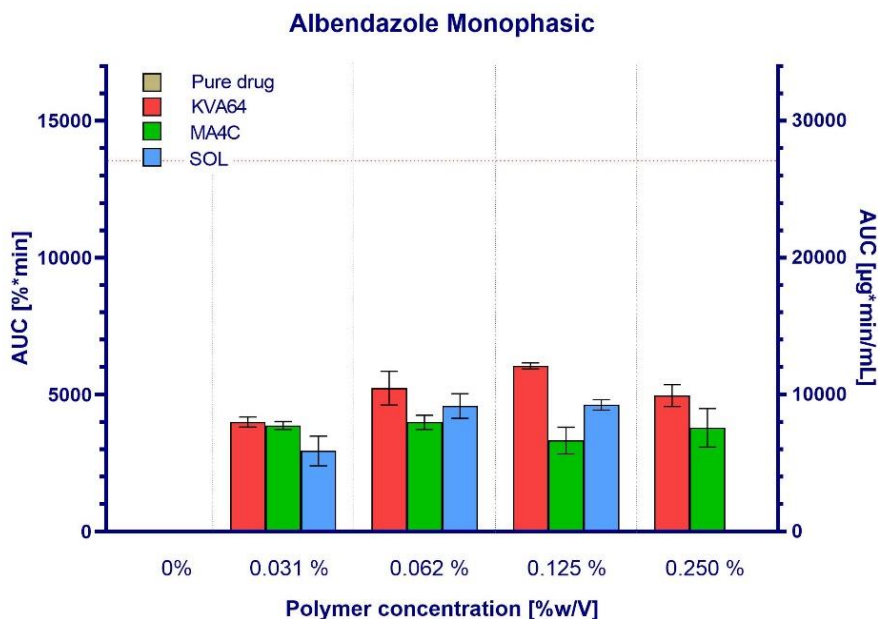


Figure 5.50: ABZ comparative AUCs obtained from the precipitation phase (pH 5.5 – pH 7.4) in the MDT approach (Mean \pm SD, n=3). The red dotted line represents 100% of dissolved drug during the entire precipitation phase, corresponding to 13500 %*min (left y-axis) or 27000 $\mu\text{g} \cdot \text{min}/\text{mL}$ (right y-axis).

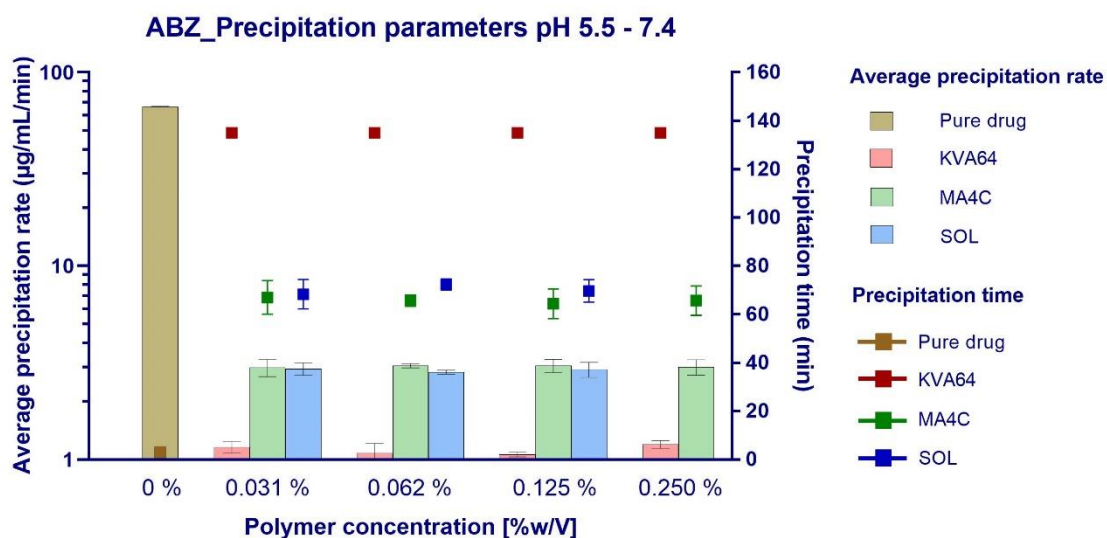


Figure 5.51: Comparative ABZ average precipitation rates (left y-axis) and precipitation times (right y-axis) (Mean \pm SD, n=3) for the pH period 5.5 – 7.4.

5. RESULTS AND DISCUSSION

Albendazole particle size distribution

The PSD of ABZ colloidal solutions clearly reflected the extent of stabilization achieved by the different polymers. In the absence of polymers, the pure drug immediately precipitated under intestinal conditions and the formed particles showed a monomodal distribution (Span value = 1.67) with d_{10} , d_{50} and d_{90} of 1.71 ± 0.01 , 5.59 ± 0.03 and 11.03 ± 0.04 μm under laser diffraction (Figure 5.52A, Figure 5.53), respectively. While KVA64 with a positive stabilization effect decreased the d_{10} , d_{50} and d_{90} (Figure 5.52A), the opposite was observed in MA4C (Figure 5.52B) and SOL (Figure 5.52C) colloidal solutions (Figure 5.53).

KVA64. The function of KVA64 as crystal growth inhibitor decreased the d_{10} , d_{50} and d_{90} values at all polymer concentrations (Figure 5.52A). In this context, a change in the ABZ crystal habit caused by the formation of H-bonds with other excipients such as benzoic acid was previously reported for ABZ (Raval et al., 2015). A similar effect might be present in ABZ/KVA64 solution, where the high degree in interaction, as well as the adsorption of polymer molecules to ABZ crystals, hindered the particle growth. Even though an identification of the crystal habit was not feasible by PLM (Figure 5.52D), the formation of needle-shaped particles, as it was the case for DPD and CLX, could be excluded. As previously observed by Raval and co-workers (Raval et al., 2015), the formation of plate-shaped particles was more likely.

MA4C. The ABZ crystals formed in MA4C colloidal solutions showed a monomodal distribution as well but with a clearly higher mean particle size than the pure drug (Figure 5.52B, Figure 5.53). These observations were supported by the lack of impact of MA4C on the ABZ solubility from a thermodynamic perspective (Figure 5.15). Additionally, it confirmed the favored aggregation of the crystalline particles in the presence of MA4C. Even when this aggregation was not detected in all cases, similar observations were reported in the literature (Bevernage et al., 2011; Dai et al., 2008; Guzmán et al., 2007b). In this sense, the gelling properties of MA4C might facilitate the formation of aggregates for certain drug molecules, as reflected for ABZ in the Figure 5.52D.

SOL. Unlike to the other two polymers, SOL achieved bimodal PSDs at polymer concentrations > 0.031 % w/V (Figure 5.52C). Even at low SOL concentrations (0.031 % w/V), for which a monomodal distribution was observed, a broader PSD and a larger mean particle size than for pure ABZ was measured. The presence of large ABZ-SOL aggregates increased the d_{90} (up to 80 – 90 μm) and the span values up to 18 (Figure 5.53). The PLM micrographs supported the formation of large crystalline particle aggregates (Figure 5.52D), which was unique for the ABZ-SOL combination, as it was not observed for any other drug-SOL combination. These observations rejected SOL as a suitable stabilizing excipient for ABZ and favored KVA64. In this sense, the spatial conformation and orientation of the drug molecules within the lipophilic SOL-cores can play a key role in the establishment of stable drug-SOL interactions. When the established interactions are not stable, the initial kinetic effect by micellization can later drive the drug precipitation into larger aggregates and broader PSDs.

The ABZ case study showed a strong dependency between the supersaturation/solubilization extent and the selected polymeric stabilization mechanism. Whether the short kinetic effect of MA4C and SOL colloidal solutions could potentially improve the partition and oral BA in combination with an absorptive compartment, will be further discussed in section 5.2.2.3.1.

5.2 Part II: *In vitro* evaluation of supersaturation and solubilization

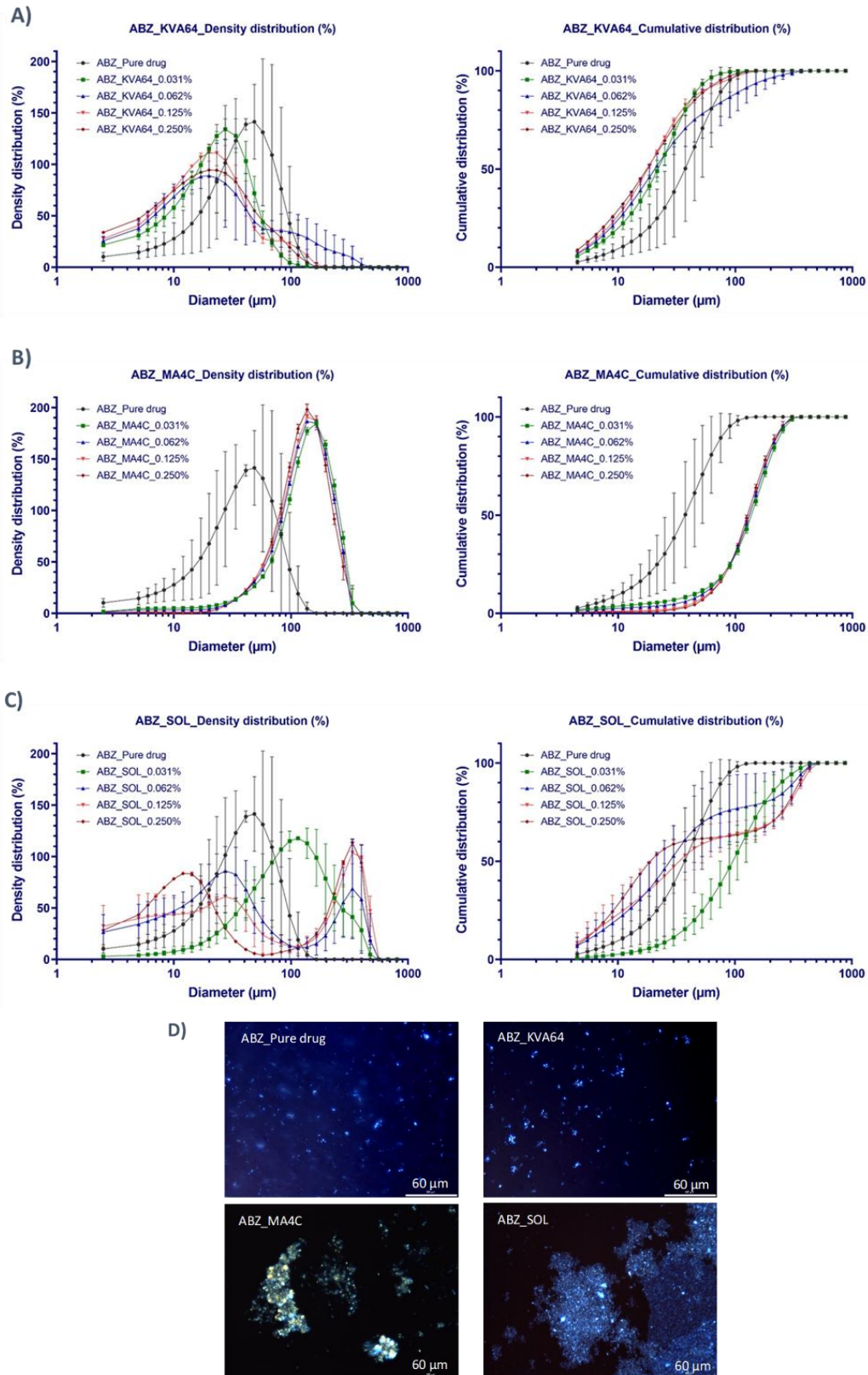


Figure 5.52: Particle size distributions obtained by laser diffractometry (Mean \pm SD, $n=3$). **A)** KVA64 **B)** MA4C **C)** SOL **D)** Micrographs obtained by PLM in a transmitted light modus (500x). The presence of crystalline microparticles or aggregates (MA4C and SOL) was characteristic.

5. RESULTS AND DISCUSSION

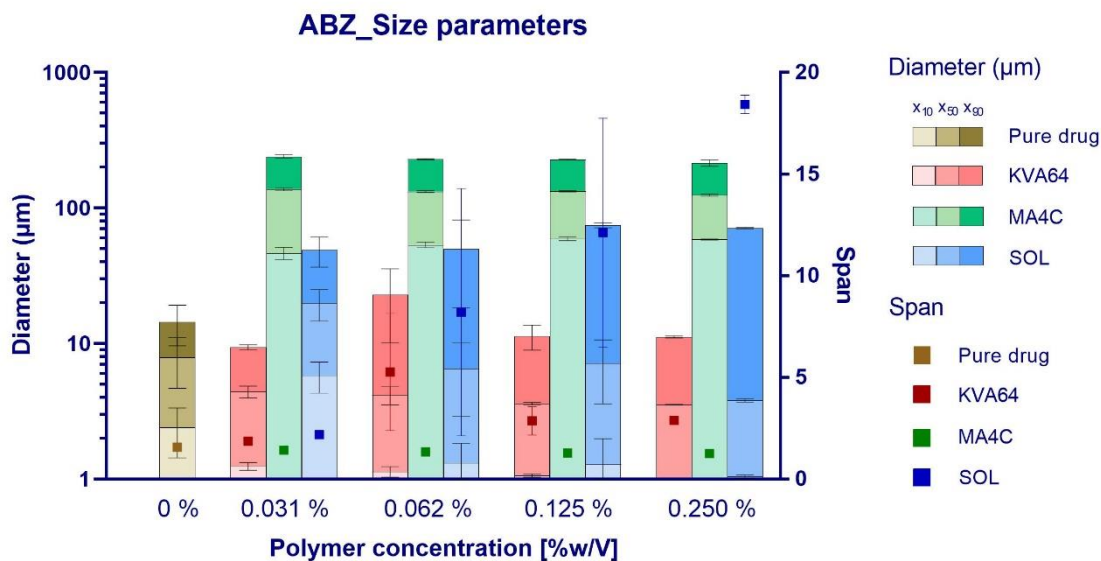


Figure 5.53: Comparative ABZ particle size parameters. Size diameters (left y-axis) and span-values (right y-axis) (Mean \pm SD, $n=3$) from ABZ particles formed by the pure drug and in KVA64, MA4C and SOL colloidal solutions.

5.2.1.3.2 Itraconazole

Similar to ABZ, the extremely poor solubility of ITZ led to immediate nucleation and complete precipitation events when intestinal conditions were simulated. Additionally, the higher initial ITZ equilibrium solubility in the gastric phase (pH 1.2) contributed to the precipitation events in the next pH period (Figure 5.54A).

KVA64. From a kinetic point of view, KVA64 had additionally no effect as precipitation inhibitor and similar to the pure drug, a complete precipitation occurred right after the pH-shift (Figure 5.54B). In this sense, ITZ served as negative control to underline the importance of the H-bond interactions with KVA64 as mechanism to kinetically stabilize supersaturated solutions. When the formation of H-bond interactions is unfeasible, as previously reported in polymeric matrices for ITZ (Bochmann et al., 2016), no solubility enhancement by KVA64 can be expected. As a result, no differences in the average dC/dt and t_p values were observed, compared to the pure drug (Figure 5.56). Supporting the kinetic observations and the lack of H-donor groups within ITZ chemical structure, no thermodynamic stabilization was achieved in KVA64 solutions, either (Figure 5.17).

On the other side, MA4C and SOL had a positive effect as precipitation inhibitors (Figure 5.54C,D, Figure 5.56). These observations are in good accordance with the intrinsic solubility results (Figure 5.16), where a stabilization of ITZ in solution by both polymers was confirmed from a thermodynamic perspective.

MA4C. MA4C stabilized ITZ in solution (concentration range: 10 - 50 µg/mL), decreased the average dC/dt by around 50-fold and prolonged the t_p over the full length of the intestinal period (Figure 5.56). Together with the viscosity increase, the establishment of hydrophobic interactions between ITZ and MA4C molecules cannot be excluded. These interactions would additionally contribute to the stabilization in solution from a kinetic and thermodynamic

perspective. Their formation was supported by the exponential decay $1/pK_a$ -curve (Figure 5.3), which supported the presence of a solubilization effect.

SOL. The potential of the SOL-micelles to solubilize the ITZ molecules was kinetically confirmed (Figure 5.54D). In all cases, the average dc/dt decreased with SOL compared to the pure drug (16 – 50 fold) therefore, increasing the t_p values (Figure 5.56). In a similar manner to ABZ, the low concentrations of solubilized drug at test end imposed challenges in the quantification by fiber optic under the applied experimental setting. Nevertheless, the intrinsic solubility determination via shaking-flask method and HPLC indicated ITZ concentrations of up to 20 – 30 $\mu\text{g}/\text{mL}$ in solution (5.16) and supported the presence of a solubilization effect.

The precipitation kinetics heavily depended on the polymer/drug ratio applied and a positive concentration-dependent effect was seen for MA4C and SOL colloidal solutions. The different stabilization mechanisms were reflected in the shape of the precipitation profiles. The precipitation kinetics were almost zero-order for all MA4C ratios, while SOL colloidal solutions achieved a first-order kinetic (Figure 5.54). The positive stabilization of ITZ by MA4C and SOL was clearly reflected in quantitative terms in the MDT by the high increase in the AUC (Figure 5.55).

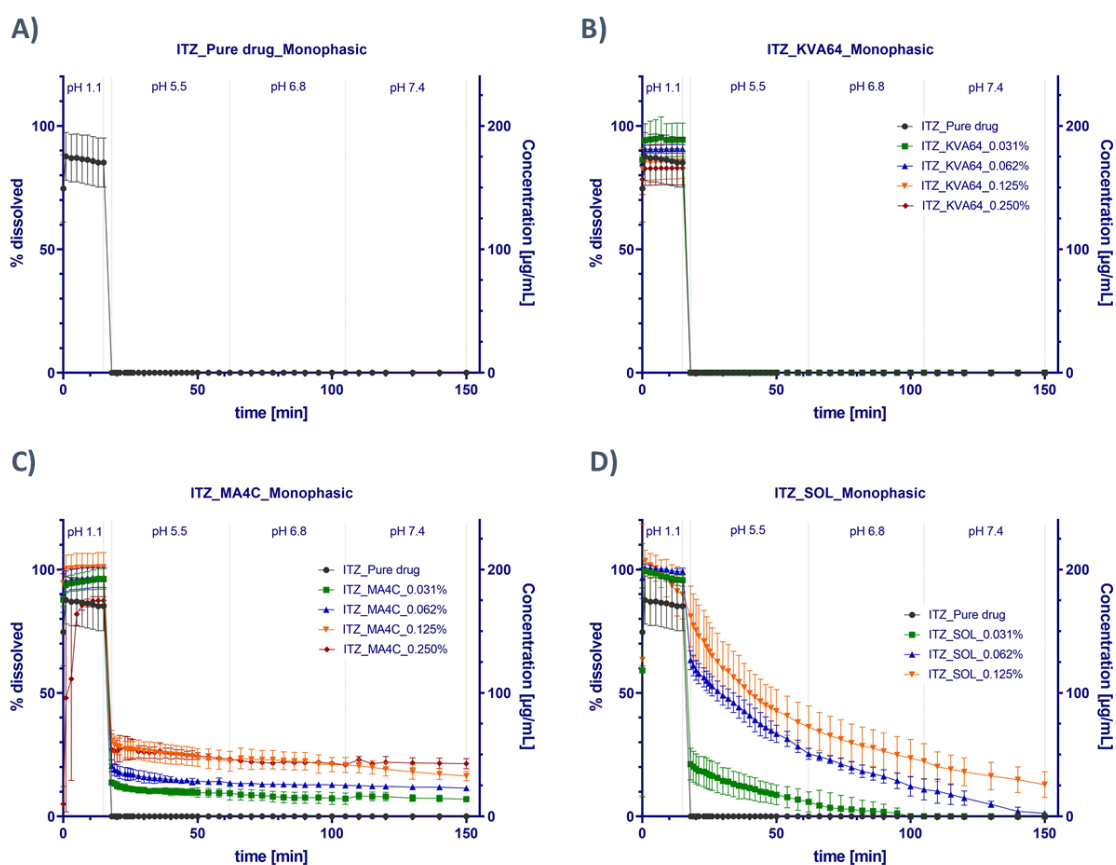


Figure 5.54: ITZ monophasic dissolution tests (Mean \pm SD, $n=3$) in NaCl 0.15 M. **A)** Pure drug, **B)** KVA64, **C)** MA4C, **D)** SOL. The extremely poor solubility of the pure drug under small intestinal conditions, as well as the stabilization achieved by MA4C and SOL colloidal solutions is highlighted.

5. RESULTS AND DISCUSSION

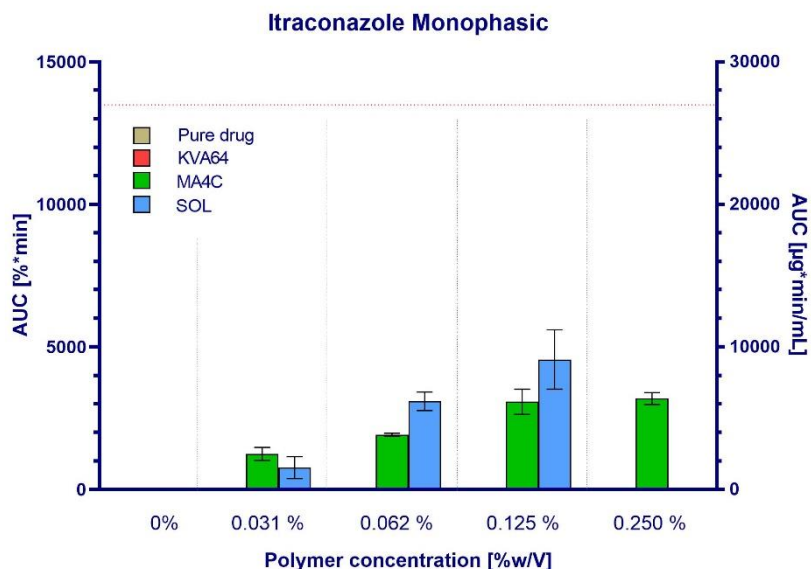


Figure 5.55: ITZ comparative AUCs obtained from the precipitation phase (pH 5.5 – pH 7.4) in the MDT approach (Mean \pm SD, n=3). The red dotted line represents 100% of dissolved drug during the entire precipitation phase, corresponding to 13500 %*min (left y-axis) or 27000 $\mu\text{g}^*\text{min}/\text{mL}$ (right y-axis).

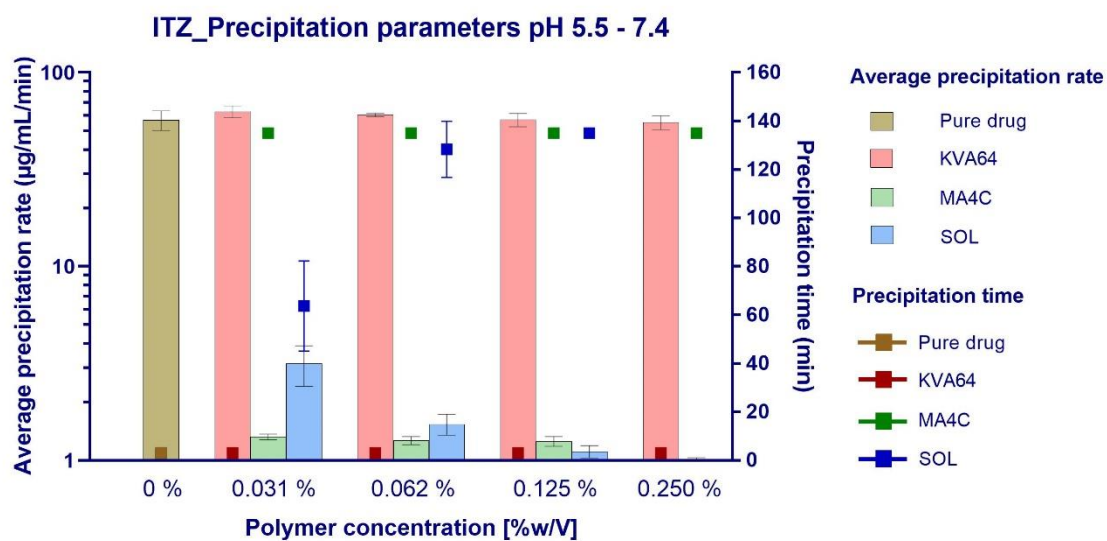


Figure 5.56: Comparative ITZ average precipitation rates (left y-axis) and precipitation times (right y-axis) (Mean \pm SD, n=3) for the pH period 5.5 – 7.4. The lack of any effect by KVA64 resulted in similar precipitation rates and times as for the pure drug. The positive effect by MA4C and SOL decelerated the precipitation rate and increased precipitation time.

Itraconazole particle size distribution

Pure ITZ immediately precipitated under intestinal conditions and the obtained particles at pH 7.4 were in the micrometer range (Figure 5.57A) with a d_{10} , d_{50} and d_{90} of 28.97, 71.59 and 125.49 μm , respectively (Figure 5.58A). A span value of 1.35 indicated a very narrow PSD. Furthermore, ITZ precipitated in small blade-shaped crystalline particles, examined by PLM (Figure 5.57D).

Previous works reported different shapes and crystal habits for ITZ in dependence of the recrystallization method and organic solvent used (Sriamornsak and Burapapadh, 2015).

All three polymers showed a crystal growth inhibition, as reflected by the decreased average particle diameters or Z-average (Figure 5.58A,B). Although these small-sized particles were unfeasible to be investigated by PLM, the certainty of initially precipitated amorphous nanoparticles in colloidal solution was not excluded. Miller and co-workers successfully investigated the formation of ITZ nanoparticle dispersions stabilized by HPMC E5 or Eudragit® L100-55 by means of antisolvent precipitation (Miller et al., 2012c). These were subsequently recovered as amorphous powders with significantly improved dissolution properties by means of rapid flocculation.

KVA64. The PSDs of KVA64 colloidal solutions were very broad and a determination by means of DLS failed, which supported the presence of ITZ microparticles in the colloidal solutions. Due to this reason, a determination under laser diffraction was additionally performed (Figure 5.57A). Compared to the pure drug, a clear reduction in the average diameters was found (\approx 50-fold decrease in d_{10} , d_{50} and d_{90}) (Figure 5.58A), but also high fractions of precipitated drug in the nanoparticle range was observed. According to the absence of a proper stabilization mechanism in solution by KVA64 for ITZ, the drug might initially precipitate as amorphous nanoparticles and crystallized over time. The adsorption of PVP – based polymers to the crystal surface was previously reported to hinder drug nucleation (Raghavan et al., 2001) or the crystal growth (Lindfors et al., 2008) by a “poisoning effect” (Simonelli et al., 1970; Ziller and Rupprecht, 1988), thus decreasing the size of the particles formed. The importance of these observations for the permeation and oral absorption will be further investigated in the section 5.2.2 in combination with an absorptive compartment.

MA4C. In the case of MA4C, the Z-average values ranged between 450 – 500 nm and no clear concentration-dependent effect was observed (Figure 5.57B). The PDI was always close to 0.2, except for the lowest polymer concentration (0.031 % w/V) (Figure 5.58B). Thus, a monodispersed distribution was assumed.

SOL. A clear concentration-dependent effect was observed in the MDT (Figure 5.54D). The formation of smaller nanoparticles as a function of increased polymer concentration decreased the Z-average values (range: 275 – 175 nm) (Figure 5.58B). However, no clear trend was observed in the PDI. In the case of SOL, for which the physicochemical characterizations indicated a high ITZ solubilization (Figure 5.3,5.16), a fraction of the nanoparticles is assumed to be SOL-micelles with solubilized ITZ in the core. Nevertheless, the precipitates could be also amorphous nanoparticles in colloidal solution, which lead to the higher PDI value.

5. RESULTS AND DISCUSSION

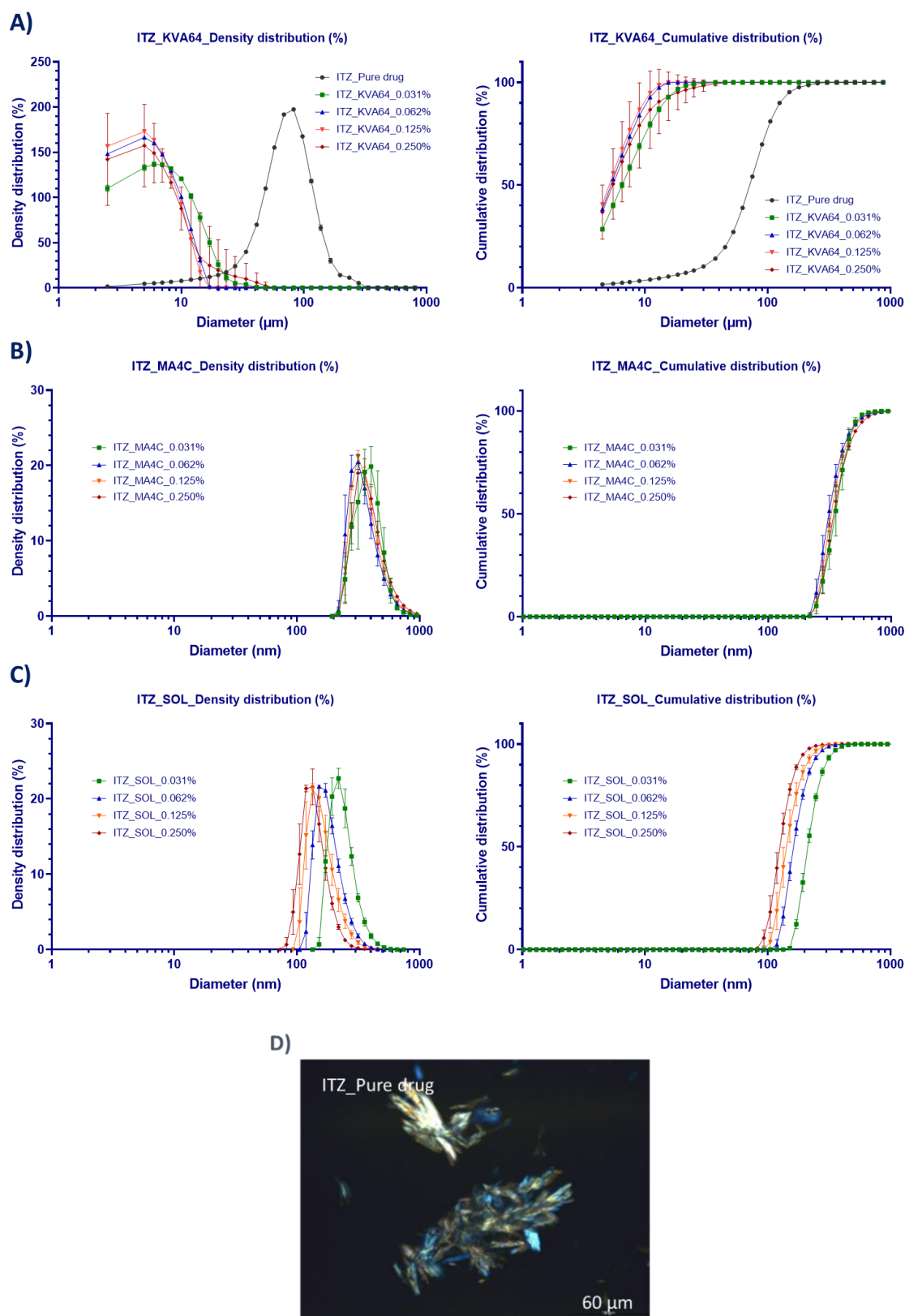


Figure 5.57: Comparative particle analysis for ITZ in colloidal solution. ITZ particle size distributions in KVA64 colloidal solution determined by laser diffractometry **(A)**. ITZ particle size distributions in MA4C **(B)** and SOL **(C)** colloidal solutions determined by dynamic light scattering (Mean \pm SD, $n=3$). **(D)** Micrographs with PLM in transmitted light modus (500 \times). ITZ pure drug precipitated immediately after the pH-shift in large crystalline particles. The decreased PSDs of colloidal solutions disabled the observation of these particles under PLM.

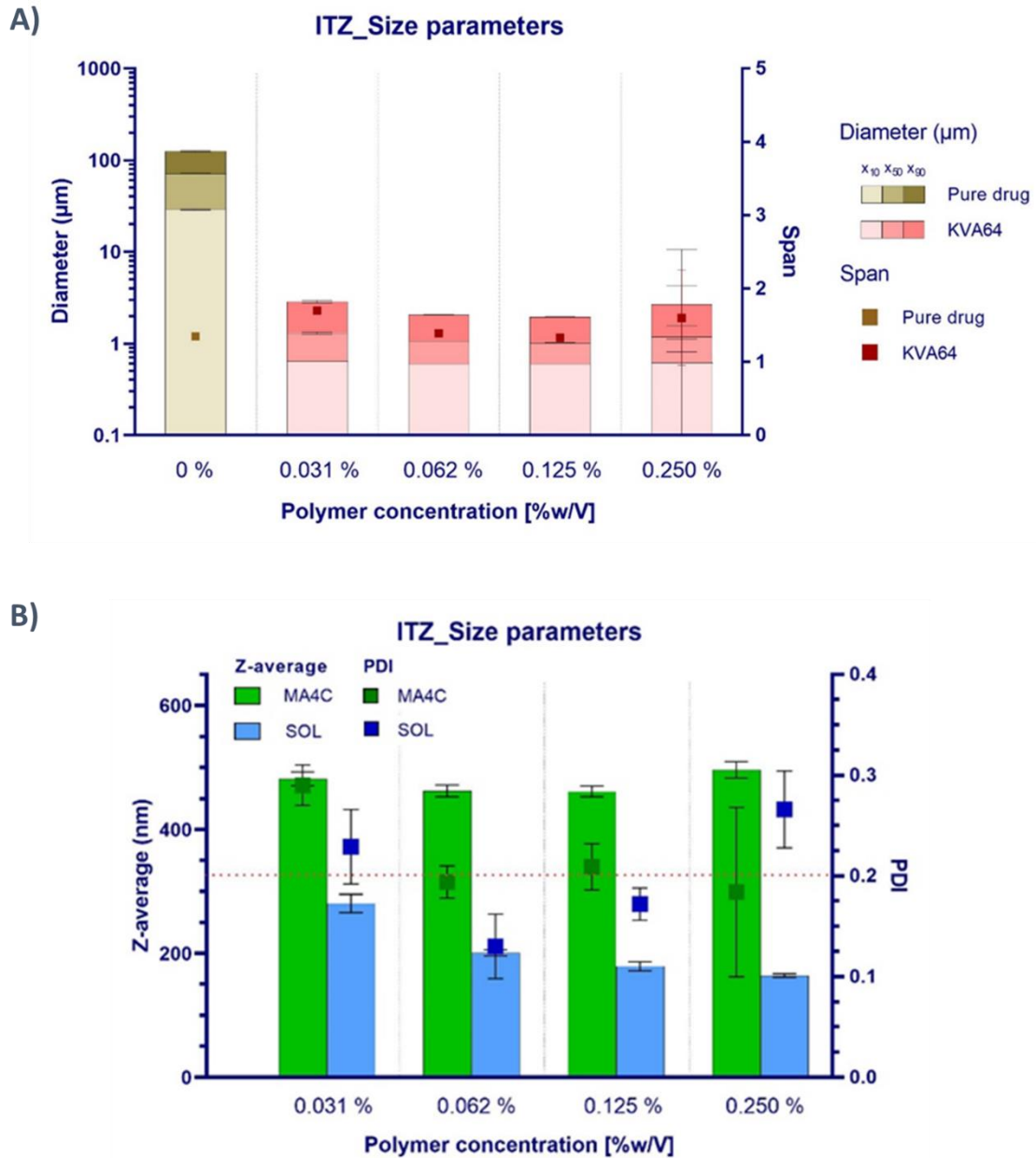


Figure 5.58: Comparative ITZ particle size parameters. **A)** Size diameters (left y-axis) and span-values (right y-axis) (Mean \pm SD, $n=3$) for ITZ particles formed by the pure drug and in KVA64 colloidal solutions. **B)** Z-average values (left y-axis) and polydispersity indexes (right y-axis) for MA4C and SOL colloidal solutions.

5. RESULTS AND DISCUSSION

5.2.1.4 Monophasic dissolution tests and particle size distributions overview

The MDT was successfully implemented as a suitable tool to investigate the supersaturation and solubilization effect of poorly soluble drugs under simulated GI tract conditions. The potential of water-soluble polymers to act as kinetic precipitation and crystal growth inhibitors was demonstrated. The polymer effect was not only investigated by the drug supersaturation and the precipitations kinetics, but also by the characterization of the precipitated particles in terms of PSD and (when feasible) physical state. Depending on the innate supersaturation ability of the drug molecules, as well as the physical state of their precipitating form, different trends were identified:

- Chaser molecules (DPD and CLX). According to the supersaturation ability of the pure drug, these molecules precipitated slowly in a crystalline form until the equilibrium solubility was reached (Comer, 2010). Both investigated chaser molecules precipitated in their pure forms as needle-shaped (acicular) particles. In the presence of supersaturating polymers, the narrowing of kinetic and intrinsic solubility values decelerated the precipitation rates and prolonged t_p . These effects were achieved by means of different stabilization mechanisms which proved in all cases to be effective as nucleation or crystal growth inhibitors. As a result of the hindering mechanisms, higher extents of stabilization (reflected as a higher AUC) and smaller particle populations were obtained. The polymers showed a high stabilization potential for chaser molecules and can be considered as suitable to enhance their oral BA.
- Non-chaser molecules (LTD and TLM). These molecules had no innate supersaturation potential and they tend to precipitate as a liquid amorphous form by means of LLPS (Comer et al., 2014; Hsieh et al., 2012). A kinetic stabilization is consequently more challenging since the precipitating form of the pure drug has already a much higher solubility than the crystalline state. However, the amorphous form is not stable from a thermodynamic point of view and the polymers kinetically inhibited crystallization. Nevertheless, this effect might not be relevant *in vivo* due to the GI transit time which might be shorter than the time needed for recrystallization (Koziolek et al., 2016). Consequently, the poor crystalline drug solubility would not heavily limit its oral BA. In this sense, the benefit of the polymers in terms of stabilization was minor for non-chaser molecules when physiological aspects, such as a normal GI transit time, are considered.
- Extremely poorly soluble molecules (ABZ and ITZ). The stabilization effects heavily depended on the drug-polymer combination used. Both pure drugs showed an immediate and complete precipitation in a crystalline form once the intestinal conditions were simulated. The function of the polymers as crystal growth inhibitors was very limited for ABZ and the formation of large crystalline aggregates when applying a polymer was found after test end. However, an initial kinetic stabilization effect was observed. The polymers heavily impacted the nucleation and crystal growth of ITZ and they seemed to drive the precipitation into amorphous nanoparticles, according to literature (Miller et al., 2012c). Due to the extremely poor solubility of the pure drug forms, the achieved stabilization extent for this molecule class was in case it appeared (e.g. ABZ-KVA64 or ITZ-MA4C) of a much higher extent than for chaser or non-chaser drug molecules.

The potential stabilization through the three proposed mechanisms (H-bond interactions, viscosity increase and solubilization) within the physicochemical characterization chapter (section 5.1) was confirmed from a kinetic biorelevant perspective.

5.2.2 Biphasic dissolution test (BDT)

The second modality of dissolution tests gained a deeper insight on the potential to enhance the oral absorption and BA from an *in vitro* approach by polymeric stabilization mechanisms. The biorelevant conditions were simulated by the inclusion of an absorptive organic phase compartment immiscible with the aqueous medium. Therefore, the complex interplay between the dissolution, supersaturation, precipitation and absorption phenomena for each drug-polymer combination in the GI tract, which influences the fraction of drug reaching the systemic circulation, can be studied. Based on the BDT, the selection of suitable drug-polymer candidates to test in *in vivo* conditions was performed. The main focus during BDT laid on the supersaturation and solubilization potential to induce changes in the oral BA. Due to the different innate supersaturation abilities of the drugs used, a variety of partition behavior into the organic phase was expected. It was additionally correlated to the physical state of the precipitating form, as well as to the species formed in solution, which have been identified to play a pivotal role in *in vivo* absorption (Wilson et al., 2018).

5.2.2.1 Chaser molecules

5.2.2.1.1 Dipyridamole

According to the chaser behavior of pure DPD, its innate supersaturation at intestinal conditions enabled the partition of 15 – 20% of the pure drug into the organic phase (Figure 5.59). This low DPD fraction found in the organic phase was related to the poor solubility and the high precipitation extent in the pH range of 5.5 – 7.4 (Figure 5.59). Due to the different stabilization mechanisms evaluated so far, the polymer effect on the partition depended on the equilibrium established between the molecularly dissolved drug and the complexed/solubilized drug fraction (Frank et al., 2012). Since only molecularly dissolved drug molecules are able to partition into the organic phase or to cross a biological membrane (Buckley et al., 2013), the equilibrium between both fractions, as well as the reversibility of the stabilization mechanisms may be the limiting step for the *in vitro* partition, as well as for the *in vivo* oral absorption.

KVA64. High DPD drug fractions (80 – 100%) partitioned into the organic phase until test end (Figure 5.59A). The 4 H-donor groups of DPD enabled the formation of low energy interactions with the KVA64 monomers. Due to the reversible character of the H-bonds, the partition into the organic phase was not hindered. At the same time, the removal of drug molecules from the aqueous phase induced the re-dissolution of undissolved drug and the formation of new reversible intermolecular interactions with the polymer. The observations correlated with the previous results, where the formation of reversible H-bonds between KVA64 and DPD provoked a kinetic (Figure 5.25) and thermodynamic (Figure 5.10) stabilization in solution.

MA4C. When using an organic compartment, MA4C provoked a lower partition rate at pH 5.5 followed by an acceleration after the solution was buffered to pH 6.8. This effect based on the higher ionization of DPD at pH 5.5 when compared to 6.8 – 7.4 and it was indicated by a 20-minutes lag time (Figure 5.59B). The total partitioned drug fraction was lower (40 – 60 %) than for KVA64. In this sense, the reduced molecular mobility in MA4C colloidal solutions impeded the accessibility of the drug molecules to the interphase between aqueous and organic solution, consequently causing a decelerated partition. However, the viscosity effect on the oral absorption might be minor in *in vivo* (Hens et al., 2017). The extensive degree of stabilization achieved by MA4C in the MDT highlighted the important role of medium viscosity as a

5. RESULTS AND DISCUSSION

precipitation inhibition mechanism (Figure 5.25C). The stabilization depended in the MDT heavily on the pH with a higher effect at pH 5.5 than at pH 6.8 or 7.4. Together with the higher ionization, the high stabilization effect of MA4C at pH 5.5 could additionally explain the lower partition rate compared to situation in the pH period 6.8 – 7.4.

SOL. DPD fractions between 30 – 60% partitioned into the organic phase from the SOL colloidal solutions. Furthermore, a negative polymer concentration-dependent effect was identified for the partition, supporting a solubilization effect in the aqueous phase (Figure 5.59C). Due to the micellization, the neutral species must be freed from the polymeric micelles to partition into the organic phase. Since the extent of drug partitioned into the organic layer was higher than for the pure drug, the SOL-micellization showed a partially reversible character. The partition rates were identical to the disappearance rates from the aqueous phase, excluding in this way the presence of precipitation events in the aqueous medium. Especially when a (micellar) solubilization effect occurred, the equilibrium between the molecularly dissolved and the solubilized drug fractions determined the partition rate and oral absorption, as previously discussed in other works (Beig et al., 2012; Buckley et al., 2013; Dahan and Miller, 2012; Frank et al., 2012). For this reason, even when SOL proved to be the most effective solubilizing agent and precipitation inhibitor of all three polymers (Figure 5.10, Figure 5.25D), the micellization could be counterproductive for the oral absorption and its benefit could be more limited as initially expected.

In conclusion, the chaser behavior of DPD molecules facilitated the stabilization in the aqueous phase, favoring partition, independently of the stabilization mechanism applied and increased in all cases the AUC_{aq} and the AUC_{oc} (Figure 5.60). However, the molecular species formed in solution (e.g. reversible or irreversible complexes or micellized drug) clearly triggered the extent of partition into the organic phase according to the established equilibrium with the molecularly dissolved DPD fraction. Surprisingly, KVA64, which showed the lowest degree of stabilization in the MDT approach (Figure 5.25B) led to the best partition behavior in the biphasic test.

5.2 Part II: *In vitro* evaluation of supersaturation and solubilization

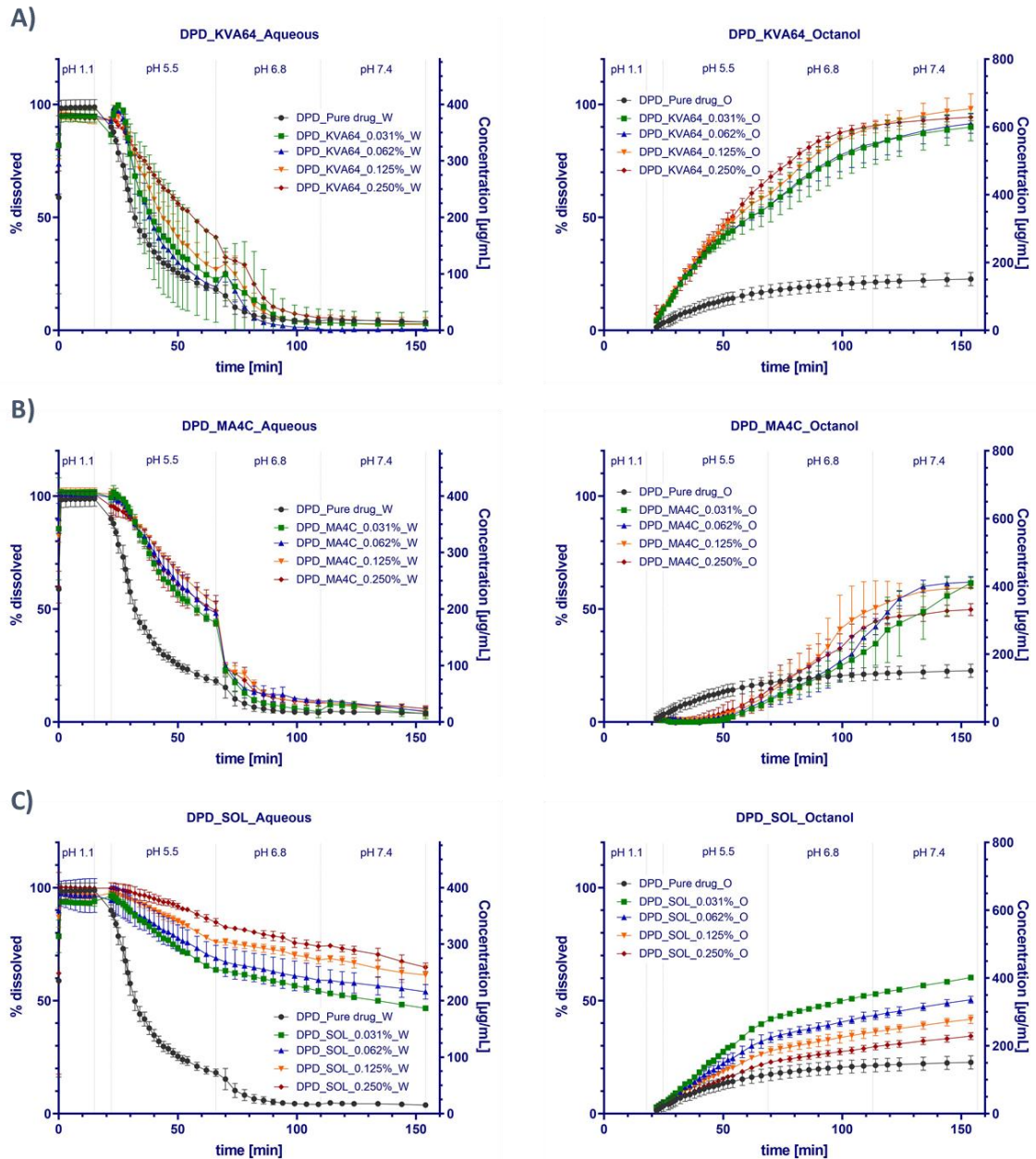


Figure 5.59: DPD biphasic dissolution tests **A) KVA64 B) MA4C C) SOL**. The left graphs indicate the fractions of dissolved drug in the aqueous phase as a function of time and the right graphs show the partitioned fractions into the octanol phase for each drug-polymer combination. The potential of DPD supersaturation and solubilization to enhance its oral bioavailability is reflected by the favored partition into the organic compartment in all cases.

5. RESULTS AND DISCUSSION

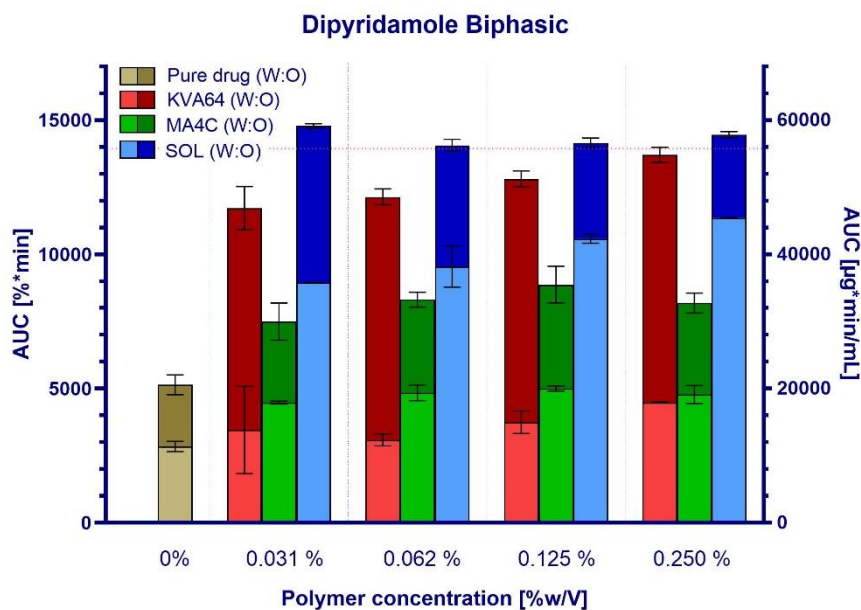


Figure 5.60: Comparative DPD AUCs of the precipitation period (pH 5.5 – pH 7.4) of aqueous and organic phases. The red dotted line indicates the presence of 100% of the dissolved drug during the entire test time (139 minutes) and it corresponds to an AUC of 13900 %*min or 55600 µg*min/mL.

5.2.2.1.2 Celecoxib

Contrary to all other drugs, CLX (weak acid, $pK_a = 9.49 \pm 0.03$) did not benefit from a dissolution under gastric conditions before simulating the intestinal medium. However, the chaser behavior of CLX and the facilitated stabilization by pharmaceutical excipients might positively impact its absorption through the intestinal barrier.

Under BDT conditions, the poor solubility of CLX in the gastric and intestinal periods considerably limited its partition into the organic phase, where only approx. 6% of the total amount was found at the end of the test (Figure 5.61). The precipitation of the pure drug in the form of needle-shaped crystals, as reported in the MDT approach (Figure 5.34), was responsible for the poor partition. When using the different polymers in the aqueous phase, an extensive stabilization was found in all cases and the crystallization was prevented. As a result, not only the dissolution during the gastric pH period was improved, but also supersaturation or solubilization under intestinal conditions was present (Figure 5.61). Besides, due to the crystal growth inhibition, CLX precipitated in the form of amorphous nanoparticles in the polymeric solutions (Figure 5.35). As a result, a quick partition and re-dissolution interplay was established under BDT conditions, which enhanced the partition.

KVA64. The inclusion of an organic absorptive compartment induced the partition of high drug fractions from the supersaturated aqueous solution into the lipophilic phase (70 – 100%)(Figure 5.61A). Additionally, a positive polymer concentration-dependent effect was found with the highest supersaturation for the highest polymer concentration applied (0.250 % w/V), facilitating the partition of the entire drug fraction into the organic phase. For the

CLX/KVA64 combination, the linear pK_a -curve (Figure 5.6) suggested the absence of a solubilization effect. In this sense, the establishment of weak intermolecular interactions were expected between the H-donor atom in CLX chemical structure and the several H-acceptors within the KVA64 monomers. Due to the reversible character of these bonds, high supersaturation extents were created and maintained over time, while the partition into the organic phase was not hindered (Figure 5.61A). Considering the predictive power of the BDT approach, these results might confirm the suitability of KVA64 to stabilize the CLX supersaturated state in the GI tract and enhance its oral exposure.

MA4C. Probably driven by the increased medium viscosity, a high stabilization of CLX in solution was observed in the aqueous phase of the BDT model (Figure 5.61B). However, despite the favored drug partition for all MA4C concentrations compared to the pure drug, the effect was lower than for KVA64 and only 40 – 65% of the drug reached the organic phase. As a result of the reduced molecular mobility in MA4C colloidal solutions, the accessibility of CLX molecules to the interface boundary is limited and consequently the partition of the drug decelerated. Despite the negative polymer concentration-dependent effect, MA4C demonstrated its potential to stabilize the CLX supersaturated state also in the CheqSol (Figure 5.11) and MDT (Figure 5.32C) approaches. The stabilization enhanced its partition with respect to the pure drug and could enhance its oral BA *in vivo*.

SOL. Due to an excess of turbidity at high polymer concentrations under the BDT conditions, the determination of the drug fraction dissolved in the aqueous phase was only feasible at the lowest polymer concentration (Figure 5.61C). Nevertheless, the partition into the organic layer could be investigated in the full polymer concentration range and indicated an inverse relationship between solubilization and partition, as previously proposed by the solubilization effect (Figure 5.6, Figure 5.11, Figure 5.32D). Anyhow, the equilibrium established between the fraction solubilized and the molecularly dissolved fraction favored the partition into the absorptive compartment (15 – 35%) with respect to the pure drug. Thus, the partial reversibility of the solubilization SOL approach for CLX was confirmed. Accordingly, SOL could also enhance the oral BA of CLX *in vivo*.

In conclusion, the CLX crystallization inhibition by all polymers led to a higher concentration of stabilized drug in the aqueous phase (increase in AUC_{aq}) (Figure 5.62). Due to the low solubility of the pure drug, the stabilization in the aqueous phase triggered a favored partition into the organic phase (increase in AUC_{oc}), which might enhance its oral exposure (Figure 5.62). Nevertheless, the reversibility of the stabilization mechanisms played a decisive role in the partition. Especially the increased medium viscosity and the solubilization limited the partition of molecularly dissolved drug into the organic phase, causing an inverse relationship between polymer concentration and partition.

5. RESULTS AND DISCUSSION

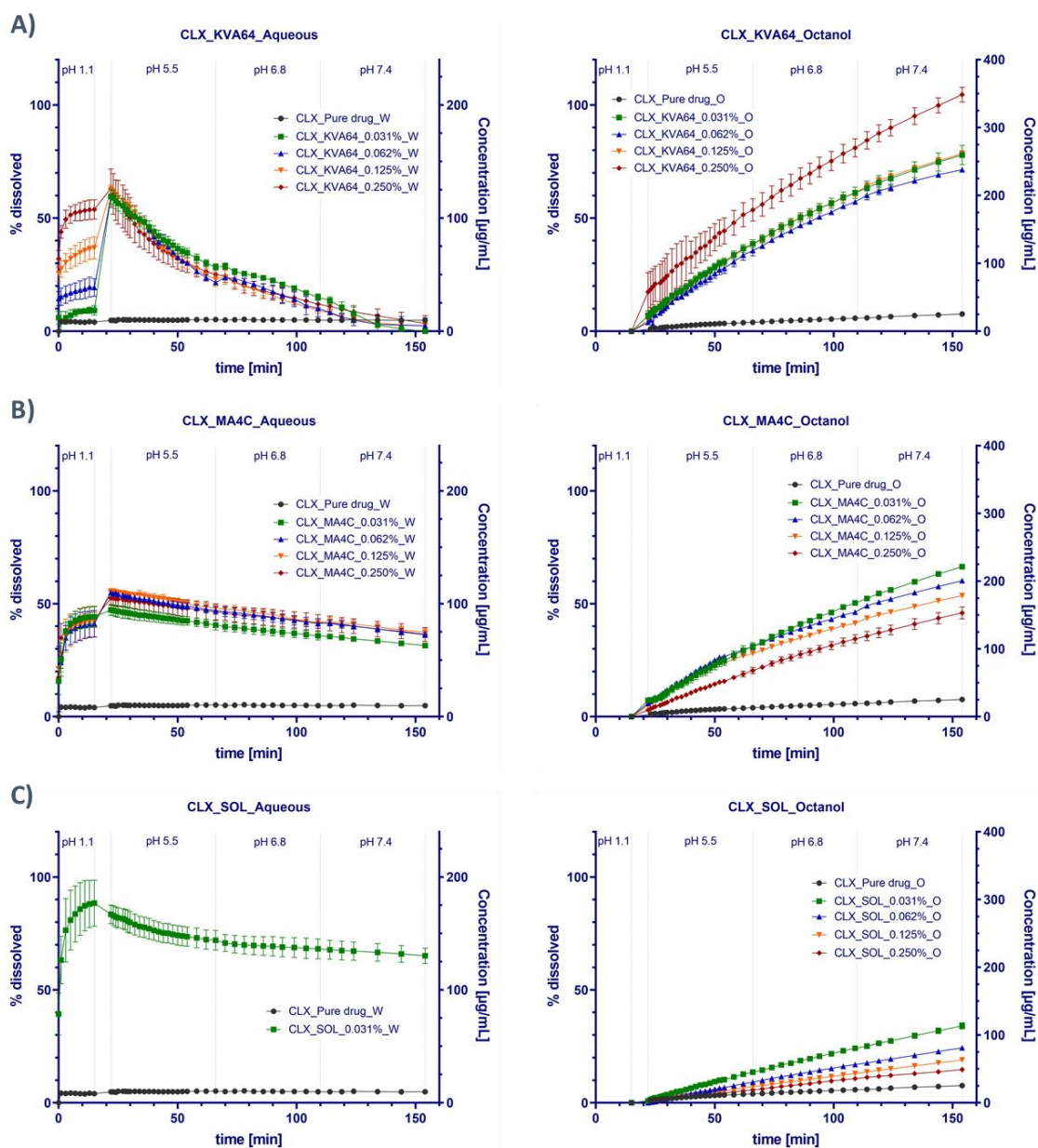


Figure 5.61: CLX biphasic dissolution tests **A)** KVA64 **B)** MA4C **C)** SOL. The left graphs depict the fractions of dissolved drug in the aqueous phase as a function of time and the right graphs show the partitioned fractions into the octanol phase for each drug-polymer combination. The potential of CLX supersaturation and solubilization to enhance its oral bioavailability is reflected by the favored partition into the organic compartment in all cases.

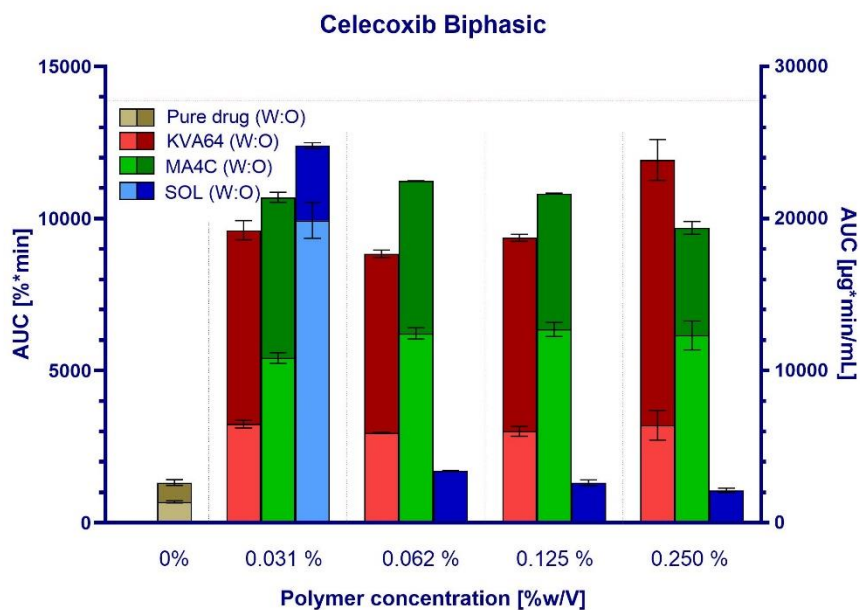


Figure 5.62: Comparative CLX AUCs obtained from the precipitation period (pH 5.5 – pH 7.4) in aqueous and organic phase. The red dotted line indicates the presence of 100% of the dissolved drug during the entire test time (139 minutes) and corresponds to an AUC of 13900 %*min or 27800 µg*min/mL. The AUC in SOL colloidal solutions (0.062 – 0.250 % w/V) could not be determined in the aqueous phase due to a high turbidity.

5.2.2.1.3 Partition rate for chaser molecules

Based on the observed shift from chaser to non-chaser behavior for DPD and CLX in polymeric colloidal solution (Figure 5.10, Figure 5.11), the stabilization was expected to increase the partition rate into the organic phase. The polymers' function as crystal growth inhibitors extended the time for drug to reach the organic phase and a faster partition rate occurred. In Figure 5.63, the higher acceleration of partition by KVA64, compared to the other two polymers, is depicted (2 – 2.5-fold acceleration for DPD and 15-fold for CLX). For KVA64, the establishment of weak intermolecular H-bond interactions was likely. Given their reversible character, the partition of freely dissolved drug molecules into the organic phase was not hindered.

For the other two polymeric approaches (MA4C and SOL), the partition into the organic phase was the result of the established equilibrium between the molecularly dissolved drug fraction and the solubilized or irreversibly bounded by polymer cluster formation drug fraction. Regarding MA4C, the partition rate was accelerated by 1.5 – 1.25-fold for DPD and 12 – 8-fold for CLX. In this sense, the achieved viscosity increase hindered the crystal growth, since it decreased the diffusion rate of a compound in the medium (Xu and Dai, 2013b). According to the Stokes-Einstein equation (Miller and Walker, 1924) this effect reduced the free mobility of drug molecules and limited the contact of the dissolved molecules with the interface between the aqueous and organic phase. Consequently, the partition was simultaneously positively impacted by the solubility enhancement factor and negatively by the viscosity effect on the molecular mobility. Therefore, the partition rate did not improve as a function of increased viscosity but showed a negative concentration-dependent effect in the case of CLX (Figure 5.63B).

5. RESULTS AND DISCUSSION

In terms of partition, the solubilization by SOL always achieved a negative polymer concentration-dependent effect, which was inversely correlated to the aqueous solubility. Despite the negative polymer concentration-dependent effect a 2-fold acceleration for DPD and 5-fold for CLX was obtained at the lowest polymer concentration (0.031% w/V). In this sense, the solubilization was interpreted as a partially irreversible stabilization mechanism that potentially limits the oral absorption. This correlates with the estimation methods for the absorbed fraction previously proposed by Sugano (Sugano, 2009; Sugano et al., 2010).

The partition rates into the organic phase heavily differed for DPD and CLX. Due to the moderate pH-dependent solubility, the partition of the pure DPD ($pK_a = 6.2$) might be initially favored during the first pH period. Thus, the DPD solubility improvement in colloidal solution was lower (Figure 5.63A) than for very poor-soluble drug molecules throughout the entire small intestine. In contrast, CLX has a very low and pH-independent solubility throughout the GI tract. Consequently, the partition of the pure drug was heavily limited by its poor solubility and therefore, the potential of the polymers to enhance its solubility and partition was much higher than for DPD (Figure 5.63B). Furthermore, the polymers used prevented the crystallization of CLX in colloidal solution and a nano-dispersed, amorphously precipitated drug was obtained, which contributed to a quick partition and re-dissolution interplay. In the case of DPD, the polymers inhibited crystal growth but did not fully prevent crystallization. Due to the crystalline state of these DPD needle-shaped precipitated particles, the partition and re-dissolution interplay was less favored.

The shift from chasers into non-chasers reflected the stabilization of dissolved drug molecules in the aqueous phase, improving the partition into the organic layer and potentially the *in vivo* oral exposure.

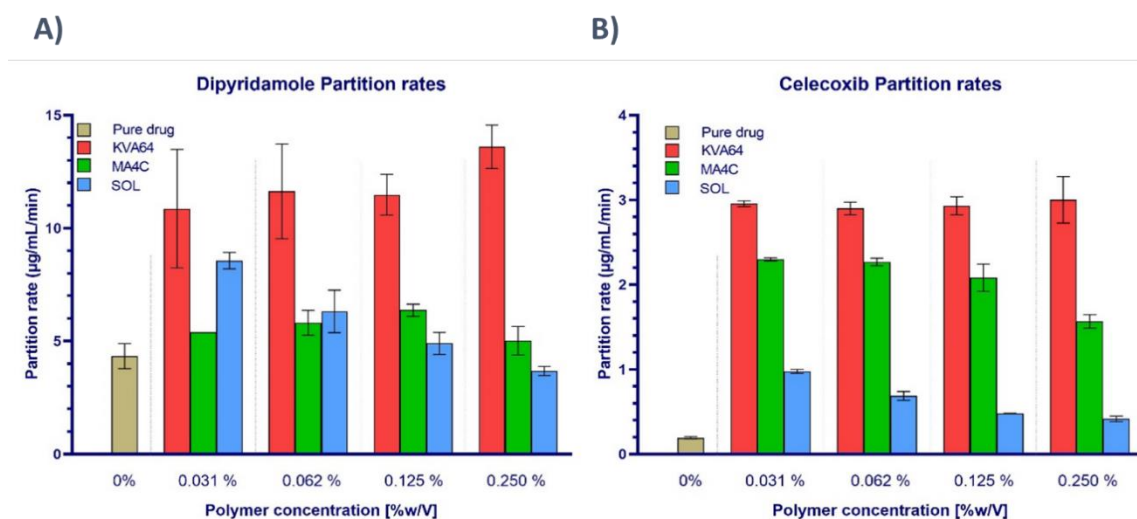


Figure 5.63: Partition rates of chaser molecules DPD (A) and CLX (B) into the octanol phase of a biphasic system. An improved partition rate, calculated by fitting the partition profile to a first-order kinetic, was always observed.

5.2.2.2 Non-chaser molecules

5.2.2.2.1 *Loratadine*

The precipitation of LTD as an amorphous liquid triggered the re-dissolution of the pure drug in aqueous medium in the MDT approach (Figure 5.37A). When combined with an absorptive compartment, such as the organic phase of the biphasic model, a quick re-dissolution – partition interplay was found for which the latter was favored by the LTD lipophilicity. As a result, for the pure drug, 80% of the total drug amount (2 mg) partitioned into the organic phase during the entire test (Figure 5.64).

KVA64. The minor drug stabilization in the aqueous phase (Figure 5.64A,B,C) did not improve the partition into the organic compartment. Only a slight improvement in the partition was observed at high KVA64 concentrations (0.250 % w/V), where 90% of the drug reached the octanol phase. At lower polymer/drug ratios, the partition remained unaffected (Figure 5.64A).

MA4C. No acceleration in partition was found for any polymer concentration and only 45 – 75% of the drug reached the organic phase (Figure 5.64B). Due to the reduced molecular mobility and the formation of LTD-MA4C hydrophobic interactions, the LTD precipitation was slightly inhibited. However, the partition into the organic phase was simultaneously impeded. Remarkably, a negative concentration-dependent effect on the partition occurred, as previously observed for chaser molecules.

SOL. The SOL-solubilization approach maintained the apparently dissolved LTD in solution in MDT. However, it failed under the biphasic model, since it hindered the accessibility of the solubilized species to partition into the organic phase (25 – 70% of the total drug amount) (Figure 5.64C). As a result, a negative polymer concentration-dependent effect was observed. Similar to the MDT test, lower polymer concentrations (0.0019 – 0.0155 % w/V) were applied because of the analytical problems associated with the low therapeutic dose used of LTD (10 mg). Furthermore, a proper quantification in the aqueous phase was not feasible for the two highest polymer concentrations used (0.0077 and 0.0155% w/V).

According to the non-chaser behavior of LTD, its amorphous precipitation and the absence of H-donor groups, the polymers KVA64 and MA4C already showed a very limited effect as LTD solubility enhancers in the kinetic (Figure 5.37) and thermodynamic (Figure 5.12) approaches. Therefore, their ability to enhance LTD partition into the organic phase was minor in a similar manner. Besides, the exponential decay 1 obtained for the pK_a -curves (Figure 5.4) suggested in both cases a low solubilization effect, which can additionally limit the partition of LTD.

The BDT results suggested that enhancing the oral exposure of the non-chaser molecule LTD might be challenging. Since the amorphous pure drug initially precipitated via LLPS, a quick interplay between re-dissolution and partition into the octanol layer was established which could not be majorly improved by the polymers used. Due to the low solubilization effect of the polymers on LTD, the partition was not favored and a decrease in the AUCs in the organic phase was determined (Figure 5.65).

5. RESULTS AND DISCUSSION

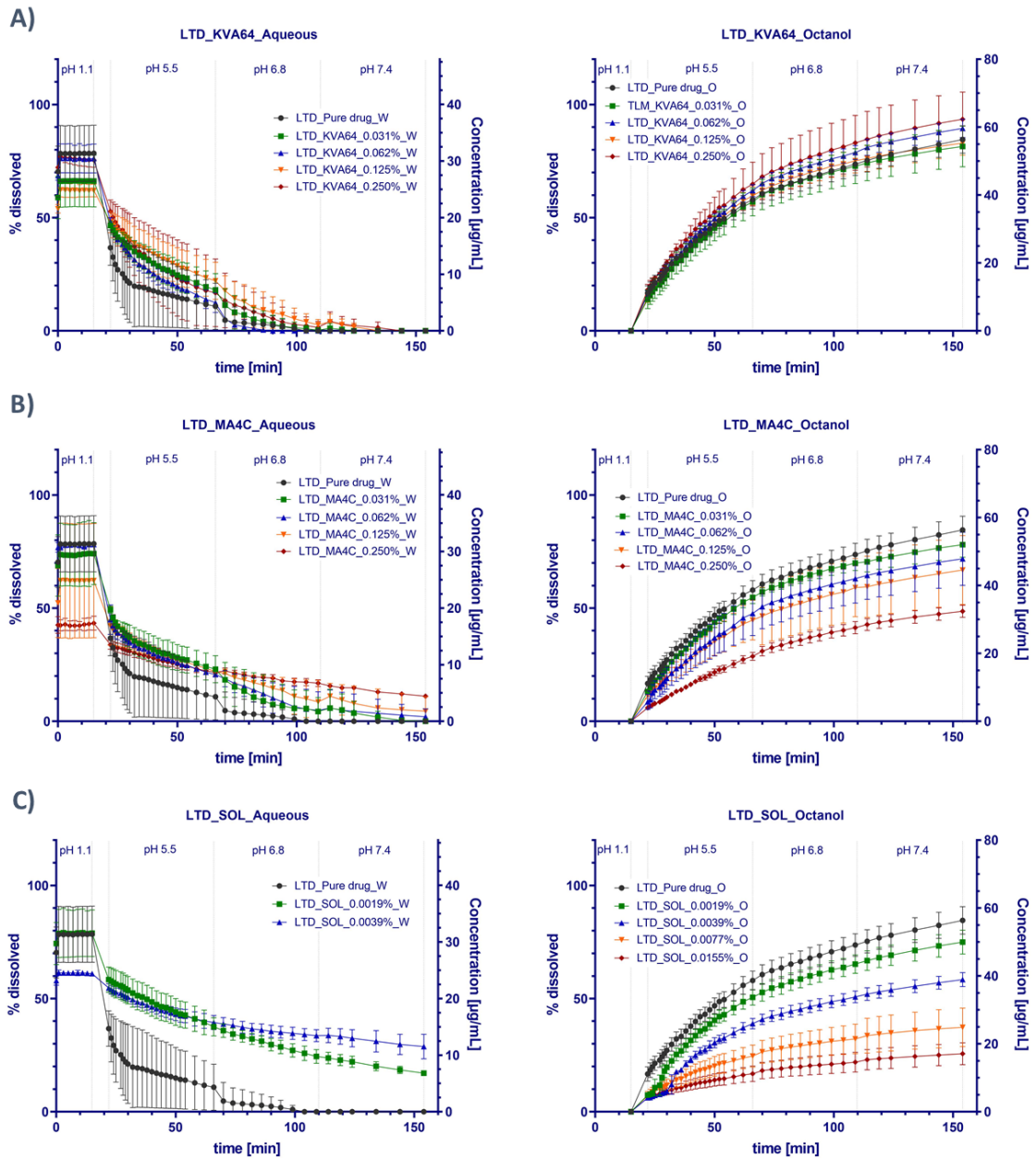


Figure 5.64: LTD biphasic dissolution tests **A) KVA64 B) MA4C C) SOL**. The left graphs represent the fractions of dissolved drug in the aqueous phase and the right graphs show the fractions partitioned into the octanol phase for each drug-polymer combination.

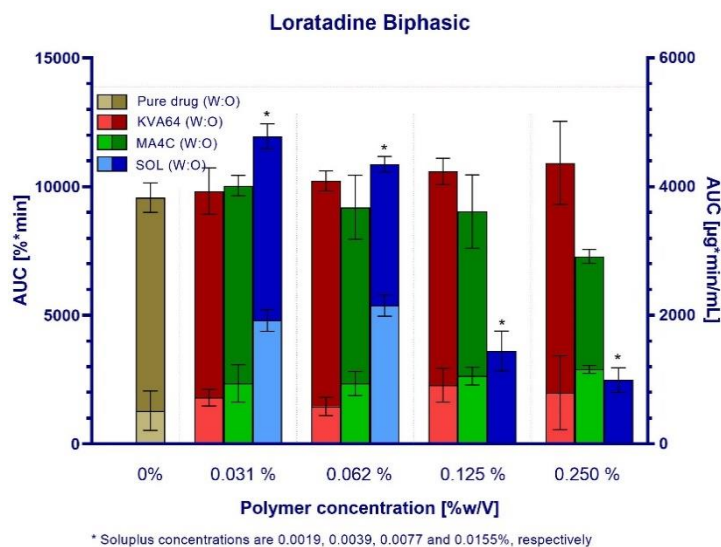


Figure 5.65: Comparative LTD AUCs from the precipitation period (pH 5.5 – pH 7.4) in the aqueous and organic phase. The red dotted line indicates 100% of the dissolved drug during entire test time (139 minutes) and corresponds to an AUC of 13900 %*min or 5560 µg*min/mL.

5.2.2.2.2 Telmisartan

The pure drug precipitated amorphously and re-dissolved easily in the aqueous phase when the conditions were thermodynamically favored (increase in pH and presence of a sink compartment). In this sense, the inclusion of an organic phase enabled the partition of the TLM molecules (85% within 139 minutes) and induced a quick interplay between partition and re-dissolution especially at pH 5.5 (Figure 5.67). Therefore, the BDT approach predicted a quick *in vivo* absorption of the pure drug.

The initial precipitation of the drug in the aqueous phase was hindered by the polymers (Figure 5.65 A,B). In the case of SOL, the high turbidity disabled the detection in the aqueous phase. Despite the polymers' positive effect, the stabilization in the aqueous phase decelerated in all cases the partition into the organic layer (50 – 70%) (Figure 5.66A-C). KVA64 showed a slightly positive concentration-dependent effect (fraction partitioned: 60 – 75%) (Figure 5.66A), while this was negative for MA4C (Figure 5.66B) and SOL (Figure 5.66C). This was caused by the additional effects of viscosity and micellization. In this sense, from a kinetic point of view, the impact of the polymers appeared to be counterproductive when a quick absorption is targeted. Consequently, an increase in the AUC_{aq} associated to the stabilization in the aqueous phase was observed in the polymeric solutions. However, and on the contrary to chasers, this involved at the same time a decrease in the AUC_{oc} values, reflecting a lower partition (Figure 5.67).

The non-chaser behavior of TLM and the precipitation of the pure drug as an amorphous highly energetic form, facilitated the interaction with the polymers and the solubilization effect. Furthermore, the zwitterionic behavior of TLM established a very complex interplay between dissolution, supersaturation, precipitation, re-dissolution and absorption.

The BDT observations were consistent with the previously determined solubilization effect in the pK_a -curves (Figure 5.5), as well as in the CheqSol/Shaking flask (Figure 5.14) and MDT approach (Figure 5.42). Furthermore, the decrease in the LogD values (Figure 5.2) of TLM in polymeric solution suggested a high impact of the polymers on the partition into the organic

5. RESULTS AND DISCUSSION

phase. In the case of KVA64 and SOL, due to the decrease in the molecularly dissolved drug fraction, as well as due to the viscosity increase in MA4C solution, the partition into the organic phase was decelerated when compared to the pure drug.

All in all, the polymers achieved a high stabilization of the non-chaser molecule TLM in the aqueous phase (approx. 2-fold for KVA64 and up to 4-fold for MA4C). However, due to the solubilization effect and decrease of the molecularly dissolved drug fraction, the partition was not favored.

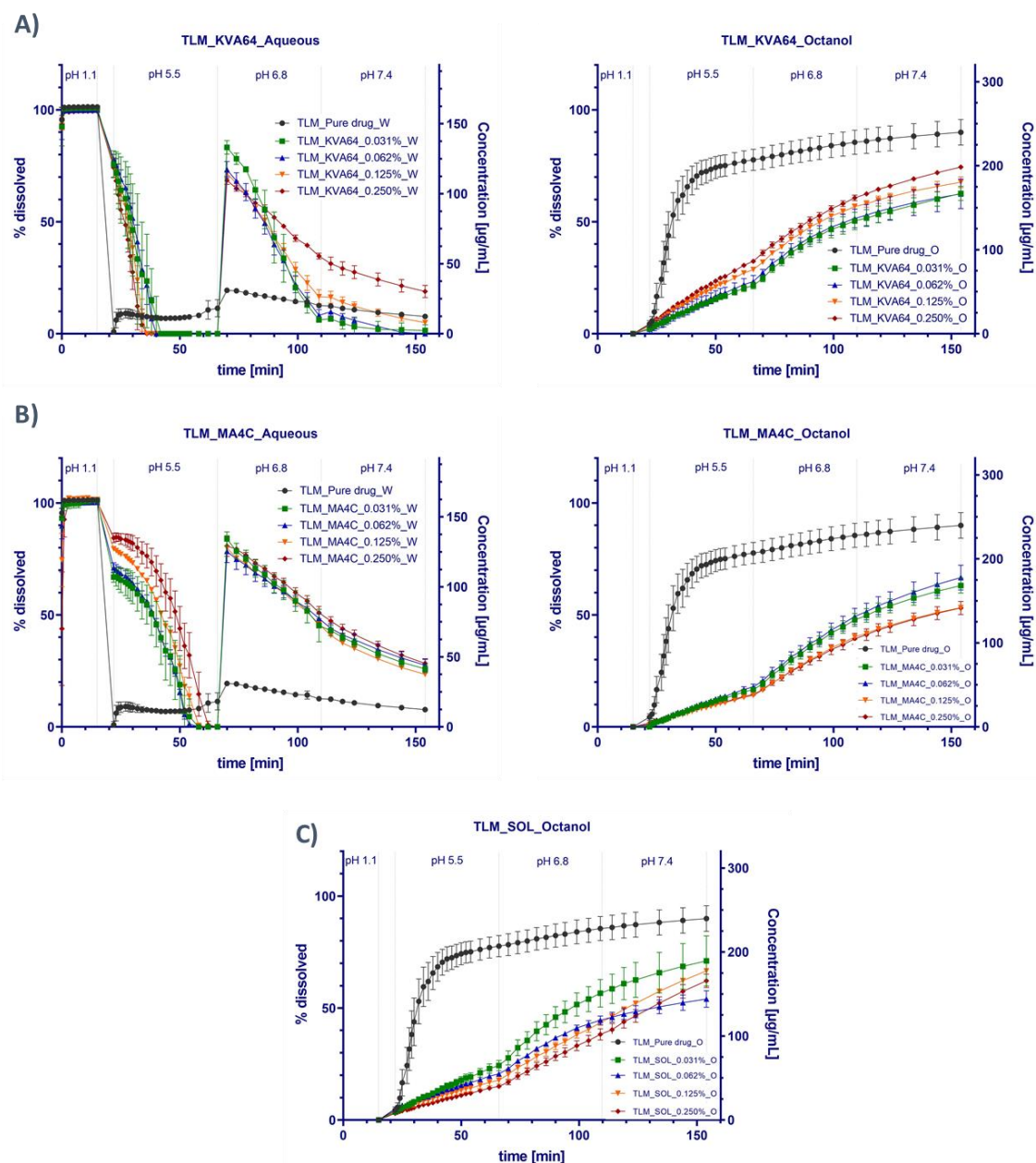


Figure 5.66: TLM biphasic dissolution tests A) KVA64 B) MA4C C) SOL. The left graphs represent the fractions of dissolved API in the aqueous phase during test time and the right graphs show the partitioned fractions into the octanol phase for each drug-polymer combination. Due to the turbidity of SOL colloidal solutions, no aqueous phase results are available. The supersaturation of TLM in colloidal solutions did not enhance the partition into the organic phase.

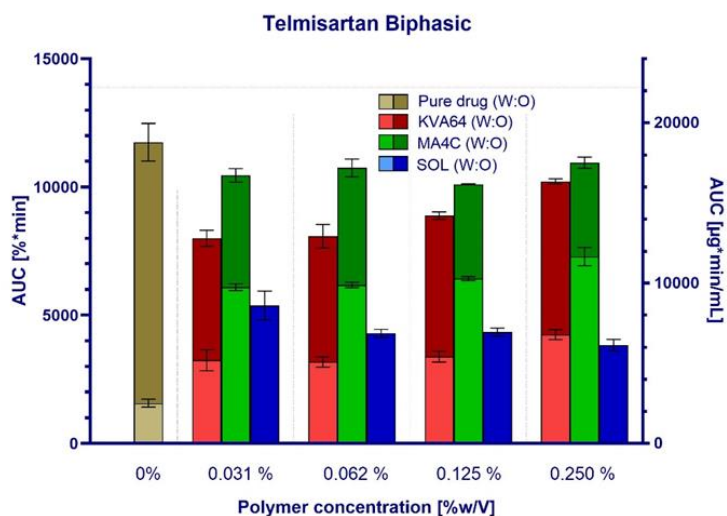


Figure 5.67: Comparative TLM AUCs obtained from the precipitation period (pH 5.5 – pH 7.4) in aqueous and organic phases. The red dotted line indicates 100% of the dissolved API during test time (139 minutes) and corresponds to an AUC of 13900 %*min or 22240 µg*min/mL. The apparently dissolved fraction in SOL colloidal solutions could not be quantified.

5.2.2.2.3 Partition rate for non-chaser molecules

The measured partition rates of LTD in KVA64 and MA4C colloidal solutions remained similar to the pure drug (around 1 µg/mL/min) (Figure 5.68A). However, in the presence of MA4C, a negative polymer concentration-dependent effect was observed, caused by the increased viscosity and decreased molecular mobility. Therefore, the partition rate decreased by the half at the highest polymer concentration (0.250% w/V). The use of SOL confirmed again a polymer concentration-dependent irreversible solubilization.

In the case of TLM, due to the complex interplay between the pH-dependent solubility, dissolution, supersaturation and precipitation phenomena, the partition rate majorly differed between the applied pH period and therefore the results were separated in two diagrams. At pH 5.5, the precipitation of the pure drug as an amorphous form and its quick re-dissolution triggered a fast initial partition rate of 25 µg/mL/min (Figure 5.68B). In the presence of polymers, the precipitation was slowed down at pH 5.5 as a result of a solubilization effect. Due to the decrease in the molecularly dissolved fraction, the potential of the molecularly dissolved drug to partition into the organic phase was lower (12.5 – 25-fold decrease in partition rate). This was supported by Log*D* results for TLM, which indicated a reduction of the overall lipophilicity of the system even at equilibrium conditions due to the presence of polymers (Table 5.2).

In Figure 5.68C, the fast drug re-dissolution at pH 6.8 improved the partition of the remaining drug fraction in the aqueous phase. In the case of the pure drug, the main drug fraction already partitioned in the first intestinal pH period (5.5) and thus, a lower partition rate in the pH period 6.8 – 7.4 was observed (0.8 µg/mL/min), as compared to the polymers (1.5 – 3 µg/mL/min).

In general, non-chaser molecules underwent a controlled partition into the organic compartment of the biphasic model from polymeric colloidal solutions. This effect was triggered due to the drug's initial precipitation as a high energetic liquid amorphous form by means of LLPS, which based on stable drug-polymer interactions associated to a solubilization effect, as

5. RESULTS AND DISCUSSION

indicated by the pK_a -curves (Figure 5.4, Figure 5.5) and the solubility determinations (Figure 5.12, Figure 5.14).

As a result, the accessibility of these solubilized species for permeation was hindered. In literature, Comer *et al.* observed an accelerated partition rate of aripiprazole in biphasic dissolution as a function of increasing drug concentrations until LLPS occurred (Comer *et al.*, 2014). After LLPS was seen, the partition became independent of the drug concentration, as it was similarly the case for LTD and TLM in the present case studies.

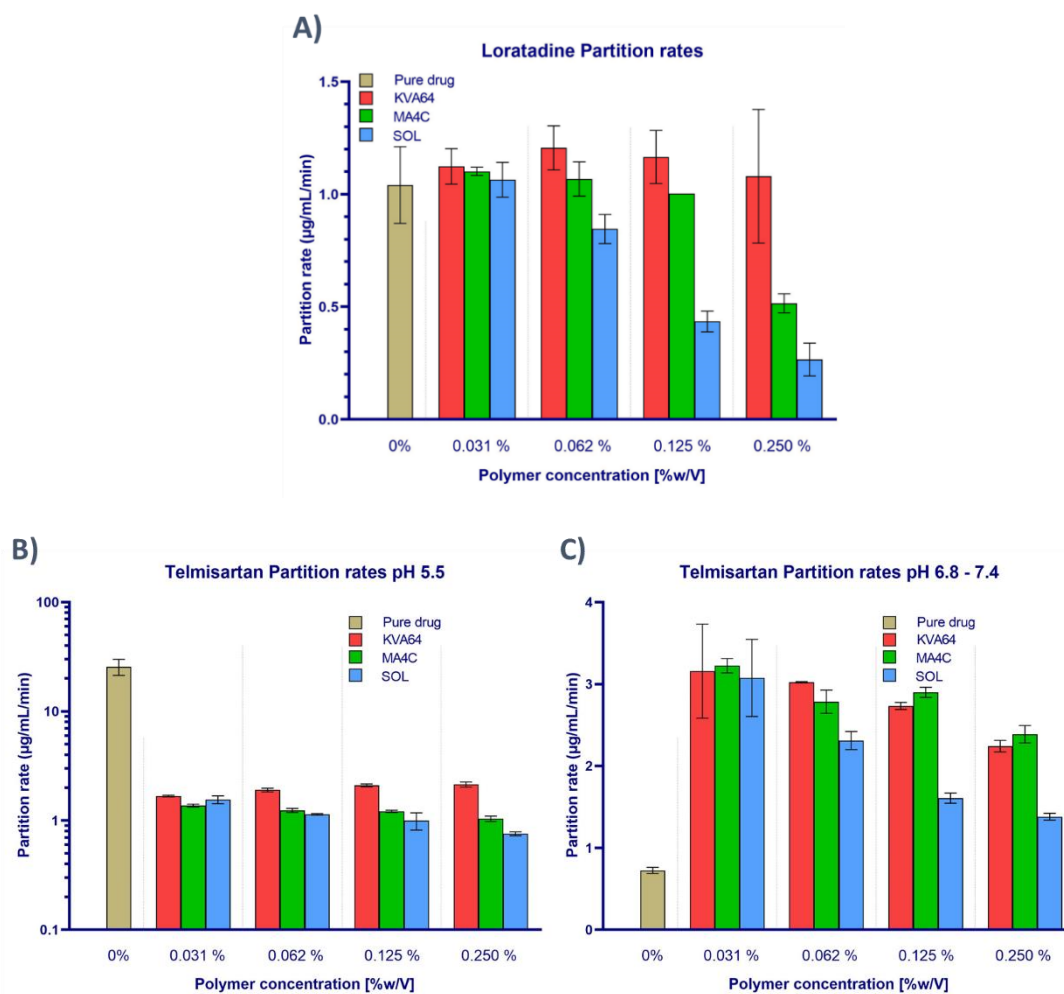


Figure 5.68: Partition rates of non-chaser molecules LTD (A) and TLM (B and C) into the octanol phase of a biphasic system. In all cases, no effect or an overall deceleration partition rate, calculated after fitting the profile to a first-order kinetic, was observed. Thus, it highlighted the difficulty to enhance the oral BA of non-chaser molecules.

5.2.2.3 Extremely poorly soluble molecules

5.2.2.3.1 *Albendazole*

According to the extremely poor solubility of ABZ, only 9 – 12 % of the pure drug reached the octanol layer at the end of the test (Figure 5.69).

KVA64. When compared to the pure drug, the partition into the organic phase was favored and up to the entire drug fraction (90 – 100%) reached the organic phase at test end (Figure 5.69A). This highlighted the potential of KVA64 to stabilize ABZ in solution, but also proved the reversibility of the drug-polymer interactions. Additionally, the partition into the octanol phase and the disappearance of drug from the aqueous compartment were identical, indicating a low precipitation in colloidal solution. Based on its shown ability as solubility enhancer (Figure 5.15) and crystal growth inhibitor (Figure 5.50), the positive effect of KVA64 for the partition of ABZ was expected (Figure 5.15, Figure 5.49). Although a solubilization effect by KVA64 occurred (Figure 5.2, Figure 5.15), the formed intermolecular interactions appeared to be reversible as the partition was not hindered, but enormously favored.

MA4C. In BDT, despite the reduced precipitation in the aqueous phase (Figure 5.69B), MA4C did not improve the partition into the organic phase (9 – 10%). As it was the case for the chaser and non-chaser drug molecules, the reduced molecular mobility in MA4C colloidal solutions impeded the partition of molecularly dissolved drug into the organic phase. However, its poor effect on the partition is not only related to the increased viscosity, since a limited kinetic (Figure 5.49C) and thermodynamic (Figure 5.15) stabilization of ABZ in solution was determined.

SOL. The inclusion of an organic phase reduced the precipitation kinetics but the partition into the organic phase remained unchanged compared to the pure drug (fraction partitioned: 9 – 11%) (Figure 5.69C). In this sense, the fraction of drug solubilized in the polymeric micelles appeared to be tightly bounded to the lipophilic core and the micellization might be partially irreversible. Consequently, SOL seemed to be unsuitable to enhance the oral BA of ABZ. In the absence of an absorptive sink compartment, the SOL-solubilization effect was kinetically limited (Figure 5.49D). Nevertheless, according to the extremely poor solubility of the pure drug, a high solubilization by SOL was observed under equilibrium conditions (Figure 5.15).

In general, the stabilization of ABZ in colloidal solution depended heavily on the polymer used. The stabilization by KVA64 showed the highest potential to limit precipitation and enhance ABZ partition into the organic phase. The drug-polymer interactions in this combination were likely reversible and the formed species in solution possessed the ability to partition into the organic phase. On the contrary, the viscosity increase or the micellization approach were not suitable to improve the partition into the organic sink compartment. Thus, only KVA64 showed a potential to stabilize ABZ in solution and facilitate the accessibility of the species in aqueous solution to partition into the organic phase, showing an increase in the AUC_{oc} (Figure 5.70). In the case of MA4C and SOL, despite the increase in the AUC_{aq} , this did not lead to an increase in the AUC_{oc} .

5. RESULTS AND DISCUSSION

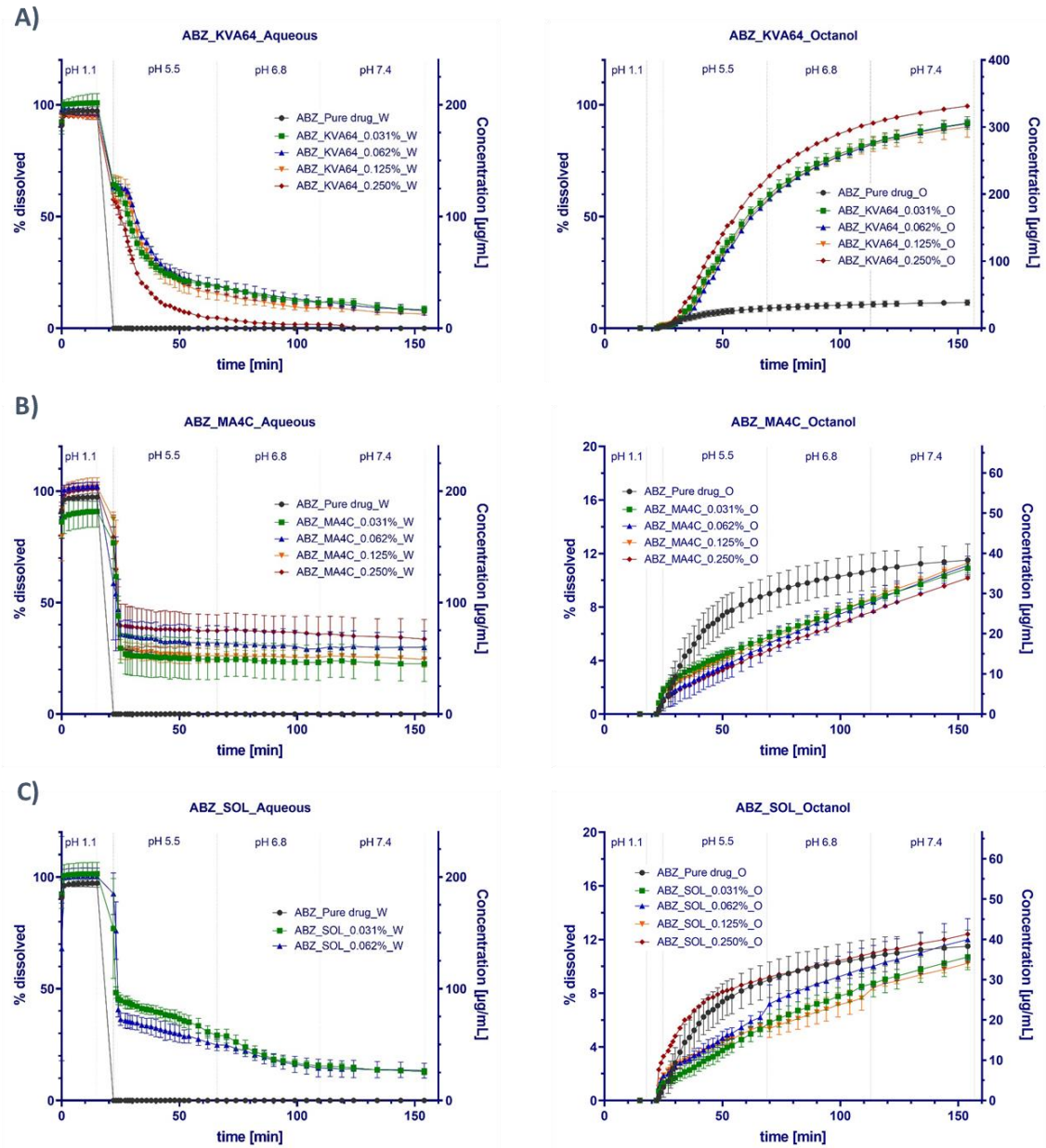


Figure 5.69: ABZ biphasic dissolution tests A) KVA64 B) MA4C C) SOL. The left graphs represent the fractions of dissolved drug in the aqueous phase as a function of time and the right graphs show the partitioned fractions into the octanol phase for each drug-polymer combination. The potential of ABZ supersaturation or solubilization to enhance its bioavailability is only found for KVA64.

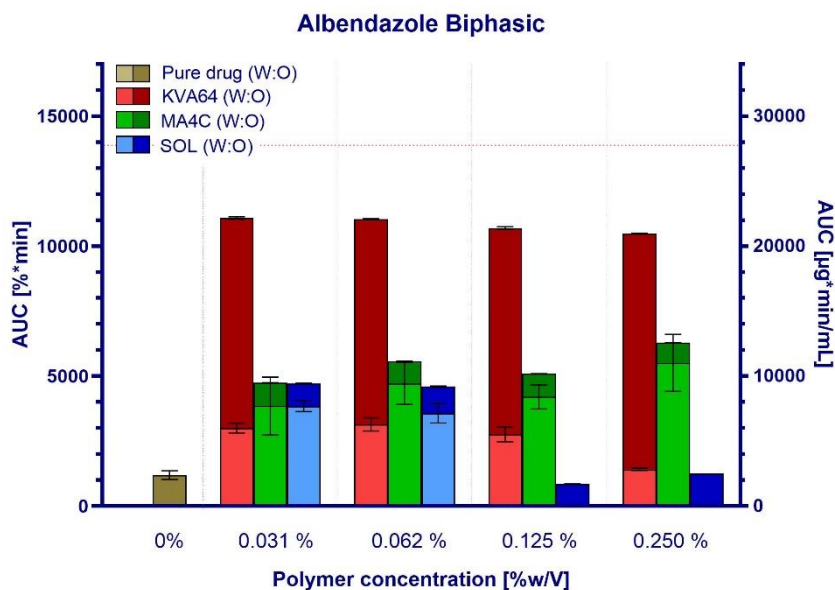


Figure 5.70: Comparative ABZ AUCs obtained from the precipitation period (pH 5.5 – pH 7.4) in aqueous and organic phases. The red dotted line indicates 100% of dissolved API during test time (139 minutes) and corresponds to an AUC of 13900 %*min or 55600 µg*min/mL.

5.2.2.3.2 Itraconazole

As reported in the literature, ITZ is able to precipitate into amorphous nanoparticles when stabilizing polymers were present (Miller et al., 2012c). Therefore, the inclusion of a sink compartment would facilitate the re-dissolution of these amorphous nanoparticles and favor the partition of ITZ into the organic phase.

In the BDT, a solubility-limited partition into the organic phase was found for the pure drug, since only 3 – 6% of the total drug fraction reached the organic phase at test end (Figure 5.72). When using the polymers, a precipitation inhibition was observed in the aqueous phase (Figure 5.72 A-C).

KVA64. In the BDT, a strong dependency between the physical state of the precipitate and the partition was found. The polymer adsorption to ITZ clusters after nucleation limited the particle growth, and very likely promoted the formation of ITZ amorphous nano-dispersed particles. The precipitation into amorphous nanoparticles contributed to the complex interplay between the supersaturation, re-dissolution and partition phenomena. Consequently, the partition into the organic phase was kinetically controlled by the re-dissolution of ITZ amorphous nanoparticles in KVA64 colloidal solution and 5 – 20% of ITZ partitioned into the organic phase by the test end (Figure 5.72A). Due to the absence of a sink compartment, no re-dissolution was observed in the MDT approach (Figure 5.54B) and the polymer itself had no solubilization effect on ITZ (5.16). This highlights the importance of including a sink compartment in order to prevent an overestimation of the precipitation in the aqueous phase.

MA4C. The precipitation of ITZ amorphous nanoparticles was also found for MA4C colloidal solutions and a re-dissolution of the drug in the aqueous phase occurred (Figure 5.72B).

5. RESULTS AND DISCUSSION

Nevertheless, the previously observed kinetic (Figure 5.54C) and thermodynamic (5.16) ITZ stabilization was not solely attributed to the viscosity increase, but also to a solubilization through the formation of stable hydrophobic drug-polymer interactions. The combination of these effects reduced the ITZ partition into the organic phase (fraction partitioned: 3%), although a high positive ITZ stabilization in the aqueous phase occurred.

SOL. In the BDT, the initial ITZ precipitation was followed by a polymer concentration-dependent re-dissolution (Figure 5.72C). In this sense, the partition of ITZ molecules was not initially improved, but the ITZ re-dissolution in the aqueous phase triggered an increased partition rate towards test end (fraction partitioned: 3 – 8%). However, the polymer concentration-dependent solubilization was counterproductive for the partition, an effect which was generally valid for all investigated drug molecules. The high SOL-solubilization extent obtained for ITZ (Figure 5.19) was attributed to its high lipophilicity ($\text{Log}P = 4.73$). The micellization of neutral ITZ species behaved as a partially irreversible process and therefore, the partition was hindered at high polymer concentrations.

All in all, despite the observed positive stabilization in all aqueous colloidal solutions (increase in the AUC_{aq}), an enhancement in the ITZ oral BA could be challenging. Since the partition heavily depended on the re-dissolution of the amorphous nanoparticles and the stabilization mechanisms used did not directly improve the accessibility of the species in solution for partition (no significant increase in AUC_{oc}), a significant *in vivo* effect is questionable (Figure 5.71).

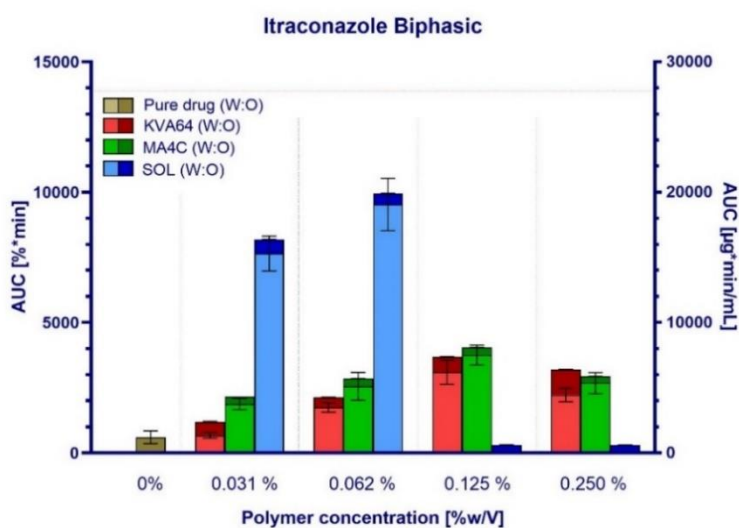


Figure 5.71: Comparative ITZ AUCs obtained from the precipitation period (pH 5.5 – pH 7.4) in aqueous and organic phases. The red dotted line indicates 100% of the dissolved API during test time (139 minutes) and corresponds to an AUC of 13900 %*min or 27800 $\mu\text{g} \cdot \text{min}/\text{mL}$.

5.2 Part II: *In vitro* evaluation of supersaturation and solubilization

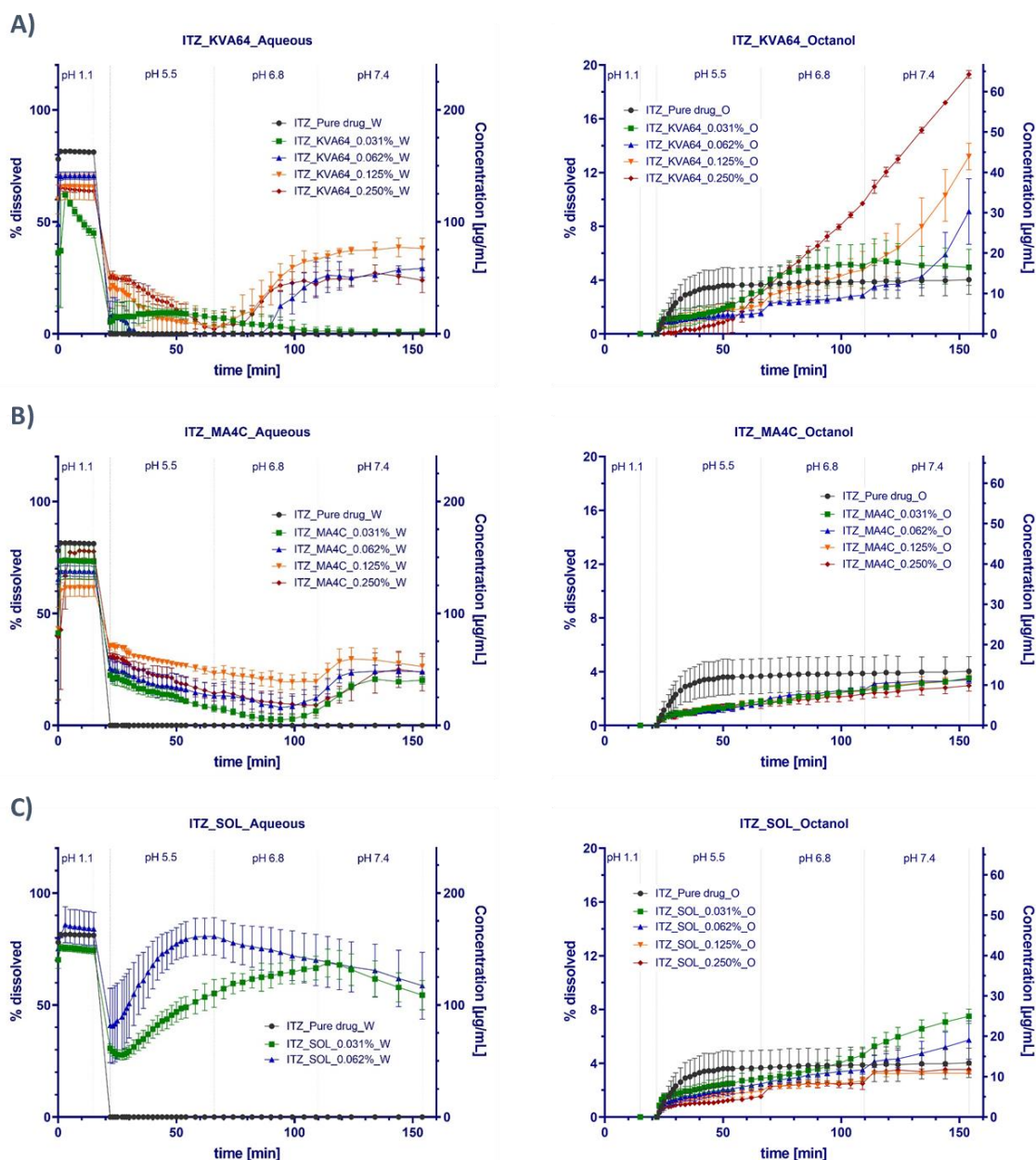


Figure 5.72: ITZ biphasic dissolution tests **A)** KVA64 **B)** MA4C **C)** SOL. The left graphs represent the fractions of dissolved API in the aqueous phase and the right graphs show the partitioned fractions into the octanol phase for each drug-polymer combination during test time.

5.2.2.3.3 Partition rate of extremely poorly soluble drug molecules.

According to their extremely poor solubility, ABZ and ITZ showed high stabilization extents in colloidal solutions under the BDT (Figure 5.70, Figure 5.71). Despite this effect, the partition into the organic phase was seldomly improved (Figure 5.73).

Only the combination ABZ-KVA64 showed an approx. 5-fold increase in the partition rate as a result of the stabilization in the aqueous phase (Figure 5.73A). Furthermore, KVA64 achieved a kinetic ITZ stabilization in the biphasic model and similarly promoted the partition of ITZ into the organic phase (Figure 5.72A). Unfortunately, the ITZ partition from the KVA64 colloidal solutions

5. RESULTS AND DISCUSSION

could not be fitted to a first-order kinetic and consequently, no partition rate was calculated for the combination.

On the contrary, MA4C and SOL did not accelerate the partition into the organic phase and the partition rates decreased by 2 – 5-fold for ABZ and 10 – 20-fold for ITZ (Figure 5.73). The viscosity increase, as well as the hydrophobic interactions in the case of ITZ/MA4C, hindered the accessibility of ABZ and ITZ to partition into the organic phase. The SOL micelles, especially for extremely poorly soluble molecules, proved to behave as a competitive lipophilic compartment or an alternative pathway to avoid precipitation, while at the same time they limited the partition.

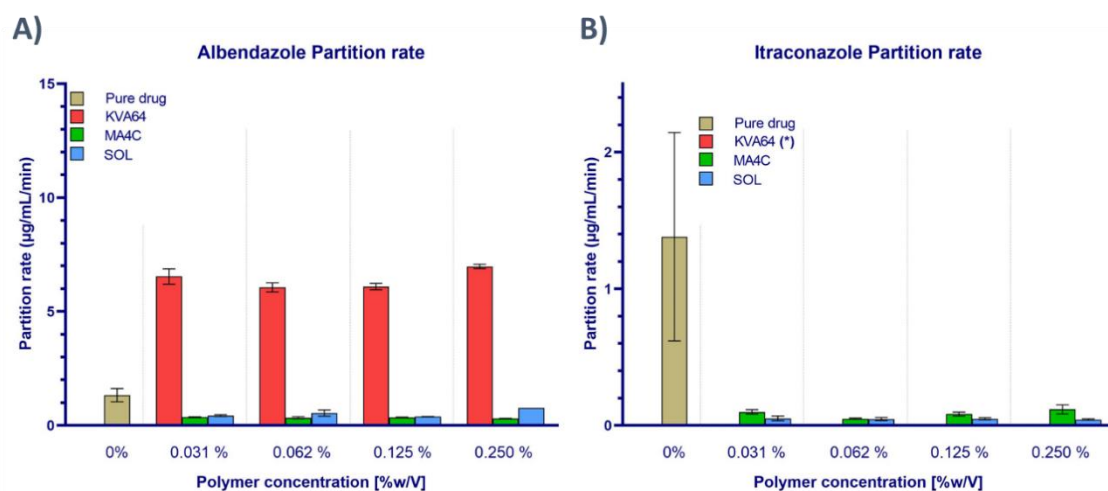


Figure 5.73: Partition rates of extremely poorly soluble molecules ABZ (A) and ITZ (B) into the octanol phase of a biphasic system. An acceleration of the partition rate was only observed for KVA64 colloidal solution. (*) The combination ITZ-KVA64 did not follow a first-order kinetic and as a result, no values were compiled here. Both MA4C and SOL were unsuitable to enhance the partition of both molecules.

5.2.2.4 Relationship between solubility enhancement and lipophilicity

In order to investigate the relationship between the observed solubility enhancement extent in equilibrium conditions (solubility enhancement ratio) and the impact on the partitioned drug fraction into the organic phase (octanol AUC enhancement), the physicochemical properties of the drugs were considered. The innate supersaturation ability of the drug molecules helped to cluster regions in the plots as a function of the partition to the solubility enhancement ratio. This investigation was important to differentiate between suitable and unsuitable polymer-drug combination candidates for further evaluation of the *in vivo* supersaturation and solubilization potential on the oral absorption.

5.2.2.4.1 Kollidon VA64

Despite the relatively low solubility enhancement by KVA64 (solubility enhancement ratios <4, except 100-200-fold for ABZ) (Figure 5.17), KVA64 improved the partition into the organic phase for almost all tested drug molecules. Clear evidence was shown that the partition extent heavily

depended on the innate supersaturation behavior of the drug molecules. This allowed the identification of different clusters in the plot:

- Chaser molecules (DPD and CLX). A cluster for chaser molecules was identified at the upper left region in the plot (Figure 5.74). Therefore, although a low solubility enhancement ratio ($\approx 2 - 4$) was found, a high partition extent for both chaser molecules into the organic phase occurred. The shift of the chaser behavior into a non-chaser (Figure 5.10, Figure 5.11) was indicative for the polymer's potential to impact nucleation and crystal growth of both drugs, which in turn favored the partition. The extent of the octanol AUC enhancement ratio also depended on the specific physicochemical properties of each molecule (e.g. pH-dependent solubility). Furthermore, the weak character of the H-bond interactions played a decisive role for the partition, since they increased the dissolved drug fraction in aqueous solution without hindering the transfer of drug molecules into the organic phase.
- Non-chaser molecules (LTD and TLM). Due to the low aqueous solubility enhancement ratios and the practically unaffected partition kinetic, the non-chaser cluster was identified at the lower left region in the plot (Figure 5.74). Thus, the potential of the polymers to enhance the oral BA of non-chaser molecules was limited. The precipitation of the pure drugs via LLPS into a high energetic amorphous form established a quick interplay between re-dissolution and partition. As a result, 80 – 90% of the pure drug reached the organic phase until test end. Due to this energetically favored “starting point” by the amorphous drug precipitate, an improved partition by supersaturating polymers was challenging. Consequently, no polymeric effect on the LTD solubility and partition was observed. In the case of TLM, the stabilization in aqueous solution was attributed to a solubilization effect as reflected by the pK_a -curve (Figure 5.5). Consequently, the decrease in the molecularly dissolved fraction slowed down the partition into the organic phase.
- Extremely poorly soluble molecules (ABZ and ITZ). Due to the high variation in solubility enhancement by KVA64 for this molecule group, no distinct cluster was identified in the plot. ABZ clearly showed a positive response to the stabilization by KVA64 in the aqueous medium, thus an improved the partition into the organic phase was found. In the case of ITZ, the lack of H-donor groups in the ITZ structure made H-bonds with the polymer unfeasible and limited the polymer's potential to enhance the ITZ solubility in aqueous solution. However, the precipitation as amorphous nanoparticles facilitated the re-dissolution and partition of the drug into the organic compartment. Thus, ITZ in KVA64 solution showed a behavior close to non-chaser molecules, while ABZ was found in a region closer to the chaser molecules (Figure 5.74).

Overall, the *in vitro* results suggested a high potential of KVA64 to enhance the oral exposure of BCS II drug molecules *in vivo*. The increased partition of the drugs into the organic phase was attributed to the reversibility of the established drug-KVA64 interactions. Furthermore, no general polymer concentration-dependency of the partition was found.

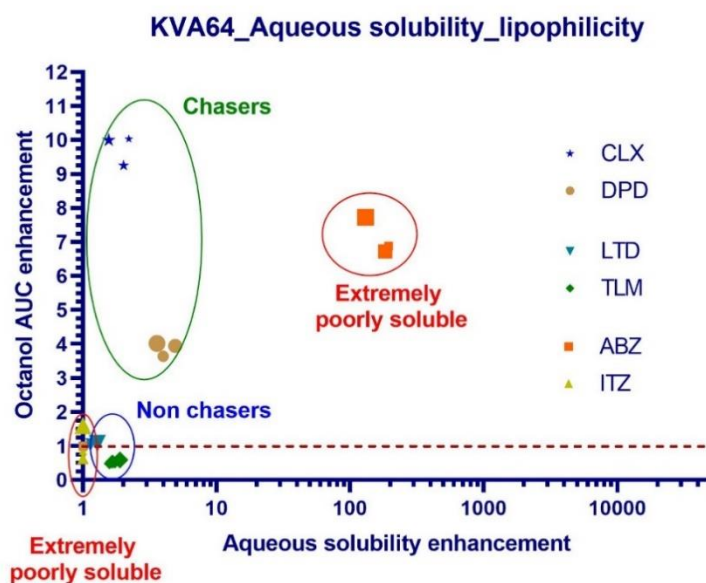


Figure 5.74: Relationship between the aqueous solubility enhancement ratios in KVA64 colloidal solutions and their potential to improve the partition of BCS II molecules into an octanol phase. Various clusters were characterized as a function of the innate supersaturation ability of the pure drug molecules. Chasers clustered in the upper left region, while non-chasers clustered in the lower left region of the plot. The partition of extremely poorly soluble molecules heavily depended on the aqueous solubility enhancement ratio. The size of the symbols corresponds to the different applied polymer concentrations (small size → low concentrations, large sizes → high concentrations).

5.2.2.4.2 Methocel A4C

Although a general positive drug stabilization by MA4C was found, only chaser molecules showed an enhanced partition. The viscosity increase, caused by the gelling properties of MA4C colloidal solutions (Table 5.4), limited the precipitation or crystal growth. However, the Brownian motion of the drug molecules in solution was simultaneously reduced and hindered their access to the aqueous-organic interface. Consequently, a negative polymer concentration-dependent effect on the partition was generally observed. In the case of the solubility-lipophilicity plot, three distinct clusters were identified (Figure 5.75):

- Chaser molecules (CLX and DPD). The chaser cluster was found in the upper left region of the plot. The potential of MA4C to limit the crystal growth and precipitation kinetics led to an improved partition, compared to the pure drug. The extent of partition depended on the precipitate's physical state: the obtained CLX nanoparticles in colloidal solutions facilitated a faster re-dissolution-absorption interplay and consequently, high drug fractions partitioned into the octanol phase (Figure 5.75). Contrary, DPD still precipitated as crystalline needles in colloidal solution, for which the re-dissolution in aqueous solution was not thermodynamically favored. However, an improved partition was observed in both cases.
- Non-chaser molecules (LTD and TLM). The non-chaser cluster was found in the lower left region of the plot (Figure 5.75), indicative for a low stabilization in aqueous solution and a low partition. The solubilization effect proposed for the non-chaser drug molecules due to the exponential pK_o -curves (Figure 5.4, Figure 5.5) and the viscosity increase limited the partition of the species into the organic phase.

- Extremely poorly soluble molecules (ABZ and ITZ). These compounds clustered in the lower left-middle region of the plot (Figure 5.75). For ITZ, the positive MA4C-solubilization effect, which was mainly attributed to the formation of intermolecular hydrophobic interactions, did not improve the partition. For ABZ, the aqueous solubility enhancement was much more limited but similarly the partition was not enhanced. The increased viscosity and the resulting decrease in the Brownian motion hindered the partition into the organic phase and caused a negative polymer concentration-dependent effect.

In general, a viscosity increase did not improve the partition of drug molecules into the organic phase in the BDT. However, due to the larger intraluminal volumes and the continuous transit triggered by peristaltic waves in the human GI tract (Hens et al., 2017; Koziolok et al., 2016), this counterproductive viscosity increase might be irrelevant *in vivo*. Nevertheless, a polymeric molar excess might promote an entrapment of the drug molecules within polymeric clusters, which would compromise the partition into the organic phase (*in vitro*) and potentially limit its oral absorption (*in vivo*).

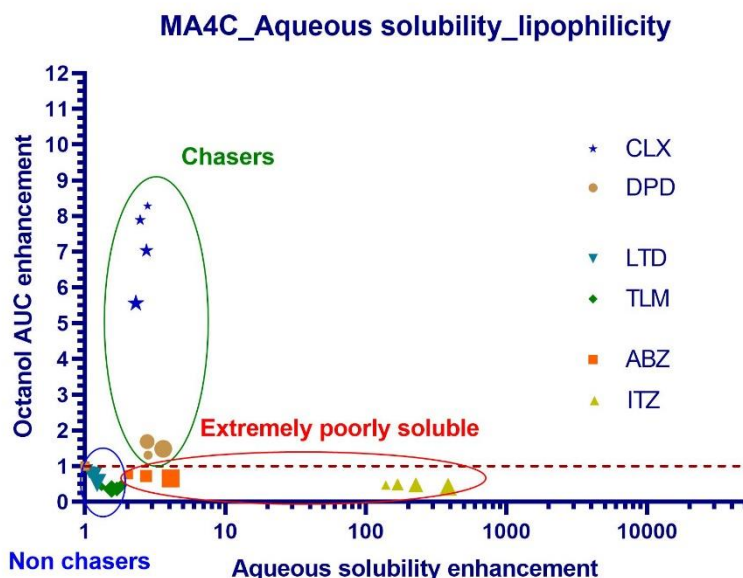


Figure 5.75: Relationship between the aqueous solubility enhancement ratios in MA4C colloidal solutions and their potential to improve the partition of BCS II molecules into an octanol phase. Various clusters were characterized as a function of the innate supersaturation ability of the pure drug molecules. Chasers can be found in the upper left region, while non-chasers and extremely poorly soluble molecules clustered in the lower left-middle region of the plot. The size of the symbols corresponds to the various applied polymer concentrations (small size \rightarrow low concentration, large size \rightarrow high concentration).

5.2.2.4.3 Soluplus

For SOL, similar trends to MA4C were observed in the plot (Figure 5.76). Since non-chaser and extremely poorly soluble molecules achieved higher solubilization extents, they clustered differently than for MA4C. The SOL-solubilization extent, as well as the irreversible internalization within the SOL-micelles, was related to the LogP of the drug molecules

5. RESULTS AND DISCUSSION

(Figure 5.19). In this sense, the partition into the organic phase was affected by the established equilibrium between the molecularly dissolved and the micellized drug fraction.

- Chaser molecules (DPD and CLX). The chasers clustered in the upper left region of the plot (Figure 5.76). Their partition into the organic phase was favored by SOL until a certain polymer concentration (0.031% w/V) was exceeded in both cases. At higher concentrations, the partition was more limited. Thus, a major negative polymer concentration-dependent effect was observed. DPD and CLX had the lowest Log*P* of the investigated drugs with 2.66 and 2.69, respectively (see section 5.1.2.1). Due to the low lipophilicity of DPD and CLX, the solubilization of chaser drugs was partially reversible and the partition was favored.
- Non-chaser molecules (LTD and TLM). The non-chaser clustered in the lower middle region of the plot (Figure 5.76). The high micellization extents (10 – 3000-fold increase in solubility) achieved by SOL, slowed down the partition kinetics for LTD and TLM. Consequently, a negative polymer concentration-dependent effect was observed. and an exponential decay relationship between the solubility enhancement ratios and the partition was determined for both molecules (Figure 5.76, Table 5.7).
- Extremely poorly soluble molecules (ABZ and ITZ). Both molecules were found in the lower middle-right region of the plot (Figure 5.76). Thus, very high solubility enhancement ratios (30 – 40000-fold) were observed in the aqueous phase. Nevertheless, the SOL-solubilization decreased the partition into the organic phase due to the entrapment of drug molecules in the SOL-micelles. Consequently, the high solubilization extents were counterproductive for the partition, thus supporting the mainly irreversible character of this stabilization for extremely poorly soluble molecules. An exponential decay relationship between the solubility enhancement ratios and the partition was similarly observed for ITZ (Figure 5.76, Table 5.7).

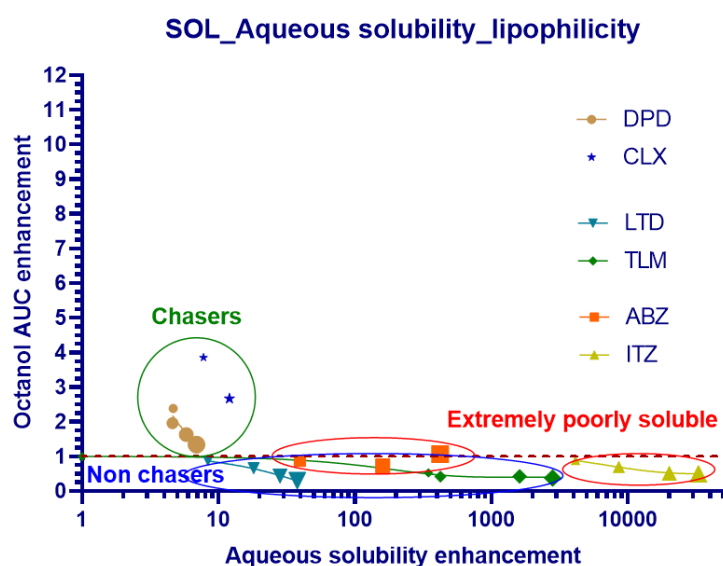


Figure 5.76: Relationship between the aqueous solubility enhancement ratios in SOL colloidal solutions and their potential to improve the partition of BCS II molecules into an octanol phase. Various regions as a function of the innate supersaturation ability of the pure drug molecules were determined. Chasers clustered in the upper left region, while non-chasers and extremely poorly soluble molecules were found in the lower middle-right region of the plot. An exponential decay relation between the aqueous solubility enhancement ratios and the extent of partition size was observed. The size of the symbols corresponds to the various applied polymer concentrations (small size → low concentration, large size → high concentration).

Table 5.7: Coefficient of determination obtained for the exponential decay relation between the solubility enhancement ratios and the extent of partition in Figure 5.76.

Drug	Exponential fitting
	R ²
DPD	0.8266
ABZ	--
ITZ	0.9986
LTD	0.9971
TLM	0.9847
CLX	--

5.2.3 Conclusion

Since the first part of this work targeted the identification of various stabilization mechanisms from a thermodynamic and physicochemical point of view (section 5.1), the second part investigated the supersaturation and solubilization potential from an *in vitro* kinetic perspective. In this sense, biorelevant conditions (e.g. pH-shifts similar to GI tract under fasted conditions and inclusion of an absorptive compartment) were introduced.

The MDT provided a deeper understanding of the polymers' potential to hinder nucleation and crystal growth from a kinetic perspective. Furthermore, the important interplay between supersaturation and precipitation was characterized and the precipitates' PSD, as well as their physical state, was determined. The implementation of the BDT facilitated a deeper understanding of the complex interplay between drug supersaturation, precipitation and re-dissolution in the presence of an absorptive sink compartment. The observed partition extent depended on the applied polymer stabilization mechanism (supersaturation vs. solubilization) but also on the innate supersaturation ability of the drug molecules and the precipitate's physical state.

For chasers, the polymers showed under the MDT their potential to hinder or delay the crystalline precipitation of the pure drugs, or even to switch the physical state of the precipitate into amorphous nanoparticles as in the case of CLX. Regardless of the stabilization mechanism in aqueous solution, under the BDT the crystallization inhibition improved in all cases the partition of the drugs into the organic phase.

In the case of non-chaser drugs, the pure drug normally precipitated by means of LLPS into a liquid amorphous form in the MDT. Moreover, this high energetic form was susceptible to undergo a quick re-dissolution when the conditions were thermodynamically favored. Thus, the inclusion of an organic sink compartment imposed a thermodynamically favored situation for the pure drug, which underwent a fast re-dissolution-partition interplay without the influence of any pharmaceutical excipient. A further solubility enhancement of the highly energetic amorphous forms by polymers was challenging for non-chasers and the established drug-polymer interactions did not affect or decreased the partition due to a solubilization effect. In this sense, the application of water-soluble polymers to enhance the oral bioavailability for non-chaser molecules would be questionable at least from a kinetic perspective.

5. RESULTS AND DISCUSSION

In the case of extremely poorly soluble molecules, the polymers generally acted as crystallization or crystal growth inhibitors in the MDT. The extent of stabilization was however heavily dependent on the drug-polymer combination applied and not only supersaturation but also solubilization events were observed. In the BDT approach, the observed drug stabilization in the aqueous phase was mainly insufficient or irreversible and a hindered partition into the organic phase occurred in most of the cases. This was the result of a viscosity increase for MA4C and micellization for SOL. Only KVA64 showed a low potential to increase the partition of ABZ and ITZ into the organic phase.

Conclusively, the combined information of physicochemical and *in vitro* biorelevant approaches facilitated the mechanistic understanding of the complex kinetic interplay present in the GI lumen. Furthermore, the potential of the polymers to trigger the partition of the drugs in the BDT model was connected to the innate supersaturation ability of the selected drug molecules, as well as to the physical changes in the precipitating form. Based on the important findings of the physicochemical and *in vitro* biorelevant approaches, the last part of the work transferred the supersaturation and solubilization approach into an *in vivo* model.

5.3 Part III: Supersaturation and solubilization in the gastrointestinal tract and its relevance for oral bioavailability: an *in vitro* vs. *in vivo* approach

The last section of this work deals with the transfer of the *in vitro* supersaturation and solubilization results into an *in vivo* model. Consequently, the predictability of the biphasic dissolution test (BDT) for an *in vivo* outcome was in focus. Thus, instead of using 0.15 M NaCl buffered solution as medium (see section 4.2.2.1), the biorelevant medium fasted simulated intestinal fluid (FaSSIF) was used during the intestinal phase to improve the quantitative predictability of this methodology. More importantly, the relevance of the *in vitro* results was investigated by a quantitative correlation to the obtained oral exposure in an *in vivo* rat model.

Based on the physicochemical characterization and *in vitro* dissolution approaches, three model drugs were selected to evaluate the *in vivo* contribution of supersaturation and solubilization to the oral bioavailability. As previously discussed in section 5.2.1, all investigated drugs were kinetically stabilized to various degrees, which might potentially affect the oral exposure. However, an enhanced oral BA cannot be automatically expected, which was assumed from the outcome of the biphasic dissolution approach (section 5.2.2). The physical state of the precipitates and the differences between real supersaturation and solubilization were critical factors which determined the partition into a lipophilic compartment. Consequently, the drug selection was based on covering a broad range of innate supersaturation and oral absorption behaviors.

- Chaser model drug (Celecoxib, CLX) → poorly soluble molecule with an innate supersaturation behavior and no pH-dependent solubility within the GI tract. It showed a high potential for oral BA enhancement in colloidal polymeric solutions (Figure 5.61).
- Non-chaser model drug (Telmisartan, TLM) → poorly soluble drug with a complex pH-dependent solubility. Although a positive stabilization was determined, it might be counterproductive for oral absorption (Figure 5.67).
- Extremely poorly soluble model drug (Itraconazole, ITZ) → Despite the observed stabilization in aqueous media, no impact on oral absorption was expected (Figure 5.72).

5.3.1 *In vitro* biphasic dissolution tests in FaSSIF

5.3.1.1 Chaser molecule: Celecoxib

Compared to the previous BDT results (Figure 5.61), the FaSSIF-BDT similarly determined a high CLX supersaturation in KVA64 and MA4C colloidal solutions (Figure 5.77A). As already stated (section 5.2.2.1), the polymers impeded crystal growth and controlled the precipitation into amorphous CLX nanoparticles. As a result, the high increase in dissolved drug fraction after the pH-shift was explainable. The stabilization clearly improved the partition of CLX into the organic phase (pure drug: 10%, KVA64: 75%, MA4C: 60%, SOL: 30%) and suggested an enhanced BA for CLX following supersaturation (Figure 5.77B). While the supersaturating effect in a KVA64 colloidal solution was quite stable (≈ 100 min), CLX underwent fast precipitation after a short supersaturation period in a MA4C colloidal solution. In the case of SOL, the solubilization of neutral CLX species in the aqueous phase increased the AUC in the octanol layer compared to the practically insoluble pure drug. Overall, the attained polymeric stabilization of a chaser

5. RESULTS AND DISCUSSION

molecule might improve its oral absorption. Noteworthy, a similar formulation ranking was obtained in the previous BDT with buffered 0.15 M NaCl solution (Figure 5.61). Nevertheless, a better quantitative discrimination between the pure drug, MA4C and KVA64 was achieved by using the biorelevant components sodium taurocholate and lecithin in the FaSSIF-like medium.

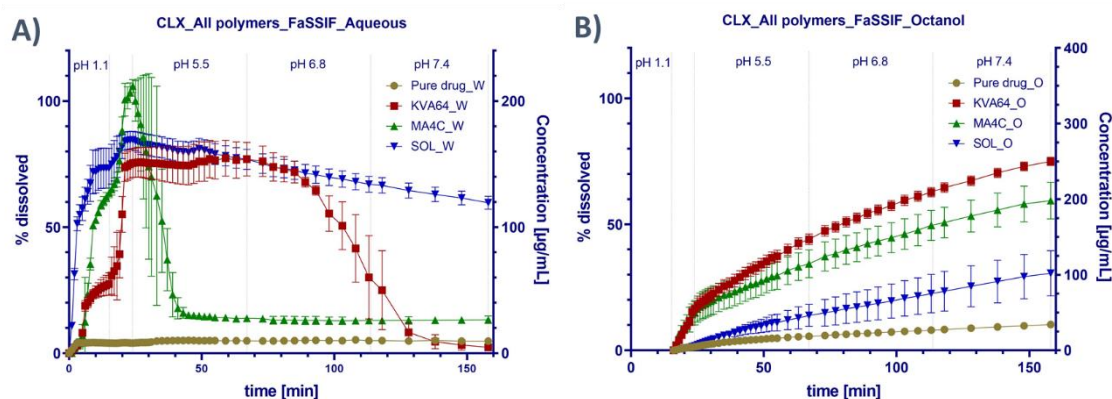


Figure 5.77: Celecoxib *in vitro* biphasic dissolution test profiles. **A)** Aqueous phase: fractions of dissolved CLX in a biorelevant FaSSIF-based medium simulating GIT pH-shift in fasted conditions. Mean \pm SD ($n=3$). **B)** Organic phase: fractions of partition CLX into 1-octanol phase as an absorptive compartment. Mean \pm SD ($n=3$).

5.3.1.2 Non chaser molecule: Telmisartan

Similar to CLX, the polymers KVA64 and MA4C achieved a stabilization of TLM in the aqueous phase (Figure 5.78A). In the case of SOL, the micellization approach entrapped the neutral TLM species in the inner lipophilic core of the polymeric micelles, which was in good agreement with the obtained exponential pK_a -curves in the physicochemical approach (Figure 5.5). However, regardless of the applied stabilization approach, the partition kinetic remained unaffected or a decreased AUC in the organic phase was observed (fraction partitioned pure drug: 85%, KVA64: 75%, MA4C: 60%, SOL: 85%) (Figure 5.78B). As already described in section 5.2.2.2.2, the physical state of the TLM precipitates enabled a quick re-dissolution-partition interplay, which was additionally favored by the TLM ionization change after buffering to pH 6.8 in the BDT. Contrary to the original BDT (Figure 5.66C), the partition of TLM into the organic phase under FaSSIF-BDT was nearly independent of the polymeric colloidal solution used (Figure 5.78B). In this context, the solubilization of TLM within the FaSSIF micelles additionally controlled and decreased the partition into the organic phase. As a result, the partition discrepancy between the pure drug and the colloidal solutions diminished (Figure 5.78B). Remarkably, regardless of the polymeric approach used, all partition profiles followed a sigmoidal curve. This was in good accordance with the pH-dependent solubility and zwitterion behavior of TLM (Figure 5.13). Noteworthy, a similar formulation ranking was obtained compared to the previous BDT without biorelevant buffers (Figure 5.67). Nevertheless, the use of FaSSIF increased the quantitative discrimination between the pure drug and the polymeric colloidal solutions and better reflected the supersaturation/solubilization and absorption interplay *in vivo*, as later discussed in this section.

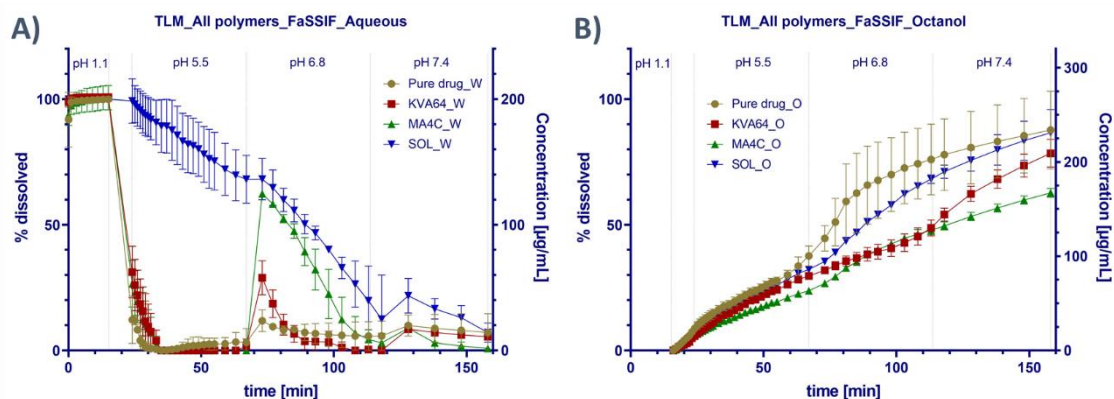


Figure 5.78: Telmisartan *in vitro* biphasic dissolution test profiles. **A)** Aqueous phase: fractions of dissolved TLM in a biorelevant FaSSIF-like medium simulating GIT pH-shift in fasted conditions. Mean \pm SD ($n=3$). **B)** Organic phase: fractions of partitioned TLM dissolved into 1-octanol as an absorptive compartment. Mean \pm SD ($n=3$).

5.3.1.3 Extremely poorly soluble molecule: Itraconazole

The ITZ results in the FaSSIF-BDT approach aligned with previous findings in the buffered 0.15 M NaCl BDT (Figure 5.72). Despite the stabilization in the aqueous phase, the polymers did not accelerate the partition of ITZ into the organic layer. Thus, the stabilization mechanisms in the aqueous phase did not facilitate the accessibility of ITZ molecules for partition but clearly inhibited the growth of the precipitates (Figure 5.56, Figure 5.58). In the polymeric colloidal solutions, ITZ precipitated in the form of (likely amorphous) nanoparticles, as previously reported in the literature for other excipients (Miller et al., 2012c). It promoted the ITZ redissolution in the aqueous phase during the intestinal pH-period (Figure 5.79A). Despite these observations, the stabilization mechanisms seemed to be irreversible or at least they limited the partition of ITZ into the organic phase (partition of pure drug and all polymers: 20%) (Figure 5.79B). Similar to TLM, the FaSSIF-BDT test reduced the discrepancy in ITZ partition from colloidal solutions compared to the pure drug. As a result, the achieved stabilizing effect by the polymers was not beneficial for partition and the advantage of the polymeric supersaturation or solubilization approaches to enhance its oral BA was questionable.

Regarding the commercial ITZ product Sporanox[®] capsule (Janssen Pharmaceutica, Titusville, N.J.) and its oral BA *in vivo* (Abuhelwa et al., 2015; Barone et al., 1998), it was selected as a positive control in both *in vitro* and *in vivo* approaches. In this formulation, ITZ is amorphously embedded in HPMC matrix pellets with a faster dissolution rate and higher solubility than the crystalline drug. However, due to analytical reasons, no profile was measurable in the aqueous phase. Compared to the ITZ polymeric colloidal solutions, the Sporanox[®] capsule achieved a faster partition kinetic at test end (fraction partitioned: 35%)(Figure 5.79B), which might enhance ITZ oral exposure. Even though a high extent of supersaturation in the aqueous phase was expected, the absence of these results impeded any further interpretation.

For the entire *in vivo* study, the FaSSIF-BDT of ITZ served as negative control to validate the qualitative predictive power of the BDT approach. Regarding the poor bioavailability of the crystalline ITZ form (Mellaerts et al., 2008b), the commercial products Sporanox[®] (FDA, 2001) or Tolsura[™] (SUBA[®]-Itraconazole, Mayne Pharma International Pty Ltd) (FDA, 2018) targeted the formulation of ITZ in a higher energy state to facilitate its dissolution and absorption.

5. RESULTS AND DISCUSSION

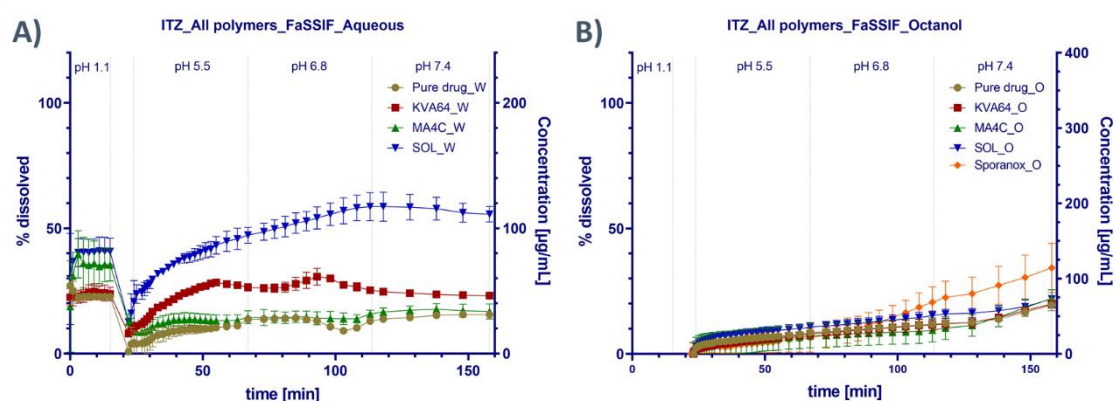


Figure 5.79: Itraconazole *in vitro* biphasic dissolution test profiles. **A)** Aqueous phase: fractions of dissolved ITZ in a biorelevant FaSSIF-based medium simulating GIT pH-shift in fasted conditions. Mean \pm SD ($n=3$). **B)** Organic phase: fractions of partitioned ITZ into 1-octanol as an absorptive compartment. Mean \pm SD ($n=3$).

5.3.2 *In vivo* pharmacokinetics

5.3.2.1 Chaser molecule: Celecoxib

The oral administration of a pure CLX suspension in 0.1 M HCl to Sprague Dawley rats ($n=4$) achieved *in vivo* PK profiles with $t_{max} = 1.29 \pm 0.29$ h, a $C_{max} = 1178.10 \pm 324.18$ ng/mL and a total $AUC_{0 \rightarrow \infty} = 9539.09 \pm 4100.84$ ng/mL*h. Regarding the administered dose = 30 mg/kg, it was in good accordance with previously published data indicating a poor oral CLX bioavailability caused by its low solubility in the entire GI tract (Cho et al., 2018; Paulson et al., 2001). Compared to the pure drug, the CLX oral exposure from polymeric solutions significantly increased due to the positive polymeric supersaturating and solubilizing effects, confirmed by the *in vivo* pharmacokinetic results (Figure 5.80). Furthermore, a similar rank order in the *in vivo* PK profiles compared to the partitioned CLX fractions in the *in vitro* FaSSIF-BDT approach was obtained. In both cases, KVA64 achieved the highest CLX bioavailability, followed by MA4C and the pure drug. As indicated by the aqueous phase of the FaSSIF-BDT, this rank order was related to the longer stabilization of the CLX supersaturated state by KVA64 in the GI tract (Figure 5.77A). Unfortunately, no intraluminal sampling in the rat model was feasible but the differences in oral exposure was considered as surrogate for the extent in drug stabilization in the gut.

The achieved stabilization by KVA64 (Figure 5.77A) enabled the absorption of neutral CLX species over a longer period through the intestinal barrier by mainly passive diffusion. Regarding the poor aqueous solubility of CLX, the 10-fold increase in the oral exposure (Table 5.8) was a considerably high enhancement in bioavailability. Moreover, this observation supported the proposed reversibility of the H-bond interactions between the KVA64 and CLX, as the kinetic stabilization in the lumen did not hinder the absorption through biological barriers. Furthermore, the precipitation of CLX as likely amorphous nanoparticles (Figure 5.36) simultaneously facilitated a quick re-dissolution and absorption interplay.

In the case of MA4C, a favored initial absorption *in vivo* (Figure 5.80) with a high C_{max} and short t_{max} was found (Table 5.8). Nevertheless, this stabilization was shorter than for KVA64 in the intestinal lumen and therefore, due to its limited absorption, a faster elimination was observed.

This correlated well with the *in vitro* supersaturation in the aqueous phase of the FaSSIF-BDT (Figure 5.77A). However, the initial stabilization and quick absorption enabled a 6-fold increase in the CLX oral bioavailability, thus highlighting the potential of MA4C to favor the oral absorption of chaser molecules *in vivo*.

The SOL-solubilization approach led to a rapid absorption of CLX and therefore, high CLX concentrations after a short time were detected in the systemic circulation (high C_{max} and low t_{max} , Table 5.8). As a result, an 8-fold increased oral bioavailability was obtained. Thus, the internalization of CLX molecules in SOL-micelles was reversible since these species were available for absorption. In this case, the reversibility of the SOL-solubilization approach might be attributed to the moderate lipophilicity of the drug molecule. In this sense, molecules like CLX with a $\text{Log}P$ of 2.69 might generally undergo a reversible micellization. Nevertheless, the oral BA of CLX from the SOL solution was not in accordance with the BDT and FaSSIF-BDT results, which suggested a moderate oral BA increase due to the slowest partition kinetic of the three tested polymers (Figure 5.77B). As a result, the BDT and FaSSIF-BDT underpredicted the *in vivo* performance of the CLX-SOL combination. Due to the amphiphilic character of SOL and its surface-active properties, the BDT results must be cautiously interpreted when trying to establish a mathematical correlation with the *in vivo* PK profiles. Evidence was shown that micellar solubilization could potentially enhance the oral BA of poorly soluble drug molecules (Rangel-Yagui et al., 2005). However, in many other cases the oral absorption was hindered, especially when using surface-active excipients (Poelma et al., 1990, 1991). Two reasons might be attributed to the underprediction of the BDT approaches for SOL-based formulations. First, the surface-active properties of SOL might change the interfacial tension between the aqueous and octanol phases in the *in vitro* model, which might slow down the partition of solubilized species. Secondly, the established intermolecular interactions between the poorly soluble drug molecule and the lipophilic inner core of the SOL micelles might hinder the partition of freely dissolved species. The drug might be stronger bound to the polymer under the biphasic model than in the *in vivo* approach. Both reasons might affect the partition rate, consequently producing a falsification of the system's predictability due to adsorbed excipients to the water-octanol interface (Xu et al., 2019).

Further *in vitro* experiments indicated the formation of a third layer between both aqueous and organic (1-octanol) phases during potentiometric $\text{Log}P$ determination at a high stirring rate (300 rpm). The formation of this third phase was attributed to the surface-active properties of SOL (Figure 5.81). These observations were in line with interfacial tension changes caused by surface-active excipients, proposed by Xu and co-workers, that might adsorb to the aqueous/octanol (W/O) interface (Xu et al., 2019). This could explain the low partition rate in the *in vitro* approach, compromising the predictability of the BDT under these experimental conditions. Similar observations were obtained for other liquid-liquid interfaces (Borwankar and Wasan, 1988; Chanda and Bandyopadhyay, 2006; Martínez et al., 2011; Novikov et al., 2017; Scholtens and Bijsterbosch, 1980; Scholtens et al., 1979; Staples et al., 2000; Tadmouri et al., 2008; Tang et al., 2014; Tiss et al., 2001). Hence, the application of surface-active excipients in biphasic dissolution approaches might be limited, since the changes in the interfacial tension might affect the partition into the organic phase. Due to this reason, the SOL results were excluded from the model to establish IVIVC.

Nevertheless, the *in vivo* results for SOL indicated a fast initial CLX absorption. As proposed by the physicochemical characterization approach, the solubilization extent for CLX was minor (\approx 10-fold) when compared to other drug molecules like TLM or ITZ (Figure 5.22). Probably, this

5. RESULTS AND DISCUSSION

was driven by the lower lipophilicity of CLX, compared to the other drug molecules. The low solubilization extent might be the key to maintain CLX long enough in solution and simultaneously not hinder its absorption. All calculated pharmacokinetic parameters were summarized in the Table 5.8.

Overall, the *in vitro* FaSSIF-BDT approach predicted well an increased oral BA for the three colloidal solutions. A similar formulation ranking for three out of four formulations was achieved when the *in vitro* FaSSIF-BDT results were compared to *in vivo* outcomes. As a result, the potential of supersaturating polymers to enhance the oral BA of chaser molecules was confirmed in an *in vivo* model. Besides, the results confirmed the suitability of the FaSSIF-BDT tool to qualitatively predict oral exposure changes under supersaturating conditions, validating additionally the observations from previous chapters.

Table 5.8: Celecoxib pharmacokinetic parameters calculated by fitting pharmacokinetic profiles to an extravasal mono-compartmental model with the help of the Kinetica 7.0 software. Mean \pm SD (n=4).

Parameter	Pure drug	KVA64	MA4C	SOL
$AUC_{0 \rightarrow \infty}$ [ng/mL*h]	9539 \pm 4101	99447 \pm 10733	61837 \pm 13401	85033 \pm 8062
t_{max} [h]	1.3 \pm 0.3	6.3 \pm 2.0	5.9 \pm 3.8	2.5 \pm 0.6
C_{max} [ng/mL]	1178.1 \pm 324.2	5595.4 \pm 576.9	6810.4 \pm 845.3	6885.6 \pm 1641.3
$t_{1/2}$ [h]	5.6 \pm 3.0	7.7 \pm 2.0	4.1 \pm 1.6	6.3 \pm 0.5
MRT [h]	9.1 \pm 4.4	13.0 \pm 2.7	7.3 \pm 1.8	9.7 \pm 0.2
k_e [h ⁻¹]	0.16 \pm 0.10	0.09 \pm 0.02	0.19 \pm 0.06	0.11 \pm 0.01
Ba_{rel} [%]	9.6 \pm 4.1	100.0 \pm 10.8	62.2 \pm 13.5	85.5 \pm 8.1

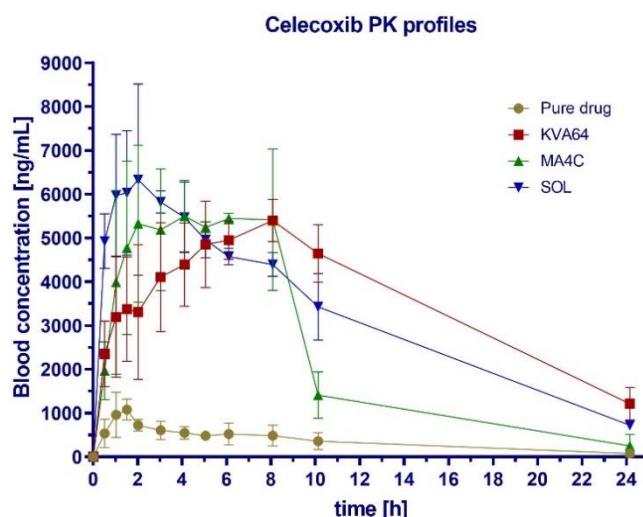


Figure 5.80: Celecoxib pharmacokinetic profiles in Sprague Dawley male albino rats following the oral administration of polymeric supersaturated suspensions. Mean \pm SD (n=4). Pharmacokinetic profiles represent the concentrations of CLX extracted from blood samples by means of liquid-liquid extraction.

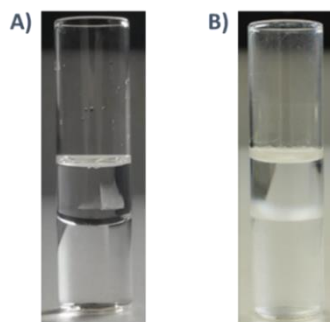


Figure 5.81: **A)** Phase separation between aqueous and organic layer in the absence of SOL followed by a $\text{Log}P$ titration under a fast stirring rate. **B)** Phase separation in the presence of SOL in the aqueous phase. The formation of a third layer containing SOL micelles between aqueous and organic phase was attributed to a change in the interfacial tension that affected the partition rate and compromised the predictability of the BDT when surface-active pharmaceutical excipients were used.

5.3.2.2 Non chaser molecule: Telmisartan

Similar to CLX, the administration of a TLM suspension (dosis = 16 mg/kg) confirmed the low oral exposure of the pure drug with a t_{max} , C_{max} and total $AUC_{0 \rightarrow \infty}$ of 4.41 ± 3.91 h, 886.23 ± 348.20 ng/mL and 12278.55 ± 5200.37 ng/mL*h, respectively. This was in good accordance with previously published data showing a poor oral BA of TLM related to its poor solubility in the upper small intestine (Bakheit et al., 2015; Wiene et al., 2000).

In contrast to CLX, no improved oral exposure for TLM was found when administered along with supersaturating or solubilizing polymers, as reflected in the PK profiles (Figure 5.82). The obtained PK parameters indicated either a decreased or unaffected $AUC_{0 \rightarrow \infty}$ and C_{max} (Table 5.9). Nevertheless, as shown *in vitro* (Figure 5.78A), a minor stabilizing effect in the aqueous phase was achieved and would occur in the upper regions of the small intestine.

In KVA64 and MA4C colloidal solutions, the low TLM absorption was attributed to the low stabilization and strong drug-polymer interactions in the GI tract. Due to the formation of these stable drug-polymer complexes, as previously discussed in the section 5.2.2.2, the accessibility of TLM species to permeate through biological membranes was limited. Furthermore, the physicochemical characterization initially showed exponential pK_a -curves in the presence of the three polymers. The shifts were especially high for KVA64 ($pK_{a,2}$ and $pK_{a,3}$) and MA4C at high polymer concentrations (0.250% w/V) (Figure 5.5) and suggested a decrease in the molecularly dissolved drug fraction, either due to a solubilization effect (KVA64) or due to a viscosity increase (MA4C). The observation supported the positive stabilization in the aqueous phase in MDT or BDT and its counterproductive effect for the oral absorption *in vivo*. Moreover, the potentiometric $\text{Log}D_{ow}$ showed a decrease in the lipophilicity of TLM in the presence of both supersaturating polymers (Table 5.2). In this way, the *in vivo* PK profiles were in line with the results from both physicochemical and *in vitro* biorelevant approaches.

The precipitation of the pure drug via LLPS and the formation of liquid amorphous particles (see section 5.2.1.2.2) facilitated the drug-polymer interactions in colloidal solutions due to the higher energetic state of the TLM precipitate. Furthermore, the amorphous precipitation enabled a much easier and faster re-dissolution, if the environmental conditions were favorable (Figure 5.78A). As a result, a re-dissolution of the pure drug and the drug in colloidal solutions was expected in the jejunum and ileum for which the pH was close to neutral. The re-dissolution would initialize a further ionization of the TLM drug molecules, as depicted in the Table 5.3. The ionized molecules were less lipophilic and a lower permeability was expected in the middle-

5. RESULTS AND DISCUSSION

distal regions of the small intestine. Thus, a quick absorption was more likely to occur in the upper regions of the small gut, where the MMC of the TLM molecules was close to neutral. It contributed to a low t_{max} value (1.5 h) for the first peak (Figure 5.82). As a result of the amorphous precipitation and of the polymer stabilization achieved in the lumen, no significant variations in the PK profiles of pure drug, KVA64 and MA4C for the t_{max} , $t_{1/2}$ and MRT were observed. Both C_{max} and AUC were identical for KVA64 and pure drug, whereas decreased values for MA4C were measured.

The absorption of TLM through the lipophilic intestinal barrier was reduced by SOL (Figure 5.82), which was reflected as a decrease in the C_{max} and AUC . Nevertheless, higher MRT and $t_{1/2}$ were observed for SOL in comparison to the pure drug, KVA64 and MA4C (Table 5.9). In this sense, although SOL decreased the TLM absorption from a kinetic perspective, it might allow a longer exposure and availability of the TLM species for absorption compared to the other two polymers. The decrease in the oral BA of TLM by means of SOL was in line with the observations from the exponential pK_a-curves (Figure 5.5), the decrease in the LogD (Table 5.2) and the decreased partition in the biphasic dissolution (Figure 5.78).

Similar to CLX, the interfacial tension between aqueous and organic phases was reduced by SOL and the partition rate of TLM was affected, which limited the predictive power of the BDT. In this sense, a SOL-solubilization might occur in the GI lumen but the formed TLM/SOL-micelles simultaneously acted as a competitive compartment to absorption. Generally, for non-chaser and very lipophilic drugs, as already described in section 5.2.2.2, the micellization through SOL became irreversible. Additionally, TLM is more lipophilic than CLX (Table 5.1 and 5.2), which might contribute to an irreversible solubilization of the TLM molecules within the lipophilic micellar cores.

Regarding other important pharmacokinetic aspects, TLM was reported to be a P-glycoprotein (P-gp) substrate (Chang et al., 2006). A condition that together with its poor solubility could limit its oral exposure. Furthermore, TLM and other Angiotensin II Receptor Blockers undergo an enterohepatic recirculation (Ieiri et al., 2011; Miura et al., 2009), which might explain the observed double maximum at $t = 10$ h in all PK-profiles.

Once more, prior any mathematical correlation, the *in vitro* FaSSIF-BDT was predictive for the absence of a positive polymeric effect on the oral BA. Similar to CLX, the *in vitro* SOL-solubilization was not quantitatively predictive for TLM oral absorption *in vivo*. In this case, the BDT clearly overestimated the partitioned drug fraction into the octanol phase *in vitro* compared to the fraction of drug absorbed *in vivo*. For this reason, the SOL approach was not regarded to establish IVIVC.

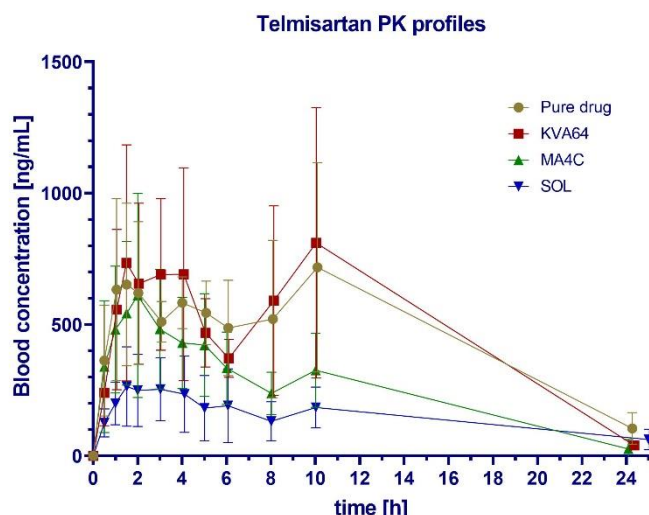


Figure 5.82: Telmisartan pharmacokinetic profiles in Sprague Dawley male albino rats following the oral administration of polymeric supersaturated suspensions. Mean \pm SD (n=4). Pharmacokinetic profiles represent the extracted concentrations of TLM from blood samples by means of liquid-liquid extraction.

Table 5.9: Telmisartan pharmacokinetic parameters calculated by fitting pharmacokinetic profiles to an extravasal mono-compartmental model by the Kinetica 7.0 software. Mean \pm SD (n=4).

Parameter	Pure drug	KVA64	MA4C	SOL
AUC [ng/mL*h]	12279 \pm 5200	11999 \pm 6227	6709 \pm 1515	4745 \pm 1891
t_{max} [h]	4.5 \pm 3.9	7.2 \pm 4.9	5.7 \pm 4.0	2.5 \pm 2.4
C_{max} [ng/mL]	886.2 \pm 348.2	887.6 \pm 468.4	691.3 \pm 377.7	331.9 \pm 124.1
$t_{1/2}$ [h]	6.3 \pm 1.2	4.1 \pm 1.1	5.1 \pm 3.2	11.1 \pm 4.5
MRT [h]	10.6 \pm 1.5	8.8 \pm 0.9	9.3 \pm 4.6	17.1 \pm 8.4
k_e [h⁻¹]	0.11 \pm 0.02	0.17 \pm 0.04	0.17 \pm 0.10	0.07 \pm 0.04
BA_{rel} [%]	100.0 \pm 42.3	97.7 \pm 50.7	54.6 \pm 12.3	38.6 \pm 15.3

5.3.2.3 Extremely poorly soluble molecule: Itraconazole

In vivo, no oral ITZ exposure was measured neither for the pure drug nor for the drug in colloidal solutions. This was in good accordance with the proposed formation of stable drug-polymer complexes in the section 5.2.2.3.2, which impacted the ITZ partition *in vitro* and now impeded absorption *in vivo*. Thus, polymeric colloidal solutions did not represent an option to enhance ITZ oral exposure.

Similar to the observations in the MDT and BDT approaches, an immediate ITZ precipitation occurred by the solvent shift method prior to the administration to the rats. Thus, the crystalline drug form was obtained at least for the pure ITZ. Worth to mention, the *in vitro* results suggested an unaffected ITZ partition into the organic phase from 0.15 M NaCl or FaSSIF by polymeric colloidal solutions (Figure 5.71, Figure 5.79). However, a positive supersaturation and

5. RESULTS AND DISCUSSION

solubilization effect was achieved by the polymers, reflected by an inhibited particle growth and the precipitation into amorphous nanoparticles (Figure 5.58).

The remaining option to enhance ITZ exposure was the formation of an ASD, which decreases the dissolution barrier and the ITZ precipitation in the GI tract as realized in Sporanox[®]. With this aim, the Sprague Dawley rats were dosed with Sporanox[®] pellets and the applied dose was 30 mg/kg weight. The administration of ITZ-ASD (Sporanox[®]) was the only tested ITZ formulation for which the drug and active metabolite were detected in the systemic circulation, thus highlighting the importance of the drug's physical form to enable its dissolution and absorption. The PK-profiles (Figure 5.83) and PK-parameters (Table 5.10) determined a rapid conversion of ITZ into its active metabolite (OH-ITZ) and indicated a fast first-pass metabolism as previously reported in literature (Quinney et al., 2008). Furthermore, the *AUC* and *C_{max}* of OH-ITZ were higher than for ITZ, indicating a high metabolization.

In general, ITZ possesses several challenges when formulated as an oral dosage form, e.g. high lipophilicity and extremely poor aqueous solubility (Kumar et al., 2015; Lang et al., 2016; Li et al., 2015). Thus, the crystalline form of the drug suffered from an extremely low oral bioavailability *in vivo* (Hardung et al., 2010). As a matter of fact, all marketed oral products avoid the formulation of its crystalline form by embedding the drug amorphously in a polymer matrix i.e., Sporanox[®] capsules (Janssen Pharmaceuticals, Titusville, N.J.) and Tolsura[®] (SUBA[®]-Itraconazole capsules, Mayne Pharma International Pty Ltd, Adelaide, Australia) or by using oral solutions (Sporanox[®] solution, Janssen Pharmaceutica, Titusville, N.J.). Using the amorphous drug in polymer matrices or solutions maintains the drug in a higher energetic state and reduces the dissolution barrier, as previously proposed by the spring and parachute approach (Guzmán et al., 2004). In this case, the ITZ oral bioavailability was only limited by the stabilization of the supersaturated state in the GI lumen, since ITZ showed a rapid absorption if dissolved (Peeters et al., 2002).

In this work, the investigations with ITZ were used as control experiments and they indicated the ineffectiveness of the applied supersaturation and solubilization approaches for extremely poorly soluble drug molecules such as ITZ. Since no significant improvements were suggested by the FaSSIF-BDT, it predicted well the situation *in vivo*. For this case study, no IVIVC was established since no oral exposure was obtained. As it was shown for Sporanox[®], the formulation of ITZ as an ASD improved its dissolution and limited its precipitation in the GIT, thus enhancing its oral absorption and bioavailability. Furthermore, other works in which ITZ was formulated as an ASD in a SOL matrix, showed an enhanced bioavailability with respect to the crystalline drug form (Hardung et al., 2010) and compared the results to the commercial Sporanox[®] capsules (Zhang et al., 2013).

5.3 Part III: Supersaturation and solubilization in the gastrointestinal tract

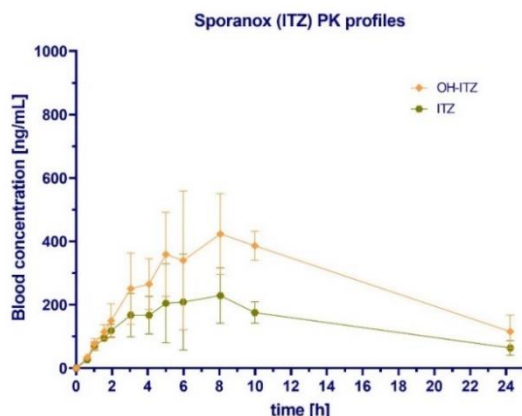


Figure 5.83: Itraconazole and hydroxyitraconazole pharmacokinetic profiles in Sprague Dawley male albino rats following the oral administration of Sporanox® pellets at a dose = 30 mg/kg. Mean \pm SD (n=4). Pharmacokinetic profiles represent the extracted concentrations of ITZ and OH-ITZ from blood samples by means of liquid-liquid extraction.

Table 5.10: Sporanox® capsules (ITZ) pharmacokinetic parameters calculated by fitting pharmacokinetic profiles to an extravasal mono-compartmental model by the Kinetica 7.0 software. Mean \pm SD (n=4).

Parameter	OH-ITZ	ITZ
AUC [ng/mL*h]	6433 \pm 607	3378 \pm 381
t_{max} [h]	8.0 \pm 2.0	8.0 \pm 2.0
C_{max} [ng/mL]	473.5 \pm 90.2	278.5 \pm 91.0

5.3.3 Deconvolution and IVIVC establishment

Following the Wagner Nelson deconvolution (Margolskee et al., 2015; Wagner and Nelson, 1964) of the PK-curves to calculate the absorption profiles (Figure 5.84), an exponential Box-Lucas equation was successfully applied (Equation 34). The obtained functions (Figure 5.84A,B) were used to determine the *in vivo* absorption as a function of time and compare them to the partition levels *in vitro*. With the help of both time-dependent curve progressions, a time scaling factor was successfully estimated for each drug, which is the slope of one linear function fitted to both curves in the Levy plots (Figure 5.85). The time scaling factors were subsequently used to calculate the absorbed drug fraction *in vivo* that corresponded timewise to the partitioned drug fraction *in vitro*. After correlating both variables, a level A IVIVC was achieved for CLX and TLM (Figure 5.86, Figure 5.87). As described in the Guidance for industry of the FDA (FDA, 1997), this correlation type is generally linear and demonstrates a point-to-point relationship between the *in vitro* dissolution/ partition and the *in vivo* input rate. Regarding the SOL solubilization approach, it was excluded from the correlation due to its biased *in vitro* results under the applied experimental conditions. Therefore, two IVIVC were established for CLX and TLM respectively, in which the pure drug, KVA64 and MA4C approaches were included (Figure 5.86, Figure 5.87).

5. RESULTS AND DISCUSSION

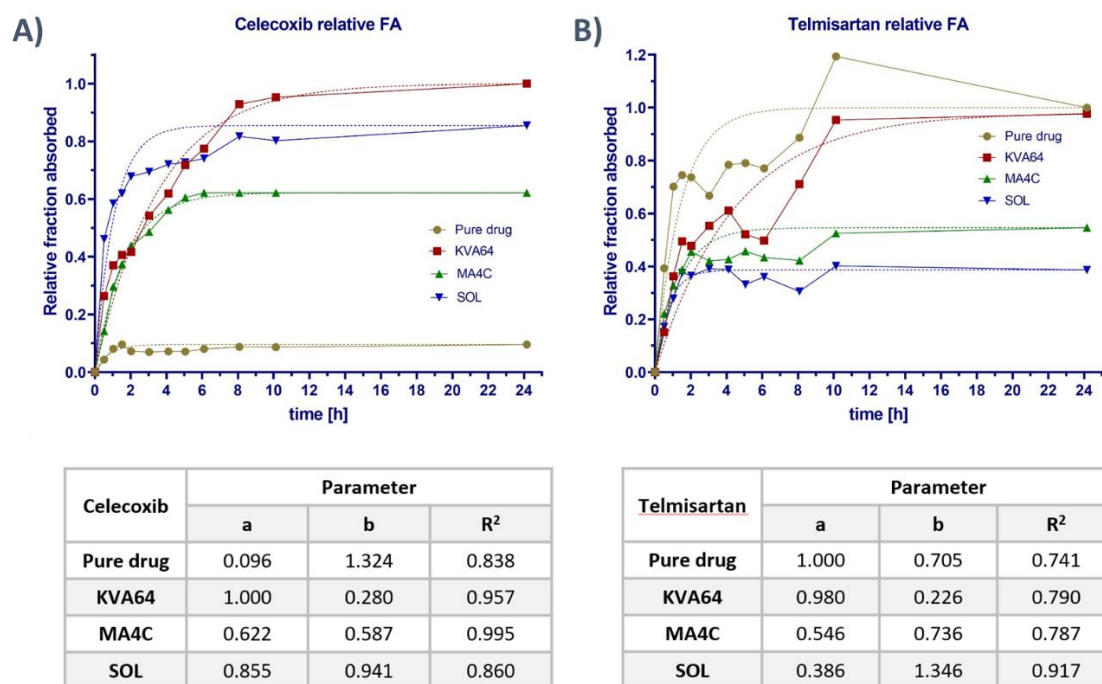


Figure 5.84: Relative absorbed *in vivo* fractions for celecoxib (A) and telmisartan (B). Mean ($n=4$). Fractions were calculated by Wagner-Nelson deconvolution from the mean pharmacokinetic profiles and normalized to the highest absorbed fraction (KVA64 for celecoxib, pure drug for telmisartan). Relative absorbed fractions were fitted to a Box-Lucas exponential function. The resulting fitting parameters (a , b and R^2) are compiled in the tables.

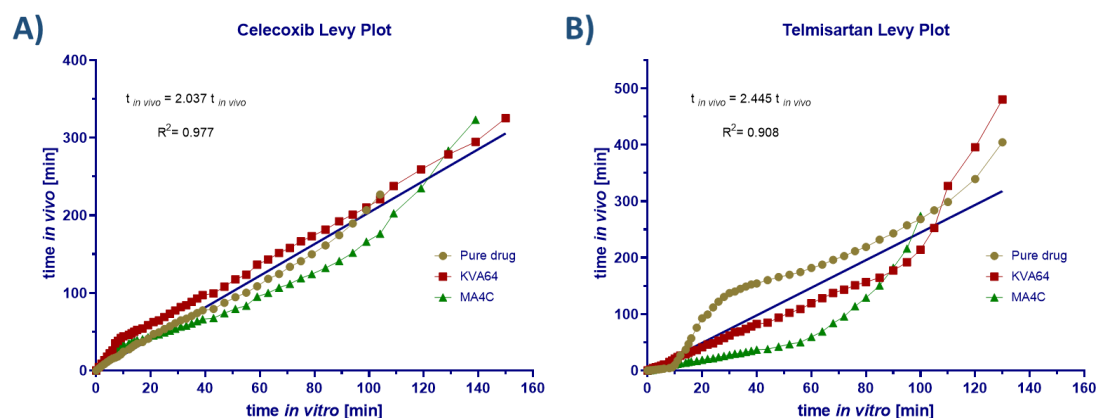


Figure 5.85: Celecoxib (A) and telmisartan (B) Levy plots. Correlation of *in vitro* and *in vivo* times and calculation of a time scaling factor defined as the slope of the linear relationship between both parameters.

5.3.3.1 Chaser molecule: Celecoxib

The Wagner Nelson deconvolution allowed the calculation of the *in vivo* absorption profile for the different CLX formulations (Figure 5.84A). The obtained profiles were fitted to an exponential Box-Lucas equation with a R^2 0.838, 0.957 and 0.995 for the pure drug, KVA64 and MA4C, respectively. These functions were used to calculate the time scaling factor of 2.037 (Figure 5.85A), which was the slope of a linear curve fit of the *in vitro* time points as a function of the calculated *in vivo* absorption profile. The calculated time factor indicated a twice faster *in vitro* partition in the FaSSIF-BDT than the *in vivo* oral absorption, since the gastric phase was not

accounted for the IVIVC calculations. Subsequently, a level A IVIVC was established between the partitioned fraction *in vitro* and the absorbed fraction *in vivo* (Figure 5.86). The R^2 of all three formulations fitted together (pure drug, KVA64 and MA4C) was 0.981. More importantly, the slope of this linear regression was 0.985, which indicated an almost 1:1 relationship between the *in vitro* (partition) and *in vivo* (oral absorption) approaches as a function of time. Both, the slope and the correlation factor confirmed the discriminatory power of the FaSSIF-BDT to predict the oral exposure of the three tested CLX supersaturated solutions.

To sum up, the observed supersaturation effect in the aqueous phase of the *in vitro* FaSSIF-BDT led to an increased partition into the organic phase. These findings correlated well with the increased oral exposure *in vivo*. Furthermore, a pure supersaturation effect in solution without being affected by the manufacturing process (e.g. ASD formulation by hot melt extrusion or spray drying) was demonstrated. In the case of CLX, a chaser molecule with an innate supersaturation ability, the pure supersaturation by the addition of polymers proved to be effective to enhance its oral BA. The facilitated dissolution and the achieved kinetic stabilization in the GI tract improved the oral absorption and exposure, compared to the pure drug.

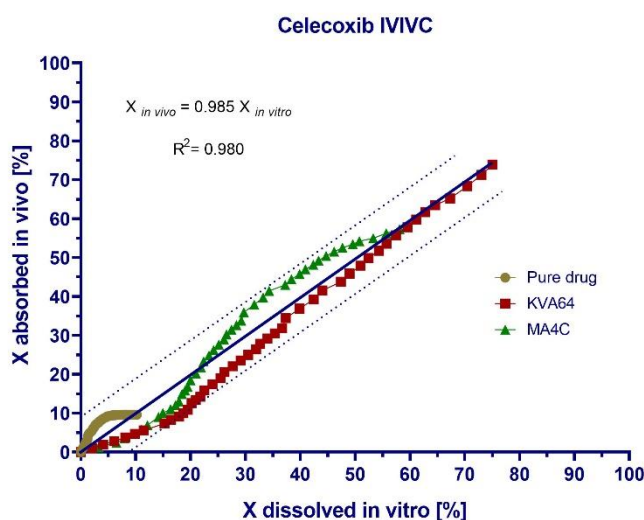


Figure 5.86: Celecoxib level A IVIVC. Point to point linear relationship between the partitioned drug fractions *in vitro* (organic phase) and absorbed drug fractions *in vivo*. The coefficients of determination (R^2) and slope indicated a linear correlation between *in vitro* partition and *in vivo* absorption. The continuous line represents the linear fit, while the dashed lines represent the lower and upper 95% prediction limits, respectively.

5.3.3.2 Non chaser molecule: Telmisartan

Similar to CLX, the absorption profiles for the three TLM formulations were calculated by using the Wagner Nelson deconvolution (Figure 5.84B). However, due to the enterohepatic recirculation of TLM (Ieiri et al., 2011; Miura et al., 2009), a double C_{max} occurred in all PK profiles (Figure 5.82). It led to an artefact in all absorption profiles and partially hindered the exponential fitting to the data. Thus, low R^2 coefficients of 0.741, 0.790 and 0.787 were obtained for the pure drug, KVA64 and MA4C, respectively. Applying the identical calculation procedure as for CLX, a time scaling factor of 2.445 was determined indicating a faster *in vitro* partition than *in vivo* absorption (Figure 5.85B).

5. RESULTS AND DISCUSSION

A level A IVIVC was achieved for TLM with a R^2 of 0.954 and a slope of 1.048. It determined again a similar *in vitro* partition and oral absorption as a function of time (Figure 5.87). It is worth to mention that the R^2 of the correlation might be considerably lower than for CLX, due to the high impact of the medium pH in the precipitation, re-dissolution and absorption interplay for TLM. Additionally, the average fasted gastric pH of rats is 4.0 and intestinal pH is 6.6 (McConnell et al., 2008), which differs from human physiological conditions and might decrease the R^2 of the IVIVC correlation.

The supersaturated state stabilization and solubilization of the non-chaser TLM did not enhance its oral absorption, which was supported by the physicochemical (exponential decay in pK_a -curves, Figure 5.5) and *in vitro* (FaSSIF-BDT, Figure 5.78B) results. The precipitation of the pure drug into a liquid amorphous form via LLPS already favored its re-dissolution in the small intestine and improved its oral absorption. In polymeric colloidal solution, the established intermolecular interactions between the liquid drug form and the polymers facilitated the formation of stable drug-polymer complexes and consequently decreased the molecularly dissolved drug fraction, thus impairing its oral absorption.

All in all, the biphasic dissolution approach predicted well the extent and direction of the oral exposure changes of two BCS II drugs with very different physicochemical properties and innate supersaturation abilities (chaser vs. non chaser). The good qualitative and quantitative performance of the BA prediction proved its potential to act as a surrogate of preclinical studies, as long as the interfacial tension between the aqueous and organic phase in FaSSIF-BDT is not affected.

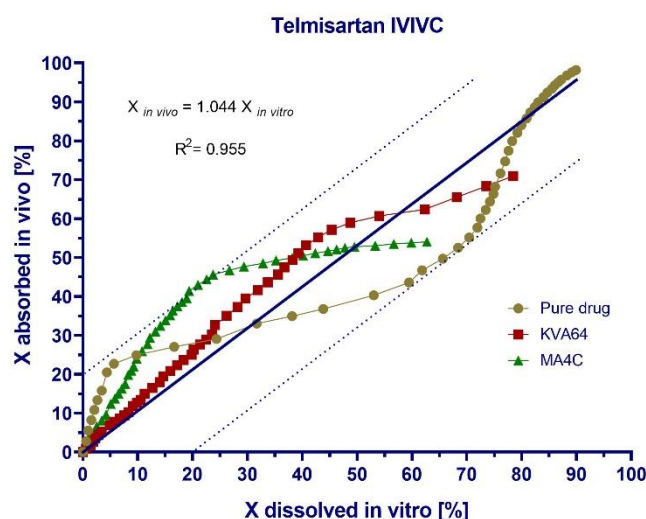


Figure 5.87: Telmisartan level A IVIVC. Point to point linear relationship between dissolved drug fraction *in vitro* (organic phase) and absorbed drug fraction *in vivo*. The coefficient of determination (R^2) and slope showed a linear relationship between *in vitro* partition and *in vivo* absorption. The continuous line represents the linear fit, while the dashed lines represent the lower and upper 95% prediction limits, respectively.

5.3.4 Conclusion

The potential of pure supersaturation or solubilization by water-soluble polymers to affect the oral BA of poorly soluble drugs *in vivo* without being biased by formulation manufacturing processes was confirmed. The extent of supersaturation *in vitro* and *in vivo* depended on the physicochemical properties of the drug molecules, as well as on the specific supersaturating mechanisms established between each polymer-drug combination. Especially, the innate supersaturation ability of the drug molecule, as well as the physical state of its precipitating form played a key role in the dissolution-absorption interplay, which was improved for amorphous drug precipitates. In this sense, identical applied supersaturation or solubilization mechanisms to CLX and TLM did not automatically lead to an identically improved oral exposure. While the stabilization achieved for the chaser molecule CLX considerably enhanced its oral BA up to 10-fold, the polymers decreased the oral absorption of the non-chaser TLM. Independently of the applied mechanism, the reversibility of the drug-polymer interactions was important to not delay or hinder oral absorption due to the limited transit time in the small intestine (Koziolek et al., 2016). In this sense, the equilibrium between molecularly dissolved and complexed (solubilized) drug played a decisive role that highlighted the importance of the interplay between supersaturation/solubilization and absorption for the extent of oral BA.

Despite the amorphous precipitation (Miller et al., 2012c) of the extremely poorly soluble drug ITZ, the supersaturation and solubilization did not affect the oral exposure. Noteworthy, the applied analytical method to detect ITZ and OH-ITZ in the blood samples might be too insensitive. Nevertheless, the commercial Sporanox® capsule, used as a positive control, achieved measurable ITZ absorption and metabolization, thus indicating the benefits of amorphously embedding ITZ in an ASD. In this sense, the formulation of ITZ as an ASD or oral solution, to decrease the energetic dissolution barrier present for the crystalline form, was mandatory to improve the absorption of the drug, as previously reported (Barone et al., 1998).

All in all, the direction and extents of the oral BA changes observed in the *in vivo* model correlated well with the FaSSIF-BDT results for the selected drug molecules. KVA64 was the most effective of all three tested polymers. In this case, the reversibility of the H-bond interactions formed did not hinder the permeation of drug molecules through biological membranes. Contrary, the achieved stabilization by MA4C and SOL limited the oral absorption to a certain extent either due to a viscosity increase or due to micellization. Thus, the *in vivo* observations were in good agreement with the physicochemical and *in vitro* approaches, which previously predicted KVA64 to be the most suitable of all polymers to enhance the oral absorption and BA of poorly soluble drug molecules.

6 Summary and outlook

This work focused on the elucidation of different solubility enhancement and supersaturation stabilization mechanisms, as well as their potential to affect the oral bioavailability of BCS II drug molecules. This aim was targeted from three different directions: 1) physicochemical 2) *in vitro* (biorelevant) 3) *in vivo* (physiological).

First, the physicochemical characterization enabled the identification of different precipitation inhibition mechanisms in colloidal solution, which depended on the nature and chemical structure of the water-soluble polymers applied:

1. The PVP derivative Kollidon VA64 (**KVA64**), rich in H-acceptor groups, showed the ability to stabilize the supersaturation of poorly soluble drugs through the formation of **intermolecular H-bond interactions**. The extent of stabilization was a function of the H-donor count of the drug molecules (itraconazole and loratadine: 0; celecoxib and telmisartan: 1; dipyridamole: 4).
2. The cellulose derivative Methocel A4C (**MA4C**) limited the precipitation of poorly soluble drugs through the **viscosity increase** achieved in colloidal solution. Its effect was heavily polymer concentration-dependent.
3. The amphiphilic graft copolymer Soluplus (**SOL**) mainly stabilized the drugs in solution by means of **micellization**. The lipophilicity of the drug molecules was similarly identified as a key parameter determining the extent of micellization.
4. Other minor stabilization mechanisms such as the **formation of hydrophobic interactions** between polymer and drug were proposed for the combinations Loratadine-MA4C and Itraconazole-MA4C.

The physicochemical characterization enabled the differentiation between supersaturating and solubilizing polymer-drug combinations. In this sense, the investigation of the ionization properties of the selected drug molecules in polymeric colloidal solution was applied as a simple tool to identify solubilization events. Due to the decrease in the molecularly dissolved drug fraction associated to solubilization, the appearance of changes in the acid-base equilibria were translated into apparent pK_a -shifts, which were indicative for solubilization events. The shape of the pK_a -curve as a function of the polymer concentration defined the nature of the stabilization mechanism. Linear pK_a -curves with a slope close to 0 were indicative for the absence of changes in the acid-base equilibria and were associated to pure supersaturating drug-polymer combinations, where the drug remained molecularly dissolved. On the other side, the presence of exponential (or in one case sigmoidal) pK_a -curves was associated to solubilization events produced due to the decrease in the molecularly dissolved drug fraction with increasing polymer concentration. While SOL induced in all cases a solubilization effect, the ability of KVA64 and MA4C to drive supersaturation or solubilization was heavily dependent on the physicochemical behavior of the drug molecules.

Depending on their innate supersaturation ability and their response to the polymers, different classes of molecules were identified:

1. **Chaser** molecules (**dipyridamole and celecoxib**). Possess an innate supersaturation ability and slowly precipitate as crystalline form. The polymers limited crystal growth and precipitation, which caused an alignment of intrinsic to kinetic solubility. As a result

of the precipitation inhibition or delay, KVA64 and MA4C induced supersaturation effects but did not act as solubilizers.

2. **Non-chaser** molecules (**loratadine and telmisartan**). Do not possess an innate supersaturation ability (Comer, 2010) and tend to quickly precipitate by means of liquid-liquid phase separation as a liquid amorphous form. Consequently, an enhancement of the aqueous solubility was attributed to solubilization effects (even when minor in some cases) and the pK_a -curves showed exponential decays in all cases (KVA64, MA4C and SOL).
3. **Extremely poorly soluble** molecules (**albendazole and itraconazole**). The pure drugs precipitated fast as crystalline form. In polymeric colloidal solutions, these drugs achieved the highest extents of stabilization but the presence of supersaturation or solubilization was heavily dependent on the polymer-drug combination applied.

In this manner, the first part of this study provided a valuable mechanistic understanding of the potential stabilization mechanisms from a thermodynamic perspective and facilitated the differentiation between solubilizing and supersaturating approaches. Furthermore, it enabled a first identification of various classes of molecules as a function of their supersaturation ability and their response to polymers.

Secondly, *in vitro* biorelevant methods were used to kinetically characterize the potential of the defined stabilization mechanisms to impact the precipitation and the partition kinetics. Furthermore, as a result of the achieved kinetic stabilization, the ability of polymers to act as precipitation inhibitors was investigated by means of endpoint particle size distribution measurements in the micron and submicron range. Finally, the shape of the formed particles in colloidal solution, as well as their physical state (crystalline vs. amorphous), was determined by polarized light microscopy. The *in vitro* biorelevant approach was carried out with or without an acceptor compartment (organic phase). The first modality (monophasic dissolution test, MDT) focused on the potential of supersaturation and solubilization to hinder or delay precipitation from a kinetic perspective under a biorelevant approach. The second modality (biphasic dissolution test, BDT) additionally targeted the potential of the achieved stabilization to enhance the partition of the drug into an organic phase, simulating the absorption into the systemic circulation. The conclusions of these investigations were summarized in the following key observations:

- The kinetic precipitation inhibition by **KVA64** in the MDT model was minor or missing compared to the other two polymers. In this sense, the low energy H-bond drug-polymer interactions and their reversible character might limit the achieved extent of stabilization in aqueous media. Nevertheless, this reversibility represented the key parameter to improve the partition of the drugs into the organic phase in the BDT approach from KVA64 colloidal solutions.
- The kinetic stabilization by **MA4C** and **SOL** was more effective than by KVA64. Both polymers showed a high potential as precipitation inhibitors. However, the underlying mechanisms for this stabilization (e.g. viscosity increase and micellization) rather complexed or solubilized the drugs and therefore, the molecularly dissolved drug fraction decreased. As a result, the partition of the drug molecules into the organic phase was hindered or at least limited. In this way, the drug-polymer species formed in colloidal solution controlled the accessibility of the drug molecules to cross biological membranes.

6. SUMMARY AND OUTLOOK

- As already seen in the physicochemical characterization, the kinetically stabilization extent in the aqueous phase depended heavily on the innate supersaturation ability of the drug molecules. In general, the polymers showed a high stabilization of the supersaturated state for chaser and extremely poorly soluble molecules, whereas the stabilization for non-chaser molecules (when present) was rather associated to solubilization events.
- Independent of the applied stabilization mechanisms, all three polymers were generally effective as precipitation or crystal growth inhibitors. The precipitate's physical state of the pure drug depended heavily on the innate supersaturation ability of the drug molecules. Chasers and extremely poorly soluble drugs precipitated as crystalline particles, while non-chasers tended to precipitate by means of LLPS as an amorphous form. In colloidal solution, the precipitation events were kinetically controlled by the underlying stabilization mechanisms. Consequently, shifts in the particle size distributions were observed for almost all drugs. In the case of celecoxib and itraconazole, the physical state of the precipitates changed from crystalline microparticles into amorphous nanoparticles in polymeric colloidal solutions. This characteristic facilitated a quick re-dissolution-partition interplay when an absorptive sink compartment (octanol phase in the BDT) was present.
- The ability of the polymers to enhance the partition into the organic phase under the BDT model did not only depend on the stabilization mechanism, but more importantly on the innate supersaturation ability of the drug molecules. For chaser molecules, which showed a stabilization of the supersaturated state, the partition was favored from polymeric colloidal solutions. For non-chaser molecules, for which the stabilization in aqueous solution was associated to solubilization events, the partition was hindered or delayed when compared to the pure drug. For extremely poorly soluble molecules, an improved partition was in most of the cases challenging but it heavily depended on the specific drug-polymer combination applied.

The third and last approach focused on the potential of supersaturation and solubilization to improve oral bioavailability in an *in vivo* Sprague Dawley rat model. The selection of celecoxib (chaser), telmisartan (non-chaser) and itraconazole (extremely poorly soluble) as model drugs was based on their various innate supersaturation behaviors in the *in vitro* biorelevant method. This was additionally confirmed with the use of fasted simulated intestinal fluid as biorelevant medium. Several conclusions were withdrawn from the *in vivo* pharmacokinetic studies:

- The potential of the polymers to induce changes in the oral absorption and bioavailability of the selected drug molecules was demonstrated. The oral exposure levels and resulting PK profiles in male Sprague Dawley rats depended on the occurred stabilization in the gastrointestinal tract as a function of the innate supersaturation ability of the selected drug molecules. In the case of the chaser celecoxib, a molecule showing a supersaturated state stabilization, all polymers improved its absorption and achieved an up to 10-fold improvement in the oral bioavailability. For the non-chaser telmisartan, a molecule easily undergoing solubilization, a decreased absorption (up to 2.6-fold) was observed. For itraconazole, a poorly soluble API, no impact of the polymers on the absorption was found. These observations were in good accordance with the partition in the organic phase observed in the FaSSIF-BDT *in vitro* approach. The achieved Level A IVIVC for celecoxib and telmisartan case studies further supported the relevance of the *in vitro* FaSSIF-BDT results to predict the extent of oral absorption and bioavailability.

- The physical state of the formed drug precipitates in the gastrointestinal tract played a key role in the precipitation-dissolution-absorption interplay. The precipitation into amorphous nanoparticles enabled a quick absorption, as seen for celecoxib in colloidal solutions. In contrast, the pure drug generated microcrystals after precipitation which led to a low exposure. The occurred LLPS for the non-chaser molecule telmisartan led to the formation of amorphous species which already favored oral absorption for the pure drug. As a result, a further improvement by polymeric colloidal solutions was questionable and the solubilization of the drug delayed or impeded the oral absorption due to the decrease in the molecularly dissolved drug fraction.
- Including the physicochemical and *in vitro* biorelevant results, KVA64 proved to be the most suitable polymer to delay or limit the precipitation kinetics and simultaneously facilitate the absorption through the intestinal barrier of the drug fraction in solution. In the case of MA4C and SOL, the increased medium viscosity and the micellization approaches limited the accessibility of the drugs for absorption either due to a reduced molecular mobility or due to the tight binding within the lipophilic micellar core, respectively. For this reason, both polymers proved to be less suitable as KVA64 to enhance the oral bioavailability of CLX and TLM.
- The FaSSIF-BDT proved to be a valuable *in vitro* model with a high prediction potential for the polymeric stabilization in the gastrointestinal tract and enhanced oral exposure. As a result, a Level A IVIVC between an *in vivo* model and the FaSSIF-BDT was established which, together with the physicochemical characterization, enabled the mechanistic understanding of the stabilization and precipitation inhibition either by supersaturation or by solubilization.

To conclude, a correlation between different stabilization mechanisms in aqueous solution from a physicochemical, *in vitro* biorelevant and *in vivo* physiological perspective was established. The potential of the polymers to supersaturate or solubilize the drug was first predicted by the physicochemical approach and afterwards confirmed by the *in vitro* kinetic approach. The potential of the polymers to act as precipitation inhibitors and affect the partition was proven to be dependent on the innate supersaturation ability of the drug molecules and on the physical state of the precipitating form. These *in vitro* observations were subsequently confirmed by the *in vivo* approach, which validated the relevance of the results generated *in vitro* and more importantly, the ability of the polymers to affect the oral absorption and to act as bioavailability enhancers.

In general, the increasing interest in enabling formulations with enhanced dissolution and delayed precipitation properties addresses the general challenge of new chemical entities with poor solubility in oral drug product development. In this context, the solubility enhancement and more concretely, the stabilization of supersaturation in the gastrointestinal lumen is important to overcome the poor oral bioavailability of poorly soluble drug molecules.

In this work, the implementation of a novel *in vitro* biorelevant tool simulating the conditions of the (human) gastrointestinal tract, as well as its complementation with a physicochemical characterization was crucial. It allows the reduction in animal or human trials due to the enabling of the selection of the most promising drug stabilization mechanism under biorelevant conditions without conducting *in vivo* trials. In the *in vitro* approach, this work showed that critical aspects for oral absorption such as the medium composition, the physiology of the gastrointestinal tract and the presence of a biological absorption membrane should be further addressed. However, the established *in vitro* model was only correlated to an *in vivo* animal

6. SUMMARY AND OUTLOOK

(rodent) trial. Therefore, trials with non-rodent species (e.g. dogs) or *in human* trials are needed to confirm the value of this *in vitro* setup for estimating bioavailability *in human*. Furthermore, material-consumption and time efficiency play nowadays a very important role in formulation development and trial-and-error approaches are often used but not favored. In this sense, the establishment of a predictive model to identify suitable excipients and formulation approaches for the design of a drug product is of major priority. With this purpose, the compilation of this data set, including drug molecules showing a high variety of chemical structures, physicochemical properties and molecular descriptors, represents the first step to the establishment of a predictive model. Under this context, the compiled data and improved mechanistic understanding from this work is the mandatory basis to establish an *in silico* computational model that enables the prediction of possible interactions between drug molecules and excipients to stabilize drugs in solution. The implementation of such *in silico* computational tool is the next logical step of this work and would reduce material and time needed to develop a final oral drug product of poorly soluble drugs. Additionally, it would cover another physiological aspects of the gastrointestinal tract, such as the gastric emptying or the intestinal transit times. The final goal would be to predict the oral absorption and pharmacokinetic profiles for various animal species or human on basis of *in vitro* results. Furthermore, the *in silico* model should provide guidance for selecting or optimizing a certain formulation candidate to obtain the best *in vivo* outcome.

Based on the key points discussed in the summary and outlook, it is clear that the stabilization of supersaturation is an important and interesting research field to improve the oral bioavailability of an increasing number of poorly soluble new chemical entities. Especially, a rational formulation selection based on supersaturation or solubilization phenomena occurring in the GI tract was enabled. Furthermore, the use of *in vitro* or *in silico* models will continuously decrease the amount of time and material needed with less animal and human trials to develop a final oral drug product in future.

7 References

- Abrahamsson, B., McAllister, M., Augustijns, P., Zane, P., Butler, J., Holm, R., Langguth, P., Lindahl, A., Müllertz, A., Pepin, X., et al. (2020). Six years of progress in the oral biopharmaceutics area – A summary from the IMI OrBiTo project. *European Journal of Pharmaceutics and Biopharmaceutics* *152*, 236–247.
- Abuhelwa, A.Y., Foster, D.J.R., Mudge, S., Hayes, D., and Upton, R.N. (2015). Population pharmacokinetic modeling of itraconazole and hydroxyitraconazole for oral SUBA-itraconazole and sporanox capsule formulations in healthy subjects in fed and fasted states. *Antimicrob Agents Chemother* *59*, 5681–5696.
- Al Durdunji, A., AlKhatib, H.S., and Al-Ghazawi, M. (2016). Development of a biphasic dissolution test for Deferasirox dispersible tablets and its application in establishing an in vitro–in vivo correlation. *European Journal of Pharmaceutics and Biopharmaceutics* *102*, 9–18.
- Albadarin, A.B., Potter, C.B., Davis, M.T., Iqbal, J., Korde, S., Pagire, S., Paradkar, A., and Walker, G. (2017). Development of stability-enhanced ternary solid dispersions via combinations of HPMCP and Soluplus® processed by hot melt extrusion. *International Journal of Pharmaceutics* *532*, 603–611.
- Alberti, S., Gladfelter, A., and Mittag, T. (2019). Considerations and Challenges in Studying Liquid-Liquid Phase Separation and Biomolecular Condensates. *Cell* *176*, 419–434.
- Alhalaweh, A., Alzghoul, A., and Bergström, C.A.S. (2019). Molecular Drivers of Crystallization Kinetics for Drugs in Supersaturated Aqueous Solutions. *Journal of Pharmaceutical Sciences* *108*, 252–259.
- Allam, A.N., El gamal, S.S., and Naggar, V.F. (2011). Bioavailability: A Pharmaceutical Review. *J Novel Drug Deliv Tech* *1*, 77–93.
- Allen, R.I., Box, K.J., Comer, J.E.A., Peake, C., and Tam, K.Y. (1998). Multiwavelength spectrophotometric determination of acid dissociation constants of ionizable drugs. *Journal of Pharmaceutical and Biomedical Analysis* *17*, 699–712.
- Almeida e Sousa, L., Sm, R.-E., Ga, S., and Ls, T. (2014). Assessment of the amorphous “solubility” of a group of diverse drugs using new experimental and theoretical approaches. *Mol Pharm* *12*, 484–495.
- Alonzo, D.E., Gao, Y., Zhou, D., Mo, H., Zhang, G.G.Z., and Taylor, L.S. (2011). Dissolution and Precipitation Behavior of Amorphous Solid Dispersions. *Journal of Pharmaceutical Sciences* *100*, 3316–3331.
- Amaral Silva, D., Al-Gousous, J., Davies, N.M., Bou Chacra, N., Webster, G.K., Lipka, E., Amidon, G.L., and Löbenberg, R. (2020). Biphasic Dissolution as an Exploratory Method during Early Drug Product Development. *Pharmaceutics* *12*, 420.
- Amidon, G.L., Lennernäs, H., Shah, V.P., and Crison, J.R. (1995). A Theoretical Basis for a Biopharmaceutic Drug Classification: The Correlation of *in Vitro* Drug Product Dissolution and *in Vivo* Bioavailability. *Pharm Res* *12*, 413–420.
- Artursson, P., and Karlsson, J. (1991). Correlation between oral drug absorption in humans and apparent drug permeability coefficients in human intestinal epithelial (Caco-2) cells. *Biochemical and Biophysical Research Communications* *175*, 880–885.
- Asare-Addo, K., Levina, M., Rajabi-Siahboomi, A.R., and Nokhodchi, A. (2011). Effect of ionic strength and pH of dissolution media on theophylline release from hypromellose matrix tablets—Apparatus USP III, simulated fasted and fed conditions. *Carbohydrate Polymers* *86*, 85–93.
- Augustijns, P., and Brewster, M.E. (2012). Supersaturating Drug Delivery Systems: Fast is Not Necessarily Good Enough. *Journal of Pharmaceutical Sciences* *101*, 7–9.
- Augustijns, P., Wuyts, B., Hens, B., Annaert, P., Butler, J., and Brouwers, J. (2014). A review of drug solubility in human intestinal fluids: Implications for the prediction of oral absorption. *European Journal of Pharmaceutical Sciences* *57*, 322–332.
- Aungst, B.J. (2017). Optimizing Oral Bioavailability in Drug Discovery: An Overview of Design and Testing Strategies and Formulation Options. *Journal of Pharmaceutical Sciences* *106*, 921–929.
- Avdeef, A. (1992). pH-Metric log P. Part 1. Difference Plots for Determining Ion-Pair Octanol-Water Partition Coefficients of Multiprotic Substances. *Quantitative Structure-Activity Relationships* *11*, 510–517.
- Avdeef, A. (1996). Assessment of Distribution-pH Profiles. In *Lipophilicity in Drug Action and Toxicology*, (John Wiley & Sons, Ltd), pp. 109–139.

7. REFERENCES

- Avdeef, A. (2007). Solubility of sparingly-soluble ionizable drugs. *Advanced Drug Delivery Reviews* 59, 568–590.
- Avdeef, A., and Berger, C.M. (2001). pH-metric solubility.: 3. Dissolution titration template method for solubility determination. *European Journal of Pharmaceutical Sciences* 14, 281–291.
- Avdeef, A., Box, K.J., Comer, J.E.A., Gilges, M., Hadley, M., Hibbert, C., Patterson, W., and Tam, K.Y. (1999). PH-metric logP 11. pKa determination of water-insoluble drugs in organic solvent–water mixtures. *Journal of Pharmaceutical and Biomedical Analysis* 20, 631–641.
- Avdeef, A., Fuguet, E., Llinàs, A., Ràfols, C., Bosch, E., Völgyi, G., Verbić, T., Boldyreva, E., and Takács-Novák, K. (2016). Equilibrium solubility measurement of ionizable drugs – consensus recommendations for improving data quality. *ADMET and DMPK* 4, 117–178.
- Avdeef, Alex., Comer, J.E.A., and Thomson, S.J. (1993). pH-Metric log P. 3. Glass electrode calibration in methanol-water, applied to pKa determination of water-insoluble substances. *Anal. Chem.* 65, 42–49.
- Baboota, S., Faiyaz, S., Ahuja, A., Ali, J., Shafiq, S., and Ahmad, S. DEVELOPMENT AND VALIDATION OF A STABILITY-INDICATING HPLC METHOD FOR ANALYSIS OF CELECOXIB (CXB) IN BULK DRUG AND MICROEMULSION FORMULATIONS. 14.
- Baghel, S., Cathcart, H., and O'Reilly, N.J. (2016). Polymeric Amorphous Solid Dispersions: A Review of Amorphization, Crystallization, Stabilization, Solid-State Characterization, and Aqueous Solubilization of Biopharmaceutical Classification System Class II Drugs. *Journal of Pharmaceutical Sciences* 105, 2527–2544.
- Bakheit, A.H.H., Abd-Elgalil, A.A., Mustafa, B., Haque, A., and Wani, T.A. (2015). Chapter Six - Telmisartan. In *Profiles of Drug Substances, Excipients and Related Methodology*, H.G. Brittain, ed. (Academic Press), pp. 371–429.
- Balani, P., Sy, W., Wk, N., E, W., Rb, T., and Sy, C. (2010). Influence of polymer content on stabilizing milled amorphous salbutamol sulphate. *Int J Pharm* 391, 125–136.
- Barone, J.A., Moskovitz, B.L., Guarnieri, J., Hassell, A.E., Colaizzi, J.L., Bierman, R.H., and Jessen, L. (1998). Enhanced Bioavailability of Itraconazole in Hydroxypropyl β -Cyclodextrin Solution versus Capsules in Healthy Volunteers. *Antimicrobial Agents and Chemotherapy* 42, 1862–1865.
- Bauer-Brandl, A., and Brandl, M. (2020). Solubility and Supersaturation. In *Solubility in Pharmaceutical Chemistry*, (Walter de Gruyter GmbH & Co KG), pp. 27–70.
- Bayer Inc. (2019). Health Canada Product Monograph: Claritin (loratadine).
- Bean, T.G., Arnold, K.E., Lane, J., Pietravalle, S., and Boxall, A.B.A. (2016). An in vitro method for determining the bioaccessibility of pharmaceuticals in wildlife. *Environmental Toxicology and Chemistry* 35, 2349–2357.
- Beig, A., Miller, J.M., and Dahan, A. (2012). Accounting for the solubility–permeability interplay in oral formulation development for poor water solubility drugs: The effect of PEG-400 on carbamazepine absorption. *European Journal of Pharmaceutics and Biopharmaceutics* 81, 386–391.
- Berben, P., Mols, R., Brouwers, J., Tack, J., and Augustijns, P. (2017). Gastrointestinal behavior of itraconazole in humans – Part 2: The effect of intraluminal dilution on the performance of a cyclodextrin-based solution. *International Journal of Pharmaceutics* 526, 235–243.
- Berben, P., Brouwers, J., and Augustijns, P. (2018). Assessment of Passive Intestinal Permeability Using an Artificial Membrane Insert System. *Journal of Pharmaceutical Sciences* 107, 250–256.
- Berge, S.M., Bighley, L.D., and Monkhouse, D.C. (1977). Pharmaceutical Salts. *Journal of Pharmaceutical Sciences* 66, 1–19.
- Bergström, C.A.S., and Avdeef, A. (2019). Perspectives in solubility measurement and interpretation. *ADMET and DMPK* 7, 88–105.
- Bergström, C.A.S., Strafford, M., Lazorova, L., Avdeef, A., Luthman, K., and Artursson, P. (2003). Absorption Classification of Oral Drugs Based on Molecular Surface Properties. *J. Med. Chem.* 46, 558–570.
- Bergström, C.A.S., Wassvik, C.M., Johansson, K., and Hubatsch, I. (2007). Poorly Soluble Marketed Drugs Display Solvation Limited Solubility. *J. Med. Chem.* 50, 5858–5862.
- Bergström, C.A.S., Andersson, S.B.E., Fagerberg, J.H., Ragnarsson, G., and Lindahl, A. (2014a). Is the full potential of the biopharmaceutics classification system reached? *European Journal of Pharmaceutical Sciences* 57, 224–231.

Bergström, C.A.S., Holm, R., Jørgensen, S.A., Andersson, S.B.E., Artursson, P., Beato, S., Borde, A., Box, K., Brewster, M., Dressman, J., et al. (2014b). Early pharmaceutical profiling to predict oral drug absorption: Current status and unmet needs. *European Journal of Pharmaceutical Sciences* 57, 173–199.

Bergström, C.A.S., Charman, W.N., and Porter, C.J.H. (2016). Computational prediction of formulation strategies for beyond-rule-of-5 compounds. *Advanced Drug Delivery Reviews* 101, 6–21.

Berthelot, M.P.E., and Jungfleisch, E.C. (1872). Sur les lois qui président au partage d'un corps entre deux dissolvants (expériences). *Ann. Chim. Phys.* 4, 396–407.

Bevernage, J., Forier, T., Brouwers, J., Tack, J., Annaert, P., and Augustijns, P. (2011). Excipient-Mediated Supersaturation Stabilization in Human Intestinal Fluids. *Mol. Pharmaceutics* 8, 564–570.

Bevernage, J., Hens, B., Brouwers, J., Tack, J., Annaert, P., and Augustijns, P. (2012a). Supersaturation in human gastric fluids. *European Journal of Pharmaceutics and Biopharmaceutics* 81, 184–189.

Bevernage, J., Brouwers, J., Annaert, P., and Augustijns, P. (2012b). Drug precipitation–permeation interplay: Supersaturation in an absorptive environment. *European Journal of Pharmaceutics and Biopharmaceutics* 82, 424–428.

Bevernage, J., Brouwers, J., Brewster, M.E., and Augustijns, P. (2013). Evaluation of gastrointestinal drug supersaturation and precipitation: Strategies and issues. *International Journal of Pharmaceutics* 453, 25–35.

Bi, M., Kyad, A., Kiang, Y.-H., Alvarez-Nunez, F., and Alvarez, F. (2011). Enhancing and Sustaining AMG 009 Dissolution from a Matrix Tablet Via Microenvironmental pH Modulation and Supersaturation. *AAPS PharmSciTech* 12, 1157–1162.

Bochmann, E.S., Neumann, D., Gryczke, A., and Wagner, K.G. (2016). Micro-scale prediction method for API-solubility in polymeric matrices and process model for forming amorphous solid dispersion by hot-melt extrusion. *European Journal of Pharmaceutics and Biopharmaceutics* 107, 40–48.

Boer, G.B.J. de, Weerd, C. de, Thoenes, D., and Goossens, H.W.J. (1987). Laser Diffraction Spectrometry: Fraunhofer Diffraction Versus Mie Scattering. *Particle & Particle Systems Characterization* 4, 14–19.

Bonnett, P.E., Carpenter, K.J., Dawson, S., and Davey, R.J. (2003). Solution crystallisation via a submerged liquid–liquid phase boundary: oiling out. *Chem. Commun.* 698–699.

Borwankar, R.P., and Wasan, D.T. (1988). Equilibrium and dynamics of adsorption of surfactants at fluid-fluid interfaces. *Chemical Engineering Science* 43, 1323–1337.

Box, K., and Comer, J. (2008). Using Measured pKa, LogP and Solubility to Investigate Supersaturation and Predict BCS Class. *Current Drug Metabolism* 9, 869–878.

Box, K., Bevan, C., Comer, J., Hill, A., Allen, R., and Reynolds, D. (2003). High-Throughput Measurement of pKa Values in a Mixed-Buffer Linear pH Gradient System. *Anal. Chem.* 75, 883–892.

Box, K., Comer, J.E., Gravestock, T., and Stuart, M. (2009). New Ideas about the Solubility of Drugs. *Chemistry & Biodiversity* 6, 1767–1788.

Box, K., Ruiz, R., Outhwaite, B., and Lee, S. (2017). Study of the impact of different salts on the intrinsic dissolution rate of pharmaceutical compounds. *British Journal of Pharmacy* 2.

Box, K.J., Völgyi, G., Baka, E., Stuart, M., Takács-Novák, K., and Comer, J.E.A. (2006). Equilibrium versus kinetic measurements of aqueous solubility, and the ability of compounds to supersaturate in solution—a validation study. *J. Pharm. Sci.* 95, 1298–1307.

Brewster, M.E., Vandecruys, R., Verreck, G., and Peeters, J. (2008). Supersaturating drug delivery systems: effect of hydrophilic cyclodextrins and other excipients on the formation and stabilization of supersaturated drug solutions. *Die Pharmazie - An International Journal of Pharmaceutical Sciences* 63, 217–220.

Brough, C., and Williams, R.O. (2013). Amorphous solid dispersions and nano-crystal technologies for poorly water-soluble drug delivery. *International Journal of Pharmaceutics* 453, 157–166.

Brouwers, J., Brewster, M.E., and Augustijns, P. (2009). Supersaturating drug delivery systems: The answer to solubility-limited oral bioavailability? *J. Pharm. Sci.* 98, 2549–2572.

Brouwers, J., Geboers, S., Mols, R., Tack, J., and Augustijns, P. (2017). Gastrointestinal behavior of itraconazole in humans – Part 1: Supersaturation from a solid dispersion and a cyclodextrin-based solution. *International Journal of Pharmaceutics* 525, 211–217.

7. REFERENCES

- Brown, C.K., Chokshi, H.P., Nickerson, B., Reed, R.A., Rohrs, B.R., and Shah, P.A. (2005). Acceptable Analytical Practices for Dissolution Testing of Poorly Soluble Compounds. *Dissolution Technologies* 12, 6–12.
- Buch, P., Langguth, P., Kataoka, M., and Yamashita, S. (2009). IVIVC in oral absorption for fenofibrate immediate release tablets using a dissolution/permeation system. *J Pharm Sci* 98, 2001–2009.
- Buchanan, C.M., Buchanan, N.L., Edgar, K.J., Klein, S., Little, J.L., Ramsey, M.G., Ruble, K.M., Wacher, V.J., and Wempe, M.F. (2007). Pharmacokinetics of itraconazole after intravenous and oral dosing of itraconazole-cyclodextrin formulations. *Journal of Pharmaceutical Sciences* 96, 3100–3116.
- Buckley, S.T., Fischer, S.M., Fricker, G., and Brandl, M. (2012). In vitro models to evaluate the permeability of poorly soluble drug entities: Challenges and perspectives. *European Journal of Pharmaceutical Sciences* 45, 235–250.
- Buckley, S.T., Frank, K.J., Fricker, G., and Brandl, M. (2013). Biopharmaceutical classification of poorly soluble drugs with respect to “enabling formulations.” *European Journal of Pharmaceutical Sciences* 50, 8–16.
- Butler, J.M., and Dressman, J.B. (2010). The Developability Classification System: Application of Biopharmaceutics Concepts to Formulation Development. *Journal of Pharmaceutical Sciences* 99, 4940–4954.
- Butler, J., Hens, B., Vertzoni, M., Brouwers, J., Berben, P., Dressman, J., Andreas, C.J., Schaefer, K.J., Mann, J., McAllister, M., et al. (2019). In vitro models for the prediction of in vivo performance of oral dosage forms: Recent progress from partnership through the IMI OrBiTo collaboration. *European Journal of Pharmaceutics and Biopharmaceutics* 136, 70–83.
- di Cagno, M., Bibi, H.A., and Bauer-Brandl, A. (2015). New biomimetic barrier Permeapad™ for efficient investigation of passive permeability of drugs. *European Journal of Pharmaceutical Sciences* 73, 29–34.
- Camenisch, G., Alsenz, J., van de Waterbeemd, H., and Folkers, G. (1998). Estimation of permeability by passive diffusion through Caco-2 cell monolayers using the drugs’ lipophilicity and molecular weight. *European Journal of Pharmaceutical Sciences* 6, 313–319.
- Cardot, J.-M., and Davit, B.M. (2012). In vitro–In Vivo Correlations: Tricks and Traps. *AAPS J* 14, 491–499.
- Carino, S.R., Sperry, D.C., and Hawley, M. (2006). Relative bioavailability estimation of carbamazepine crystal forms using an artificial stomach-duodenum model. *Journal of Pharmaceutical Sciences* 95, 116–125.
- Carlert, S., Pålsson, A., Hanisch, G., Corswant, C. von, Nilsson, C., Lindfors, L., Lennernäs, H., and Abrahamsson, B. (2010). Predicting Intestinal Precipitation—A Case Example for a Basic BCS Class II Drug. *Pharm Res* 27, 2119–2130.
- Caron, G., Reymond, F., Carrupt, P.A., Girault, H.H., and Testa, B. (1999). Combined molecular lipophilicity descriptors and their role in understanding intramolecular effects. *Pharm Sci Technol Today* 2, 327–335.
- CDER/FDA (2000). Guidance for industry: waiver of in vivo bioavailability and bioequivalence studies for immediate-release solid oral dosage forms based on a Biopharmaceutics Classification System.
- Center for Drug Evaluation and Research, USFDA (2017). Waiver of In Vivo Bioavailability and Bioequivalence Studies for Immediate-Release Solid Oral Dosage Forms Based on a Biopharmaceutics Classification System. Guidance for Industry (FDA).
- Chanda, J., and Bandyopadhyay, S. (2006). Molecular Dynamics Study of Surfactant Monolayers Adsorbed at the Oil/Water and Air/Water Interfaces. *J. Phys. Chem. B* 110, 23482–23488.
- Chandran, S., Gesenberg, C., Levons, J., Hubert, M., and Raghavan, K. (2011). A high-throughput spectrophotometric approach for evaluation of precipitation resistance. *Journal of Pharmaceutical and Biomedical Analysis* 56, 698–704.
- Chandrasekhar, S. (1943). Stochastic Problems in Physics and Astronomy. *Rev. Mod. Phys.* 15, 1–89.
- Chang, C., Bahadduri, P.M., Polli, J.E., Swaan, P.W., and Ekins, S. (2006). Rapid Identification of P-glycoprotein Substrates and Inhibitors. *Drug Metab Dispos* 34, 1976–1984.
- Chavan, R.B., Rathi, S., Jyothi, V.G.S.S., and Shastri, N.R. (2019). Cellulose based polymers in development of amorphous solid dispersions. *Asian Journal of Pharmaceutical Sciences* 14, 248–264.
- Chen, C.-S., and Brown, C.W. (1994). A Drug Dissolution Monitor Employing Multiple Fiber Optic Probes and a UV/Visible Diode Array Spectrophotometer. *Pharmaceutical Research* 11, 979–983.
- Chevillard, C., and Axelos, M.A.V. (1997). Phase separation of aqueous solution of methylcellulose. *Colloid Polym Sci* 275, 537–545.

- Childs, S.L., Kandi, P., and Lingireddy, S.R. (2013). Formulation of a Danazol Cocrystal with Controlled Supersaturation Plays an Essential Role in Improving Bioavailability. *Mol. Pharmaceutics* *10*, 3112–3127.
- Cho, K.H., Jee, J.-P., Yang, D.A., Kim, S.T., Kang, D., Kim, D.-Y., Sim, T., Park, S.Y., Kim, K., and Jang, D.-J. (2018). Improved Dissolution and Oral Bioavailability of Celecoxib by a Dry Elixir System. *J Nanosci Nanotechnol* *18*, 1482–1486.
- Colombo, M., Staufenbiel, S., Rühl, E., and Bodmeier, R. (2017). In situ determination of the saturation solubility of nanocrystals of poorly soluble drugs for dermal application. *International Journal of Pharmaceutics* *521*, 156–166.
- Colorcon (2009). How to Prepare Aqueous Solutions of METHOCEL™.
- Comer, J. (2010). Supersaturation effects in drug development. *Chimica Oggi* *28*, 4.
- Comer, J., Chamberlain, K., and Evans, A. (1995). Validation of pH-Metric Technique for Measurement of pKa and log Pow of Ionizable Herbicides. *SAR and QSAR in Environmental Research* *3*, 307–313.
- Comer, J., Box, K., and Taylor, R. (2014). Biopharmaceutics and formulation. New experimental methods for supersaturation and precipitation. *Chimica Oggi* *32*, 6.
- Comyn, J. (1985). Introduction to Polymer Permeability and the Mathematics of Diffusion. In *Polymer Permeability*, J. Comyn, ed. (Dordrecht: Springer Netherlands), pp. 1–10.
- Dahan, A., and Miller, J.M. (2012). The Solubility-Permeability Interplay and Its Implications in Formulation Design and Development for Poorly Soluble Drugs. *AAPS J.* *14*, 244.
- Dahan, A., Miller, J.M., Hoffman, A., Amidon, G.E., and Amidon, G.L. (2010). The Solubility–Permeability Interplay in Using Cyclodextrins as Pharmaceutical Solubilizers: Mechanistic Modeling and Application to Progesterone. *Journal of Pharmaceutical Sciences* *99*, 2739–2749.
- Dai, W.-G. (2010). In vitro methods to assess drug precipitation. *International Journal of Pharmaceutics* *393*, 1–16.
- Dai, W.-G., Dong, L.C., Li, S., and Deng, Z. (2008). Combination of Pluronic/Vitamin E TPGS as a potential inhibitor of drug precipitation. *International Journal of Pharmaceutics* *355*, 31–37.
- Dardonville, C. (2018). Automated techniques in pKa determination: Low, medium and high-throughput screening methods. *Drug Discovery Today: Technologies* *27*, 49–58.
- Davis, M.T., Potter, C.B., Mohammadpour, M., Albadarin, A.B., and Walker, G.M. (2017). Design of spray dried ternary solid dispersions comprising itraconazole, soluplus and HPMCP: Effect of constituent compositions. *International Journal of Pharmaceutics* *519*, 365–372.
- Davis, S.S., Hardy, J.G., and Fara, J.W. (1986). Transit of pharmaceutical dosage forms through the small intestine. *Gut* *27*, 886–892.
- Dayan, A.D. (2003). Albendazole, mebendazole and praziquantel. Review of non-clinical toxicity and pharmacokinetics. *Acta Tropica* *86*, 141–159.
- Denninger, A., Westedt, U., Rosenberg, J., and Wagner, K.G. (2020). A Rational Design of a Biphasic Dissolution Setup—Modelling of Biorelevant Kinetics for a Ritonavir Hot-Melt Extruded Amorphous Solid Dispersion. *Pharmaceutics* *12*, 237.
- Desai, P., Thakkar, A., Ann, D., Wang, J., and Prabhu, S. (2019). Loratadine self-microemulsifying drug delivery systems (SMEDDS) in combination with sulforaphane for the synergistic chemoprevention of pancreatic cancer. *Drug Deliv Transl Res.*
- DeSesso, J.M., and Jacobson, C.F. (2001). Anatomical and physiological parameters affecting gastrointestinal absorption in humans and rats. *Food and Chemical Toxicology* *39*, 209–228.
- Di, L., Fish, P.V., and Mano, T. (2012). Bridging solubility between drug discovery and development. *Drug Discovery Today* *17*, 486–495.
- DiNunzio, J.C., Miller, D.A., Yang, W., McGinity, J.W., and Williams, R.O. (2008). Amorphous Compositions Using Concentration Enhancing Polymers for Improved Bioavailability of Itraconazole. *Mol. Pharmaceutics* *5*, 968–980.
- DiNunzio, J.C., Brough, C., Miller, D.A., Williams, R.O., and McGinity, J.W. (2010). Applications of KinetiSol® Dispersing for the production of plasticizer free amorphous solid dispersions. *European Journal of Pharmaceutical Sciences* *40*, 179–187.

7. REFERENCES

- Ditzinger, F., Price, D.J., Ilie, A.-R., Köhl, N.J., Jankovic, S., Tsakiridou, G., Aleandri, S., Kalantzi, L., Holm, R., Nair, A., et al. (2019). Lipophilicity and hydrophobicity considerations in bio-enabling oral formulations approaches – a PEARRL review. *Journal of Pharmacy and Pharmacology* *71*, 464–482.
- Djuric (2011). Soluplus. In *Solubility Enhancement with BASF Pharma Polymers - Solubilizer Compendium*, pp. 67–72.
- Dokoumetzidis, A., and Macheras, P. (2006). A century of dissolution research: From Noyes and Whitney to the Biopharmaceutics Classification System. *International Journal of Pharmaceutics* *321*, 1–11.
- Dong, W.Y., Maincent, P., and Bodmeier, R. (2007). In vitro and in vivo evaluation of carbamazepine-loaded enteric microparticles. *International Journal of Pharmaceutics* *331*, 84–92.
- Donovan, S.F., and Pescatore, M.C. (2002). Method for measuring the logarithm of the octanol–water partition coefficient by using short octadecyl–poly(vinyl alcohol) high-performance liquid chromatography columns. *Journal of Chromatography A* *952*, 47–61.
- Douroumis, D., and Fahr, A. (2007). Stable carbamazepine colloidal systems using the cosolvent technique. *European Journal of Pharmaceutical Sciences* *30*, 367–374.
- Dow (2013). Methocel™ - Technical Bulletin.
- Dow Chemical (2013). Chemistry of Methocel(TM) - Cellulose Ethers - A Technical Review.
- Dressman, J.B., and Reppas, C. (2000). In vitro–in vivo correlations for lipophilic, poorly water-soluble drugs. *European Journal of Pharmaceutical Sciences* *11*, S73–S80.
- Dressman, J.B., Amidon, G.L., Reppas, C., and Shah, V.P. (1998). Dissolution Testing as a Prognostic Tool for Oral Drug Absorption: Immediate Release Dosage Forms. *Pharm Res* *15*, 11–22.
- Edueng, K., Mahlin, D., Larsson, P., and Bergström, C.A.S. (2017). Mechanism-based selection of stabilization strategy for amorphous formulations: Insights into crystallization pathways. *Journal of Controlled Release* *256*, 193–202.
- Edwards, F., Tsakmaka, C., Mohr, S., R. Fielden, P., J. Goddard, N., Booth, J., and Y. Tam, K. (2013). Using droplet-based microfluidic technology to study the precipitation of a poorly water-soluble weakly basic drug upon a pH-shift. *Analyst* *138*, 339–345.
- Einstein, A. (1905). Über die von der molekularkinetischen Theorie der Wärme geforderte Bewegung von in ruhenden Flüssigkeiten suspendierten Teilchen. *Annalen Der Physik* *322*, 549–560.
- El Seoud, O.A. (1989). Effects of organized surfactant assemblies on acid-base equilibria. *Advances in Colloid and Interface Science* *30*, 1–30.
- Elworthy, P.H., and Patel, M.S. (1982). Demonstration of maximum solubilization in a polyoxyethylene alkyl ether series of non-ionic surfactants. *Journal of Pharmacy and Pharmacology* *34*, 543–546.
- European Pharmacopoeia 9th Edition (2017). *European Pharmacopoeia* 9.2.
- Fagerberg, J.H., Karlsson, E., Ulander, J., Hanisch, G., and Bergström, C.A.S. (2015). Computational Prediction of Drug Solubility in Fasted Simulated and Aspirated Human Intestinal Fluid. *Pharm Res* *32*, 578–589.
- Fallingborg, J., Christensen, L.A., Ingeman-Nielsen, M., Jacobsen, B.A., Abildgaard, K., and Rasmussen, H.H. (1989). pH-Profile and regional transit times of the normal gut measured by a radiotelemetry device. *Alimentary Pharmacology & Therapeutics* *3*, 605–614.
- Fallingborg, J., Christensen, L.A., Ingeman-Nielsen, M., Jacobsen, B.A., Abildgaard, K., Rasmussen, H.H., and Rasmussen, S.N. (1990). Gastrointestinal pH and transit times in healthy subjects with ileostomy. *Alimentary Pharmacology & Therapeutics* *4*, 247–253.
- FDA (1997). *Extended Release Oral Dosage Forms: Development, Evaluation, and Application of In Vitro/In Vivo Correlations* (FDA).
- FDA (2001). *Drug Approval Package: Sporanox (Itraconazole) NDA #20-966/S1, 3 & 4 & 20-657/S4 & 5*.
- FDA (2018). *Drug Approval Package: Tolsura*.
- FDA Guidance for Industry (1997). *Dissolution testing of immediate release solid oral dosage forms*. Food and Drug Administration, Center for Drug Evaluation and Research.

FDA/CDER (2017). Guidance for Industry: Waiver on In Vivo Bioavailability and Bioequivalence Studies for Immediate-Release Solid Oral Dosage Forms Based on a Biopharmaceutics Classification System. US Department of Health and Human Services.

Flaten, G.E., Dhanikula, A.B., Luthman, K., and Brandl, M. (2006). Drug permeability across a phospholipid vesicle based barrier: A novel approach for studying passive diffusion. *European Journal of Pharmaceutical Sciences* 27, 80–90.

Fong, S.Y.K., Bauer-Brandl, A., and Brandl, M. (2017a). Oral bioavailability enhancement through supersaturation: an update and meta-analysis. *Expert Opin Drug Deliv* 14, 403–426.

Fong, S.Y.K., Poulsen, J., Brandl, M., and Bauer-Brandl, A. (2017b). A novel microdialysis-dissolution/permeation system for testing oral dosage forms: A proof-of-concept study. *European Journal of Pharmaceutical Sciences* 96, 154–163.

Frank, K.J., Rosenblatt, K.M., Westedt, U., Hölig, P., Rosenberg, J., Mägerlein, M., Fricker, G., and Brandl, M. (2012). Amorphous solid dispersion enhances permeation of poorly soluble ABT-102: True supersaturation vs. apparent solubility enhancement. *International Journal of Pharmaceutics* 437, 288–293.

Frank, K.J., Locher, K., Zecevic, D.E., Fleth, J., and Wagner, K.G. (2014). In vivo predictive mini-scale dissolution for weak bases: Advantages of pH-shift in combination with an absorptive compartment. *European Journal of Pharmaceutical Sciences* 61, 32–39.

Fuchs, A., and Dressman, J.B. (2014). Composition and Physicochemical Properties of Fasted-State Human Duodenal and Jejunal Fluid: A Critical Evaluation of the Available Data. *Journal of Pharmaceutical Sciences* 103, 3398–3411.

Fule, R., and Amin, P. (2014a). Development and evaluation of lafutidine solid dispersion via hot melt extrusion: Investigating drug-polymer miscibility with advanced characterisation. *Asian Journal of Pharmaceutical Sciences* 9, 92–106.

Fule, R., and Amin, P. (2014b). Hot melt extruded amorphous solid dispersion of posaconazole with improved bioavailability: investigating drug-polymer miscibility with advanced characterisation. *Biomed Res Int* 2014, 146781.

Gan, Y., Zhang, X., Xu, D., Zhang, H., Baak, J.P., Luo, L., Xia, Y., Wang, J., Ke, X., and Sun, P. (2020). Evaluating supersaturation in vitro and predicting its performance in vivo with Biphasic gastrointestinal Simulator: A case study of a BCS IIB drug. *International Journal of Pharmaceutics* 578, 119043.

Gao, P., and Shi, Y. (2012). Characterization of Supersaturable Formulations for Improved Absorption of Poorly Soluble Drugs. *AAPS J* 14, 703–713.

Gao, P., Akrami, A., Alvarez, F., Hu, J., Li, L., Ma, C., and Surapaneni, S. (2009a). Characterization and optimization of AMG 517 supersaturable self-emulsifying drug delivery system (S-SEDDS) for improved oral absorption. *J. Pharm. Sci.* 98, 516–528.

Gao, P., Akrami, A., Alvarez, F., Hu, J., Li, L., Ma, C., and Surapaneni, S. (2009b). Characterization and optimization of AMG 517 supersaturable self-emulsifying drug delivery system (S-SEDDS) for improved oral absorption. *Journal of Pharmaceutical Sciences* 98, 516–528.

Gao et al. (2003). Development of a Supersaturable SEDDS (S-SEDDS) Formulation of Paclitaxel with Improved Oral Bioavailability.

Ginski, M.J., Taneja, R., and Polli, J.E. (1999). Prediction of dissolution-absorption relationships from a continuous dissolution/Caco-2 system. *AAPS PharmSci* 1, 27.

Göke, K., Lorenz, T., Repanas, A., Schneider, F., Steiner, D., Baumann, K., Bunjes, H., Dietzel, A., Finke, J.H., Glasmacher, B., et al. (2018). Novel strategies for the formulation and processing of poorly water-soluble drugs. *European Journal of Pharmaceutics and Biopharmaceutics* 126, 40–56.

Granger, D.N., Barrowman, J.A., and Kviety, P.R. (1985). *Clinical gastrointestinal physiology* (WB Saunders Company).

Gravestock, T., Box, K., Comer, J., Frake, E., Judge, S., and Ruiz, R. (2011). The “GI dissolution” method: a low volume, in vitro apparatus for assessing the dissolution/precipitation behaviour of an active pharmaceutical ingredient under biorelevant conditions. *Anal. Methods* 3, 560–567.

Grès, M.-C., Julian, B., Bourrié, M., Meunier, V., Roques, C., Berger, M., Boulenc, X., Berger, Y., and Fabre, G. (1998). Correlation Between Oral Drug Absorption in Humans, and Apparent Drug Permeability in TC-7 Cells, A Human Epithelial Intestinal Cell Line: Comparison with the Parental Caco-2 Cell Line. *Pharm Res* 15, 726–733.

Gribbon, P., and Andreas, S. (2005). High-throughput drug discovery: What can we expect from HTS? *Drug Discovery Today* 10, 17–22.

Grujić, M., Popović, M., Popović, G., Nikolic, K., and Agbaba, D. (2016). Protolytic Equilibria of Sartans in Micellar Solutions of Differently Charged Surfactants. *Journal of Pharmaceutical Sciences* 105, 2444–2452.

7. REFERENCES

- Guzmán, H., Tawa, M., Zhang, Z., Ratanabanangkoon, P., Shaw, P., Mustonen, P., Gardner, C., Chen, H., Moreau, J., Almarsson, O., et al. (2004). A “spring and parachute” approach to designing solid celecoxib formulations having enhanced oral absorption. *AAPS J* 6, T2189.
- Guzmán, H.R., Tawa, M., Zhang, Z., Ratanabanangkoon, P., Shaw, P., Gardner, C.R., Chen, H., Moreau, J., Almarsson, Ö., and Remenar, J.F. (2007a). Combined Use of Crystalline Salt Forms and Precipitation Inhibitors to Improve Oral Absorption of Celecoxib from Solid Oral Formulations. *Journal of Pharmaceutical Sciences* 96, 2686–2702.
- Guzmán, H.R., Tawa, M., Zhang, Z., Ratanabanangkoon, P., Shaw, P., Gardner, C.R., Chen, H., Moreau, J.-P., Almarsson, Ö., and Remenar, J.F. (2007b). Combined use of crystalline salt forms and precipitation inhibitors to improve oral absorption of celecoxib from solid oral formulations. *J. Pharm. Sci.* 96, 2686–2702.
- Halter, J.B., Tinetti, M.E., Studenski, S., High, K.P., and Asthana, S. (2009). Hazzard’s geriatric medicine and gerontology. In *Hazzard’s Geriatric Medicine and Gerontology*, (New York: McGraw-Hill Companies), p.
- Hancock, B.C., and Parks, M. (2000). What is the True Solubility Advantage for Amorphous Pharmaceuticals? *Pharm Res* 17, 397–404.
- Hansch, C., and Fujita, T. (1964). A Method for the Correlation of Biological Activity and Chemical Structure. *Journal of the American Chemical Society* 86, 11.
- Hardung, H., Djuric, D., and Ali, S. (2010). Combining HME & Solubilization: Soluplus® - The Solid Solution. *10*, 7.
- Hasselbalch, K.A. (1916). The calculation of blood pH via the partition of carbon dioxide in plasma and oxygen binding of the blood as a function of plasma pH. *Biochem Z* 78, 112–144.
- Heigoldt, U., Sommer, F., Daniels, R., and Wagner, K.-G. (2010). Predicting in vivo absorption behavior of oral modified release dosage forms containing pH-dependent poorly soluble drugs using a novel pH-adjusted biphasic in vitro dissolution test. *European Journal of Pharmaceutics and Biopharmaceutics* 76, 105–111.
- Helander, H.F., and Fändriks, L. (2014). Surface area of the digestive tract – revisited. *Scandinavian Journal of Gastroenterology* 49, 681–689.
- Henderson, L. (1908). Concerning the relationship between the strength of acids and their capacity to preserve neutrality. *Am J Physiol* 21, 427–448.
- Hens, B., Corsetti, M., Brouwers, J., and Augustijns, P. (2016a). Gastrointestinal and Systemic Monitoring of Posaconazole in Humans After Fasted and Fed State Administration of a Solid Dispersion. *Journal of Pharmaceutical Sciences* 105, 2904–2912.
- Hens, B., Brouwers, J., Corsetti, M., and Augustijns, P. (2016b). Supersaturation and Precipitation of Posaconazole Upon Entry in the Upper Small Intestine in Humans. *Journal of Pharmaceutical Sciences*.
- Hens, B., Corsetti, M., Spiller, R., Marciani, L., Vanuytsel, T., Tack, J., Talatof, A., Amidon, G.L., Koziolk, M., Weitschies, W., et al. (2017). Exploring gastrointestinal variables affecting drug and formulation behavior: Methodologies, challenges and opportunities. *International Journal of Pharmaceutics* 519, 79–97.
- Herve, G. (1989). *Allosteric Enzymes* (CRC Press).
- Higashino, H., Hasegawa, T., Yamamoto, M., Matsui, R., Masaoka, Y., Kataoka, M., Sakuma, S., and Yamashita, S. (2014). In Vitro–in Vivo Correlation of the Effect of Supersaturation on the Intestinal Absorption of BCS Class 2 Drugs. *Mol. Pharmaceutics* 11, 746–754.
- HIGUCHI, T. (1960). Physical Chemical analysis of Percutaneous Absorption Process from Creams and Ointments. *J. Soc. Cosmet. Chem* 11, 85–97.
- Hill, A.P., and Young, R.J. (2010). Getting physical in drug discovery: a contemporary perspective on solubility and hydrophobicity. *Drug Discovery Today* 15, 648–655.
- Hoffman, J.D. (1958). Thermodynamic Driving Force in Nucleation and Growth Processes. *J. Chem. Phys.* 29, 1192–1193.
- Homayouni, A., Sadeghi, F., Varshosaz, J., Afrasiabi Garekani, H., and Nokhodchi, A. (2014). Promising dissolution enhancement effect of soluplus on crystallized celecoxib obtained through antisolvent precipitation and high pressure homogenization techniques. *Colloids and Surfaces B: Biointerfaces* 122, 591–600.
- Homayouni, A., Sadeghi, F., Nokhodchi, A., Varshosaz, J., and Afrasiabi Garekani, H. (2015). Preparation and Characterization of Celecoxib Dispersions in Soluplus®: Comparison of Spray Drying and Conventional Methods. *Iran J Pharm Res* 14, 35–50.

- Hörter, D., and Dressman, J.B. (1997). Influence of physicochemical properties on dissolution of drugs in the gastrointestinal tract. *Advanced Drug Delivery Reviews* 25, 3–14.
- Hsieh, Y.-L., Ilevbare, G.A., Eerdenbrugh, B.V., Box, K.J., Sanchez-Felix, M.V., and Taylor, L.S. (2012). pH-Induced Precipitation Behavior of Weakly Basic Compounds: Determination of Extent and Duration of Supersaturation Using Potentiometric Titration and Correlation to Solid State Properties. *Pharm Res* 29, 2738–2753.
- Hu, J., Rogers, T.L., Brown, J., Young, T., Johnston, K.P., and Williams III, R.O. (2002). Improvement of Dissolution Rates of Poorly Water Soluble APIs Using Novel Spray Freezing into Liquid Technology. *Pharm Res* 19, 1278–1284.
- Huang, L.-F., and Tong, W.-Q. (Tony) (2004). Impact of solid state properties on developability assessment of drug candidates. *Advanced Drug Delivery Reviews* 56, 321–334.
- Hunter, E., Fell, J.T., and Sharma, H. (1982). The Gastric Emptying of Pellets Contained in Hard Gelatin Capsules. *Drug Development and Industrial Pharmacy* 8, 751–757.
- Ieiri, I., Nishimura, C., Maeda, K., Sasaki, T., Kimura, M., Chiyoda, T., Hirota, T., Irie, S., Shimizu, H., Noguchi, T., et al. (2011). Pharmacokinetic and pharmacogenomic profiles of telmisartan after the oral microdose and therapeutic dose. *Pharmacogenet. Genomics* 21, 495–505.
- Ilevbare, G.A., and Taylor, L.S. (2013). Liquid–Liquid Phase Separation in Highly Supersaturated Aqueous Solutions of Poorly Water-Soluble Drugs: Implications for Solubility Enhancing Formulations. *Crystal Growth & Design* 13, 1497–1509.
- Ilevbare, G.A., Liu, H., Pereira, J., Edgar, K.J., and Taylor, L.S. (2013a). Influence of Additives on the Properties of Nanodroplets Formed in Highly Supersaturated Aqueous Solutions of Ritonavir. *Mol. Pharmaceutics* 10, 3392–3403.
- Ilevbare, G.A., Liu, H., Edgar, K.J., and Taylor, L.S. (2013b). Maintaining Supersaturation in Aqueous Drug Solutions: Impact of Different Polymers on Induction Times. *Crystal Growth & Design* 13, 740–751.
- Indulkar, A.S., Box, K.J., Taylor, R., Ruiz, R., and Taylor, L.S. (2015). pH-Dependent Liquid–Liquid Phase Separation of Highly Supersaturated Solutions of Weakly Basic Drugs. *Molecular Pharmaceutics* 12, 2365–2377.
- Institute for Laboratory Animal Research, National Research Council (2010). *Guide for the Care and Use of Laboratory Animals: Eighth Edition* (National Academies Press).
- Jackson, M.J., Kestur, U., Hussain, M., and Taylor, L. (2016). Characterization of Supersaturated Danazol Solutions – Impact of Polymers on Solution Properties and Phase Transitions. *Pharmaceutical Research*.
- Jantravid, E., and Dressman, J. (2009). Biorelevant Dissolution Media Simulating the Proximal Human Gastrointestinal Tract: An Update. *Dissolution Technologies* 16, 21–25.
- Jantravid, E., Janssen, N., Reppas, C., and Dressman, J.B. (2008). Dissolution Media Simulating Conditions in the Proximal Human Gastrointestinal Tract: An Update. *Pharm Res* 25, 1663.
- Jonsson, U., Alpsten, M., Bogenhoft, C., Eriksson, R., and Sjögren, J. (1983). Gastric emptying of pellets and tablets in healthy subjects under fasting and nonfasting conditions.
- Josefson, Mats., Johansson, Erik., and Torstensson, Arne. (1988). Optical fiber spectrometry in turbid solutions by multivariate calibration applied to tablet dissolution testing. *Anal. Chem.* 60, 2666–2671.
- Kansy, M., Senner, F., and Gubernator, K. (1998). Physicochemical High Throughput Screening: Parallel Artificial Membrane Permeation Assay in the Description of Passive Absorption Processes. *J. Med. Chem.* 41, 1007–1010.
- Kararli, T.T. (1995). Comparison of the gastrointestinal anatomy, physiology, and biochemistry of humans and commonly used laboratory animals. *Biopharmaceutics & Drug Disposition* 16, 351–380.
- Kashchiev, D., and van Rosmalen, G.M. (2003). Review: Nucleation in solutions revisited. *Cryst. Res. Technol.* 38, 555–574.
- Kataoka, M., Masaoka, Y., Yamazaki, Y., Sakane, T., Sezaki, H., and Yamashita, S. (2003). In Vitro System to Evaluate Oral Absorption of Poorly Water-Soluble Drugs: Simultaneous Analysis on Dissolution and Permeation of Drugs. *Pharm Res* 20, 1674–1680.
- Kaur, T., Madgulkar, A., Bhalekar, M., and Asgaonkar, K. (2019). Molecular Docking in Formulation and Development. *Current Drug Discovery Technologies* 16, 30–39.

7. REFERENCES

- Kawabata, Y., Wada, K., Nakatani, M., Yamada, S., and Onoue, S. (2011). Formulation design for poorly water-soluble drugs based on biopharmaceutics classification system: Basic approaches and practical applications. *International Journal of Pharmaceutics* 420, 1–10.
- Kenneth Wolfenbarger, J., and Seinfeld, J.H. (1990). Inversion of aerosol size distribution data. *Journal of Aerosol Science* 21, 227–247.
- Khan, M.Z.I., Rausl, D., Zanoski, R., Zidar, S., Mikulčić, J.H., Krizmanić, L., Eskinja, M., Mildner, B., and Knezević, Z. (2004). Classification of loratadine based on the biopharmaceutics drug classification concept and possible in vitro-in vivo correlation. *Biol. Pharm. Bull.* 27, 1630–1635.
- Kleberg, K., Jacobsen, J., and Müllertz, A. (2010). Characterising the behaviour of poorly water soluble drugs in the intestine: application of biorelevant media for solubility, dissolution and transport studies. *J. Pharm. Pharmacol.* 62, 1656–1668.
- Klein, S. (2010). The Use of Biorelevant Dissolution Media to Forecast the In Vivo Performance of a Drug. *AAPS J* 12, 397–406.
- Klein, C.E., Chiu, Y.-L., Awni, W., Zhu, T., Heuser, R.S., Doan, T., Breitenbach, J., Morris, J.B., Brun, S.C., and Hanna, G.J. (2007). The tablet formulation of lopinavir/ritonavir provides similar bioavailability to the soft-gelatin capsule formulation with less pharmacokinetic variability and diminished food effect. *J. Acquir. Immune Defic. Syndr.* 44, 401–410.
- Kobayashi, M., Sada, N., Sugawara, M., Iseki, K., and Miyazaki, K. (2001). Development of a new system for prediction of drug absorption that takes into account drug dissolution and pH change in the gastro-intestinal tract. *International Journal of Pharmaceutics* 221, 87–94.
- Kole, P.L., Venkatesh, G., Kotecha, J., and Sheshala, R. (2011). Recent advances in sample preparation techniques for effective bioanalytical methods. *Biomed. Chromatogr.* 25, 199–217.
- Koltzenburg, S. (2011). Formulation of problem drugs - and they are all problem drugs. In *Solubility Enhancement with BASF Pharma Polymers - Solubilizer Compendium*, pp. 9–26.
- Kostewicz, E.S., Wunderlich, M., Brauns, U., Becker, R., Bock, T., and Dressman, J.B. (2004). Predicting the precipitation of poorly soluble weak bases upon entry in the small intestine. *Journal of Pharmacy and Pharmacology* 56, 43–51.
- Kostewicz, E.S., Abrahamsson, B., Brewster, M., Brouwers, J., Butler, J., Carlert, S., Dickinson, P.A., Dressman, J., Holm, R., Klein, S., et al. (2014). In vitro models for the prediction of in vivo performance of oral dosage forms. *European Journal of Pharmaceutical Sciences* 57, 342–366.
- Kourentas, A., Vertzoni, M., Stavrinoudakis, N., Symillidis, A., Brouwers, J., Augustijns, P., Reppas, C., and Symillides, M. (2016a). An in vitro biorelevant gastrointestinal transfer (BioGIT) system for forecasting concentrations in the fasted upper small intestine: Design, implementation, and evaluation. *European Journal of Pharmaceutical Sciences* 82, 106–114.
- Kourentas, A., Vertzoni, M., Symillides, M., Goumas, K., Gibbon, R., Butler, J., and Reppas, C. (2016b). Effectiveness of supersaturation promoting excipients on albendazole concentrations in upper gastrointestinal lumen of fasted healthy adults. *European Journal of Pharmaceutical Sciences* 91, 11–19.
- Kourentas, A., Vertzoni, M., Khadra, I., Symillides, M., Clark, H., Halbert, G., Butler, J., and Reppas, C. (2016c). Evaluation of the Impact of Excipients and an Albendazole Salt on Albendazole Concentrations in Upper Small Intestine Using an In Vitro Biorelevant Gastrointestinal Transfer (BioGIT) System. *Journal of Pharmaceutical Sciences* 105, 2896–2903.
- Kourentas, A., Vertzoni, M., Symillides, M., Hens, B., Brouwers, J., Augustijns, P., and Reppas, C. (2016d). In vitro evaluation of the impact of gastrointestinal transfer on luminal performance of commercially available products of posaconazole and itraconazole using BioGIT. *International Journal of Pharmaceutics* 515, 352–358.
- Koziolek, M., Grimm, M., Garbacz, G., Kühn, J.-P., and Weitschies, W. (2014). Intra-gastric Volume Changes after Intake of a High-Caloric, High-Fat Standard Breakfast in Healthy Human Subjects Investigated by MRI. *Mol. Pharmaceutics* 11, 1632–1639.
- Koziolek, M., Grimm, M., Becker, D., Iordanov, V., Zou, H., Shimizu, J., Wanke, C., Garbacz, G., and Weitschies, W. (2015a). Investigation of pH and Temperature Profiles in the GI Tract of Fasted Human Subjects Using the Intellicap® System. *Journal of Pharmaceutical Sciences* 104, 2855–2863.
- Koziolek, M., Schneider, F., Grimm, M., Modeß, C., Seekamp, A., Roustom, T., Siegmund, W., and Weitschies, W. (2015b). Intra-gastric pH and pressure profiles after intake of the high-caloric, high-fat meal as used for food effect studies. *Journal of Controlled Release* 220, 71–78.
- Koziolek, M., Grimm, M., Schneider, F., Jedamzik, P., Sager, M., Kühn, J.-P., Siegmund, W., and Weitschies, W. (2016). Navigating the human gastrointestinal tract for oral drug delivery: Uncharted waters and new frontiers. *Advanced Drug Delivery Reviews* 101, 75–88.

- Kraemer, E.O., and Dexter, S.T. (1927). The Light-Scattering Capacity (Tyndall Effect) and Colloidal Behavior of Gelatine Sols and Gels. *The Journal of Physical Chemistry* *31*, 764–782.
- Krämer, S.D. (1999). Absorption prediction from physicochemical parameters. *Pharmaceutical Science & Technology Today* *2*, 373–380.
- Ku, M.S. (2008). Use of the Biopharmaceutical Classification System in Early Drug Development. *AAPS J* *10*, 208–212.
- Kumar, S., Jog, R., Shen, J., Zolnik, B., Sadrieh, N., and Burgess, D.J. (2015). In Vitro and In Vivo Performance of Different Sized Spray-Dried Crystalline Itraconazole. *Journal of Pharmaceutical Sciences* *104*, 3018–3028.
- Lafferrère, L., Hoff, C., and Veessler, S. (2004). In Situ Monitoring of the Impact of Liquid–Liquid Phase Separation on Drug Crystallization by Seeding. *Crystal Growth & Design* *4*, 1175–1180.
- Lang, B., Liu, S., McGinity, J.W., and Williams, R.O. (2016). Effect of hydrophilic additives on the dissolution and pharmacokinetic properties of itraconazole-enteric polymer hot-melt extruded amorphous solid dispersions. *Drug Development and Industrial Pharmacy* *42*, 429–445.
- Le Chatelier, H. (1888). *Recherches expérimentales et théoriques sur les équilibres chimiques* (Dunod).
- Lefebvre, A.H., and McDonnell, V.G. (2017). *Atomization and Sprays* (CRC Press).
- Lennernäs, H., Aarons, L., Augustijns, P., Beato, S., Bolger, M., Box, K., Brewster, M., Butler, J., Dressman, J., Holm, R., et al. (2014). Oral biopharmaceutics tools – Time for a new initiative – An introduction to the IMI project OrBiTo. *European Journal of Pharmaceutical Sciences* *57*, 292–299.
- Leuner, C., and Dressman, J. (2000). Improving drug solubility for oral delivery using solid dispersions. *European Journal of Pharmaceutics and Biopharmaceutics* *50*, 47–60.
- Li, J., Bukhtiyarov, Y., Spivey, N., Force, C., Hidalgo, C., Huang, Y., Owen, A.J., and Hidalgo, I.J. (2019). In Vitro and In Vivo Assessment of the Potential of Supersaturation to Enhance the Absorption of Poorly Soluble Basic Drugs. *Journal of Pharmaceutical Innovation*.
- Li, P., Vishnuvajjala, R., Tabibi, S.E., and Yalkowsky, S.H. (1998). Evaluation of in vitro precipitation methods. *Journal of Pharmaceutical Sciences* *87*, 196–199.
- Li, Z., He, X., Gao, X., Xu, Y., Wang, Y., Gu, H., Ji, R., and Sun, S. (2011). Study on dissolution and absorption of four dosage forms of isosorbide mononitrate: Level A in vitro–in vivo correlation. *European Journal of Pharmaceutics and Biopharmaceutics* *79*, 364–371.
- Li, Z., Han, X., Zhai, Y., Lian, H., Zhang, D., Zhang, W., Wang, Y., He, Z., Liu, Z., and Sun, J. (2015). Critical determinant of intestinal permeability and oral bioavailability of pegylated all trans-retinoic acid prodrug-based nanomicelles: Chain length of poly (ethylene glycol) corona. *Colloids and Surfaces B: Biointerfaces* *130*, 133–140.
- Lindenberg, M., Kopp, S., and Dressman, J.B. (2004). Classification of orally administered drugs on the World Health Organization Model list of Essential Medicines according to the biopharmaceutics classification system. *European Journal of Pharmaceutics and Biopharmaceutics* *58*, 265–278.
- Lindfors, L., Forssén, S., Westergren, J., and Olsson, U. (2008). Nucleation and crystal growth in supersaturated solutions of a model drug. *Journal of Colloid and Interface Science* *325*, 404–413.
- Linn, M., Collnot, E.-M., Djuric, D., Hempel, K., Fabian, E., Kolter, K., and Lehr, C.-M. (2012). Soluplus® as an effective absorption enhancer of poorly soluble drugs in vitro and in vivo. *Eur J Pharm Sci* *45*, 336–343.
- Lipinski, C.A. (2000). Drug-like properties and the causes of poor solubility and poor permeability. *Journal of Pharmacological and Toxicological Methods* *44*, 235–249.
- Lipinski, C.A., Lombardo, F., Dominy, B.W., and Feeney, P.J. (1997). Experimental and computational approaches to estimate solubility and permeability in drug discovery and development settings. *Advanced Drug Delivery Reviews* *23*, 3–25.
- Liu, H., Taylor, L.S., and Edgar, K.J. (2015). The role of polymers in oral bioavailability enhancement; a review. *Polymer* *77*, 399–415.
- Llinàs, A., and Goodman, J.M. (2008). Polymorph control: past, present and future. *Drug Discovery Today* *13*, 198–210.

7. REFERENCES

- Locatelli, I., Mrhar, A., and Bogataj, M. (2009). Gastric Emptying of Pellets under Fasting Conditions: A Mathematical Model. *Pharm Res* 26, 1607–1617.
- Locher, K., Borghardt, J.M., Frank, K.J., Kloft, C., and Wagner, K.G. (2016). Evolution of a mini-scale biphasic dissolution model: Impact of model parameters on partitioning of dissolved API and modelling of in vivo-relevant kinetics. *European Journal of Pharmaceutics and Biopharmaceutics* 105, 166–175.
- Locher, K., Borghardt, J.M., Wachtel, H., Schaefer, K.J., and Wagner, K.G. (2018). Mechanistic study on hydrodynamics in the mini-scale biphasic dissolution model and its influence on in vitro dissolution and partitioning. *European Journal of Pharmaceutical Sciences* 124, 328–338.
- Loftsson, T., and Brewster, M.E. (2011). Pharmaceutical Applications of Cyclodextrins: Effects on Drug Permeation through Biological Membranes. *J. Pharm. Pharmacol.* 63, 1119.
- Lombardo, F., Shalaeva, M.Y., Tupper, K.A., and Gao, F. (2001). ElogDoct: A Tool for Lipophilicity Determination in Drug Discovery. 2. Basic and Neutral Compounds. *J. Med. Chem.* 44, 2490–2497.
- Lu, X., Lozano, R., and Shah, P. (2003). In-Situ Dissolution Testing Using Different UV Fiber Optic Probes and Instruments. *Dissolution Technologies* 10, 6–15.
- Ma, X., Taw, J., and Chiang, C.-M. (1996). Control of drug crystallization in transdermal matrix system. *International Journal of Pharmaceutics* 142, 115–119.
- Ma, Y., Gao, S., and Hu, M. (2015). Quantitation of celecoxib and four of its metabolites in rat blood by UPLC-MS/MS clarifies their blood distribution patterns and provides more accurate pharmacokinetics profiles. *J Chromatogr B Analyt Technol Biomed Life Sci* 1001, 202–211.
- Mackie, A., and Rigby, N. (2015). InfoGest Consensus Method. In *The Impact of Food Bioactives on Health: In Vitro and Ex Vivo Models*, K. Verhoeckx, P. Cotter, I. López-Expósito, C. Kleiveland, T. Lea, A. Mackie, T. Requena, D. Swiatecka, and H. Wichers, eds. (Cham: Springer International Publishing), pp. 13–22.
- Madhav, K.V., and Kishan, V. (2018). Self microemulsifying particles of loratadine for improved oral bioavailability: preparation, characterization and in vivo evaluation. *J. Pharm. Investig.* 48, 497–508.
- Margolskee, A., Darwich, A.S., Galetin, A., Rostami-Hodjegan, A., and Aarons, L. (2015). Deconvolution and IVIVC: Exploring the Role of Rate-Limiting Conditions. *AAPS J* 18, 321–332.
- Martinez, M.N., and Amidon, G.L. (2002). A Mechanistic Approach to Understanding the Factors Affecting Drug Absorption: A Review of Fundamentals. *The Journal of Clinical Pharmacology* 42, 620–643.
- Martínez, H., Chacón, E., Tarazona, P., and Bresme, F. (2011). The intrinsic interfacial structure of ionic surfactant monolayers at water–oil and water–vapour interfaces. *Proceedings of the Royal Society A: Mathematical, Physical and Engineering Sciences* 467, 1939–1958.
- McAllister, M. (2010). Dynamic Dissolution: A Step Closer to Predictive Dissolution Testing? *Mol. Pharmaceutics* 7, 1374–1387.
- McConnell, E.L., Basit, A.W., and Murdan, S. (2008). Measurements of rat and mouse gastrointestinal pH, fluid and lymphoid tissue, and implications for in-vivo experiments. *J. Pharm. Pharmacol.* 60, 63–70.
- McGovern, S.L., Caselli, E., Grigorieff, N., and Shoichet, B.K. (2002). A Common Mechanism Underlying Promiscuous Inhibitors from Virtual and High-Throughput Screening. *J. Med. Chem.* 45, 1712–1722.
- McGovern, S.L., Helfand, B.T., Feng, B., and Shoichet, B.K. (2003). A specific mechanism of nonspecific inhibition. *J. Med. Chem.* 46, 4265–4272.
- Mellaerts, R., Mols, R., Kayaert, P., Annaert, P., Van Humbeeck, J., Van den Mooter, G., Martens, J.A., and Augustijns, P. (2008a). Ordered mesoporous silica induces pH-independent supersaturation of the basic low solubility compound itraconazole resulting in enhanced transepithelial transport. *International Journal of Pharmaceutics* 357, 169–179.
- Mellaerts, R., Mols, R., Jammaer, J.A.G., Aerts, C.A., Annaert, P., Van Humbeeck, J., Van den Mooter, G., Augustijns, P., and Martens, J.A. (2008b). Increasing the oral bioavailability of the poorly water soluble drug itraconazole with ordered mesoporous silica. *European Journal of Pharmaceutics and Biopharmaceutics* 69, 223–230.
- Miao, L., Liang, Y., Pan, W., Gou, J., Yin, T., Zhang, Y., He, H., and Tang, X. (2019). Effect of supersaturation on the oral bioavailability of paclitaxel/polymer amorphous solid dispersion. *Drug Deliv. and Transl. Res.* 9, 344–356.
- Michaelis, L., and Menten, M.L. (1913). Die kinetik der invertinwirkung. *Biochem. Zeitung* 49, 333–369.

- Mie, G. (1908). Beiträge zur Optik trüber Medien, speziell kolloidaler Metallösungen. *Annalen Der Physik* 330, 377–445.
- Miller, C.C., and Walker, J. (1924). The Stokes-Einstein law for diffusion in solution. *Proceedings of the Royal Society of London. Series A, Containing Papers of a Mathematical and Physical Character* 106, 724–749.
- Miller, D.A., McConville, J.T., Yang, W., Williams, R.O., and McGinity, J.W. (2007). Hot-melt extrusion for enhanced delivery of drug particles. *J. Pharm. Sci.* 96, 361–376.
- Miller, D.A., DiNunzio, J.C., Yang, W., McGinity, J.W., and III, R.O.W. (2008a). Enhanced In Vivo Absorption of Itraconazole via Stabilization of Supersaturation Following Acidic-to-Neutral pH Transition. *Drug Development and Industrial Pharmacy* 34, 890–902.
- Miller, D.A., DiNunzio, J.C., Yang, W., McGinity, J.W., and Iii, R.O.W. (2008b). Targeted Intestinal Delivery of Supersaturated Itraconazole for Improved Oral Absorption. *Pharm Res* 25, 1450–1459.
- MILLER, J.M., RODRÍGUEZ-HORNEDO, N., BLACKBURN, A.C., MACIKENAS, D., and COLLMAN, B.M. (2007). Solvent Systems for Crystallization and Polymorph Selection. In *Solvent Systems and Their Selection in Pharmaceuticals and Biopharmaceuticals*, P. Augustijns, and M.E. Brewster, eds. (New York, NY: Springer), pp. 53–109.
- Miller, J.M., Beig, A., Carr, R.A., Spence, J.K., and Dahan, A. (2012a). A Win–Win Solution in Oral Delivery of Lipophilic Drugs: Supersaturation via Amorphous Solid Dispersions Increases Apparent Solubility without Sacrifice of Intestinal Membrane Permeability. *Mol. Pharmaceutics* 9, 2009–2016.
- Miller, J.M., Beig, A., Carr, R.A., Webster, G.K., and Dahan, A. (2012b). The Solubility–Permeability Interplay When Using Cosolvents for Solubilization: Revising the Way We Use Solubility-Enabling Formulations. *Mol. Pharmaceutics* 9, 581–590.
- Miller, M.A., DiNunzio, J., Matteucci, M.E., Ludher, B.S., Williams, R.O., and Johnston, K.P. (2012c). Flocculated amorphous itraconazole nanoparticles for enhanced in vitro supersaturation and in vivo bioavailability. *Drug Development and Industrial Pharmacy* 38, 557–570.
- Minekus, M. (2015). The TNO gastro-intestinal model (TIM). In *The Impact of Food Bioactives on Health*, (Springer, Cham), pp. 37–46.
- Miura, M., Satoh, S., Inoue, K., Saito, M., Habuchi, T., and Suzuki, T. (2009). Telmisartan pharmacokinetics in Japanese renal transplant recipients. *Clin Chim Acta* 399, 83–87.
- Morgen, M., Bloom, C., Beyerinck, R., Bello, A., Song, W., Wilkinson, K., Steenwyk, R., and Shamblin, S. (2012). Polymeric Nanoparticles for Increased Oral Bioavailability and Rapid Absorption Using Celecoxib as a Model of a Low-Solubility, High-Permeability Drug. *Pharm Res* 29, 427–440.
- Morrison, J.S., Nophsker, M.J., and Haskell, R.J. (2014). A Combination Turbidity and Supernatant Microplate Assay to Rank-Order the Supersaturation Limits of Early Drug Candidates. *Journal of Pharmaceutical Sciences* 103, 3022–3032.
- Mudie, D.M., Amidon, G.L., and Amidon, G.E. (2010). Physiological Parameters for Oral Delivery and in Vitro Testing. *Mol. Pharmaceutics* 7, 1388–1405.
- Murdande, S.B., Pikal, M.J., Shanker, R.M., and Bogner, R.H. (2010). Solubility advantage of amorphous pharmaceuticals: I. A thermodynamic analysis. *J Pharm Sci* 99, 1254–1264.
- Mutschler, E., Thews, G., Schaible, H.G., and Vaupel, P. (2007). *Anatomie, Physiologie, Pathophysiologie des Menschen* (Wissenschaftliche Verlagsgesellschaft mbh Stuttgart).
- Nernst, W. (1904). Theorie der Reaktionsgeschwindigkeit in heterogenen Systemen. *Zeitschrift Für Physikalische Chemie* 47, 52–55.
- Niazi, S.K. (2019). Bioavailability and Bioequivalence Studies Submitted in NDAs or INDs—General Considerations. In *Handbook of Pharmaceutical Manufacturing Formulations*, (CRC Press), pp. 201–213.
- Novikov, A.A., Semenov, A.P., Monje-Galvan, V., Kuryakov, V.N., Klauda, J.B., and Anisimov, M.A. (2017). Dual Action of Hydrotropes at the Water/Oil Interface. *J. Phys. Chem. C* 121, 16423–16431.
- Noyes, A.A., and Whitney, W.R. (1897). THE RATE OF SOLUTION OF SOLID SUBSTANCES IN THEIR OWN SOLUTIONS. *J. Am. Chem. Soc.* 19, 930–934.
- O’Dwyer, P.J., Litou, C., Box, K.J., Dressman, J.B., Kostewicz, E.S., Kuentz, M., and Reppas, C. (2019). In vitro methods to assess drug precipitation in the fasted small intestine – a PEARRL review. *Journal of Pharmacy and Pharmacology* 71, 536–556.

7. REFERENCES

- Olmo, M., Ferrer, E., Curto, J., Barragán, P., Saumoy, M., Perulero, N., and Podzamczar, D. (2008). Improved tolerability and quality of life with the new lopinavir/ritonavir tablet formulation. *J. Infect.* *57*, 503–505.
- Overhoff, K.A., McConville, J.T., Yang, W., Johnston, K.P., Peters, J.I., and Iii, R.O.W. (2007). Effect of Stabilizer on the Maximum Degree and Extent of Supersaturation and Oral Absorption of Tacrolimus Made By Ultra-Rapid Freezing. *Pharm Res* *25*, 167–175.
- Ozaki, S., Minamisono, T., Yamashita, T., Kato, T., and Kushida, I. (2012). Supersaturation–Nucleation Behavior of Poorly Soluble Drugs and its Impact on the Oral Absorption of Drugs in Thermodynamically High-Energy Forms. *Journal of Pharmaceutical Sciences* *101*, 214–222.
- Pal, A., Brasseur, J.G., and Abrahamsson, B. (2007). A stomach road or “Magenstrasse” for gastric emptying. *Journal of Biomechanics* *40*, 1202–1210.
- Palermo, R.N., Anderson, C.A., and Drennen, J.K. (2012). Review: Use of Thermal, Diffraction, and Vibrational Analytical Methods to Determine Mechanisms of Solid Dispersion Stability. *J Pharm Innov* *7*, 2–12.
- Palmelund, H., Madsen, C.M., Plum, J., Müllertz, A., and Rades, T. (2016). Studying the Propensity of Compounds to Supersaturate: A Practical and Broadly Applicable Approach. *JPharmSci* *105*, 3021–3029.
- Park, J., Cho, W., Cha, K.-H., Ahn, J., Han, K., and Hwang, S.-J. (2013). Solubilization of the poorly water soluble drug, telmisartan, using supercritical anti-solvent (SAS) process. *International Journal of Pharmaceutics* *441*, 50–55.
- Paulson, S.K., Vaughn, M.B., Jessen, S.M., Lawal, Y., Gresk, C.J., Yan, B., Maziasz, T.J., Cook, C.S., and Karim, A. (2001). Pharmacokinetics of celecoxib after oral administration in dogs and humans: effect of food and site of absorption. *J. Pharmacol. Exp. Ther.* *297*, 638–645.
- Peeters, J., Neeskens, P., Tollenaere, J.P., Van Remoortere, P., and Brewster, M.E. (2002). Characterization of the interaction of 2-hydroxypropyl- β -cyclodextrin with itraconazole at pH 2, 4, and 7. *Journal of Pharmaceutical Sciences* *91*, 1414–1422.
- Pentafragka, C., Symillides, M., McAllister, M., Dressman, J., Vertzoni, M., and Reppas, C. (2019). The impact of food intake on the luminal environment and performance of oral drug products with a view to in vitro and in silico simulations: a PEARRL review. *Journal of Pharmacy and Pharmacology* *71*, 557–580.
- Pestieau, A., and Evrard, B. (2017). In vitro biphasic dissolution tests and their suitability for establishing in vitro-in vivo correlations: A historical review. *European Journal of Pharmaceutical Sciences* *102*, 203–219.
- Pestieau, A., Krier, F., Lebrun, P., Brouwers, A., Streel, B., and Evrard, B. (2015). Optimization of a PGSS (particles from gas saturated solutions) process for a fenofibrate lipid-based solid dispersion formulation. *International Journal of Pharmaceutics* *485*, 295–305.
- Pestieau, A., Lebrun, S., Cahay, B., Brouwers, A., Streel, B., Cardot, J.-M., and Evrard, B. (2017). Evaluation of different in vitro dissolution tests based on level A in vitro–in vivo correlations for fenofibrate self-emulsifying lipid-based formulations. *European Journal of Pharmaceutics and Biopharmaceutics* *112*, 18–29.
- Phillips, D.L. (1962). A Technique for the Numerical Solution of Certain Integral Equations of the First Kind. *J. ACM* *9*, 84–97.
- Phillips, D.J., Pygall, S.R., Cooper, V.B., and Mann, J.C. (2012). Toward Biorelevant Dissolution: Application of a Biphasic Dissolution Model as a Discriminating Tool for HPMC Matrices Containing a Model BCS Class II Drug. *Dissolution Technologies* *19*, 25–34.
- Plum, J., Bavnthøj, C.G., Eliassen, J.N., Rades, T., and Müllertz, A. (2020). Comparison of induction methods for supersaturation: Amorphous dissolution versus solvent shift. *European Journal of Pharmaceutics and Biopharmaceutics* *152*, 35–43.
- Poelma, F.G., Breäs, R., and Tukker, J.J. (1990). Intestinal absorption of drugs. III. The influence of taurocholate on the disappearance kinetics of hydrophilic and lipophilic drugs from the small intestine of the rat. *Pharm. Res.* *7*, 392–397.
- Poelma, F.G.J., Breäs, R., Tukker, J.J., and Crommelin, D.J.A. (1991). Intestinal Absorption of Drugs. The Influence of Mixed Micelles on the Disappearance Kinetics of Drugs from the Small Intestine of the Rat. *Journal of Pharmacy and Pharmacology* *43*, 317–324.
- Pouton, C.W. (2000). Lipid formulations for oral administration of drugs: non-emulsifying, self-emulsifying and “self-microemulsifying” drug delivery systems. *Eur J Pharm Sci* *11 Suppl 2*, S93–98.
- Psachoulas, D., Vertzoni, M., Goumas, K., Kalioras, V., Beato, S., Butler, J., and Reppas, C. (2011). Precipitation in and Supersaturation of Contents of the Upper Small Intestine After Administration of Two Weak Bases to Fasted Adults. *Pharm Res* *28*, 3145–3158.

- Pudlas, M., Kyeremateng, S.O., Williams, L.A.M., Kimber, J.A., van Lishaut, H., Kazarian, S.G., and Woehle, G.H. (2015). Analyzing the impact of different excipients on drug release behavior in hot-melt extrusion formulations using FTIR spectroscopic imaging. *European Journal of Pharmaceutical Sciences* 67, 21–31.
- Qiu, Y., Chen, Y., Zhang, G.G.Z., Liu, L., and Porter, W. (2009). *Developing Solid Oral Dosage Forms: Pharmaceutical Theory & Practice* (Academic Press).
- Quinney, S.K., Galinsky, R.E., Jiyamapa-Serna, V.A., Chen, Y., Hamman, M.A., Hall, S.D., and Kimura, R.E. (2008). Hydroxyitraconazole, formed during intestinal first-pass metabolism of itraconazole, controls the time course of hepatic CYP3A inhibition and the bioavailability of itraconazole in rats. *Drug Metab. Dispos.* 36, 1097–1101.
- Raghavan, S.L., Trividic, A., Davis, A.F., and Hadgraft, J. (2001). Crystallization of hydrocortisone acetate: influence of polymers. *International Journal of Pharmaceutics* 212, 213–221.
- Ramirez, E., Laosa, O., Guerra, P., Duque, B., Mosquera, B., Borobia, A.M., Lei, S.H., Carcas, A.J., and Frias, J. (2010). Acceptability and characteristics of 124 human bioequivalence studies with active substances classified according to the Biopharmaceutic Classification System. *Br J Clin Pharmacol* 70, 694–702.
- Rangel-Yagui, C.O., Pessoa-Jr, A., and Tavares, L.C. (2005). Micellar solubilization of drugs. *J. Pharm. Pharm. Sci* 8, 147–163.
- Rao, S.S.C., Kuo, B., McCallum, R.W., Chey, W.D., DiBaise, J.K., Hasler, W.L., Koch, K.L., Lackner, J.M., Miller, C., Saad, R., et al. (2009). Investigation of Colonic and Whole-Gut Transit With Wireless Motility Capsule and Radiopaque Markers in Constipation. *Clinical Gastroenterology and Hepatology* 7, 537–544.
- Raval, M.K., Vaghela, P.D., Vachhani, A.N., and Sheth, N.R. (2015). Role of excipients in the crystallization of Albendazole. *Advanced Powder Technology* 26, 1102–1115.
- Reintjes (2011). Soluble Kollidon (R) grades. In *Solubility Enhancement with BASF Pharma Polymers - Solubilizer Compendium*, pp. 112–118.
- Rodríguez-hornedo, N., and Murphy, D. (1999). Significance of controlling crystallization mechanisms and kinetics in pharmaceutical systems. *J. Pharm. Sci.* 88, 651–660.
- Rudin, A., and Choi, P. (2012). *The Elements of Polymer Science and Engineering* (Academic Press).
- Ruff, A., Holm, R., and Kostewicz, E.S. (2017). Evaluating the predictability of the in vitro transfer model and in vivo rat studies as a surrogate to investigate the supersaturation and precipitation behaviour of different Albendazole formulations for humans. *European Journal of Pharmaceutical Sciences* 105, 108–118.
- Sassano, M.F., Doak, A.K., Roth, B.L., and Shoichet, B.K. (2013). Colloidal Aggregation Causes Inhibition of G Protein-Coupled Receptors. *J Med Chem* 56, 2406–2414.
- Schenck, H.-U., Simak, P., and Haedicke, E. (1979). Structure of Polyvinylpyrrolidone-Iodine (Povidone-Iodine). *JPharmSci* 68, 1505–1509.
- Schiller, C., Fröhlich, C.-P., Giessmann, T., Siegmund, W., Mönnikes, H., Hosten, N., and Weitschies, W. (2005). Intestinal fluid volumes and transit of dosage forms as assessed by magnetic resonance imaging. *Alimentary Pharmacology & Therapeutics* 22, 971–979.
- Scholtens, B.J.R., and Bijsterbosch, B.H. (1980). The influence of molecular architecture on the surface activity of vinyl alcohol-acetate copolymers. *Journal of Colloid and Interface Science* 77, 162–173.
- Scholtens, B.J.R., Bruin, S., and Bijsterbosch, B.H. (1979). Liquid-liquid mass transfer and its retardation by macromolecular adsorption. *Chemical Engineering Science* 34, 661–670.
- Sengupta, P., Chatterjee, B., Mandal, U.K., Gorain, B., and Pal, T.K. (2017). Development and validation of a high throughput LC–MS/MS method for simultaneous quantitation of pioglitazone and telmisartan in rat plasma and its application to a pharmacokinetic study. *Journal of Pharmaceutical Analysis* 7, 381–387.
- Shakeel, F., Baboota, S., Ahuja, A., Ali, J., and Shafiq, S. (2008). Celecoxib nanoemulsion: Skin permeation mechanism and bioavailability assessment. *Journal of Drug Targeting* 16, 733–740.
- Shedlovsky (1962). The behaviour of carboxylic acids in mixed solvents. *Electrolytes*, Pesce, B., Ed.
- Shi, Y., Gao, P., Gong, Y., and Ping, H. (2010). Application of a Biphasic Test for Characterization of In Vitro Drug Release of Immediate Release Formulations of Celecoxib and Its Relevance to In Vivo Absorption. *Mol. Pharmaceutics* 7, 1458–1465.

7. REFERENCES

- Shi, Y., Erickson, B., Jayasankar, A., Lu, L., Marsh, K., Menon, R., and Gao, P. (2016). Assessing Supersaturation and Its Impact on In Vivo Bioavailability of a Low-Solubility Compound ABT-072 With a Dual pH, Two-Phase Dissolution Method. *Journal of Pharmaceutical Sciences* *105*, 2886–2895.
- Shrivastava, M., Khunt, D., Shrivastava, M., Choudhari, M., Rathod, R., and Misra, M. (2019). Advances in In Vivo Predictive Dissolution Testing of Solid Oral Formulations: How Closer to In Vivo Performance? *J Pharm Innov.*
- Siegel, J.A., Urbain, J.L., Adler, L.P., Charkes, N.D., Maurer, A.H., Krevsky, B., Knight, L.C., Fisher, R.S., and Malmud, L.S. (1988). Biphasic nature of gastric emptying. *Gut* *29*, 85–89.
- Simonelli, A.P., Mehta, S.C., and Higuchi, W.I. (1970). Inhibition of Sulfathiazole Crystal Growth by Polyvinylpyrrolidone. *Journal of Pharmaceutical Sciences* *59*, 633–638.
- Singhal, D., and Curatolo, W. (2004). Drug polymorphism and dosage form design: a practical perspective. *Advanced Drug Delivery Reviews* *56*, 335–347.
- Sirius Analytical Instruments (2009a). Presentation: Introduction to pH-metric solubility measurement.
- Sirius Analytical Instruments (2009b). Presentation: Introduction to pH-metric logP measurement.
- Sjögren, E., Abrahamsson, B., Augustijns, P., Becker, D., Bolger, M.B., Brewster, M., Brouwers, J., Flanagan, T., Harwood, M., Heinen, C., et al. (2014). In vivo methods for drug absorption – Comparative physiologies, model selection, correlations with in vitro methods (IVIVC), and applications for formulation/API/excipient characterization including food effects. *European Journal of Pharmaceutical Sciences* *57*, 99–151.
- Skolnik, S.M., Geraci, G.M., and Dodd, S. (2018). Automated Supersaturation Stability Assay to Differentiate Poorly Soluble Compounds in Drug Discovery. *Journal of Pharmaceutical Sciences* *107*, 84–93.
- Slater, B., McCormack, A., Avdeef, A., and Comer, J.E.A. (1994). Ph-metric log P. 4. Comparison of partition coefficients determined by HPLC and potentiometric methods to literature values. *Journal of Pharmaceutical Sciences* *83*, 1280–1283.
- Smoluchowski, M. von (1906). Zur kinetischen Theorie der Brownschen Molekularbewegung und der Suspensionen. *Annalen Der Physik* *326*, 756–780.
- Sriamornsak, P., and Burapapadh, K. (2015). Characterization of recrystallized itraconazole prepared by cooling and anti-solvent crystallization. *Asian Journal of Pharmaceutical Sciences* *10*, 230–238.
- Staples, E., Penfold, J., and Tucker, I. (2000). Adsorption of Mixed Surfactants at the Oil–Water Interface. *J. Phys. Chem. B* *104*, 606–614.
- Stegemann, S., Leveiller, F., Franchi, D., de Jong, H., and Lindén, H. (2007). When poor solubility becomes an issue: From early stage to proof of concept. *European Journal of Pharmaceutical Sciences* *31*, 249–261.
- Steiner, T. (2002). The Hydrogen Bond in the Solid State. *Angewandte Chemie International Edition* *41*, 48–76.
- Steingoetter, A., Fox, M., Treier, R., Weishaupt, D., Marincek, B., Boesiger, P., Fried, M., and Schwizer, W. (2006). Effects of posture on the physiology of gastric emptying: A magnetic resonance imaging study. *Scandinavian Journal of Gastroenterology* *41*, 1155–1164.
- Strindberg, S., Plum, J., Stie, M.B., Christiansen, M.L., Hagner Nielsen, L., Rades, T., and Müllertz, A. (2020). Effect of supersaturation on absorption of indomethacin and tadalafil in a single pass intestinal perfusion rat model, in the absence and presence of a precipitation inhibitor. *European Journal of Pharmaceutics and Biopharmaceutics* *151*, 108–115.
- Stuart, M., and Box, K. (2005a). Chasing Equilibrium: Measuring the Intrinsic Solubility of Weak Acids and Bases. *Anal. Chem.* *77*, 983–990.
- Stuart, M., and Box, K. (2005b). Chasing Equilibrium: Measuring the Intrinsic Solubility of Weak Acids and Bases. *Anal. Chem.* *77*, 983–990.
- Sugano, K. (2009). Estimation of Effective Intestinal Membrane Permeability Considering Bile Micelle Solubilisation. *Int. J. Pharm.* *368*, 116.
- Sugano, K., Kataoka, M., Da Costa Mathews, C., and Yamashita, S. (2010). Prediction of Food Effect by Bile Micelles on Oral Drug Absorption Considering Free Fraction in Intestinal Fluid. *Eur. J. Pharm. Sci.* *40*, 118.

- Sugawara, M., Kadomura, S., He, X., Takekuma, Y., Kohri, N., and Miyazaki, K. (2005). The use of an in vitro dissolution and absorption system to evaluate oral absorption of two weak bases in pH-independent controlled-release formulations. *European Journal of Pharmaceutical Sciences* 26, 1–8.
- Sun, D.D., Wen, H., and Taylor, L.S. (2016). Non-Sink Dissolution Conditions for Predicting Product Quality and In Vivo Performance of Supersaturating Drug Delivery Systems. *Journal of Pharmaceutical Sciences* 105, 2477–2488.
- Sympatec GmbH Laser Diffraction.
- Tadmouri, R., Zedde, C., Routaboul, C., Micheau, J.-C., and Pimienta, V. (2008). Partition and Water/Oil Adsorption of Some Surfactants. *J. Phys. Chem. B* 112, 12318–12325.
- Takács-Novák, K., and Avdeef, A. (1996). Interlaboratory study of log P determination by shake-flask and potentiometric methods. *J Pharm Biomed Anal* 14, 1405–1413.
- Takács-Novák, K., Box, K.J., and Avdeef, A. (1997). Potentiometric pKa determination of water-insoluble compounds: validation study in methanol/water mixtures. *International Journal of Pharmaceutics* 151, 235–248.
- Takeuchi, S., Tsume, Y., Amidon, G.E., and Amidon, G.L. (2014). Evaluation of a Three Compartment In Vitro Gastrointestinal Simulator Dissolution Apparatus to Predict In Vivo Dissolution. *Journal of Pharmaceutical Sciences* 103, 3416–3422.
- Tallarida, R.J., and Murray, R.B. (1987). Area under a Curve: Trapezoidal and Simpson's Rules. In *Manual of Pharmacologic Calculations: With Computer Programs*, R.J. Tallarida, and R.B. Murray, eds. (New York, NY: Springer), pp. 77–81.
- Tang, X., Huston, K.J., and Larson, R.G. (2014). Molecular Dynamics Simulations of Structure–Property Relationships of Tween 80 Surfactants in Water and at Interfaces. *J. Phys. Chem. B* 118, 12907–12918.
- Terhaag, B., Donath, F., Le Petit, G., and Feller, K. (1986). The absolute and relative bioavailability of dipyridamole from different preparations and the in vitro-in vivo comparison. *Int J Clin Pharmacol Ther Toxicol* 24, 298–302.
- Thiry, J., Kok, M.G.M., Collard, L., Frère, A., Krier, F., Fillet, M., and Evrard, B. (2017). Bioavailability enhancement of itraconazole-based solid dispersions produced by hot melt extrusion in the framework of the Three Rs rule. *European Journal of Pharmaceutical Sciences* 99, 1–8.
- Tian, F., Saville, D.J., Gordon, K.C., Strachan, C.J., Zeitler, J.A., Sandler, N., and Rades, T. (2007). The influence of various excipients on the conversion kinetics of carbamazepine polymorphs in aqueous suspension. *Journal of Pharmacy and Pharmacology* 59, 193–201.
- Tiss, A., Ransac, S., Lengsfeld, H., Hadvary, P., Cagna, A., and Verger, R. (2001). Surface behaviour of bile salts and tetrahydrolipstatin at air/water and oil/water interfaces. *Chemistry and Physics of Lipids* 111, 73–85.
- Trasi, N.S., and Taylor, L.S. (2012). Effect of Additives on Crystal Growth and Nucleation of Amorphous Flutamide. *Crystal Growth & Design* 12, 3221–3230.
- Tsume, Y., Mudie, D.M., Langguth, P., Amidon, G.E., and Amidon, G.L. (2014). The Biopharmaceutics Classification System: Subclasses for in vivo predictive dissolution (IPD) methodology and IVIVC. *Eur J Pharm Sci* 57, 152–163.
- Tsume, Y., Takeuchi, S., Matsui, K., Amidon, G.E., and Amidon, G.L. (2015). In vitro dissolution methodology, mini-Gastrointestinal Simulator (mGIS), predicts better in vivo dissolution of a weak base drug, dasatinib. *European Journal of Pharmaceutical Sciences* 76, 203–212.
- Tsume, Y., Matsui, K., Searls, A.L., Takeuchi, S., Amidon, G.E., Sun, D., and Amidon, G.L. (2017). The impact of supersaturation level for oral absorption of BCS class IIb drugs, dipyridamole and ketoconazole, using in vivo predictive dissolution system: Gastrointestinal Simulator (GIS). *European Journal of Pharmaceutical Sciences* 102, 126–139.
- Twomey, S. (1963). On the Numerical Solution of Fredholm Integral Equations of the First Kind by the Inversion of the Linear Produced by Quadrate. *JACM* 10.
- U.S. Food and Drug Administration (2020). Novel Drug Approvals for 2020. 2020.
- USP (2011). <711> Dissolution. In *United States Pharmacopeia*, p.
- Usui, F., Maeda, K., Kusai, A., Nishimura, K., and Yamamoto, K. (1997). Inhibitory effects of water-soluble polymers on precipitation of RS-8359. *International Journal of Pharmaceutics* 154, 59–66.

7. REFERENCES

- Van Den Abeele, J., Brouwers, J., Mattheus, R., Tack, J., and Augustijns, P. (2016). Gastrointestinal Behavior of Weakly Acidic BCS Class II Drugs in Man—Case Study of Diclofenac Potassium. *Journal of Pharmaceutical Sciences* *105*, 687–696.
- Van den Mooter, G. (2012). The use of amorphous solid dispersions: A formulation strategy to overcome poor solubility and dissolution rate. *Drug Discovery Today: Technologies* *9*, e79–e85.
- Van Speybroeck, M., Mellaerts, R., Mols, R., Thi, T.D., Martens, J.A., Van Humbeeck, J., Annaert, P., Van den Mooter, G., and Augustijns, P. (2010a). Enhanced absorption of the poorly soluble drug fenofibrate by tuning its release rate from ordered mesoporous silica. *European Journal of Pharmaceutical Sciences* *41*, 623–630.
- Van Speybroeck, M., Mols, R., Mellaerts, R., Thi, T.D., Martens, J.A., Humbeeck, J.V., Annaert, P., Mooter, G.V. den, and Augustijns, P. (2010b). Combined use of ordered mesoporous silica and precipitation inhibitors for improved oral absorption of the poorly soluble weak base itraconazole. *European Journal of Pharmaceutics and Biopharmaceutics* *75*, 354–365.
- Vandercruys, R., Peeters, J., Verreck, G., and Brewster, M.E. (2007). Use of a screening method to determine excipients which optimize the extent and stability of supersaturated drug solutions and application of this system to solid formulation design. *International Journal of Pharmaceutics* *342*, 168–175.
- Vangani, S., Li, X., Zhou, P., Del-Barrio, M.-A., Chiu, R., Cauchon, N., Gao, P., Medina, C., and Jasti, B. (2009). Dissolution of poorly water-soluble drugs in biphasic media using USP 4 and fiber optic system. *Clinical Research and Regulatory Affairs* *26*, 8–19.
- Vasconcelos, T., Sarmento, B., and Costa, P. (2007). Solid dispersions as strategy to improve oral bioavailability of poor water soluble drugs. *Drug Discovery Today* *12*, 1068–1075.
- Vatier, J., Harman, A., Castela, N., Droy-Lefaix, M.T., and Farinotti, R. (1994). Interactions of cimetidine and ranitidine with aluminum-containing antacids and a clay-containing gastric-protective drug in an “artificial stomach-duodenum” model. *Journal of Pharmaceutical Sciences* *83*, 962–966.
- Veesler, S., Lafferrère, L., Garcia, E., and Hoff, C. (2003). Phase Transitions in Supersaturated Drug Solution. *Org. Process Res. Dev.* *7*, 983–989.
- Veesler, S., Revalor, E., Bottini, O., and Hoff, C. (2006). Crystallization in the Presence of a Liquid–Liquid Phase Separation. *Org. Process Res. Dev.* *10*, 841–845.
- Verma, S., Huey, B.D., and Burgess, D.J. (2009). Scanning Probe Microscopy Method for Nanosuspension Stabilizer Selection. *Langmuir* *25*, 12481–12487.
- Vertzoni, M., Dressman, J., Butler, J., Hempenstall, J., and Reppas, C. (2005). Simulation of fasting gastric conditions and its importance for the in vivo dissolution of lipophilic compounds. *European Journal of Pharmaceutics and Biopharmaceutics* *60*, 413–417.
- Vertzoni, M., Augustijns, P., Grimm, M., Koziolok, M., Lemmens, G., Parrott, N., Pentafragka, C., Reppas, C., Rubbens, J., Van Den Abeele, J., et al. (2019). Impact of regional differences along the gastrointestinal tract of healthy adults on oral drug absorption: An UNGAP review. *European Journal of Pharmaceutical Sciences* *134*, 153–175.
- Verwei, M., Minekus, M., Zeijdner, E., Schilderink, R., and Havenaar, R. (2016). Evaluation of two dynamic in vitro models simulating fasted and fed state conditions in the upper gastrointestinal tract (TIM-1 and tiny-TIM) for investigating the bioaccessibility of pharmaceutical compounds from oral dosage forms. *International Journal of Pharmaceutics* *498*, 178–186.
- Veseli, A., Žakelj, S., and Kristl, A. (2019). A review of methods for solubility determination in biopharmaceutical drug characterization. *Drug Development and Industrial Pharmacy* *45*, 1717–1724.
- Vishweshwar, P., McMahon, J.A., Bis, J.A., and Zaworotko, M.J. (2006). Pharmaceutical Co-Crystals. *Journal of Pharmaceutical Sciences* *95*, 499–516.
- Völgyi, G., Baka, E., Box, K.J., Comer, J.E.A., and Takács-Novák, K. (2010). Study of pH-dependent solubility of organic bases. Revisit of Henderson-Hasselbalch relationship. *Analytica Chimica Acta* *673*, 40–46.
- Wagner, J.G., and Nelson, E. (1964). Kinetic Analysis of Blood Levels and Urinary Excretion in the Absorptive Phase after Single Doses of Drug. *Journal of Pharmaceutical Sciences* *53*, 1392–1403.
- Wankhede, S.B., Tajne, M.R., Gupta, K.R., and Wadodkar, S.G. (2007). RP-HPLC method for simultaneous estimation of telmisartan and hydrochlorothiazide in tablet dosage form. *Indian Journal of Pharmaceutical Sciences* *69*, 298.
- Warren, D.B., Benameur, H., Porter, C.J.H., and Pouton, C.W. (2010). Using polymeric precipitation inhibitors to improve the absorption of poorly water-soluble drugs: A mechanistic basis for utility. *Journal of Drug Targeting* *18*, 704–731.

- van de Waterbeemd, H., Carter, R.E., Grassy, G., Kubinyi, H., Martin, Y.C., Tute, M.S., and Willett, P. (1997). Glossary of terms used in computational drug design (IUPAC Recommendations 1997). *Pure and Applied Chemistry* 69, 1137–1152.
- Wenlock, M.C., Austin, R.P., Barton, P., Davis, A.M., and Leeson, P.D. (2003). A Comparison of Physicochemical Property Profiles of Development and Marketed Oral Drugs. *J. Med. Chem.* 46, 1250–1256.
- Wiener, W., Entzeroth, M., Meel, J.C.A. van, Stangier, J., Busch, U., Ebner, T., Schmid, J., Lehmann, H., Matzek, K., Kempthorne-Rawson, J., et al. (2000). A Review on Telmisartan: A Novel, Long-Acting Angiotensin II-Receptor Antagonist. *Cardiovascular Drug Reviews* 18, 127–154.
- Williams, J.M. (1975). Combining residual entropy and diffraction results to understand crystal structure. *J. Chem. Educ.* 52, 210.
- Williams, H.D., Trevaskis, N.L., Charman, S.A., Shanker, R.M., Charman, W.N., Pouton, C.W., and Porter, C.J.H. (2013). Strategies to Address Low Drug Solubility in Discovery and Development. *Pharmacol Rev* 65, 315–499.
- Wilson, V., Lou, X., Osterling, D.J., Stolarik, D.F., Jenkins, G., Gao, W., Zhang, G.G.Z., and Taylor, L.S. (2018). Relationship between amorphous solid dispersion in vivo absorption and in vitro dissolution: phase behavior during dissolution, speciation, and membrane mass transport. *Journal of Controlled Release* 292, 172–182.
- Wu, C.-Y., and Benet, L.Z. (2005). Predicting Drug Disposition via Application of BCS: Transport/Absorption/ Elimination Interplay and Development of a Biopharmaceutics Drug Disposition Classification System. *Pharm Res* 22, 11–23.
- Wu, H., and Khan, M.A. (2011). Quality-by-Design: An Integrated Process Analytical Technology Approach to Determine the Nucleation and Growth Mechanisms During a Dynamic Pharmaceutical Coprecipitation Process. *Journal of Pharmaceutical Sciences* 100, 1969–1986.
- Xie, S., Poornachary, S.K., Chow, P.S., and Tan, R.B.H. (2010). Direct Precipitation of Micron-Size Salbutamol Sulfate: New Insights into the Action of Surfactants and Polymeric Additives. *Crystal Growth & Design* 10, 3363–3371.
- Xu, S., and Dai, W.-G. (2013a). Drug precipitation inhibitors in supersaturable formulations. *International Journal of Pharmaceutics* 453, 36–43.
- Xu, S., and Dai, W.-G. (2013b). Drug precipitation inhibitors in supersaturable formulations. *International Journal of Pharmaceutics* 453, 36–43.
- Xu, H., Wang, W., Shi, Y., and Gao, P. (2019). Characterization of the Partition Rate of Ibuprofen Across the Water-Octanol Interface and the Influence of Common Pharmaceutical Excipients. *Journal of Pharmaceutical Sciences* 108, 525–537.
- Yamashita, K., Nakate, T., Okimoto, K., Ohike, A., Tokunaga, Y., Ibuki, R., Higaki, K., and Kimura, T. (2003). Establishment of new preparation method for solid dispersion formulation of tacrolimus. *International Journal of Pharmaceutics* 267, 79–91.
- Yamashita, T., Kokubo, T., Zhao, C., and Ohki, Y. (2010). Antiprecipitant Screening System for Basic Model Compounds using Bio-Relevant Media. *JALA: Journal of the Association for Laboratory Automation* 15, 306–312.
- Yamashita, T., Ozaki, S., and Kushida, I. (2011). Solvent shift method for anti-precipitant screening of poorly soluble drugs using biorelevant medium and dimethyl sulfoxide. *International Journal of Pharmaceutics* 419, 170–174.
- Yani, Y., Chow, P.S., and Tan, R.B.H. (2011). Molecular Simulation Study of the Effect of Various Additives on Salbutamol Sulfate Crystal Habit. *Mol. Pharmaceutics* 8, 1910–1918.
- Yasuda, M. (1959). Dissociation Constants of Some Carboxylic Acids in Mixed Aqueous Solvents. *BCSJ* 32, 429–432.
- Young, A.T. (1981). Rayleigh scattering. *Appl. Opt.*, AO 20, 533–535.
- Zecevic, D. E., Meier, R., Daniels, R., & Wagner, K. G. (2014). Site specific solubility improvement using solid dispersions of HPMC-AS/HPC SSL - Mixtures. *European Journal of Pharmaceutics and Biopharmaceutics*, 87(2), 264–270. <https://doi.org/10.1016/j.ejpb.2014.03.018>
- Zhang, K., Yu, H., Luo, Q., Yang, S., Lin, X., Zhang, Y., Tian, B., and Tang, X. (2013). Increased dissolution and oral absorption of itraconazole/Soluplus extrudate compared with itraconazole nanosuspension. *European Journal of Pharmaceutics and Biopharmaceutics* 85, 1285–1292.
- Zhao, H., Xie, C., Xu, Z., Wang, Y., Bian, L., Chen, Z., and Hao, H. (2012). Solution Crystallization of Vanillin in the Presence of a Liquid-Liquid Phase Separation. *Ind. Eng. Chem. Res.* 51, 14646–14652.
- Zhao, Y.H., Abraham, M.H., Le, J., Hersey, A., Luscombe, C.N., Beck, G., Sherborne, B., and Cooper, I. (2002). Rate-Limited Steps of Human Oral Absorption and QSAR Studies. *Pharm Res* 19, 1446–1457.

7. REFERENCES

- Zhong, Y., Jing, G., Tian, B., Huang, H., Zhang, Y., Gou, J., Tang, X., He, H., and Wang, Y. (2016). Supersaturation induced by Itraconazole/Soluplus® micelles provided high GI absorption in vivo. *Asian Journal of Pharmaceutical Sciences* 11, 255–264.
- Ziller, K.H., and Rupprecht, H. (1988). Control of Crystal Growth in Drug Suspensions: 1) Design of a Control Unit and Application to Acetaminophen Suspensions). *Drug Development and Industrial Pharmacy* 14, 2341–2370.
- Zimmermann, A., Millqvist-Fureby, A., Elema, M.R., Hansen, T., Müllertz, A., and Hovgaard, L. (2009). Adsorption of pharmaceutical excipients onto microcrystals of siramesine hydrochloride: Effects on physicochemical properties. *European Journal of Pharmaceutics and Biopharmaceutics* 71, 109–116.

